# SYNTHESIS, CHARACTERIZATION AND ANTICANCER STUDIES OF OSMIUM-CYMENE COMPLEXES WITH O,O′- AND P,P′-CHELATORS AS WELL AS MONODENTATE N- AND P-DONOR LIGANDS

by

**KGAUGELO CORNELIUS TAPALA**

Submitted in accordance with the requirements for the degree of

**MASTER OF SCIENCE**

In the subject

**CHEMISTRY**

At the

University of South Africa

Supervisor: Dr. H.S. Clayton

August 2017

**DECLARATION**

Student number: 4090 7333

I, Kgaugelo Cornelius Tapala, declare that "**SYNTHESIS, CHARACTERIZATION AND ANTICANCER STUDIES OF OSMIUM-CYMENE COMPLEXES WITH O,O′- AND P,P′-CHELATORS AS WELL AS MONODENTATE N- AND P-DONOR LIGANDS**" is my own work and that all the sources that I have used or quoted have been indicated and acknowledged by means of complete references.

_____ _____

SIGNATURE DATE

(Mr)

# PUBLICATIONS

**Crystal structure of dibromido μ-oxalato-$\kappa^2O,O'$:$\kappa^2O'',O'''$-$\eta^6$-*p*-cymenediosmium(II), $C_{22}H_{28}Br_2O_4Os_2$**

Hadley S. Clayton, Kgaugelo C. Tapala and Andreas Lemmerer

Zeitschrift für Kristallographie - New Crystal Structures, **2016**, 231(4), 1055–1056.

# CONFERENCES

Part of this work was presented at the SACI Convention 2015 in Durban.

## DEDICATION

To my parents, Maake *Snr* and Keleganne Tapala as well as my son Goitsemodimo Maake *Jnr* Tapala.

# ABSTRACT

Seventeen novel osmium cymene complexes with O,O′- and P,P′-chelating ligands as well as N- and P-monodentate ligands are reported. The osmium cymene complexes were synthesised and characterised by spectroscopic techniques (NMR, IR and Raman), elemental analysis, thermal analysis, conductivity studies and X-ray crystallography. The molecular structures of complexes **1(b)**, **2**, **4**, **6**, **7(a)-(d)** and **11** in this study are reported. The cymene rings of these complexes show different conformations due to loss of planarity influenced by the ancillary ligands as a result of M–L back bonding.

Osmium cymene complexes of the type $[Os(\eta^6\text{-p-cymene})BrL_2]^+$ (where $L_2$ = chelating P,P′ ligand) and binuclear $[\{Os(\eta^6\text{-}p\text{-cymene})Br_2\}_2\ L_2]$ (where $L_2$ = bridging P,P′ ligand) were evaluated for anticancer activity against renal, melanoma, breast and HeLa cancer cells. The chelated-diphosphine osmium cymene complexes exhibited significant anticancer activities relative to the bridged-diphosphine osmium analogues. A series of O,O′-chelated osmium complexes exhibited moderate and poor anticancer activities.

Key words: osmium, anticancer, cymene, diphosphine, oxalate, tropolone.

# TABLE OF CONTENTS

## List of Figures

## List of Charts



## List of Schemes

## List of Tables

## Abbreviations

| | |
|---|---|
| *ca*. | circa |
| $CDCl_3$ | Deuterated chloroform |
| Dppm | 1,1-bis(diphenylphosphino)methane |
| Dppe | 1,2-bis(diphenylphosphino)ethane |
| Dppp | 1,3-bis(diphenylphosphino)propane |
| Dppb | 1,4-bis(diphenylphosphino)butane |
| DMSO-$d_6$ | Deuterated dimethylsulfoxide |
| HSQC | Heteronuclear Single Quantum Correlation |
| $IC_{50}$ | Inhibitory Concentration 50% |
| IR/Raman m | medium peak |
| IR/Raman s | strong peak |
| IR/Raman sh | shoulder peak |
| IR/Raman vs | very strong peak |
| IR/Raman w | weak peak |
| NMR br | broad |
| NMR d | doublet |
| NMR dd | doublet of doublets |
| NMR m | multiplet |
| NMR s | singlet |
| NMR sept | septet |
| NMR tt | triplet of triplets |
| trop | tropolone |

**Acknowledgements**

I would like to express my sincere gratitude to my supervisor Dr. Hadley S. Clayton for his excellent guidance, support and encouragement throughout this study, for proofreading and correcting my manuscripts, abstracts, posters, presentations and this MSc thesis. Your methods of teaching and patience are extremely appreciated.

Thanks to Natasha Kolesnikova at the Council of Scientific and Industrial Research (CSIR) Bioscience laboratories for the anticancer data. Also, thanks to Mike Philport at the Agricultural Research Council-Institute for Soil, Climate and Water for elemental analysis data. I would also like to extend my appreciation to Professor Andreas Lemmerer (University of Witwatersrand) for collection of crystallography data. I express gratitude Kabelo Ledwaba from Chemical Engineering Department (UNISA) for assisting in collection of Raman data. I thank everyone in the Chemistry Department for their contributions in this study. To all my friends who stood by me through my academic and social challenges, I am highly indebted to you.

The financial support of the National Research Foundation (NRF) of South Africa towards this research is extremely acknowledged. Opinions expressed and conclusions arrived at, are those of the author and are not necessarily to be attributed to the NRF. We also thank the Anglo-Platinum Research Laboratories for the generous donation of potassium osmate. The financial support of UNISA Chemistry Department and Grow Your Own Timber is highly acknowledged.

Special thanks to my parents and siblings for all the loyal support and encouragement I acquired from you.

# CHAPTER 1

## INTRODUCTION

### 1.1 The role of metals in medicine

Currently, transition metals regardless of their general toxicity play an important role in the mammalian biological systems as well as treatment of certain diseases.[1,2] There are transitional metals that are approved for clinical use as supplements such as chromium, manganese, iron, cobalt, nickel, copper and molybdenum.[3] These metals are known to perform unique functions in the body such as catalysis in biological reactions. Copper and zinc are found to play a role in the healing processes of wounds and burns.[4,5] Copper is known to play an essential role in the cellular uptake of iron. Mercury complexes utilized in ancient Greece for treatment of scabies and lice.[6] Gold cyanide was used to treat tuberculosis.[7] Bismuth complexes were applied for treatment of syphilis, gastrointestinal disorder and exhibit anti-microbial, anti-cancer, anti-leishmanial properties.[8] The iron complex, ferroquine is undergoing clinical trials against chloroquine resistant malaria parasite.[6] Also, the ruthenium complex $[RuCl_2(\text{chloroquine})]_2$ relative to chloroquine exhibits 2-5 times greater potency against chloroquine resistant malaria parasite.[9]

Vanadium complexes are found to be potent with less toxicity against human cancer cells [10] The deficiency of vanadium is responsible for malfunctioning of thyroid, glucose and lipid metabolism.[11] Titanium metal complexes with mixed ligand system are found to enhance solubility in aqueous media as well as exhibit increased anticancer activities relative to titanocene dichloride complex.[12] Also the titanium complex dichlorobis(1-phenylbutane-1,3-dionato)titanium(IV) entered clinical trials for its potency against colon cancer.[13] Molybdenum and tungsten complexes also were found to be cytotoxic against the HeLa, MCF-7 and N1E-115 cell lines *in vitro* screening.[14]

## 1.2 Brief background of metal arene complexes

Arenes are purely organic hydrocarbons with π-electrons delocalised around the ring of carbon atoms. The C–C bonds with delocalised electrons are shorter than the C–C single bonds. The arenes are part of a family of π-ligand systems which donate π-electrons to the metal with hapticity ranging from one to six ($\eta^1$- $\eta^6$) (*chart 1.1*). The simplest of these arenes is the benzene ring, which usually donates six electrons to the metal centre during complexation. In this study, only the cymene ligand was used, which donates electrons in the range $\eta^1$- $\eta^6$ to the metal centre.

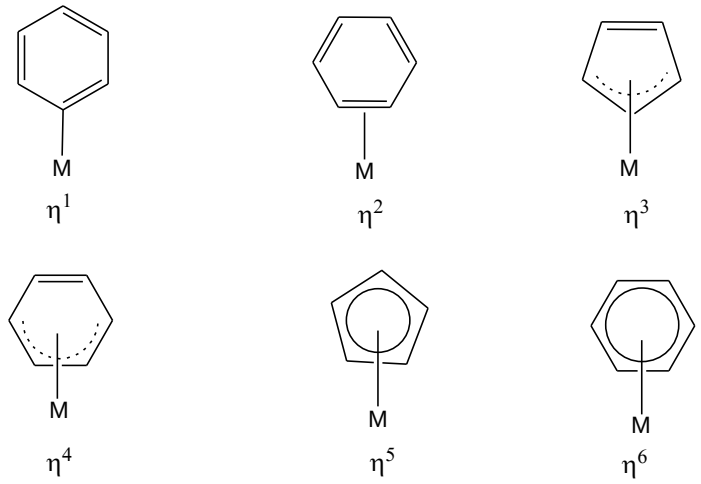


*Chart 1.1: Bonding possibilities of the arene ligands.*

The bonding of metal arenes is based mostly on the orbital interactions between the metal and the arene ligands (*see figure 1.1*). Here, the central metal acts as a Lewis acid and the arene ligand acts as the Lewis base. The interaction occurs by donation of π-electrons from the arene ligand to the σ d-orbitals of the metal atom ($\pi \rightarrow d_\sigma$). Back bonding of the electrons from the metal atom to the arene ligand is possible resulting in shortened M−C bonds due to metal-arene bond reinforcement. The reinforcement arises when the metal centre has more electrons and the arene ligand is electron deficient;[15] therefore, back donation ($d_\pi \rightarrow \pi^*$) reduces electron density on the metal centre.

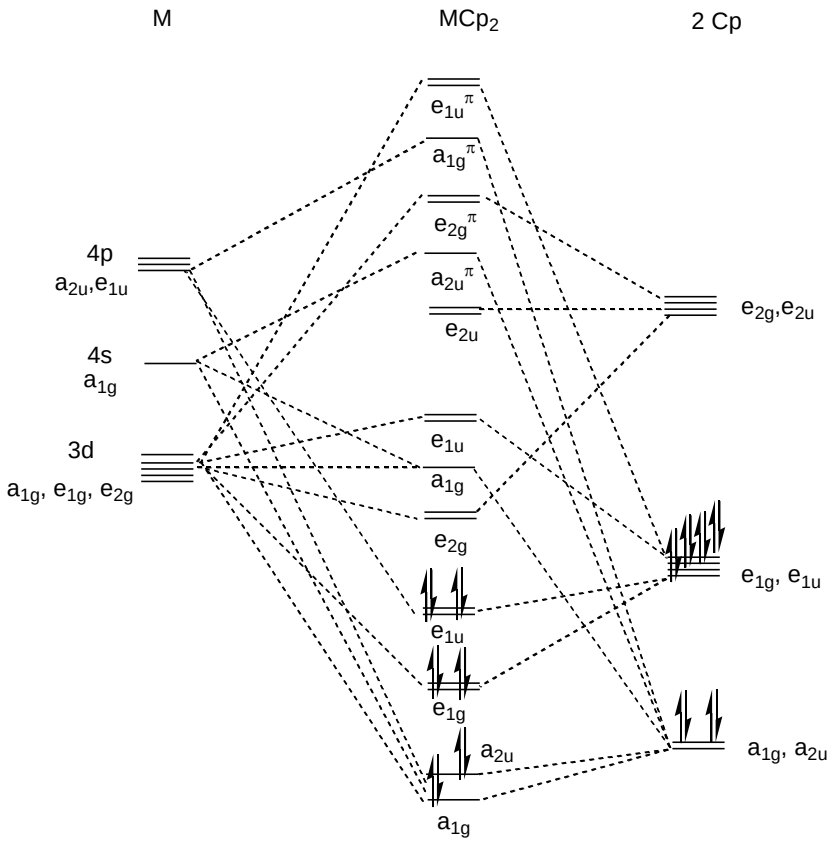


*Figure 1.1: The $MCp_2$ molecular orbital diagram showing arene orbitals involved in bonding.*[16]

Back bonding is an important phenomenon in organometallic chemistry. The free arene ligand has electrons delocalised around the C−C atoms of the arene ligand. However, when the arene ligand is bonded to a metal centre, electrons are localised between the adjacent carbons of the bound carbon on the arene, with the consequence of C−C bonds longer than those of the free arene. This would suggest that alternating C=C and C−C bonds would be observed in the coordinated arene ring. The interaction changes the shape as well as the reactivity of the arene ligand. The shape of the $\eta^6$-arene ligand may change from planar to pseudo boat and to pseudo chair conformation. The metal-arene bond that reduces the electron density on the arene ligand causing the arene ligand to have a slight positive charge and the central metal to have slight negative charge causes the change in reactivity of the arene ligand.

Substituents on the arene ligand play an important role in metal complex stability because of electronic and steric effects[17]. The substituents also influence the reactivity of the arene ligand on coordination to the metal centre. Electron donating groups on the arene ligand such

as alkyls can assist in stabilizing the bound arene when electron poor metals deplete electron density. On the other hand, electron withdrawing groups such as fluorides on the arene further destabilizes the arene promoting nucleophilic attack on the arene ligand (*see figure 1.2*).[15] Furthermore, ancillary ligands on the metal complex play a role in the reactivity of the arene ligand. Strong π-acceptor ligands at positions *trans* to carbons on the arene weaken the metal-carbon bonds of the arene. The phenomenon may be observed through different M-$C_{arene}$ bond lengths found in the molecular structures of the complexes.

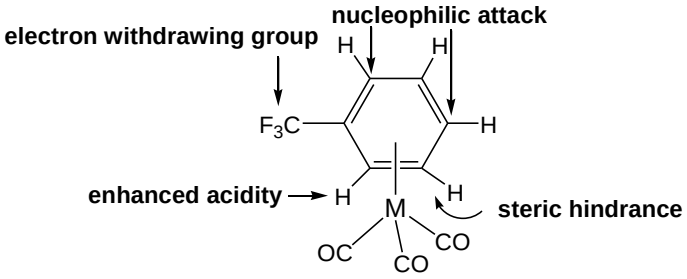


*Figure 1.2: Illustration of influence of substituents on the arene ligand.*[18]

Metal arene complexes were developed by the pioneering work of Pauson and Kealy[19] in 1951 when the two accidentally discovered ferrocene in an attempt to synthesize fulvalene ($C_{10}H_8$). Metal arene chemistry was further explored by Fischer and Hafner in 1955 on their work of developing metal arenes complexes with $\eta^6$-ligands, such as bis(benzene)chromium(0). Jellinek[20] reported the crystal structure of bis(benzene) chromium(0) at room temperature relative to the data reported by Weiss and Fischer. In 1979 Muetterties and co-workers[21] studied the arene exchange stability of transition metal complexes with $\eta^2$, $\eta^4$ and $\eta^6$ ligands. The group discovered that metal arene complexes with $\eta^6$ coordination required higher temperatures to replace the arene compared to $\eta^4$- and $\eta^2$-metal arene complexes, which required less energy to break bonds. The chemistry of metal arene complexes play an important role in the field of catalysis.[22] The arene ligands stabilize metal centres with high oxidation states and contribute to selectivity depending on the substituents and the ancillary ligands.

Arenes play an important role in bioinorganic chemistry as agents that effect cellular uptake of metal complexes.[23] The presence of arenes on the metal complex provides the hydrophobicity which is important for the passage of the metal complex across cell

membranes.[24] The study of cellular uptake of osmium arene (arene = *p*-cymene, biphenyl) complexes revealed that the *p*-cymene complexes are taken up by the cell 2-3 times more than the biphenyl complexes and cisplatin. In addition, complexes with biphenyl as an arene ligand were found to have a non-covalent interaction with the DNA.[25] Therefore, the arenes assist in increasing the cytotoxicity of the metal complex by intercalating the DNA structure causing distortions.[26,27]

Habtemariam and co-workers[28] investigated the effect of arene ligands on the anticancer activity of some ruthenium complexes (*see chart 1.2*). The group discovered that the cytotoxicity of arene complexes was depended on the size of the arene ligand. The more fused rings in the arene ligand the greater the potency, with the order: cyclophane << tetralin < indan, dibenzosuberane < dihydroanthracene, fluorene < 5,6-dihydrophenanthrene < tetrahydroanthracene. This trend is consistent with the study reported in 2002 by Aird and co-workers[27] where they observed that tetrahydroanthracene complexes are more cytotoxic than the dihydroanthracene complexes > biphenyl complexes > *p*-cymene complexes > benzene complexes.

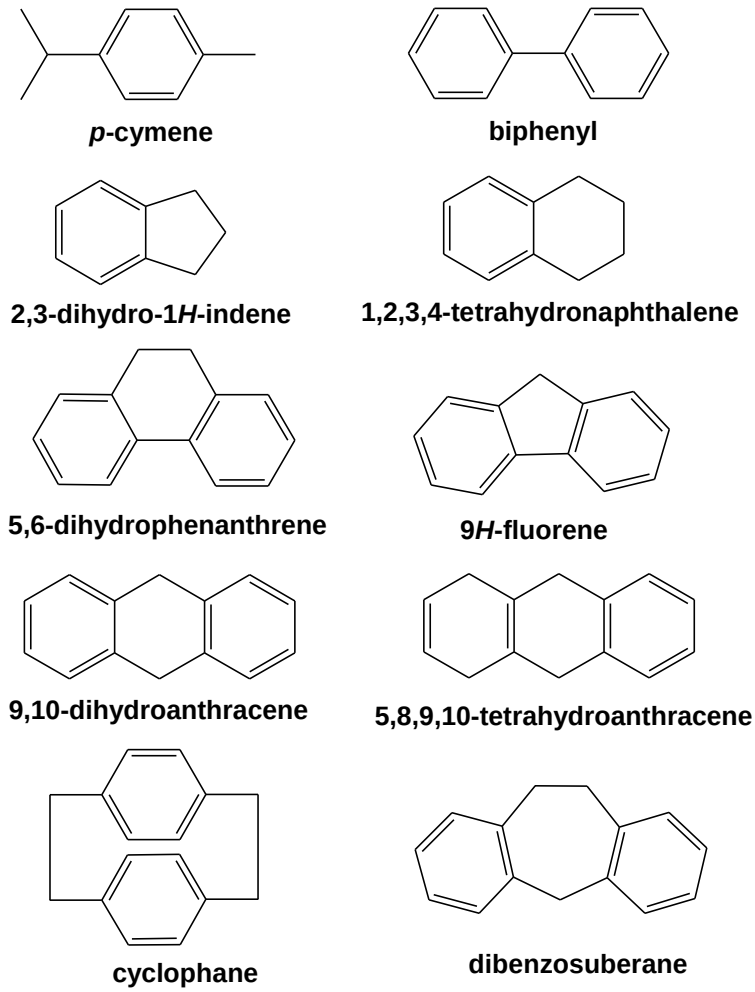


*Chart 1.2: Structures of arene ligands investigated for their influences on the cytotoxicity in cancer cell lines.*[27,28]

## 1.3 Ruthenium arene complexes

The chemistry of ruthenium arene complexes has been extensively studied in bioorganometallic chemistry and catalysis. There are a number of reports of ruthenium complexes with different arene ligands as well as different modes of arene coordination. In 1972 Zelonka and Baird[22] reported the synthesis of the first ruthenium arene complexes. Bennett and Smith[29] in 1974 isolated the ruthenium arene dimer with $\mu^2$-chlorido ligands by dehydrogenation of cyclohexa-1,3-diene/cyclohexa-1,4-diene with ruthenium(III) trichloride in ethanol solution. Robertson and Stephenson[30] reported stable $\eta^5$-cyclohexadienyl complexes of ruthenium in 1977. Two groups of researchers reported neutral ruthenium $\eta^6$-arene complexes $[Ru(C_6H_6)Cl_2L]$ (L = $C_5H_5N$, $Me_2SO$, $PR_3$), negatively charged

$Cs[Ru(C_6H_6)Cl_3]$ and the cationic complex with $\mu^3$-chlorido ligands $[Ru_2(C_6H_6)_2(\mu^3\text{-}Cl_3)]PF_6$ in 1978.[29,31] In 1979 Bennett and Matheson[32] reported the preparation of bis-arene ruthenium cationic complexes with varied arenes. Suravajjala and co-workers[33] in 1993 reported the synthesis of the dicationic bis($\eta^6$-*p*-cymene) complex $[Ru(\eta^6\text{-}p\text{-cymene})_2](BF_4)_2$ from refluxing the $\mu^2$-chlorido ruthenium dimer $[Ru(\eta^6\text{-}p\text{-cymene})Cl_2]_2$ with $AgBF_4$ in acetone and then further refluxing the intermediate in trifluoroacetic acid and excess *p*-isopropyltoluene.

The success of Cisplatin and second-generation platinum complexes as well as subsequent limitations led to the investigation of ruthenium complexes as future pharmaceutical agents. In 2001 Morris and co-workers[34] reported ruthenium arene complexes which inhibit the *in vitro* growth of human ovarian cancer cells. In 2008 Bugarcic and co-workers[24] reported ruthenium complexes with terphenyl arenes which showed different cytotoxicity, cell uptake and DNA binding properties depending on the *ortho*-, *meta*- and *para*- substituents of the two phenyl groups. The *para*-terphenyl complex was reported to have a "piano-stool geometry", determined from X-ray crystallography, and the potency of this complex was reported to be similar to that of Cisplatin.

### 1.4 Osmium arene complexes

In contrast, osmium arene chemistry has received less attention compared to the ruthenium analogue. This may be a consequence of the inertness of osmium complexes because of its low spin $5d^n$ configuration. Furthermore, the toxicity of osmium tetroxide as a starting material in the past has contributed to the difficulty in preparation of osmium complexes.[35] In 1984 Bandy and co-workers[36] reported the preparation of bis(benzene) osmium complexes from co-condensation of osmium atoms with benzene. In 1990, Kiel and co-workers[37] reported the first hexamethylbenzene osmium complex when they investigated intermolecular C−H activations. In 1994 Gross and co-workers[38] reported a new synthetic route for $[Os(C_5Me_5)_2Br_4]$ as a starting material for the synthesis of osmium pentamethylcyclopentadienyl complexes with the aim of increasing interest in osmium chemistry. Field and co-workers[39] reported the synthesis and characterisation of $[Os(\eta^5\text{-}C_5Ph_5)(CO)_2Br]$ from the reaction of osmium carbonyl cluster $[Os_3(CO)_{12}]$ with pentaphenylcyclopentadienylbromide and 1-chlorobenzene. In 2012, Albertin and co-workers[40] reported the osmium cymene complexes with $\eta^2$-alkene ligands.

Recently, osmium arene complexes with some anticancer activities have been reported. Kostrhunova and co-workers[25] investigated DNA interactions of mononuclear osmium arene complexes. The group discovered that the osmium complex with a biphenyl arene ligand is more cytotoxic towards cancer cells relative to the analogous *p*-cymene osmium complex. In 2010 van Rijt and co-workers[41] reported the anticancer study of osmium complexes with four different $\eta^6$-arene ligands (benzene, *p*-cymene, biphenyl and tetrahydroanthracene). In their study, the group revealed that biphenyl osmium complexes are easily taken up by cells. In addition, the biphenyl osmium complexes exhibit potency equivalent to the tetrahydroanthracene, however, better than the *p*-cymene complexes followed by the benzene complexes. In 2014 van Rijt and co-workers[42] reported osmium arene complexes with higher anticancer activity compared to the ruthenium analogues. The osmium complexes were found to accumulate to higher concentrations in cell membranes resulting in disruption of the mitochondrial membranes as a result encourages cell death. Bergamo and co-workers[43] reported the anticancer activity of osmium biphenyl complex which is isostructural with the ruthenium analogue. The osmium biphenyl complex was found to be 6 times more potent than the ruthenium analogue.

### 1.5 Osmium versus ruthenium complexes

Ruthenium is a 4d transition metal whereas osmium is a heavier 5d congener. Ruthenium complexes are found to exhibit faster ligand exchange rates relative to the isostructrural osmium complexes.[44] In addition, ruthenium arene complexes hydrolyse faster than the osmium arene analogues.[45] Ruthenium complexes were found to be 40 times more reactive than the osmium analogues in anticancer studies.[46] The inertness of osmium complexes is an advantage in anticancer activity, because the osmium complexes may reach the target with all ligands still coordinated to the osmium centre. Some osmium complexes were found to exhibit higher anticancer activities compared to the ruthenium analogue.[43] Therefore, the hypothesis is that osmium complexes may offer greater anticancer activity based on enhanced stability and slow ligand exchange rates.

### 1.6 Chelating and monodentate ligands

Chelating ligands are able to bond to the central metal through two or more donor atoms. These chelate ligands can be classified as bidentate, tridentate, tetradentate or more depending on the availability of electron-pair donor atoms on the chelate ligands. Chelate ligands are known to have very interesting properties once they are bounded to the metal centre; such properties include the chelate effect, which brings stability to the metal complex by forming metallacyclic rings. Chelate rings have different stability depending on the ring size. Three- to seven-membered chelate rings are well known and even larger chelate rings are known. The most common and stable chelate ring is the five-membered ring because of less sterically hindered bond angles, which are favourable for metal ions with larger radii resulting in no ring strains.[47] The six-membered chelate rings are found to be reasonably stable if their formation results in electron delocalization.[48]

The delocalization of electrons in the chelate ring is possible, and can contribute to the stability of the complex. Strong π-acceptor ligands can accept π-electrons from the electron rich metal atom to stabilize the whole metal complex depending on the type of substituents on the ligand system. Three-, four-, seven-membered and larger chelate rings are less common because of the resulting distortions of bond angles and unfavourable steric interactions.

Chelate ligands also have the ability to bridge two metal centres which may give stable binuclear complex depending on the type of ligand systems. Diphosphine ligands may also bridge two metal centres, resulting in a flexible binuclear complex as a consequence of elongated alkyl chain length.[49] Oxalates are known to bridge two metal centres resulting in two five-membered chelate rings on the binuclear complexes.

Generally, chelate ligands have played important roles in the chemistry of catalysis, removal of toxic metals from the environment as well as human/animal biological systems and continue to play a key role in the development of metallopharmaceutical agents. Chelated diphosphine complexes of Ag(I) have shown some antitumour activity in *in vitro* studies as well as animal trials.[50] In 1990 Berners-Price and co-workers[51] reported the cytotoxicity and antitumour activity of gold(I) chelated with diphosphine ligands.

The titanium-based complex cis[$(EtO)_2(bzac)_2Ti$] (where bzac = 1-phenylbutane-1,3-diketonate) is reported to undergo clinical trials against colon cancer in animal models.[13] The

O,O′-chelating ligands are found to bring stability to the metal complex as well as electron delocalization in the resulting chelate rings.[48] The chelate effect of diketones can also be observed in the anticancer studies of Carboplatin and Oxaliplatin[52] which are in clinical use against Cisplatin resistant tumours. In 2004 Thompson and co-workers[53] reported the effect of bis(maltolato)oxovanadium(IV) on type 2 diabetes in both *in vivo* and *in vitro* testing. Habtemariam and co-workers[28] reported a ruthenium arene complex with an O,O′ chelating ligand [Ru($\eta^6$-*p*-cymene)(PhCOCHCOPh)Cl] which was found to be highly potent with an $IC_{50}$ value of 11 μM. Turel and co-workers[54] studied the ruthenium cymene complex with ofloxacin ($C_{18}H_{20}FN_3O_4$). This ligand chelated the ruthenium metal through the oxygen atoms and the complex was found to interact with DNA in solution.

Monodentate ligands also play an important role in coordination chemistry. The phosphine ligands ($PR_3$) are known as good σ-donor as well as good π-accepter depending on the R substituents (where R = alkyl or aryl). The $PPh_3$ ligand is one of the most studied among monodentate phosphine ligands with almost all transition metals. In anticancer studies, the $PPh_3$ ligand was found to bring stability on the ruthenium complex [Ru($\eta^6$-*p*-cymene)Cl(PTA)($PPh_3$)]$BF_4$ consequently enhancing the anticancer activity of the ruthenium complex.[55]

### 1.7 Aims and Objectives of the study

The aim of this study was to synthesize osmium-cymene complexes with chelating O,O′- and P,P′- ligands as well as monodentate N- and P-donor ligands. Characterize the complexes using spectroscopic techniques (NMR, IR and Raman), elemental analysis, thermogravimetric analysis (TGA), conductivity studies and single crystal X-ray diffraction. The structure-activity relationship of the complexes against a range of cancer cells was to be investigated. The main objectives of this study were:

- To synthesize and characterize osmium-cymene complexes with O,O′ and P,P′ chelating ligands as well as monodentate N- and P-donor ligands.
- To evaluate the synthesized osmium-cymene complexes on the *in vitro* anticancer activities.
- To establish structure reactivity patterns on the anticancer activities of osmium-cymene complexes.

## 1.8 References


(1) Fraga, C. G. *Mol. Aspects Med.* **2005**, *26*, 235.

(2) Siddik, Z. H. *Oncogene* **2003**, *22*, 7265.

(3) Berners-Price, S. J.; Sadler, P. J. *Coord. Chem. Rev.* **1996**, *151*, 1.

(4) Berger, M. M.; Binnert, C.; Chiolero, R. L.; Taylor, W.; Raffoul, W.; Cayeux, M.-C.; Benathan, M.; Shenkin, A.; Tappy, L. *Am. J. Clin. Nutr.* **2007**, *85*, 1301.

(5) Stucki, P.; Perez, M.-H.; Cotting, J.; Shenkin, A.; Berger, M. M. *Crit. Care* **2010**, *14*, 1.

(6) Jaouen, G.; Beck, W.; McGlinchey, M. J. In *Bioorganometallics: Biomolecules, Labeling, Medicine.*; G., J., Ed.; 2006 Wiley-VCH Verlag GmbH & Co. KGaA: Weinheim, 2006, p 1.

(7) Kopf-Maier, P. *Eur. J. Clin. Pharmacol.* **1994**, *47*, 1.

(8) Keogan, D. M.; Griffith, D. M. *Molecules* **2014**, *19*, 15258.

(9) Allardyce, C. S.; Dyson, P. J. *Platin. Met. Rev.* **2001**, *45*, 62.

(10) Evangelou, A. M. *Crit. Rev. Oncol. Hematol.* **2002**, *42*, 249.

(11) Mukherjee, B.; Patra, B.; Mahapatra, S.; Banerjee, P.; Tiwari, A.; Chatterjee, M. *Toxicol. Lett.* **2004**, *150*, 135.

(12) Hernandez, R.; Mendez, J.; Lamboy, J.; Torres, M.; Roman, F. R.; Meledez, E. *Toxicol. In Vitro* **2011**, *24*, 1.

(13) Melendez, E. *Crit. Rev. Oncol. Hematol.* **2002**, *42*, 309.

(14) Bandarra, D.; Lopes, M.; Lopes, T.; Almeida, J.; Saraiva, M. S.; Vasconcellos-Dias, M.; Nunes, C. D.; Felix, V.; Brandao, P.; Vaz, P. D.; Meireles, M.; Calhorda, M. J. *J. Inorg. Biochem.* **2010**, *104*, 1171.

(15) Le Magueres, P.; Lindeman, S. V.; Kochi, J. K. *Organomet.* **2001**, *20*, 115.

(16) Fery-Forgues, S.; Delavaux-Nicot, B. *J. Photochem. Photobiol.:A Chem.* **2000**, *132* 137

(17) Egger, A. E.; Hartinger, C. G.; Renfrew, A. K.; Dyson, P. J. *J. Biol. Inorg. Chem.* **2010**, *15*, 919.

(18) Abd-El-Aziz , A. S.; Bernardin, S. *Coord. Chem. Rev.* **2000**, *203* 219.

(19) Werner, H. *Angew. Chem. Int. Ed.* **2012**, *51*, 6052.

(20) Jellinek, F. *J. Organomet. Chem.* **1963**, *1*, 43.

(21) Muetterties, E. L.; Bleeke, J. R.; Sievert, A. C. *J. Organomet. Chem.* **1979**, *178*, 197.

(22) Zelonka, R. A.; Baird, M. C. *Can. J. Chem.* **1972**, *50*, 3063.

(23) Schubert, U.; Werner, R.; Zinner, L.; H., W. *J. Organomet. Chem.* **1983**, *253*, 363.

(24) Bugarcic, T.; Novakova, O.; Halamikova, A.; Zerzankova, L.; Vrana, O.; Kasparkova, J.; Habtemariam, A.; Parsons, S.; Sadler, P. J.; Brabec, V. *J. Med. Chem.* **2008**, *51*, 5310.

(25) Kostrhunova, H.; Florian, J.; Novakova, O.; Peacock, A. F. A.; Sadler, P. J.; Brabec, V. *J. Med. Chem.* **2008**, *51*, 3635.

(26) Hanif, M.; Meier, S. M.; Nazarov, A. A.; Risse, J.; Legin, A.; Casini, A.; Jakupec, M. A.; Keppler, B. K.; Hartinger, C. G. *Inorg. Chem.* **2013**, *1*, 1.

(27) Aird, R. E.; Cummings, J.; Ritchie, A. A.; Muir, M.; Morries, R. E.; Chen, H.; Salder, P. J.; Jodrell, D. I. *Br. J. Cancer* **2002**, *86*, 1652.

(28) Habtemariam, A.; Melchart, M.; Fernandez, R.; Parsons, S.; Oswald, I. D. H.; Parkin, A.; Fabbiani, F. P. A.; Davidson, J. E.; Dawson, A.; Aird, R. E.; Jodrell, D. I.; Sadler, P. J. *J. Med. Chem.* **2006**, *49*, 6858.

(29) Bennett, M. A.; Smith, A. K. *J.C.S. Dalton* **1974**, *3*, 1236.

(30) Robertson, D. R.; Stephenson, T. A. *J. Organomet. Chem.* **1977**, *142*, 31.

(31) Robertson, D. R.; Stephenson, T. A.; Arthur, T. *J. Organomet. Chem.* **1978**, *162*, 121.

(32) Bennett, M. A.; Matheson, T. W. *J. Organomet. Chem.* **1979**, *175*, 87.

(33) Suravajjala, S.; Polam, J. R.; Porter, L. C. *J. Organomet. Chem.* **1993**, *461*, 201.

(34) Morris, R. E.; Aird, R. E.; Murdoch, P. d. S.; Chen, H.; Cummings, J.; Hughes, N. D.; Parsons, S.; Parkin, A.; Boyd, G.; Jodrell, D. I.; Sadler, P. J. *J. Med. Chem.* **2001**, *44*, 3616.

(35) Peacock, A. F. A.; Sadler, P. J. *Chem. Asian J.* **2008**, *3*, 1890.

(36) Bandy, J. A.; Green, M. L. H.; O'Hare, D.; Prout, K. *J. Chem. Soc., Chem. Commun.* **1984**, 1402.

(37) Kiel, W. A.; Ball, R. G.; Graham, W. A. G. *J. Organomet. Chem.* **1990**, *383*, 481.

(38) Gross, C. L.; Wilson, S. R.; Girolami, G. S. *J. Am. Chem. Soc.* **1994**, *116*, 10294.

(39) Field, L. D.; Hambley, T. W.; Humphrey, P. A.; Masters, A. F.; Turner, P. *Polyhedron* **1998**, *17*, 2587.

(40) Albertin, G.; Albinati, A.; Antoniutti, S.; Bortoluzzi, M.; Rizzato, S. *J. Organomet. Chem.* **2012**, *702*, 45.

(41) van Rijt, S. H.; Mukherjee, A.; Pizarro, A. M.; Sadler, P. J. *J. Med. Chem.* **2010**, *53*, 840.

(42) van Rijt, S. H.; Romero-Canelon, I.; Fu, Y.; Shnyder, S. D.; Sadler, P. J. *Metallomics* **2014**, *6*, 1014.

(43) Bergamo, A.; Masi, A.; Peacock, A. F. A.; Habtemariam, A.; Sadler, P. J.; Sava, G. *J. Inorg. Biochem.* **2010**, *104*, 79.

(44) Bruijnincx, P. C. A.; Sadler, P. J. *Adv. Inorg. Chem.* **2011**, *61*, 1.

(45) Hanif, M.; Nazarov, A. A.; Hartinger, C. G.; Kandioller, W.; Jakupec, M. A.; Arion, V. B.; Dyson, P. J.; Keppler, B. K. *Dalton Trans.* **2010**, *39*, 7345.

(46) Peacock, A. F. A.; Parsons, S.; Sadler, P. J. *J. Am. Chem. Soc.* **2007**, *129*, 3348.

(47) Hancock, R. D. *J. Chem. Educ.* **1992**, *69*, 615.

(48) Biro, L.; Farkas, E.; Buglyo, P. *Dalton Trans.* **2010**, *39*, 10272.

(49) Karami, K.; Hosseini-Kharat, M.; Sadeghi-Aliabadi, H.; Lipkowski, J.; Mirian, M. *Eur. J. Med. Chem.* **2014**, *73*, 8.

(50) Berners-Price, S. J.; Johnson, R. K.; Giovenella, A. J.; Faucettem, L. F.; Mirabelli, C. K.; Sadler, P. J. *J. Inorg. Biochem.* **1988**, *33*, 285.

(51) Berners-Price, S. J.; Girard, G. R.; Hill, D. T.; Sutton, B. M.; Jarrett, P. S.; Faucette, L. F.; Johnson, R. K.; Mirabelli, C. K.; Sadler, P. J. *J. Med. Chem.* **1990**, *33*, 1386.

(52) Stordal, B.; Pavlakis, N.; Davey, R. *Cancer Treat. Rev.* **2007**, *33*, 347.

(53) Thompson, K. H.; Chiles, J.; Yuen, V. G.; Tse, J.; McNeill, J. H.; Orvig, C. *J. Inorg. Biochem.* **2004**, *98*, 683.

(54) Turel, I.; Kljun, J.; Perdih, F.; Morozova, E.; Bakulev, V.; Kasyanenko, N.; Byl, J. A. W.; Osheroff, N. *Inorg. Chem.* **2010**, *49*, 10750.

(55) Scolaro, C.; Chaplin, A. B.; Hartinger, C. G.; Bergamo, A.; Cocchietto, M.; Keppler, B. K.; Sava, G.; Dyson, P. J. *Dalton Trans.* **2007**, 5065.

# CHAPTER 2

## SYNTHESIS AND CHARACTERIZATION OF O,O′-CHELATED OSMIUM CYMENE COMPLEXES

### 2.1 Background

Diketones are well known in the field of medicine as active ingredients or substrates in pharmaceuticals as well as industrial polymerisation catalysts.[1,2] These compounds have also been applied in environment remediation for the removal of heavy metals due to their chelating properties.[3] Studies have indicated that diketones preferably form neutral complexes with metal ions.[4,5] However, a number of mononuclear as well as the binuclear complexes bearing positive charges have been reported.[6] Another interesting property of diketones is their ability to bridge two, three and four metal complexes. The chemical and physical properties of diketones have been investigated with a range of transition metals.[6-14] Verma and co-workers[15] reported the synthesis of O,O′-chelated complexes of various transition metals.

There are many types of diketones and those that are common are; α-diketones and β-diketones, which differ in positions of the carbonyl carbons on the carbon framework. The carbonyl carbons on the α-diketone are adjacent to each other whereas the carbonyl carbons of the β-diketone are at a 1,3 position to each other. The α-diketone forms a five-membered chelate ring with metal centres which are considered to be the most stable chelate ring size favoured by metal centres with larger ionic radii.[16] In contrast, β-diketones form six-membered chelate rings, which are considered more stable than four- and seven-membered chelate rings but less stable than five-membered chelate rings.

The most common O,O′-chelating ligand in the α-diketone family is the oxalate ligand. The oxalate ligand has shown the ability to bridge two metal centres forming a bis-chelate.[6] This property has led to the oxalate ligand being incorporated to many transition metals such as copper,[10] chromium,[17] cobalt,[17] iron,[17] manganese,[18] molybdenum,[19] nickel,[20] platinum,[21] palladium[22] and ruthenium.[6,23] The magnetic properties of oxalate complexes of several

transition metals such as copper dimers,[24] chromium-manganese and iron-manganese binuclear species[25,26] have been reported.

The chelate effect of the oxalato ligand plays a vital role in the medicinal properties of Oxaliplatin.[27] Carboplatin and Oxaliplatin were introduced in 1999 and 2003 respectively as metal complexes bearing O,O′-bidentate ligands and are currently both in clinical use world-wide.[27] The chelate effect of the O,O′ ligands delay the hydrolysis of these platinum complexes relative to Cisplatin, consequently changing the overall biological reactivity of Carboplatin and Oxaliplatin towards cancer cells.

Complexes of α-diketones attached to π-systems such as tropolone are known. Ligands of this type have interesting chemical and electronic properties because of their electron rich π-systems. The tropolone has six π-electrons in the seven-membered carbon ring, which can act as an electron-donating group during complexation to form complexes with $\eta^7$ hapticity. The tropolone ligand can chelate an additional metal centre through the O atoms.[28] Since the oxygen on the carbonyl carbon is more reactive towards the metal ions than the π-bonds on the tropolone ring, the chelated O,O′ complex can be isolated. Melchart and co-workers[9] reported the synthesis of [Ru($\eta^6$-*p*-cymene)($\kappa^2$-O,O′-$C_7H_5O_2$)Cl] which is isostructural with complex **3** reported in this study. This group also studied the interaction of the ruthenium tropolonate complex with DNA bases. Their findings show that the ruthenium complex interacts with N1 of the guanine as well as N1 and N7 of the adenine DNA nucleobases.

In this chapter, the synthesis and characterization of osmium cymene complexes with oxalate and tropolone ligands will be discussed.

## 2.2 Preparation of O,O′-osmium cymene complexes

Complex **1(a)** was prepared by reacting the osmium dimer [Os($\eta^6$-*p*-cymene)$Br_2$]$_2$ with $Ag_2C_2O_4$ in $CH_2Cl_2$/$CH_3OH$ at room temperature. Further reaction of **1(a)** with $PPh_4Br$ in $CH_2Cl_2$ at room temperature for 30 minutes resulted in the formation of **1(b)**. Synthesis of complexes **2, 4** and the attempted synthesis of [{Os($\eta^6$-*p*-cymene)($PPh_3$)}$_2$ μ–$C_2O_4$)]($BF_4$)$_2$ were carried out by the method reported by Yan and co-workers[6] with some modifications. Complex **2** was prepared by reaction of Ag[Os($\eta^6$-*p*-cymene)Br($C_2O_4$)] **1(a)** and $PPh_3$ in $CH_2Cl_2$/$CH_3OH$ solution at 44 ºC. Complex **3** was prepared by reacting the osmium dimer

and sodium tropolonate ($NaC_7H_5O_2$) in $CH_2Cl_2/CH_3OH$ at room temperature. Complex **4** was prepared by the reaction of the osmium dimer with ammonium oxalate in $CH_2Cl_2/CH_3OH$. Complex **5** was prepared by the method reported by Clayton and co-workers[29] with some modifications. The osmium dimer and $PPh_3$ were stirred in $CH_2Cl_2$ at room temperature for an extended period. The attempted preparation of $[\{Os(\eta^6\text{-}p\text{-cymene})(PPh_3)\}_2\ \mu\text{–}C_2O_4)](BF_4)_2$ by reacting **4** and $PPh_3$ in $CH_2Cl_2$ at room temperature resulted in a mixture of two products (**2** and **5**). The two complexes in the mixture were identified by the NMR and IR data of the pure complexes **2** and **5** prepared separately. All the complexes reported in this chapter were synthesized under the conditions reported in *scheme 2.1*. The oxalate ligand in **1(a)**, **1(b)** and **2** contribute two electrons using the neutral electron counting method while in **4** it contributes three electrons because of the delocalised electrons on both five-membered chelate rings.

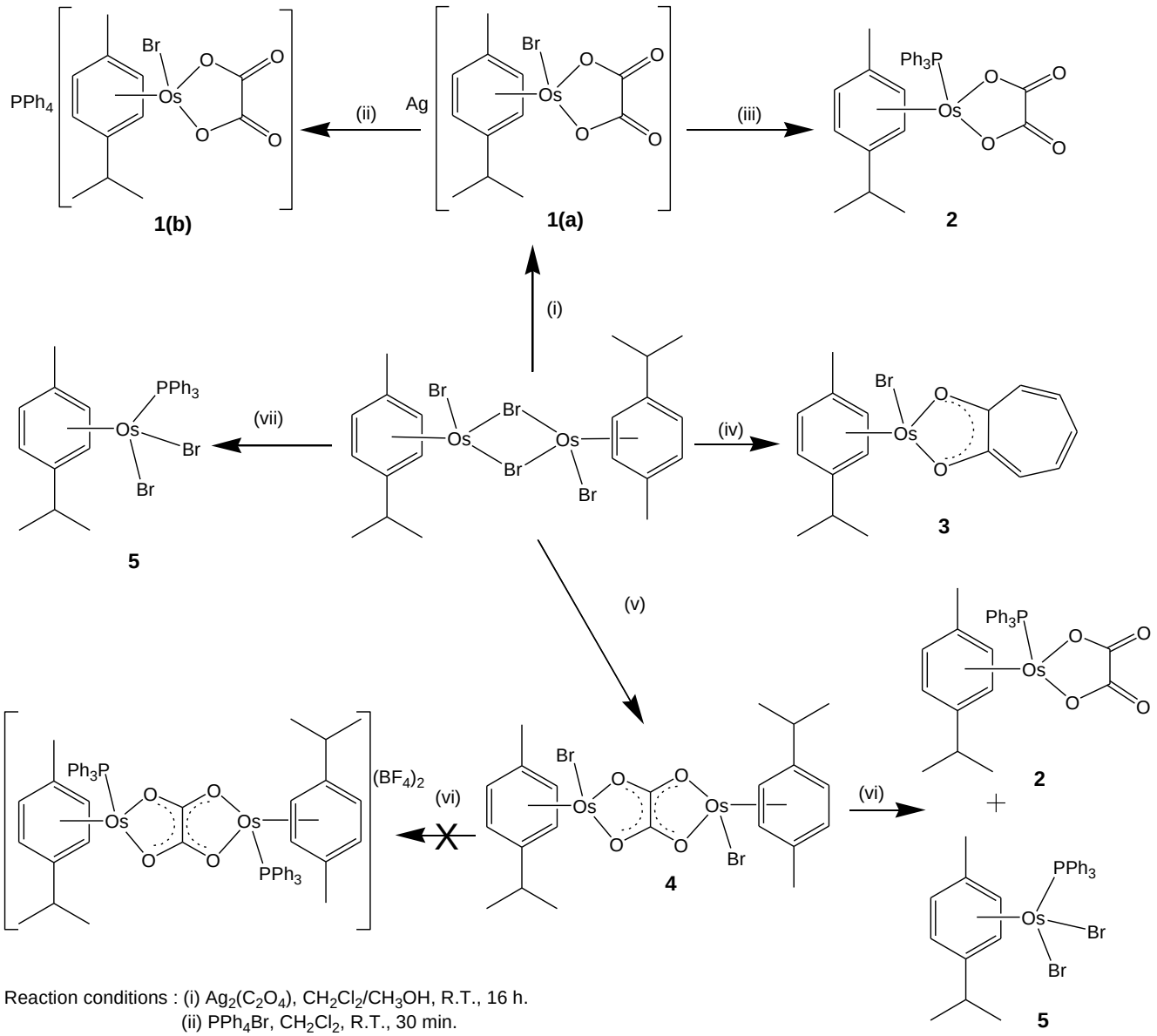


Reaction conditions : (i) $Ag_2(C_2O_4)$, $CH_2Cl_2/CH_3OH$, R.T., 16 h.
(ii) $PPh_4Br$, $CH_2Cl_2$, R.T., 30 min.
(iii) $PPh_3$, $CH_2Cl_2/CH_3OH$, 44 $^oC$, 16 h.
(iv) $NaC_7H_5O_2$, $CH_3OH$, R.T., 16 h.
(v) $(NH_4)_2C_2O_4.H_2O$, $CH_2Cl_2/CH_3OH$, R.T., 16 h.
(vi) $2PPh_3$, $NH_4BF_4$, $CH_2Cl_2$, R.T., 16 h.
(vii) $PPh_3$, $CH_2Cl_2$, R.T., 16 h.

**Scheme 2.1**

The reaction of the osmium dimer with excess $(NH_4)_2C_2O_4{\cdot}H_2O$ did not result in the formation of the mononuclear complex $NH_4[Os(\eta^6\text{-}p\text{-cymene})(C_2O_4)Br]$ (*see scheme 2.2*). However, the reaction with the $Ag_2C_2O_4$ did give the expected product. The failure to obtain the mononuclear complex $NH_4[Os(\eta^6\text{-}p\text{-cymene})(C_2O_4)Br]$ may be rationalized using the hard-soft-acid-base (HSAB) principle. The $NH_4^+$ ion is a hard acid and the anion complex $[Os(\eta^6\text{-}p\text{-cymene})(C_2O_4)Br]^-$ is a soft base, which may result in a poorly stable complex $NH_4[Os(\eta^6\text{-}p\text{-cymene})(C_2O_4)Br]$ which readily reverts to the formation of the neutral binuclear complex **4**. In addition, the $NH_4^+$ ion and the $Ag^+$ ion have different ionic radii,

which may cause noticeable differences in electrostatic interactions. Furthermore, the $NH_4^+$ ion depend entirely on the electrostatic forces whereas the $Ag^+$ ion has empty *s*-orbitals, which may contribute to the reactivity of this metal ion. Size selectivity due to large electrostatic interactions combined with hard/soft character of the cations played a role in the unsuccessful preparation of $NH_4[Os(\eta^6\text{-}p\text{-cymene})(C_2O_4)Br]$ and successful preparation of $Ag[Os(\eta^6\text{-}p\text{-cymene})(C_2O_4)Br]$.[30]

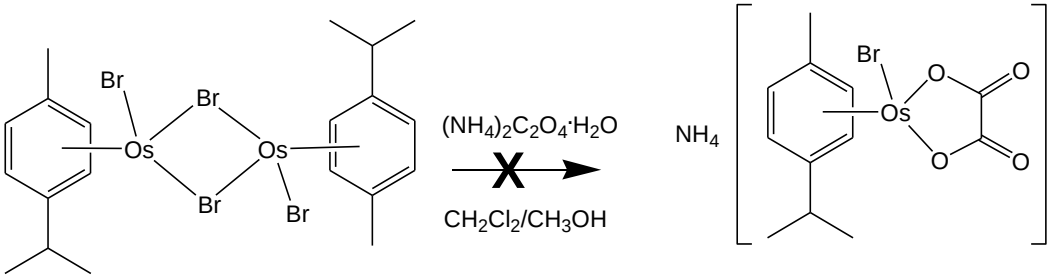


**Scheme 2.2**

Below is a proposed mechanism for the reaction of **4** with $PPh_3$. Two possible reaction pathways will be discussed (*see scheme 2.3*).

The interchange associative ($I_a$) mechanism was proposed to proceed via the following pathway. The first step involves the addition of the $PPh_3$ ligand to form an intermediate **(I)**. The $\eta^6$-cymene at one of the Os centres ($Os_A$) undergoes ring-slippage to an $\eta^4$-cymene to accommodate the $PPh_3$.[31] In this arrangement, the cymene ligand occupies two coordination sites instead of three. Elimination of the labile Br ligand proceeds fast ($S_N2$) which results in formation of the positively charged intermediate **(III)** with $PPh_3$ and Br ligands at the $Os_A$ and $Os_B$ centres respectively.

In contrast, for an interchange dissociative ($I_d$) mechanism the first step is proposed to involve the slow elimination of the Br ligand forming a five-coordinate complex on the $Os_A$ centre. The fast addition of the $PPh_3$ ligand forming the positively charged (located on $Os_A$ centre) asymmetrically substituted binuclear osmium complex with $PPh_3$ and Br ligands at different osmium centres.

The second step for both the interchange associative and dissociative mechanism is assumed the same (*see scheme 2.3*). Addition of the second $PPh_3$ ligand at $Os_B$ cleaves the $Os_B$-O bond

forming intermediate **(IV).** This happens because steric factors may not allow two $PPh_3$ bulky ligands on the $Os_A$ centre while the $Os_B$ centre is less sterically crowded. The steric effect of the $PPh_3$ ligand on $Os_A$ exerted on the $C_2O_4$ ligand and the bulkiness of the entering $PPh_3$ ligand favours the elimination of the $Os_B$-O bond before the entering of the $PPh_3$ ligand. Intermediate **(IV)** undergoes a second $Os_B$-O bond cleavage to form the neutral complex **2**. The Br ligand in the solution occupies the vacant site completing the coordination geometry of the osmium centre by forming the neutral complex **5**.

Since **4** is a low-spin octahedral complex, it is expected that the interchange dissociative mechanism will be favoured. Under similar reaction conditions, the ruthenium analogue $[\{Ru(\eta^6\text{-}p\text{-cymene})Cl\}_2\ (\mu\text{–}C_2O_4)]$ is reported to afford the $[\{Ru(\eta^6\text{-}p\text{-cymene})(PPh_3)\}_2\ \mu\text{–}C_2O_4)](CF_3SO_3)_2$ complex,[6] formed by substitution of the chloride ligands by $PPh_3$. The reason for the differences in reactivity of **4** compared to the ruthenium analogue may be due to the change in metal–ligand orbital overlap provided by the 5d metal orbitals.[32] The Br is a stronger ligand than chloride and the 5d osmium metal form the more stable complexes compared to the 4d ruthenium metal. In addition, the osmium complexes are found to react slowly compared to their ruthenium analogues, that is, Os−Br complex is found to be less labile than the Ru−Cl analogue.[33] Hence, the differences in electronic properties of **4** compared to the ruthenium analogue as well as the difference in electronegativity between the chlorido and bromido ligands are factors which could account for the observed differences in reactivity.

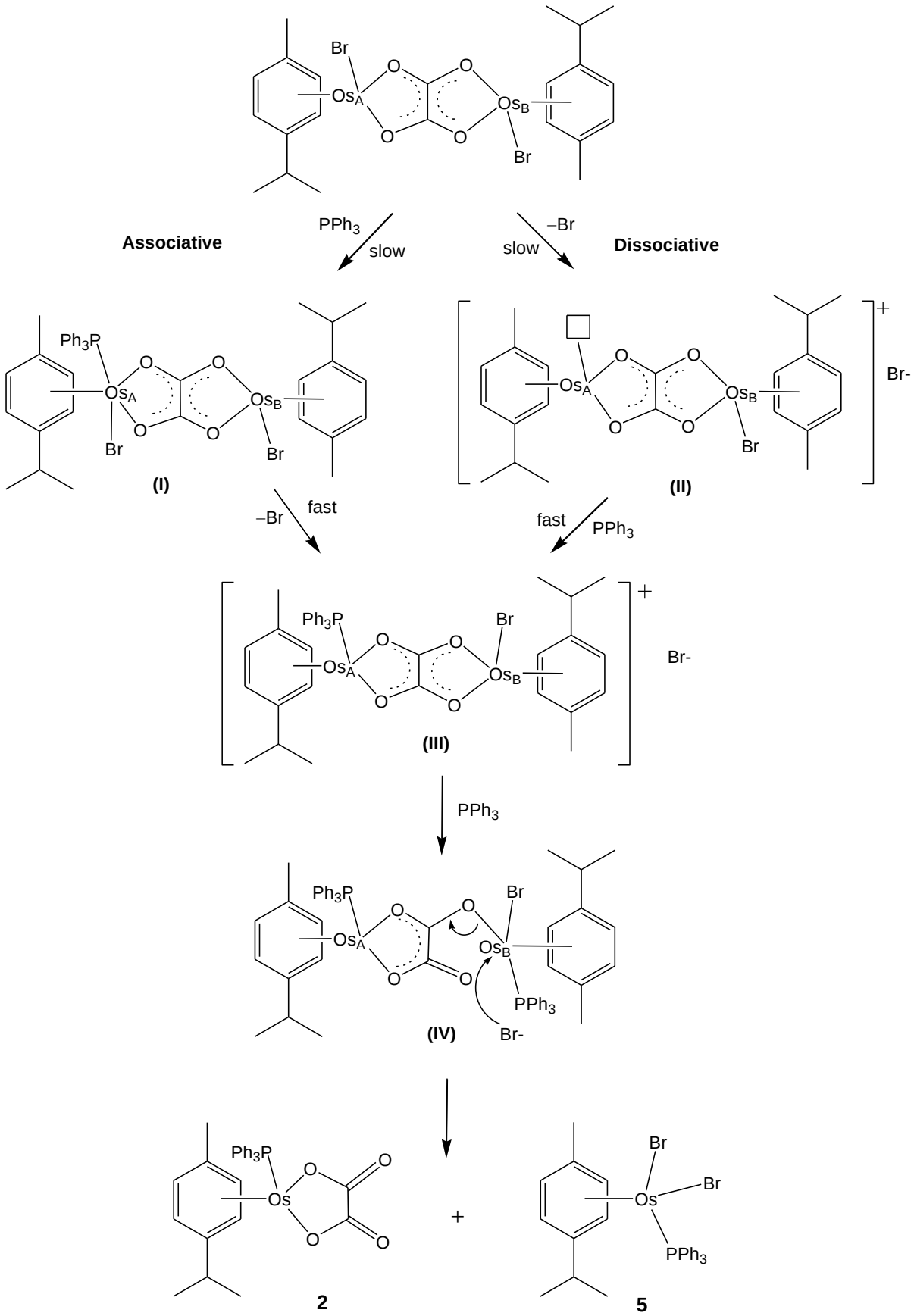
Br
OsA
OsB
O
Br
PPh3
slow
Associative
−Br
slow
Dissociative
Ph3P
Br
(I)
(II)
Br-
−Br
fast
fast
PPh3
(III)
Br-
PPh3
(IV)
Br-
Ph3P
Os
2
+
Br
Os
PPh3
5

**Scheme 2.3**

## 2.3 Results and Discussion

### 2.3.1 Nuclear Magnetic Resonance (NMR) Spectroscopy

#### 2.3.1.1 $^{1}$H NMR data


*Figure 2.1: The $^{1}$H NMR of (i) cymene ligand and (ii) tropolone ligand will be discussed with these assignments.*

The $^{1}$H NMR data for complexes **1(a)**, **1(b)**, **2**, **3** and **4** are reported in Table 2.1. The proton signals of $H_b$ and $H_c$ for **1(a)** showed peaks slightly shifted downfield compared to those of **1(b)**. This observation may be attributed to solvent effects because **1(a)** was only soluble in DMSO-$d_6$ whereas **1(b)** was soluble in $CDCl_3$ solvent. The two mononuclear complexes **1(a)** and **1(b)** are isostructural but differ with the cations. In addition, the slight difference in chemical shifts may be attributed to the change from the $Ag^+$ cation to the $PPh_4^+$ cation. The cation-π interaction was reported to have an influence on the NMR chemical shifts of complexes.[34,35] In this case, the $Ag^+$ cation may interact with the π-electrons of the cymene ligand to a larger extent than the $PPh_4^+$ cation, deshielding $H_b$ and $H_c$ protons as well as enhancing the acidity.

Complex **2** displayed $H_b$ and $H_c$ signals upfield relative to those of **1(a)** and **1(b)**. The upfield shift of **2** was due to $PPh_3$. The binuclear complex **4** displays similar $H_b$ and $H_c$ signals to that of **1(a)** whereas complex **1(b)** exhibits an upfield shift relative to **4**. Complex **3** shows the signals due to $H_b$ and $H_c$ downfield relative to complex **1(b)** and upfield relative to complexes **1(a)** and **4**. The results of complex **5** were found to be comparable to $^{1}$H NMR data in literature.[29]

*Table 2.1: $^{1}H$ NMR data of **1(a)**, **1(b)**, **2**, **3**, and **4**.*

| Assignment | **1(a)*** | | **1(b)** | | **2** | | **3** | | **4** | |
|---|---|---|---|---|---|---|---|---|---|---|
| | δ(ppm) | J(Hz) | δ(ppm) | J(Hz) | δ(ppm) | J(Hz) | δ(ppm) | J(Hz) | δ(ppm) | J(Hz) |
| $H_e$ (d) | 1.24 | 6.9 | 1.27 | 6.8 | 1.16 | 6.9 | 1.29 | 6.9 | 1.32 | 6.8 |
| $H_a$ (s) | 2.17 | - | 2.23 | - | 2.01 | - | 2.38 | - | 2.28 | - |
| $H_d$ (sept) | 2.67 | 6.8 | 2.80 | 6.9 | 2.47 | 6.8 | 2.76 | 6.9 | 2.77 | 6.8 |
| $H_b$ (d) | 6.09 | 6.4 | 5.64 | 5.9 | 5.29 | 5.4 | 5.78 | 5.5 | 5.97 | 5.9 |
| $H_c$ (d) | 6.22 | 5.9 | 5.91 | 5.4 | 5.51 | 5.9 | 6.00 | 5.8 | 6.21 | 5.9 |
| $H_h$ (t) | - | - | - | - | - | - | 6.80-6.87 | 8.8 | - | - |
| $H_f$ and $H_g$ (m) | - | - | - | - | - | - | 7.20-7.31 | - | - | - |
| m, 15H, Ph | - | - | - | - | 7.41-7.50 | - | - | - | - | - |
| m, 20H,Ph | - | - | 7.57-7.91 | - | - | - | - | - | - | - |

*Spectra were recorded in $CDCl_3$ except for **1(a)**, which was recorded in DMSO-$d_6$

### 2.3.1.2 $^{13}C$ NMR data

The $^{13}C$ NMR data for complexes **1(a)**, **1(b)**, **2**, **3** and **4** are reported in Table 2.2, which supports the $^{1}H$ NMR data. The influence of the O,O′- and P- ligand systems on the cymene ligand was observed. Complex **1(b)** showed the most downfield carbon shift with respect to the aromatic carbons of the cymene in comparison to **1(a)**. Regardless of the similarity with respect to the anionic osmium complex, the $Ag^+$ ion and $PPh_4^+$ ion have a unique electrostatic influence on the two complexes **1(a)** and **1(b)**. The cation-π interaction of the soft $Ag^+$ ion with the π-electrons of the cymene ligand may have contributed to the upfield shift in the $^{13}C$ signals of the cymene. In contrast, the $PPh_4^+$ ion of **1(b)** has four π-systems, which may have stronger π-π interactions with the π-electrons of the cymene, deshielding the cymene aromatic carbons.

Complex **2** displayed carbon signals due to $\eta^6$-$C_6H_4$ of the cymene upfield relative to **1(b)** and downfield relative to **1(a)**. This may be attributed to the influence of $PPh_3$ as a strong σ-donor as well as strong π-acceptor ligand. The P atom in complex **2** competes with the C atoms of the cymene for back-bonding electrons. The binuclear complex **4** displayed four signals due

to $\eta^6$-$C_6H_4$ carbons of the cymene ligand upfield relative to **1(a)**, **1(b)** and **2**. This shift was due to increased π-back bonding from Os to the $\eta^6$-$C_6H_4$ carbon atoms. Complex **3** displayed signals due to aromatic cymene carbons upfield relative to **1(a)**, **1(b)** and **2** but shifted downfield compared to **4**. The positions of these signals in complex **3** were attributed to the contribution of π-electrons from the tropolone ring.

The ancillary ligands of the osmium cymene complexes have an effect on the CO signals of the oxalate moeity. The CO signals were observed as singlets at 163.78 ppm for **1(a)**, 166.90 ppm for **1(b)**, 164.22 ppm for **2**, 185.85 ppm for **3** and 175.39 ppm for **4**. The CO signal of complex **1(a)** appears upfield relative to that of **1(b)** and **2**. The carbonyl shift of **1(b)** may be influenced by $PPh_4^+$ cation and the carbonyl shift of **2** may be influenced by the presence of $PPh_3$ ligand (*see table 2.2*). The cation-π interaction of the $PPh_4^+$ cation with the cymene may influence carbonyl shift on the NMR. Also, the solvent effect may be one factor that influenced the CO signals of **1(a)**, **1(b)** and **2**. Complex **4** shows the most downfield carbonyl signal than the mononuclear complexes **1(a)**, **1(b)** and **2**. This downfield shift was attributed to the oxalate ligand donating electrons to both osmium centres. Hence, the oxygen atoms pull electrons from the carbon atoms by induction resulting in the carbonyl carbons being deshielded. Complex **3** displayed a CO signal downfield compared to complexes **1(a)**, **1(b)**, **2**, **3** and **4** due to the presence of the tropolone ligand which has π-bonds in the ring. The NMR data for the CO signals of the mononuclear complexes suggest that the tropolonate ligand is a stronger σ-donor ligand compared to the oxalato ligand.

*Table 2.2: $^{13}C$ NMR data of **1(a)**, **1(b)**, **2**, **3** and **4**.*

| Assignment | **1(a)*** | **1(b)** | **2** | **3** | **4** |
|---|---|---|---|---|---|
| $\underline{C}H_3C_6H_4$ | 17.25 | 18.91 | 18.04 | 19.56 | 19.51 |
| $CH(\underline{C}H_3)_2$ | 22.34 | 23.01 | 22.70 | 23.00 | 22.94 |
| $\underline{C}H(CH_3)_2$ | 30.65 | 31.66 | 31.00 | 32.02 | 32.07 |
| $\eta^6$-$C_6H_4$ | 95.41, 90.77, 78.80, 77.46 | 117.82, 117.15, 71.76, 68.86 | 98.82, 88.39, 79.35, 79.10 | 91.00, 87.26, 71.76, 69.63 | 90.68, 86.64, 71.97, 69.75 |
| trop-3C | - | - | | 127.42, 127.23 | - |
| trop-C | - | - | | 138.07 | - |
| $C_{Aromatic}$ | - | 130.79-135.75 | 128.91-134.40 | - | - |
| $\underline{C}O$ | 163.78 | 166.90 | 164.22 | 185.85 | 175.39 |

*Spectra were recorded in $CDCl_3$ except for **1(a)** which was recorded in DMSO-$d_6$

trop = tropolonate ligand

2.3.1.3 Heteronuclear Single Quantum Correlation (HSQC) NMR

The Heteronuclear Single Quantum Correlation (HSQC) is a 2D NMR study of the correlation of $^1H$ with other nuclei such as $^{13}C$, $^{15}N$, $^{31}P$, $^{29}Si$ NMR that are observed as cross-peaks on a two-dimensional spectrum. The correlation of quaternary carbons is not possible due to the absence of C–H bonds. In this thesis, the experiments carried out involved proton-carbon ($^1H$–$^{13}C$) correlations and the magnetisation transfer between these nuclei allowed for the identification of protons bonded to different nuclei ($^{13}C$), assisting with assignment of $^1H$ and $^{13}C$ resonances.

Complex **3** has been characterised by 2D HSQC NMR. Data from this study suggests that the tropolone ligand becomes symmetrical upon coordination to the osmium centre. The free tropolone ligand is asymmetrical (*see figure 2.1(i)*). The singlet due to $H_a$ correlates with the carbon signal at 19.56 ppm ($\underline{C}H_3C_6H_4$). The doublet due to $H_e$ correlates with the carbon signal at 23.00 ppm ($CH(\underline{C}H_3)_2$) (*see figure 2.2*). The septet due to $H_d$ correlates with the carbon signal at 32.02 ppm ($\underline{C}H(CH_3)_2$). The $H_b$ protons on the cymene group were assigned as protons at *ortho* position to the methyl group while the $H_c$ protons were assigned at *meta* position to the methyl group on the cymene ligand. The two sets of doublets due to $H_b$ and $H_c$ correlates with the carbon signals at 69.63 and 71.76 ppm respectively. For the tropolonate ligand, the triplet due to $H_h$ correlates with the carbon signal at 127.42 ppm. The $H_g$ protons correlate with the carbon signal at 127.23 ppm. The $H_f$ protons correlate with the carbon

signal at 138.07 ppm (*see figure 2.2*). The HSQC spectrum allows for the unambiguous assignment of the aromatic cymene protons $H_b$ and $H_c$.

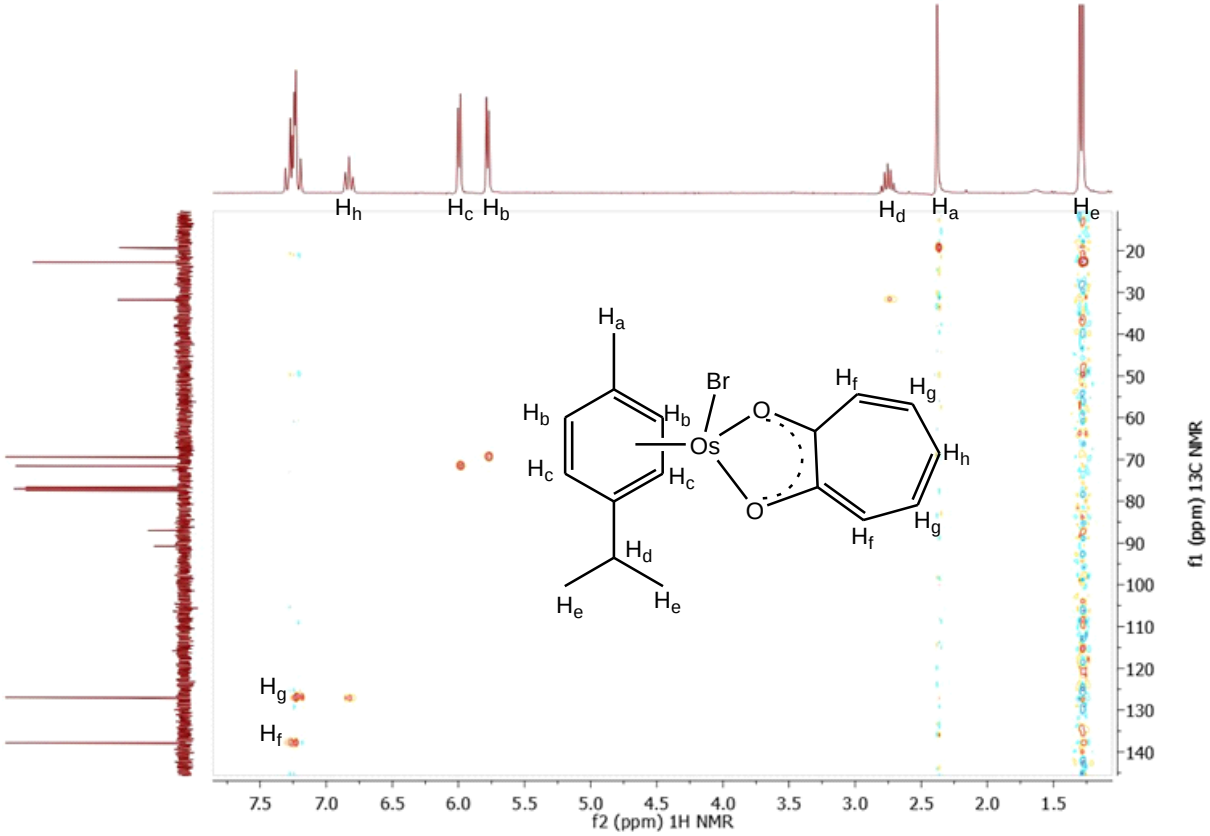


*Figure 2.2: The 2D HSQC spectra of **3** showing C–H correlation.*

2.3.1.4 $^{31}$P NMR data of **1(b)** and **2**

The $^{31}$P NMR data for complexes **1(b)** and **2** are reported below. The single P signal for complex **1(b)** due to the $PPh_4$ cation was observed at 24.06 ppm with two satellite peaks at 24.43 and 23.69 ppm. The P signal of the $PPh_4^+$ cation in **1(b)** is deshielded compared to the P signal of $PPh_4Br$ (23.09 ppm). The P chemical shift for complex **1(b)** was attributed to change in electrostatic interaction from the small Br anion to the larger osmium complex anion. The $^{31}$P spectrum of **2** showed a single signal at 1.78 ppm and satellite peaks at 1.90 and 1.64 ppm which may be due to spinning side bands with $^1J$= 53 Hz which is less than $^1J(^{187}Os\text{-}^{31}P)$ = 77 Hz observed for octahedral pentaosmium phosphinidene clusters.[36] A second set of satellite peaks at 2.54 and 1.02 ppm was assigned to $^{187}$Os coupling with $^1J(^{187}Os\text{-}^{31}P)$ = 309 Hz (*see figure 2.3*).

The two sets of satellites were attributed to the NMR active isotope of osmium which is $^{187}$Os (I = 1/2) with higher J-coupling constant and side spinning bands with lower J-coupling constant.[37] In solution, only satellite signals are expected for the less abundant isotope $^{187}$Os, as the more abundant $^{189}$Os isotope has extremely efficient quadrupolar relaxation in solution. However, in solid-state $^{31}$P NMR, satellite peaks for $^{189}$Os isotope are also observed because of longer relaxation times.[38,39]

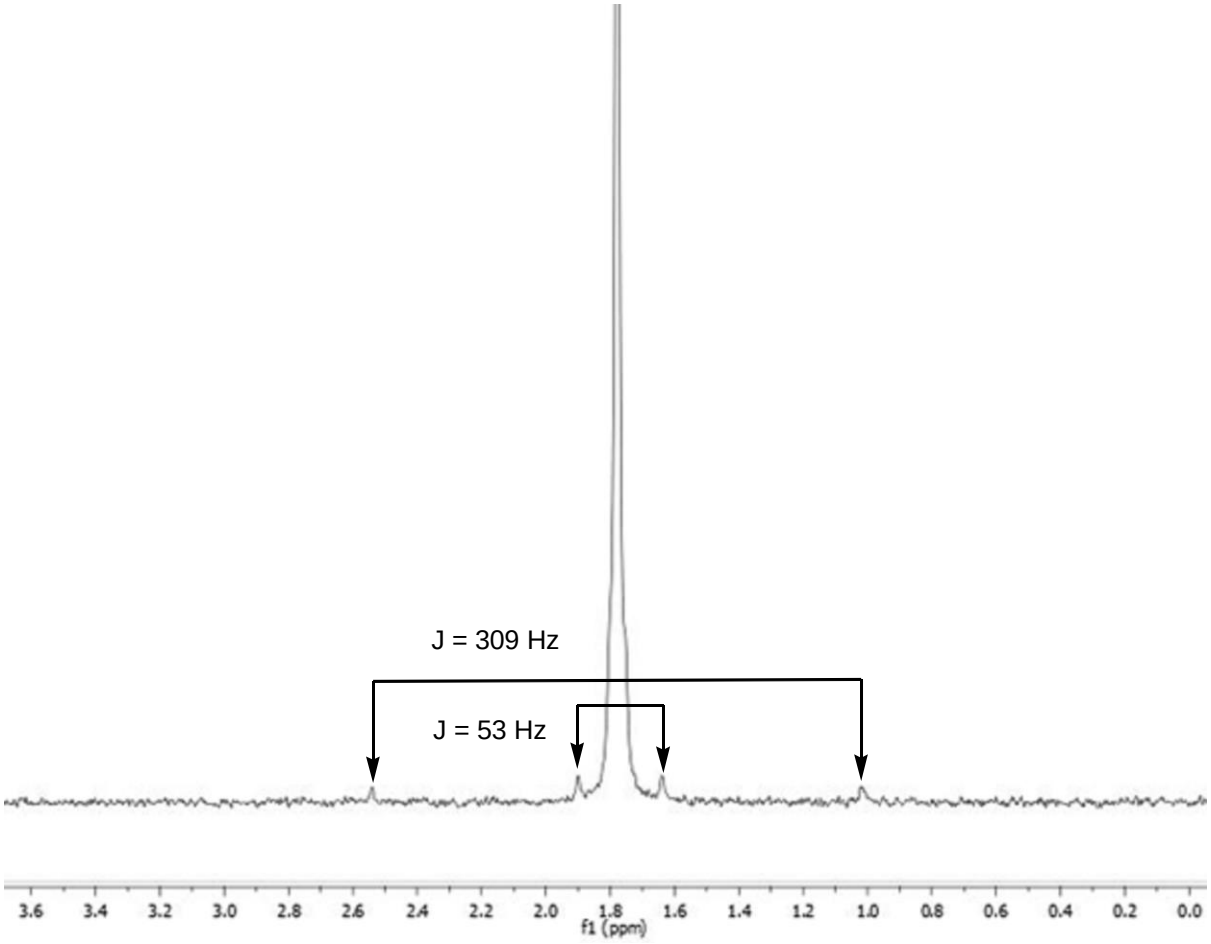


*Figure 2.3: $^{31}$P NMR spectrum of **2** showing two sets of satellite peaks.*

## 2.3.2 Infra-Red (IR) Spectroscopy

Studies of carboxylate groups have shown that symmetric and asymmetric stretching bands of oxalate are found in the ranges 1400-1500 cm$^{-1}$ and 1500-1700 cm$^{-1}$ respectively.[40] The infra-red spectrum of **1(a)** showed two very strong stretching bands with shoulder peaks at 1688vs/1671sh/1640sh cm$^{-1}$ and at 1595vs/1574sh cm$^{-1}$ which were attributed to $\nu_{asym(OCO)}$

bands (*see figure 2.4*).[41] A very weak band at 1457 $cm^{-1}$ and a medium band at 1422 $cm^{-1}$ were assigned to $\nu_{sym(OCO)} + \nu_{(CC)}$. At 1265 $cm^{-1}$ another medium stretching band was assigned to $\nu_{sym(OCO)}$. The very weak and weak stretching bands at 911 $cm^{-1}$ and 876 $cm^{-1}$ respectively were assigned to $\nu_{(CC)}$. The strong stretching band at 794 $cm^{-1}$ was assigned to $\nu_{(CC)} + \delta_{(OCO)}$.[42] Surprisingly, complex **1(b)** showed three strong stretching bands at 1695 $cm^{-1}$, 1674 $cm^{-1}$ and 1653 $cm^{-1}$ attributed to $\nu_{asym(OCO)}$. The two stretching bands at 1483 $cm^{-1}$ weak and 1436 $cm^{-1}$ medium were assigned to $\nu_{sym(OCO)} + \nu_{(CC)}$. At 1378 $cm^{-1}$ and 1371 $cm^{-1}$ a strong peak and weak peak were observed respectively, and were assigned to $\nu_{sym(OCO)}$. The two very weak stretching bands at 910 $cm^{-1}$ and 886 $cm^{-1}$ were assigned to $\nu_{(CC)}$. A strong band at 787 $cm^{-1}$ was assigned to $\nu_{(CC)} + \delta_{(OCO)}$.[42] The mononuclear complex **2** also displayed three stretching bands at 1706 $cm^{-1}$, 1693 $cm^{-1}$ and 1669 $cm^{-1}$ attributed to $\nu_{asym(OCO)}$. A very weak band and a weak band were observed at 1482 $cm^{-1}$ and 1433 $cm^{-1}$ respectively attributed to $\nu_{sym(OCO)} + \nu_{(CC)}$. A very strong broad stretching band with three splitting was observed at 1371/1363/1356 $cm^{-1}$ was assigned to $\nu_{sym(OCO)}$. A very weak band at 904 $cm^{-1}$ and a weak band at 875 $cm^{-1}$ was assigned to $\nu_{(CC)}$. The strong stretching band at 786 $cm^{-1}$ was assigned to $\nu_{(CC)} + \delta_{(OCO)}$.[42]

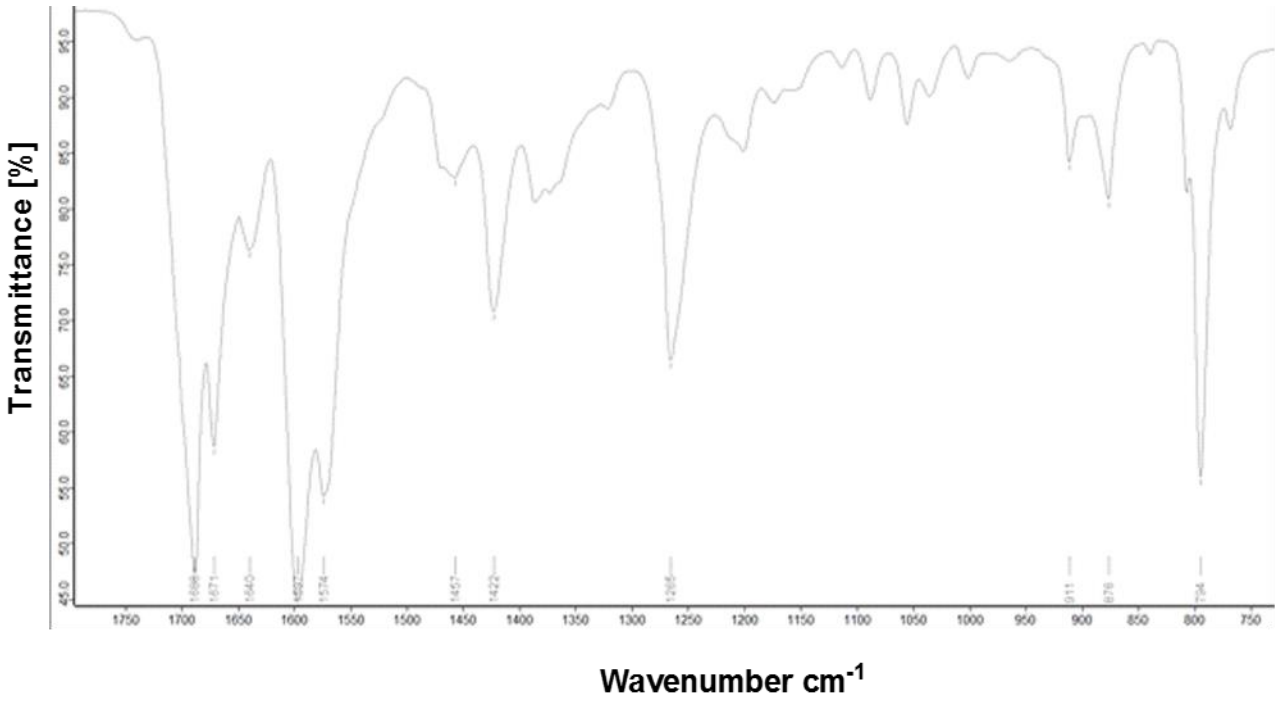


*Figure 2.4: Infra-red spectrum of complex **1(a)**.*

Complex **3** showed a single strong stretching band at 1588 $cm^{-1}$ attributed to $\nu_{(CC)}$ (*see figure 2.5*). The second strong peak at 1512 $cm^{-1}$ was attributed to $\nu_{(CO)} + \nu_{(CC)}$. The strong peak with a shoulder was attributed to $\nu_{(CC)}$ at 1424 $cm^{-1}$ and $\delta_{(C\text{-}H)}$ at 1407 $cm^{-1}$. The broad peak was attributed to $\nu_{(CO)}$ at 1353/1341 $cm^{-1}$.[43] Complex **4** showed the characteristics bands of a bridging oxalate ligand $\nu_{asym(OCO)}$ at 1611 $cm^{-1}$ which is a very strong band, $\nu_{sym(OCO)} + \nu_{(CC)}$ at 1468 $cm^{-1}$ which is a weak band and $\nu_{sym(OCO)}$ at 1387/1341 $cm^{-1}$ which is also a very strong band. A weak band at 881 $cm^{-1}$ with a shoulder at 891 $cm^{-1}$ were attributed to $\nu_{(CC)}$ and another weak band assigned as $\nu_{(CC)} + \delta_{(OCO)}$ at 803/796 $cm^{-1}$.[19,24,41,42,44] The delocalised electrons in the chelate rings of the binuclear osmium complex results in a weakened C–O bond and consequently lower stretching frequency compared to the C=O band. The stretching band of **4** was similar to that of the ruthenium analogue reported to be 1614 $cm^{-1}$ by Yan and co-workers.[6] Complex **1(b)** displayed higher stretching bands for M–O–C bonds relative to **1(a)** and **4**. Terminal C–O bonds have higher stretching frequencies while the bridging alkoxy exhibits lower stretching frequencies. Complex **3** exhibits lower stretching frequencies because of the electrons delocalised in the 5-membered chelate ring.

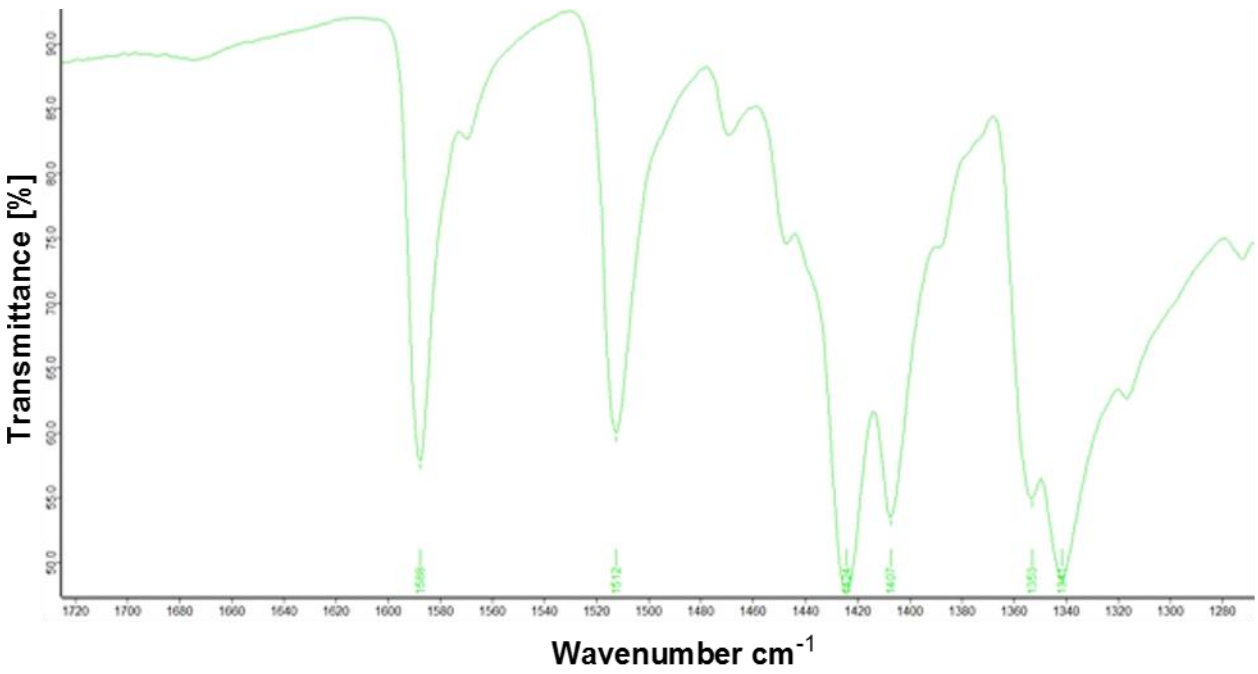


*Figure 2.5: Infra-red spectrum of complex **3**.*

2.3.3 Raman Spectroscopy

The Raman spectroscopy of **1(a)**, **1(b)**, **2** and **4** support the NMR and IR data, however, the Raman data of complex **3** was not obtained due to the dark colour of the sample. Complex **1(a)** displayed two stretching bands at 1695/1688 $cm^{-1}$ weak and 1609/1575 $cm^{-1}$ very weak attributed to $\nu_{asym(OCO)}$ (*see figure 2.6*). The stretching bands due to $\nu_{sym(OCO)}$ + $\nu_{(CC)}$ were observed at 1457 $cm^{-1}$ a shoulder and at 1426 $cm^{-1}$ which is a very strong band. A medium band at 1269 $cm^{-1}$ was assigned to $\nu_{sym(OCO)}$. A weak stretching band at 912 $cm^{-1}$ and a very weak band at 893 $cm^{-1}$ were assigned to $\nu_{(CC)}$.[41,42] Additional weak band due to $\nu_{(Os\text{-}Br)}$ was observed at 182 $cm^{-1}$. Complex **1(b)** shows three medium stretching bands at 1697/1680/1654 $cm^{-1}$ attributed to $\nu_{asym(OCO)}$. The very weak stretching bands at 1483/1460/1440 $cm^{-1}$ were assigned to $\nu_{sym(OCO)}$ + $\nu_{(CC)}$. A medium stretching band at 1384 $cm^{-1}$ and a very weak band at 1317 $cm^{-1}$ were attributed to $\nu_{sym(OCO)}$. A very weak stretching band at 907 $cm^{-1}$ was assigned to $\nu_{(CC)}$. Also a medium stretching band due to $\nu_{(Os\text{-}Br)}$ was observed at 197 $cm^{-1}$. The Os–Br bands for **1(a)** and **1(b)** appeared at different wavelengths attributed to the difference in cations, which exhibit different electrostatic interactions towards the osmium complex anion.

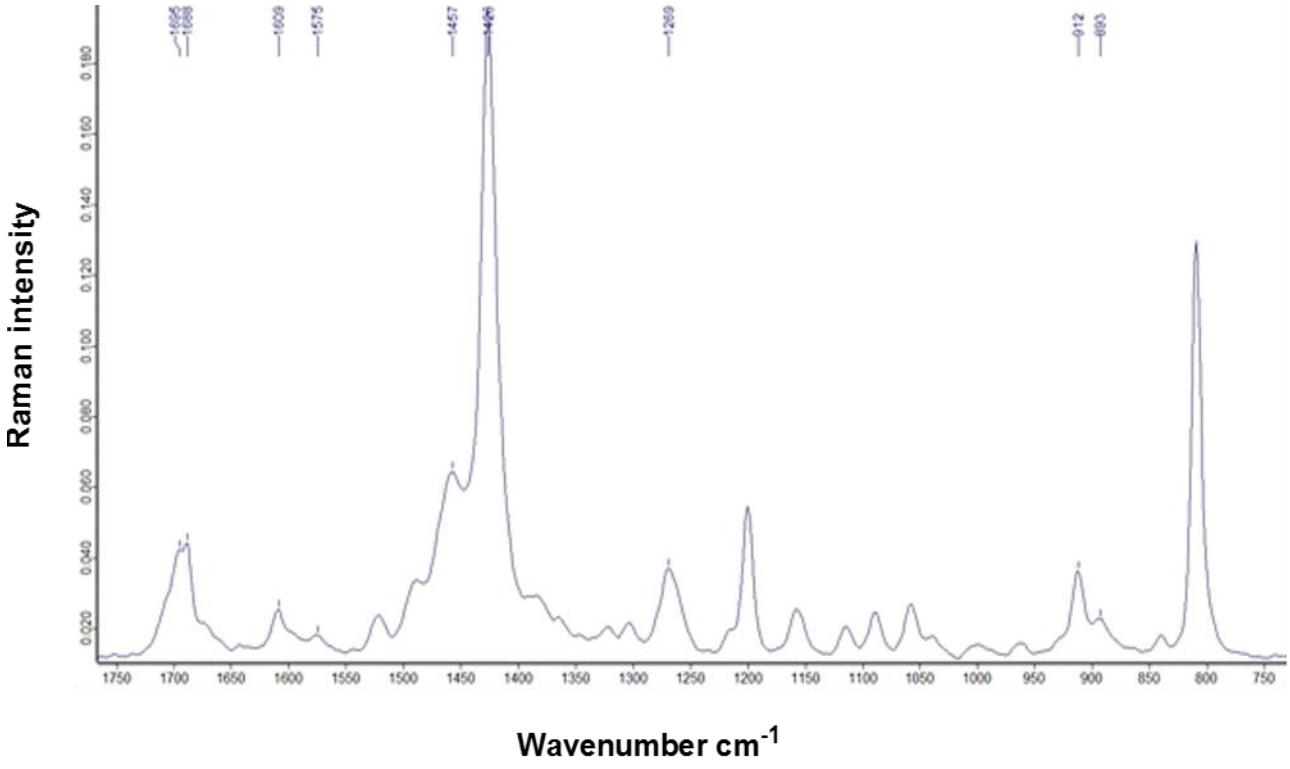


*Figure 2.6: Raman spectrum of complex **1(a)**.*

Complex **2** showed two weak stretching bands at 1697 $cm^{-1}$ and 1669 $cm^{-1}$ due to $v_{asym(OCO)}$. The very weak bands due to $v_{sym(OCO)} + v_{(CC)}$ were observed at 1483 $cm^{-1}$,1455 $cm^{-1}$ and 1440 $cm^{-1}$. A very weak stretching band at 1388 $cm^{-1}$ and a medium stretching band at 1364 $cm^{-1}$ were attributed to $v_{sym(OCO)}$. The two very weak bands were observed at 906 $cm^{-1}$ and 889 $cm^{-1}$ due to $v_{(CC)}$. Complex **4** displayed a weak single stretching band at 1655 $cm^{-1}$ due to $v_{asym(OCO)}$. A very strong stretching band at 1480 $cm^{-1}$ and a strong stretching band at 1445 $cm^{-1}$ were assigned to $v_{sym(OCO)} + v_{(CC)}$. The very weak stretching bands at 1380/1361 $cm^{-1}$ and 1319/1301 $cm^{-1}$ were assigned to $v_{sym(OCO)}$. A very weak stretching band at 921/904 $cm^{-1}$ were assigned to $v_{(CC)}$. In addition, a medium peak due to $v_{(Os\text{-}Br)}$ was observed at 200 $cm^{-1}$. Because of the symmetry of the binuclear complex **4**, a single Os−Br peak was observed. The Os–Br bands in this study were assigned according to literature data.[45]

### 2.3.4 Thermogravimetric analysis (TGA)

Thermal stability studies on all complexes reported in this chapter were carried out using TGA. Complex **1(a)** displayed remarkable thermal stability with three distinct degradation steps. The first step around 50 – 97.6 ºC was attributed the residual $CH_2Cl_2$ solvent. The second step showed the onset of decomposition at 160.1 to 322.8 ºC accounting for 44.3% mass loss attributed to the loss of the cymene, $C_2O_4$. The third step showed mass loss at 648.3 ºC attributed to the loss of Br ligand which was followed by oxidation of Ag(I) to AgO and Os(II) to $OsO_2$ and/or $OsO_4$ with 29% residue of silver and osmium beyond 800 ºC (*see figure 2.7*).[46]

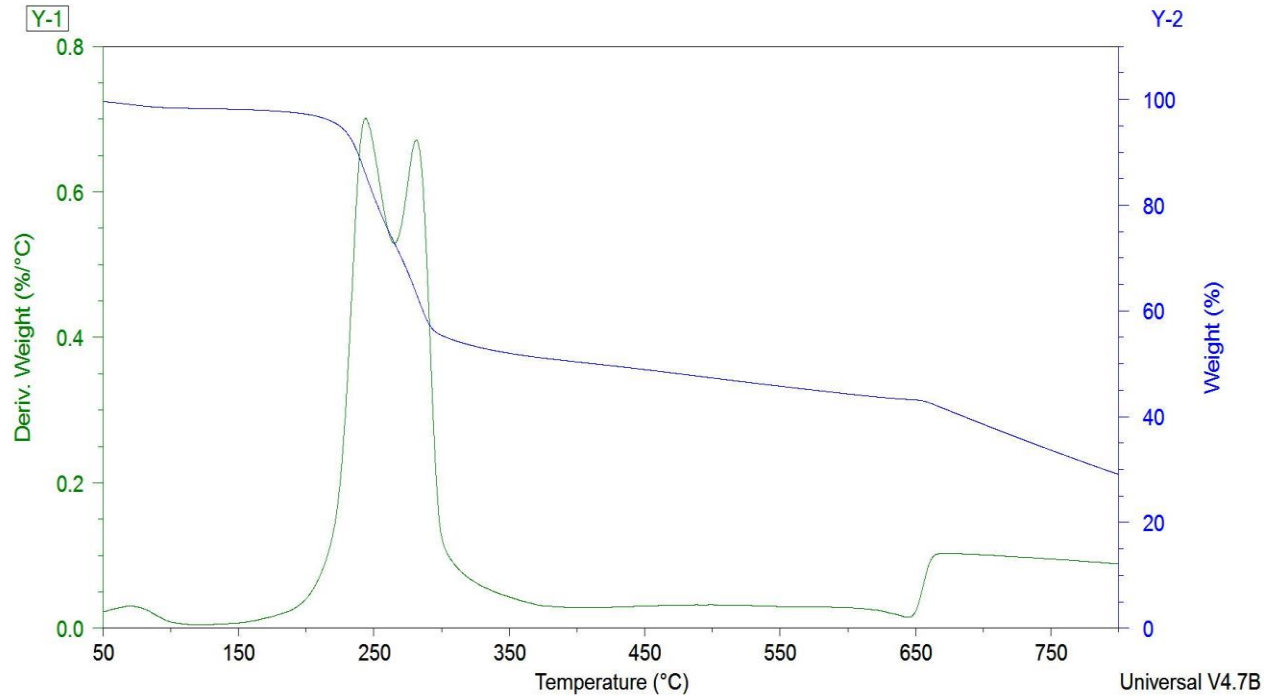


*Figure 2.7*: *TGA thermograms of* ***1(a)*** *with DTG curve.*

Complex **1(b)** shows four distinct degradation steps. The loss of the $CH_2Cl_2$ solvent was observed at 123.8 to 199.8 ºC. The first degradation step due to the onset decomposition of 22.1% mass loss at 245.2 ºC attributed to the loss of the cymene and $C_2O_4$ ligands. The second degradation step of 8.2% mass loss corresponds to the loss of one phenyl group of the $PPh_4^+$ counter ion at 298.2 to 345.6 ºC. The third step of degradation at 345.6 to 400.5 ºC corresponds to the loss of second phenyl group with 10.8% mass loss. The third step of degradation at 400.5 to 469.1 ºC corresponds to the loss of two phenyl groups with about 16.0% mass loss. The fourth step was incomplete below 800 ºC with about 27% remaining fragment attributed to [OsPBr]. Complexes **1(a)** and **1(b)** degrade in different pathways because of the different electrostatic forces between the cations and the complex anion (*see figure 2.8*). The $PPh_4^+$ cation has a positive influence on the thermal stability of **1(b)**. In **1(b)**, there is a systematic loss of four phenyl groups from $PPh_4^+$ at 295.1 to 469.1 ºC which results in the possible Os–P bond formation. The boiling point of P at 280.5 ºC supports our theory of a chemical vapour deposition reaction to yield [OsBrP].

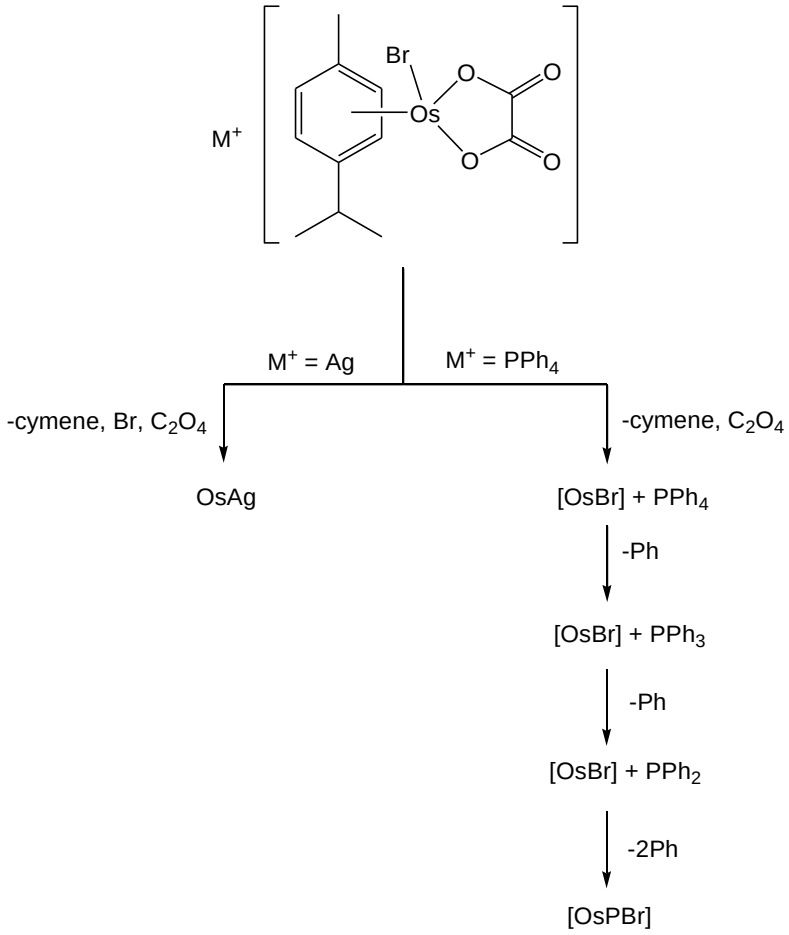


*Figure 2.8: The proposed decomposition pathways of **1(a)** and **1(b)**.*

Complex **2** shows three degradation steps, the onset decomposition of 33.6% mass at 168.1 to 331.0 ºC was attributed to the loss of cymene and the $C_2O_4$. The second degradation of 11.6% mass loss at 314.3 to 424.2 ºC was attributed to the loss of one phenyl group. The third degradation step of 19.7% mass loss was attributed to the loss of the two-phenyl groups at 424.2 to 627.0 ºC. The remaining 37% was attributed to [OsPBr] fragment. In contrast, complex **3** was observed to decompose in three distinct steps. For this complex the first step corresponds to the loss of the cymene ligand at 236.1 to 304.2 ºC accounting for 26.9% mass loss (*see figure 2.9*). The second step corresponds to the loss of the tropolonate ligand at 304.2 to 446.4 ºC accounting for 24.2% mass loss. The last step was attributed to the breaking of Os−Br bond and probably the loss of $OsO_2$ and $OsO_4$ resulting in the 14% residue remaining attributed to Os metal.[46]

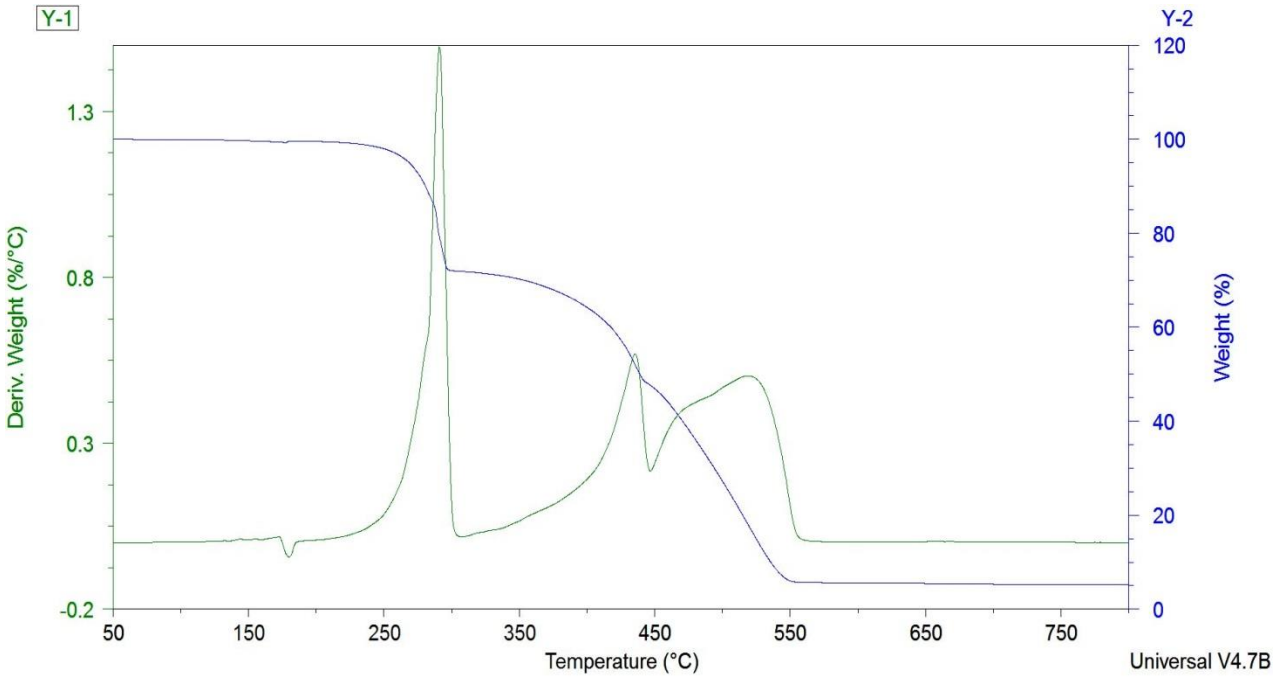


*Figure 2.9: TGA thermogram of **3** with DTG curve.*

Complex **4** decomposes in two distinct steps. The first degradation step corresponds to the loss of two cymene groups and the oxalate ligand at 248.8 to 316.3 ºC account for 41.2% mass loss. The second degradation step shows 14.4% mass loss which corresponds to two bromide ligands at 368.0 to 483.5 ºC (*see figure 2.10*). The osmium metal undergo oxidation to $OsO_2$ and/or $OsO_4$ followed by reduction to Os metal accounting for 41.4% mass loss at temperatures between 483.5 to 731.6 ºC.

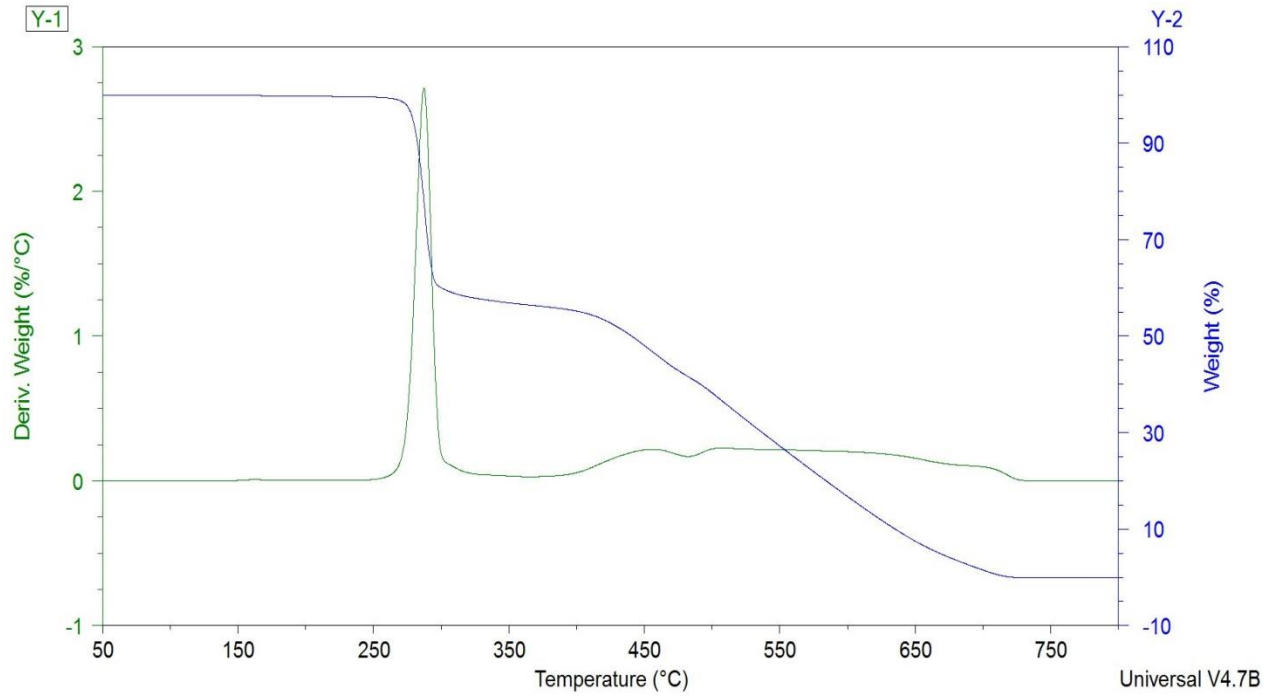


*Figure 2.10: TGA thermogram of **4** with DTG curve.*

2.3.5 Conductivity studies

The conductivity of ionic complexes **1(a)** and **1(b)** were measured at a concentration of $10^{-3}$ M in nitrobenzene solvent. From literature reports, 1:1 complexes are expected to give conductivities within the range 20-30 $Scm^2mol^{-1}$.[47] The results for complex **1(a)** at a concentration of $1.5 \times 10^{-3}$ M was not observed because the conductance of the complex was below the detection limit. The non-conductivity behaviour of this complex was attributed to low mobility of the ions involved and the interference of the solvent. Complex **1(b)** gave a molar conductivity value of 15.43 $Scm^2.mol^{-1}$ at a concentration of $1.2 \times 10^{-3}$ M. The molar conductivity of **1(b)** appeared to be below the range. This was attributed to the low mobility of ions involved as well as the bulkiness of the $PPh_4$ cation.

The results for complex **1(b)** were calculated using the following equations.

$$\kappa = G \times K \quad \ldots\ldots [1]$$

Where $\kappa$ = conductivity (S/cm), G = conductance (S), K = cell constant ($cm^{-1}$)

Converting the conductivity to the molar conductivity the following equation was used:

$\Lambda_M = \kappa / C_M$ . . . . . [2]

Where $\Lambda_M$ is the molar conductivity and $C_M$ is the molar concentration of complex **1(b)** = $1.2 \times 10^{-3}$ M

Then by substituting values obtained from equations [1] and [2], we obtained the following,

$\Lambda_M = 15.43$ S $cm^2$/mol

NB: The conductance of the samples were obtained after subtracting the value of the blank; Nitrobenzene = 3.45 μS from the measured values.

2.3.6 Crystallography

Single crystal X-ray crystallography confirmed the molecular structures of **1(b)**, **2** and **4**. Table 2.3 contains the crystal data and structural refinement parameters of **1(b)**, **2** and **4**. The general assignments of atoms in the three molecular structures are as indicated below (*see figure 2.11*).

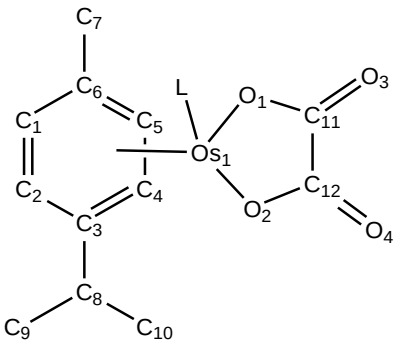


*Figure 2.11: General assignment of atoms in the molecular structures of **1(b)**, **2** and **4** discussed in this chapter.*

2.3.6.1 Molecular structure of **1(b)**.

Crystals of **1(b)** suitable for X-ray diffraction were obtained by slow diffusion of diethyl ether into a dichloromethane solution at room temperature. Complex **1(b)** measured the Os-centroid$_{cymene}$ distance as 1.642 Å. Loss of aromaticity was observed in the cymene ligand

through short and long C−C bonds which shows the localization of the C=C bonds in three sets of bonds C(1)−C(2), C(2)−C(3), C(3)−C(4) (*see table 2.4*). The Os−C bond lengths were observed to be slightly longer for Os(1)−C(1), Os(1)−C(3) and Os(1)−C(5) bonds. The loss of planarity in the cymene ring was observed in the deviation of the ring carbons from the mean plane defined by C(1), C(2), C(4) and C(5). The C(3) deviated by 0.083 Å below the mean plane and C(6) deviated by 0.049 Å also below the mean plane, which resulted in the cymene ligand adopting an inverted boat conformation. The oxalate bite angle O(1)−Os(1)−O(2) was measured at 77.05º.

The torsion angle C(3)−C(4)−C(5)−C(6) was found to be slightly higher than zero which indicates the distortion of the cymene ligand (*see table 2.4*). Complex **1(b)** showed intermolecular hydrogen bond between O(2) and a H atom on one of the phenyl rings of the $PPh_4^+$ ion. A C−H···O contact distance measured as 2.479 Å at an angle 149.22º. Also, found was a C−H···O intramolecular hydrogen bond between the hydrogen of C(10) and O(2) which measured 2.673 Å at 149.01º. Further intermolecular hydrogen bonding was observed between O(4) atom and a H atom of the phenyl ring of $PPh_4^+$ ion. A C−H···O hydrogen bond was measured as 2.582 Å at an angle 145.22º (*see figure 2.12*). A C−H···Br intermolecular hydrogen bonding was also observed between the hydrogen on the phenyl ring with Br(1) which measured 2.996 Å at 150.08º (*see figure 2.12*). The two C−H···O and one C−H···Br hydrogen bonds play a significant role in holding the two oppositely charged ions.

The effects of coordination of the oxalato ligand in **1(b)** are discussed below in comparison with the molecular structure of the uncoordinated oxalate ligand. The molecular structure of the uncoordinated oxalate ion (AMOXAL02[†1]) has been reported to have O(1)−C−C and O(2)−C−C bond angles of 117.79º and 117.00º respectfully as well as an O(1)−C−O(2) bond angle of 125.21º.[48] Also the free oxalate ligand bond lengths C−O(1), C−O(2) and C−C have been reported as 1.255 Å, 1.258 Å, and 1.548 Å respectively. In comparison, the coordinated oxalate ligand of complex **1(b)** has the following bond angles O(1)−C(11)−C(12), O(2)−C(12)−C(11), O(3)−C(11)−C(12), O(4)−C(12)−C(11), O(1)−C(11)−O(3) and O(2)−C(12)−O(4) which were measured at 114.29º, 114.63º, 121.10º, 120.33º, 124.48º and 124.96º respectively. The oxalate ligand in **1(b)** was affected upon coordination to the osmium centre, which can be observed through slight changes to the bond angles. The bond lengths of the coordinated oxalate ligand were measured as 1.300 Å for O(1)−C(11), 1.291 Å

†1 The CIF file used for comparison was obtained from the CCDC database.

for O(2)−C(12), 1.214 Å for O(3)−C(11), 1.221 Å for O(4)−C(12) and 1.543 Å for C(11)−C(12). The C(11)–O(3) and C(12)–O(4) of **1(b)** were shorter than those of the free ligand which may be attributed to introduction of electron density from Os into the chelate ring.

Similarly, the effects of electrostatic interactions on the $PPh_4^+$ ion in **1(b)** relative to the $PPh_4^+$ ion in $PPh_4Br$ (DEMYEZ03[†2]) were compared. The $PPh_4^+$ ion in complex **1(b)** measured similar C−P bond lengths and C−P−C bond angles relative to the $PPh_4Br$.[49] Hence, the electrostatic interaction between $PPh_4^+$ and the osmium complex has a negligible effect on the $PPh_4^+$ ion.

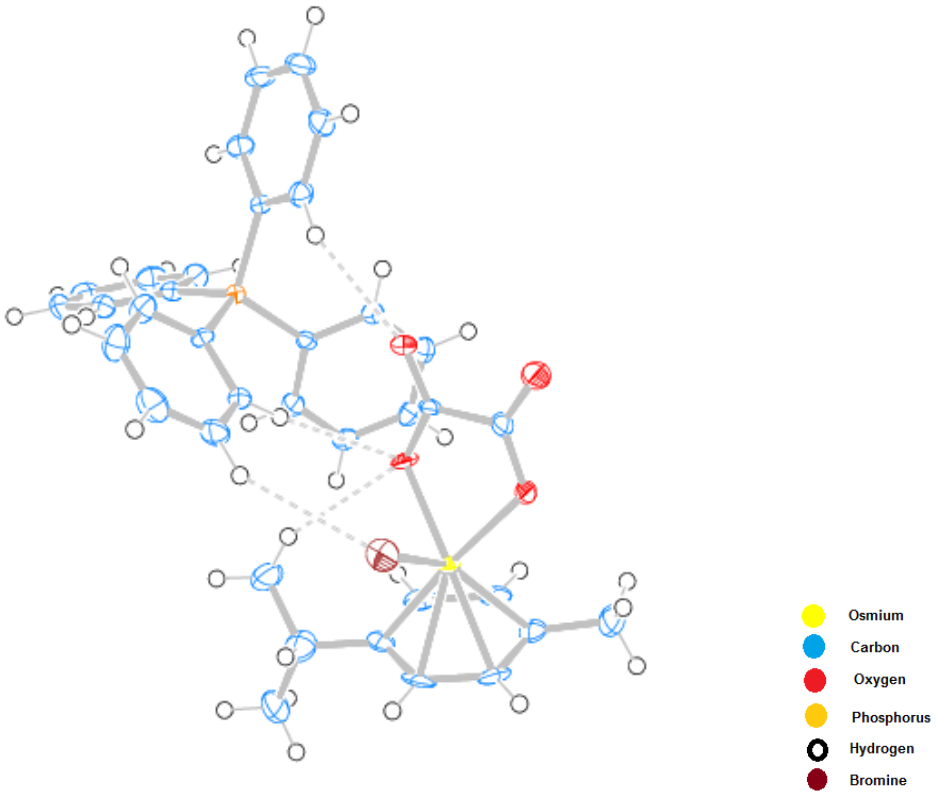


*Figure 2.12: Molecular structure of **1(b)** at 50% probability thermal ellipsoids.*

[†2] The CIF file used for comparison was obtained from the CCDC database.

2.3.6.2 Molecular structure of **2**.

Crystals of **2** were obtained from slow diffusion of diethyl ether into a dichloromethane solution at room temperature. The complex has a monoclinic crystal system with *P2₁* space group. The neutral complex **2** has both oxalate and $PPh_3$ ligands attached to the same osmium centre. Evidence of loss of aromaticity was observed with alternating shorter and longer C−C bonds around the cymene ligand. The three sets of carbons; C(1)−C(2), C(3)−C(4) and C(5)−C(6) have shorter distances than C(2)−C(3), C(4)−C(5) and C(6)−C(1) (*see table 2.3*). The *trans* influence of the $PPh_3$ ligand was observed on C(1) and C(2) with longer Os−C bond lengths than the four carbon atoms; C(3), C(4), C(5), and C(6) around the cymene. This was caused by competing of back bonding electrons from the osmium centre between aromatic carbon atoms and phosphorus atom. The Os−C bond lengths due to C(3), C(4), C(5) and C(6) were shorter because oxygen atoms *trans* to the four carbon atoms exert a weaker *trans* influence than C($sp^2$) atoms (*see table 2.4*).[50]

The distance from the centroid of the cymene ring to the osmium centre was measured as 1.700 Å whereas the ruthenium analogue (RUJHOT[†3]) was found to be 1.704 Å.[6] The difference in M−centroid distance was attributed to the stronger interaction of the osmium to the cymene in this study relative to the ruthenium analogue. The O(1)−Os(1)−O(2) bite angle was measured at 77.77º. The Os(1)−P(1) bond length at 2.350 Å was slightly shorter than that reported for the analogous Ru complex (2.367 Å).[6] The bond lengths C(11)–O(1) and C(12)–O(2) measured as 1.283 and 1.295 Å respectively were slightly longer than that of the C(11)–O(3) and C(12)–O(4) measured as 1.209 Å and 1.225 Å respectively.

The presence of weak intramolecular hydrogen bonding between O(1) and a H atom on the phenyl ring of $PPh_3$ was observed. The C−H···O contact distance was measured as 2.741 Å at an angle of 115.11º (*see figure 2.13*). A second interaction of the bridging oxygen atom (O(2)) with one of the H atoms of the isopropyl group of the cymene ligand was observed. Here, the C−H···O bond distance measured 2.545 Å at an angle of 133.46º (*see figure 2.13*). This contact is classified as a weak hydrogen bonding in literature.[51] Loss of planarity was observed in the cymene ring with deviation from planarity of C(3) measured as 0.047 Å

†3 The CIF file used for comparison was obtained from the CCDC database.

above the mean plane. The C(6) was deviated by 0.053 Å below the mean plane, which resulted in the cymene ligand adopting a pseudo-chair conformation.

The free oxalate and the coordinated oxalato ligands were compared in order to deduce the effects of coordination on the oxalato ligand in **2**. The free oxalate ligand shows O−C−C bond angles which are measured at 117.79º and 117.00º as well as the O−C−O bond angle at 125.21º.[48] The free oxalate ligand reported bond lengths due to C−O and C−C, which are 1.255 Å and 1.258 Å as well as 1.548 Å respectively. In this study, the parameters for **2** have been determined for O(1)−C(11)−O(3) and O(2)−C(12)−O(4) bond angles which were measured at 125.50º and 124.40º respectively. The torsion angle O(1)−C(11)−C(12)−O(2) was measured at 3.66º which indicated that the chelate ring was slightly distorted from the planar (*see table 2.4*).

The bond angles due to O(1)−C(11)−C(12) and O(2)−C(12)−C(11) were at 114.8º and 114.1º respectively. There was a slight difference in bond angles of the coordinated and the free oxalate ligand. The bond lengths of the coordinated oxalate ligand due to O(1)−C(11), O(2)−C(12) and C(11)−C(12) were measured as 1.283 Å, 1.296 Å and 1.548 Å respectively. The bond lengths of the carbonyl groups, C(11)−O(3) and C(12)−O(4) were measured as 1.226 Å and 1.209 Å respectively. This observation may be attributed to possible hydrogen bonding of O(1) and O(2) because the C−H···O bond length seems to be slightly longer for C(11)–O(3) bond but shorter for C(12)–O(4). The bond lengths [C(11)–O(3) and C(12)–O(4)] were slightly different from that of the free oxalate ligand, as expected.

The free $PPh_3$ and the coordinated $PPh_3$ ligands were also compared to determine the effects of coordination on the bond lengths and angles of $PPh_3$ in **2**. The free $PPh_3$ ligand (PTRPHE03[†4]) has the C−P−C bond angles which were measured at 103.08º, 103.44º and 101.66º.[52] The P−C bond lengths of the free $PPh_3$ ligand have been reported as 1.827 Å, 1.831 Å and 1.832 Å.[52] The C−P−C bond angles of the coordinated $PPh_3$ ligand in **2** were measured at 102.23º, 105.27º and 104.62º. The coordinated $PPh_3$ ligand P−C bond lengths were found be 1.819 Å, 1.820 Å and 1.834 Å. The deviation of two C−P−C bond angles for **2** from that of the free ligand was attributed to the combination of steric demand and Os–P–C back-bonding. The bond lengths were slightly less than that of the free ligands, which may be due to back bonding.

†4 The CIF file used for comparison was obtained from the CCDC database.

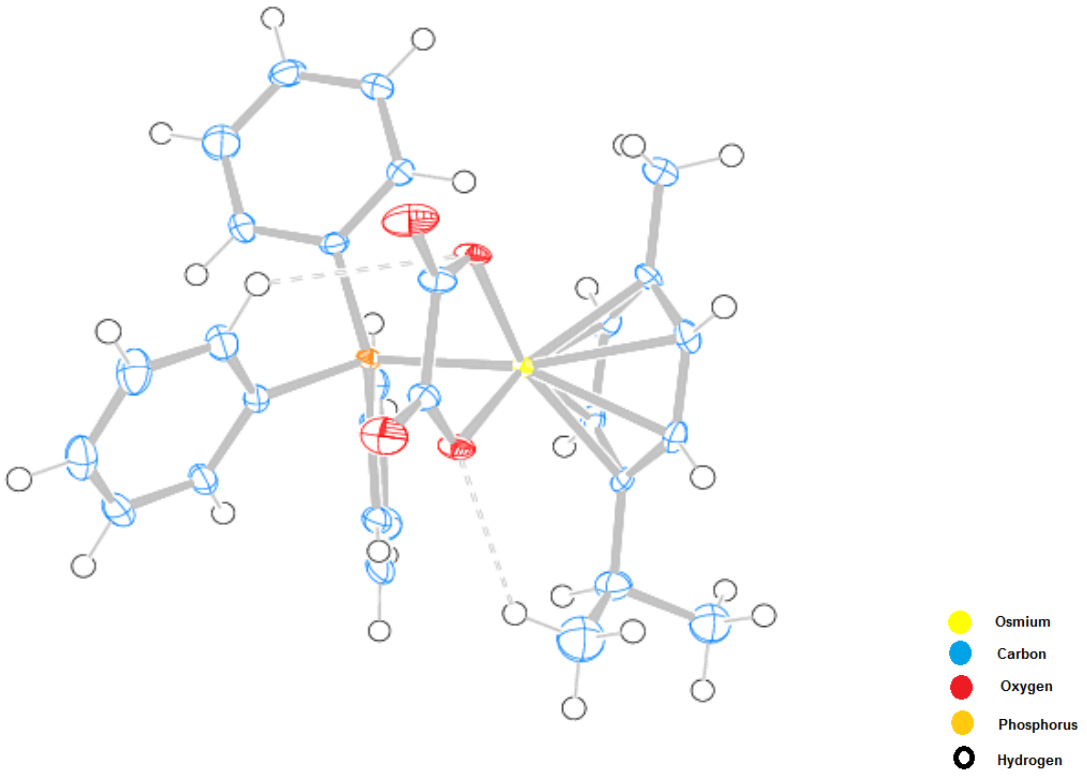


*Figure 2.13: Molecular structure of **2** at 50% probability thermal ellipsoids.*

2.3.6.3 Molecular structure of **4**.

Crystals of **4** suitable for X-ray diffraction were obtained by slow diffusion of diethyl ether into dichloromethane solution at room temperature. Complex **4** was found to crystalize in orthorhombic system with space group *Pbca*. The complex has a centre of symmetry hence the two nuclear fragmentations have equal bond distances as well as bond angles. Complex **4** gives a molecular structure with bis-chelated five-membered rings on both osmium centres. There was a difference in bond distances observed from the aromatic carbons to the osmium centre. The distance from the aromatic carbon atoms C(1), C(3) and C(6) on the cymene to Os(1) were longer than the other three aromatic carbon atoms C(2), C(4) and C(5) (*see table 2.4*). An indication of weaker interaction due to Os–$C_{cymene}$ long bond lengths may be attributed to the *trans* influence caused by the oxygen atoms adjacent to the three atoms. The shortest distance was observed for the Os(1)–C(2) bond which indicates a stronger interaction between the Os(1) and C(2) atoms.

The carbons in the cymene ligand showed different C−C bond distances, which indicated a loss of aromaticity of the cymene ligand once bounded to the osmium metal (*see table 2.4*). The distance from the osmium centre to the cymene centroid was found to be 1.636 Å. In contrast, the ruthenium analogues have Ru−centroid$_{cymene}$ distance of 1.644 Å (RUJHIN[†5]) and 1.650 Å (RUJHEJ[†6]) which were slightly longer compared to the Os−centroid$_{cymene}$ distance.[6] The observation may be attributed to the characteristics of the 5d transition metals to favour formation of more stable complexes relative to the 4d analogues. A weak C−H···Br intramolecular hydrogen bond was observed between the hydrogen of C(8) and Br atoms (*see figure 2.14*). The C−H···Br contact measures a distance of 3.081 Å at an angle 133.01º.

The bite angle O(1)−Os(1)−O(2) was measured at 77.10º which is significantly less than the ideal octahedral complex of 90º (*see figure 2.14*). The distortion of the bond angle O(1)−Os(1)−O(2) was caused by the oxalato ligand since the oxalato ligand has shorter carbon chain length. The interatomic distance between the two donor oxygen atoms [O(1) and O(2)] was measured as 2.664 Å. The torsion angle O(1)−C(11)−C(12)−O(2) measured at −0.63º indicates that the oxalate ligand was slightly distorted. The minor distortion was observed because of the *trans* influence due to aromatic carbons on the cymene equally affect the bridged-oxalato ligand from both osmium centres. The loss of planarity was observed in the cymene via the mean plane defined by C(1), C(2), C(4) and C(5). The deviation of C(3) was observed to be 0.003 Å below the mean plane and C(6) was measured as 0.030 Å also below the mean plane. The deviation of C(6) was found to be 10 times more than the deviation of C(3) because of the different substituents on these two carbon atoms. The cymene ligand adopted an inverted boat conformation. The torsion angle C(6)−C(1)−C(2)−C(3) was found to be −2.80º which also indicates the loss of planarity of the cymene. The intramolecular distances between the two osmium centres was found to be 5.540 Å.

The effects of the bis-chelating mode of the oxalato ligand in **4** relative to the free oxalate ligand were compared. The bond angles O(1)−C(11)−C(12) and O(2)−C(12)−C(11) were measured at 117.31º and 116.74º respectively. The bond angles of the coordinated oxalato ligand were found to be slightly deviated from the bond angles of the free ligands (117.79º and 117.00º).[48] The O(1)−C(11)−O(3) bond angle was measured at 125.94º for **4** while in the

†5 The CIF file used for comparison was obtained from the CCDC database.
†6 The CIF file used for comparison was obtained from the CCDC database.

free oxalate ligand it was measured at 125.21º. The slight difference may be attributed to the coordination of the oxalato ligand to two osmium centres. The O(1)−C(11), O(2)−C(12) and C(11)−C(12) bond lengths are measured to be 1.256 Å, 1.256 Å and 1.523 Å respectively. In free oxalate ligand these bond lengths are O−C (1.250 and 1.230 Å), and C−C (1.580 Å). Surprisingly, the bond lengths of the free oxalate ligand and the bridging oxalate ligand were similar.

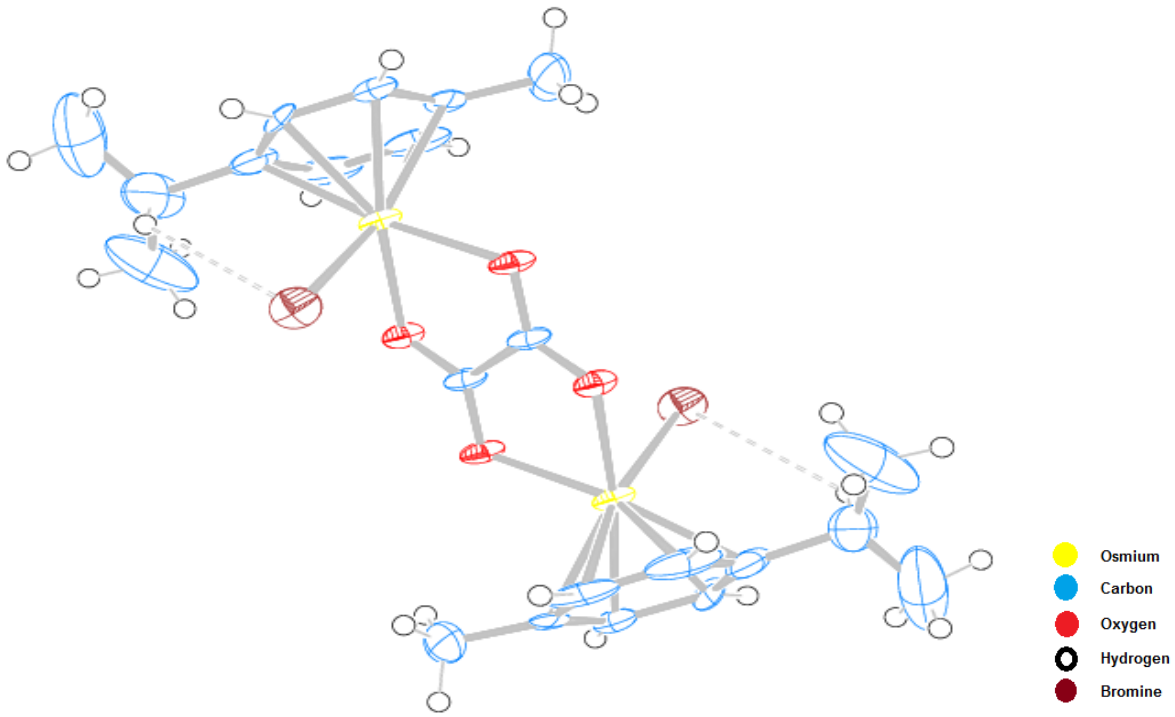


*Figure 2.14: Molecular structure of **4** at 50% probability thermal ellipsoids.*

*Table 2.3: Crystal data and structure refinement of **1(b)**, **2**, and **4**.*

| | **1(b)** | **2** | **4** |
|---|---|---|---|
| Chemical formula | $C_{36}H_{34}BrO_4OsP$ | $C_{30}H_{29}O_4OsP$ | $C_{22}H_{28}Br_2O_4Os_2$ |
| Molecular mass | 831.71 | 674.70 | 896.66 |
| Crystal system | Monoclinic | Monoclinic | Orthorhombic |
| Space group | $P2_1$ | $P2_1$ | Pbca |
| Crystal colour and shape | Yellow sheets | Yellow-brownish cubes | Yellow needle |
| a(Å) | 7.5565(8) | 9.745(5) | 10.8433(5) |
| b(Å) | 10.7431(12) | 11.825(5) | 11.8395(5) |
| c(Å) | 19.144(2) | 11.403(5) | 18.7871(8) |
| α(°) | 90.00 | 90.000(5) | 90.00 |
| β(°) | 100.154(4) | 99.261(5) | 90.00 |
| γ(°) | 90.00 | 90.000(5) | 90.00 |
| V(Å$^3$) | 1529.8(3) | 1296.9(10) | 2411.87(18) |
| Z | 2 | 2 | 4 |
| T(K) | 173(2) | 173(2) | 173(2) |
| $D_{calc}$ (mg/m$^3$) | 1.806 | 1.728 | 2.469 |
| Absorption coefficient | 5.566 mm$^{-1}$ | 5.012 mm$^{-1}$ | 13.865 mm$^{-1}$ |
| Reflections collected | 70605 | 59101 | 34419 |
| Independent reflections | 7361 [R(int) = 0.0939] | 6222 [R(int) = 0.0398] | 2911 [R(int) = 0.0903] |
| Data / restraints / parameters | 7361 / 1 / 391 | 6222 / 1 / 308 | 2911 / 0 / 139 |
| F(000) | 816 | 664 | 1656 |
| Final R indices [I>2σ(I)] | R1 = 0.0240, wR2 = 0.0623 | R1 = 0.0206, wR2 = 0.0529 | R1 = 0.0511, wR2 = 0.1041 |
| R indices (all data) | R1 = 0.0245, wR2 = 0.0636 | R1 = 0.0210, wR2 = 0.0532 | R1 = 0.0555, wR2 = 0.1061 |
| Goodness-of-fit on F$^2$ | 0.421 | 0.945 | 1.3811 |
| Largest diff. peak and hole | 0.727 and −2.154 e.Å$^{-3}$ | 0.815 and −2.134 e.Å$^{-3}$ | 2.308 and −2.853 e.Å$^{-3}$ |

*Table 2.4: Selected bond lengths (Å), Os-centroid$_{cymene}$ (Å), bond and torsion angles (º) of **1(b)**, **2** and **4**.*

| **Atom type label** | **1(b)** | **2** | **4** |
|---|---|---|---|
| Os(1)–C(1) | 2.175(6) | 2.234(4) | 2.179(10) |
| Os(1)–C(2) | 2.165(5) | 2.245(4) | 2.138(11) |
| Os(1)–C(3) | 2.184(6) | 2.208(3) | 2.176(11) |
| Os(1)–C(4) | 2.150(6) | 2.194(3) | 2.161(9) |
| Os(1)–C(5) | 2.182(6) | 2.210(3) | 2.162(9) |
| Os(1)–C(6) | 2.163(6) | 2.201(4) | 2.177(9) |
| C(1)–C(2) | 1.414(12) | 1.387(5) | 1.420(2) |
| C(2)–C(3) | 1.414(11) | 1.436(5) | 1.420(2) |
| C(3)–C(4) | 1.415(10) | 1.418(5) | 1.431(16) |
| C(4)–C(5) | 1.438(10) | 1.430(5) | 1.397(15) |
| C(5)–C(6) | 1.417(9) | 1.407(5) | 1.404(14) |
| C(6)–C(1) | 1.416(9) | 1.446(6) | 1.441(17) |
| Os(1)–O(1) | 2.099(4) | 2.078(3) | 2.136(7) |
| Os(1)–O(2) | 2.100(4) | 2.093(3) | 2.137(6) |
| Os(1)–Br(1) | 2.5324(7) | – | 2.5168(11) |
| Os(1)–P(1) | – | 2.3503(11) | – |
| Os–centroid$_{cymene}$ | 1.642 | 1.700 | 1.636 |
| **Bond angles** | | | |
| O(1)–Os(1)–O(2) | 77.05(16) | 77.77(10) | 77.1(2) |
| **Torsion angles** | | | |
| C(6)–C(1)–C(2)–C(3) | 0.54 | −0.5(6) | 0.4(15) |
| C(3)–C(4)–C(5)–C(6) | −4.14 | −1.1(5) | 2.8(16) |
| O(1)–C(11)–C(12)–O(2) | −1.04 | 3.7(5) | −0.63 |

## 2.4 Conclusions

Five novel O,O′-chelated osmium cymene complexes have been synthesized and characterized. The synthesis of the mononuclear complex $NH_4[Os(\eta^6\text{-}p\text{-cymene})(C_2O_4)Br]$ was not achieved instead a novel binuclear complex **4** was isolated. In addition, attempts to synthesize $[\{Os(\eta^6\text{-}p\text{-cymene})(PPh_3)\}_2\ \mu\text{-}C_2O_4](BF_4)_2$ were unsuccessful, instead a mixture of two neutral complexes **2** and **5** were obtained. The reaction of **4** with $PPh_3$ cleaved the Os−O bonds of the five membered O,O′-chelate ring at one osmium centre to afford a mixture of two neutral mononuclear complexes **2** and **5.** The spectroscopic techniques (NMR, IR and Raman) have played an important role in the identification of the two complexes. The binuclear osmium complex **4** exhibited unique reactivity compared to that reported for the ruthenium analogue.

The presence of $PPh_4^+$ as a counter ion improves the solubility, electrolytic properties and have a significant impact on vibrational modes of the carboxylate group of **1(b)**. Thermal studies showed that **1(a)** and **2** were less thermally stable with lower decomposition temperatures *ca.* 210 ºC relative to **1(b)**, **3** and **4**. The Os−O thermal stability was observed to follow the trend: **3** > **4** > **1(b)** > **1(a)** > **2**.

Single crystal X-ray diffraction confirmed the molecular structures of **1(b)**, **2** and **4**. The bridged-oxalato in **4** showed less distortion compared to the oxalato ligand in mononuclear complexes **1(b)** and **2**. The strong *trans* influence due to the $PPh_3$ ligand in **2** elongates the Os−C bonds *trans* to the $PPh_3$ ligand. In addition, **2** has the longest Os−$centroid_{cymene}$ distance than **1(b)** and **4,** attributed to the *trans* influence by $PPh_3$ ligand. The Os−O bond lengths increases in the following trend: **4** > **1(b)** > **2** which suggest that the stability of the bond may depend on other factors other than the length. The coordination of the cymene ligand to the osmium metal and the *trans* influence have shown to affect the aromaticity and planarity of the cymene ligand. The loss of aromaticity and planarity were found to be dependent on the ligand system around the osmium centre. The *in vitro* anticancer activity results of complexes **1(b)**, **3** and **4** will be discussed in Chapter 5.

## 2.5 References


(1) Urbaniak, W.; Jurek, K.; Witt, K.; Goraczko, A. *Chemik* **2011**, *65*, 273.

(2) Lewis, F. D.; Miller, A. M.; Salvi, G. D. *Inorg. Chem.* **1995**, *34*, 3173.

(3) Hammad, E. M.; Mubarak, M. S. *J. Appl. Polym. Sci.* **2007**, *108*, 2415.

(4) Hall, B. J.; Brodbelt, J. S. *J. Am. Soc. Mass Spectrom* **1999**, *10*, 402.

(5) Fanou, D.; Yao, B.; Siaka, S.; Ado, G. *J. Applied Sci.* **2007**, *7*, 310.

(6) Yan, H.; Suss-Fink, G.; Neels, A.; Stoeckli-Evans, H. *J. Chem. Soc., Dalton Trans.* **1997**, 4345.

(7) Kuhn, A.; Conradie, J. *Dalton Trans.* **2015**, *44*, 5106.

(8) Govindaswamy, P.; Mobin, S. M.; Thone, C.; Kollipara, M. R. *J. Organomet. Chem.* **2005**, *690*, 1218.

(9) Melchart, M.; Habtemariam, A.; Parsons, S.; Moggach, S. A.; Sadler, P. J. *Inorg. Chim. Acta* **2006**, *359*, 3020.

(10) Youngme, S.; Cheansirisomboon, A.; Danvirutai, C.; Chaichit, N.; Pakawatchai, C.; van Albada, G. A.; Reedijk, J. *Inorg. Chem. Comm.* **2006**, *9*, 973.

(11) Melchart, M.; Habtemariam, A.; Parsons, S.; Sadler, P. J. *J. Inorg. Biochem.* **2007**, *101*, 1903.

(12) Patil, K. C.; Gajapathy, D.; Kishore, K. *Thermochim. Acta* **1982**, *52*, 113.

(13) Lin, C.-T.; Bear, J. L. *J. Inorg. nucl. Chem.* **1969**, *31*, 263.

(14) Simmons, E. L.; Wendlandt, W. W. *J. Inorg. Nucl. Chem.* **1965**, *27*, 2325.

(15) Verma, P. N.; Juneja, H. D. *Int. J. ChemTech Res.* **2012**, *4*, 1000.

(16) Hancock, R. D. *J. Chem. Educ.* **1992**, *69*, 615.

(17) Feist, M.; Troyanov, S.; Kemnitz, E. *Inorg. Chem.* **1996**, *35*, 3067.

(18) Garcia-Couceiro, U.; Castillo, O.; Cepeda, J.; Luque, A.; Perez-Yanez, S.; Roman, P. *Inorg. Chim. Acta* **2009**, *362*, 4212.

(19) Modec, B.; Brencic, J. V.; Dolenc, D.; Zubieta, J. *J. Chem. Soc., Dalton Trans.* **2002**, 4582.

(20) Mautner, F. A.; Louka, F. R.; Massoud, S. S. *J. Mol. Struct.* **2009**, *921*, 333.

(21) Stordal, B.; Pavlakis, N.; Davey, R. *Cancer Treat. Rev.* **2007**, *33*, 347.

(22) Dey, S.; Banerjee, P. *Transition Met. Chem.* **2003**, *28*, 765.

(23) Barry, N. P. E.; Zava, O.; Furrer, J.; Dyson, P. J.; Therrien, B. *Dalton Trans.* **2010**, *39*, 5272.

(24) Zhang, Z.; Shao, D.-L.; Geng, Z.-R.; Wang, Z.-L. *Z. Anorg. Allg. Chem.* **2012**, *638*, 821.

(25) Nastase, S.; Maxim, C.; Tuna, F.; Duhayon, C.; Sutter, J.-P.; Andruh, M. *Polyhedron* **2009**, *28*, 1688.

(26) Pellaux, R.; Schmalle, H. W.; Huber, R.; Fischer, P.; Hauss, T.; Ouladdiaf, B.; Decurtins, S. *Inorg. Chem.* **1997**, *36*, 2301.

(27) Johnstone, T. C.; Suntharalingam, K.; Lippard, S. J. *Chem. Rev.* **2016**, *116*, 3436.

(28) Pittracher, M.; Frisch, U.; Kopacka, H.; Wurst, K.; Muller, T.; Oehninger, L.; Ott, I.; Wuttke, E.; Scheerer, S.; Winter, R. F.; Bildstein, B. *Organomet.* **2014**, *33*, 1630.

(29) Clayton, H. S.; Makhubela, B. C. E.; Su, H.; Smith, G. S.; Moss, J. R. *Polyhedron* **2009**, *28*, 1511.

(30) Fransen, J. R.; Dutton, P. J. *Can. J. Chem.* **1995**, *73*, 2217.

(31) Gamelas, C. A.; Bandeira, N. A. G.; Pereira, C. C. L.; Calhorda, M. J.; Herdtweck, E.; Machuqueiro, M.; Romaoa, C. C.; Veirose, L. F. *Dalton Trans.* **2011**, *40*, 10513.

(32) Huang, J.; Serron, S.; Nolan, S. P. *Organomet.* **1998**, *17*, 4004.

(33) Fernández-Zúmel, M. A.; Kiefer, G.; Thommes, K.; Scopelliti, R.; Severin, K. *Eur. J. Inorg. Chem.* **2010**, 3596.

(34) Hunter, C. A.; Low, C. M. R.; Rotger, C.; Vinter, J. G.; Zonta, C. *Proc. Natl. Acad. Sci.* **2002**, *99*, 4873.

(35) Cox, R. H. *Can. J. Chem.* **1971**, *49*, 1377.

(36) Colbran, S. B.; Johnson, B. F. G.; Lewis, J.; Sorrell, R. M. *J. Chem. Soc. Chem. Commun.* **1986**, 525.

(37) Kühl, O. *Phosphorus-31 NMR Spectroscopy A Concise Introduction for the Synthetic Organic and Organometallic Chemist*; Springer-Verlag: Berlin Heidelberg, 2008.

(38) Bell, A. G.; Kozminski, W.; Linden, A.; von Philipsborn, W. *Organomet.* **1996**, *15*, 3124.

(39) Eichele, K.; Wasylishen, R. E.; Corrigan, J. F.; Taylor, N. J.; Carty, A. J.; Feindel, K. W.; Bernard, G. M. *J. Am. Chem. Soc.* **2002**, *124*, 1541.

(40) Kuroda, D. G.; Hochstrasser, R. M. *J. Chem. Phys.* **2011**, *135*, 1.

(41) D'Antonio, M. C.; Wladimirsky, A.; Palacios, D.; Coggiola, L.; González-Baró, A. C.; Baran, E. J.; Mercaderd, R. C. *J. Braz. Chem. Soc.* **2009**, *20*, 445.

(42) Torres, M. M.; Palacios, D.; Dantonio, M. C.; González-Baróc, A. C.; Baran, E. J. *Spectroscopy Letters* **2016**, *49*, 238.

(43) Burden, K. J.; Thornton, D. A.; Watkins, G. M. *Spectrochim. Acta* **1989**, *45A*, 1179.

(44) Zhang, L.; Bu, W.-M.; Yan, S.-P.; Jiang, Z.-H.; Liao, D.-Z.; Wang, G.-L. *Polyhedron* **2000**, *19*, 1105.

(45) Bottger, G. L.; Damsgard, C. V. *Spectrochim. Acta* **1972**, *28A*, 1631.

(46) Brown, M. E. *Introduction to thermal analysis: techniques and applications*; Chapman and Hall Ltd: London and New York 1988.

(47) Geary, W. J. *Coord. Chem. Rev.* **1971**, *7*, 81.

(48) Taylor, J. C.; Sabine, T. M. *Acta Cryst.* **1972**, *28*, 3340.

(49) Burgess, K. M. N.; Korobkov, I.; Bryce, D. L. *Chem. Eur. J.* **2012**, *18*, 5748.

(50) Kapoor, P. N.; Kakkar, R. *J. Mol. Struct.* **2004**, *679*, 149.

(51) Steiner, T.; Desiraju, G. R. *Chem. Commun.* **1998**, 891.

(52) Bruckmann, J.; Kruger, C.; Lutz, F. *Z. Naturforsch.* **1995**, *50*, 351.

# CHAPTER 3

## SYNTHESIS OF MONODENTATE PHOSPHINE AND P,P′-CHELATED OSMIUM CYMENE COMPLEXES

### 3.1 Background

Phosphine ligands are ubiquitous in organometallic chemistry. The electronic and steric properties of phosphine ligands brought more interest in the study of phosphines from catalysis to medicinal applications.[1] In 1993 Polam and Porter[2] reported the molecular structure of the ruthenium arene complex $[Ru(\eta^6\text{-}C_6H_5CH_3)(PPh_3)_2Cl]BF_4$ obtained by refluxing $[Ru(PPh_3)_3Cl_2]$ and $AgBF_4$ in toluene. Their findings show that the toluene moiety was coordinated to ruthenium centre upon the cleavage of one $PPh_3$ and chloride ligand. Lalrempuia and co-workers[3] in 2003 reported the molecular structure of the ruthenium complex with a cymene ligand $[Ru(\eta^6\text{-}p\text{-cymene})(PPh_3)_2Cl]BF_4$. These two complexes are similar to complex **6** reported in this chapter but differ in the binding of the arene, halide and most importantly differs with respect to the metal centre.

The chemistry of diphosphine ligands has been known in coordination chemistry because of their wide range of applications in the fields of catalysis and metallopharmaceuticals. The diphosphine ligands are good π-acceptor ligands bringing stability to the whole complex by reducing electron density on the metal centre through π-back donation to the empty P 3d-orbitals. Hence, these ligands have been incorporated to a wide range of transition metals such as copper,[4] gold,[4] silver,[4] osmium,[5] ruthenium,[6,7] palladium,[8] chromium,[9] molybdenum,[9] tungsten,[9] rhodium.[10] Diphosphine ligands are capable of coordinating as monodentate as well as bidentate ligands. As bidentate, these species form chelate rings with metals resulting in stable complex formation compared to monodentate coordination. Furthermore, these ligands can also bridge two metals centres acting as a monodentate ligand at each metal centre.[5]

As bridging ligands, the diphosphines with shorter carbon chain length such as $[R_2P(CH_2)_nPR_2$ (where n = 1 or 2)] are capable of locking the two metal centres into close proximity. The diphosphine with longer carbon chain length such as $R_2P(CH_2)_nPR_2$ (where n = 3, 4 and higher) are more flexible with the two metal centres further apart. The electronic

communication of the two metal centres with bridging ligands is observed to be stronger depending on the ancillary ligands and the nature of the bridging ligand.[11] In the bridging diphosphine ligands, the electronic communication was reported to be stronger with shorter carbon chain length [$R_2P(CH_2)_nPR_2$ (where n = 1 or 2)] and the presence of non π-acceptor ancillary ligands.[12]

Chaplin and co-workers[7] reported a series of chelated diphosphine ruthenium cymene complexes [Ru($\eta^6$-*p*-cymene)Cl(P−P)]$PF_6$ (where P−P = diphenylphospinomethane (dppm), diphenylphosphinovinyl (dppv), diphenylphosphinoethane (dppe), diphenylphosphinopropane (dppp) and diphenylphosphinoferrocene (dppf). The group investigated chelation kinetics of the diphosphine ruthenium cymene complexes in $CH_2ClCH_2Cl$ upon heating which resulted in the loss of $PPh_3$ ligand that activated the ring closing process. Their findings show that the Ru−dppm complex chelates at the same rate ($t_{1/2}$ = 30 minutes) as the Ru−dppv complex. The Ru−dppp complex undergoes the chelation process slightly faster ($t_{1/2}$ = 22 minutes) than the Ru−dppe complex ($t_{1/2}$ = 28 minutes). The Ru−dppf undergoes ring closing process in $t_{1/2}$ = 1 minute. In another mechanistic study, ruthenium cymene complexes [Ru($\eta^6$-*p*-cymene)($\eta^1$-(P−P)$Cl_2$] (where P−P = dppm and dppv) were investigated for their rate of chelation in different solvents to afford [Ru($\eta^6$-*p*-cymene)(P−P)Cl]Cl. The Ru−dppm was found to chelate 4 times more slowly in different mixed ratios of $CH_3OH/CH_2ClCH_2Cl$ (solvent (v/v); 2:1, 1:1, 1:2) than the Ru-dppv complex.

Jensen and co-workers[6] reported the synthesis of the diphosphine complexes from the bis(acetonitrile) ruthenium cymene complex [Ru($\eta^6$-*p*-cymene)$(CH_3CN)_2Cl]^+$. The group reported the ring contributions to $^{31}$P NMR coordination shifts calculated relative to suitable monodentate analogues of the bidentate complexes. Therefore, the ring contributions to $^{31}$P NMR coordination shifts of complexes of this type [Ru($\eta^6$-*p*-cymene)(P−P)Cl]$PF_6$ (where P−P = dppm, dppe and dppp) complexes were calculated relative to methyldiphenylphosphine ($PCH_3Ph_2$) monodentate analogue. The Ru−dppm complex was found to have an upfield ring contribution compared to the Ru−dppe and Ru−dppp complexes. The Ru−dppe complex was found to have a downfield ring contribution compared to the Ru−dppp complex.

The synthesis methods reported by Chaplin and co-workers as well as Jensen and co-workers were used in this study to achieve the synthesis of osmium cymene complexes with chelating- and bridging-diphosphines (*see scheme 3.1*).

### 3.2 Preparation of P,P′-osmium cymene complexes

The preparation of the monodentate and chelated complexes **6** and **7(a)-(d)** were carried out by the method reported by Jensen and co-workers.[6] Complex **6** was prepared by reacting $[Os(\eta^6\text{-}p\text{-cymene})(CH_3CN)_2Br]BF_4$ and $PPh_3$ in $CH_2Cl_2$ at room temperature. The $PPh_3$ ligands slowly substitute the more labile $CH_3CN$ ligands. Complexes **7(a)-(d)** were prepared by reacting $[Os(\eta^6\text{-}p\text{-cymene})(CH_3CN)_2Br]BF_4$ and the corresponding diphosphine ligand $[PPh_2{-}(CH_2)_n{-}PPh_2$ (where n = 1 – 4)] in $CH_2Cl_2$ at room temperature. The substitution of the more labile $CH_3CN$ ligands gave the chelated diphosphine complexes as positively charged complexes. Complexes **8(a)-(d)** were prepared by drop-wise addition of the solution of the corresponding diphosphine ligand $[PPh_2{-}(CH_2)_n{-}PPh_2$ (where n = 1 – 4)] in $CH_2Cl_2$ to a stirred solution of the osmium dimer $[Os(\eta^6\text{-}p\text{-cymene})Br_2]_2$. Under these conditions the diphosphine ligand coordinate to two osmium centers in a bridging mode, affording a neutral binuclear complex (*see scheme 3.1*).

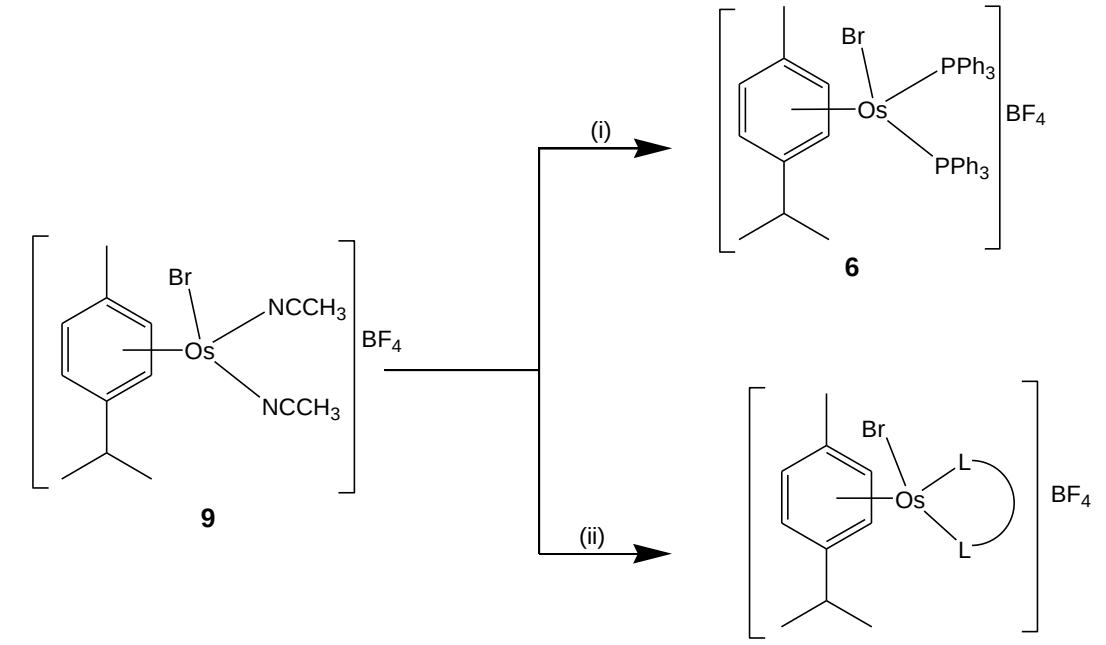


**7(a)** $L_2$ = dppm
**7(b)** $L_2$ = dppe
**7(c)** $L_2$ = dppp
**7(d)** $L_2$ = dppb

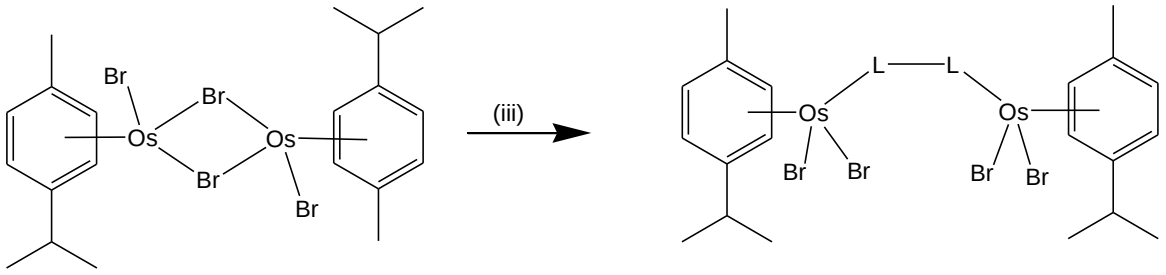


**8(a)** $L_2$ = dppm
**8(b)** $L_2$ = dppe
**8(c)** $L_2$ = dppp
**8(d)** $L_2$ = dppb

Reaction conditions (i) $2PPh_3$, $CH_2Cl_2$, R.T., 16 h.
(ii) $PPh_2(CH_2)_nPPh_2$, $CH_2Cl_2$, R.T., 16 h.
(iii) $PPh_2(CH_2)_nPPh_2$, $CH_2Cl_2$, R.T., 16h.

**Scheme 3.1**

## 3.3 Results and Discussion

### 3.3.1 Nuclear Magnetic Resonance (NMR) Spectroscopy

#### 3.3.1.1 $^1$H NMR data

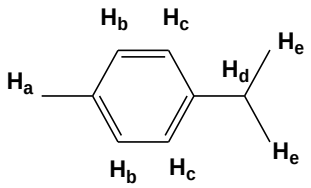


*Figure 3.1: $^1$H NMR data of the cymene ligand will be discussed with these assignments.*

The $^1$H NMR data for complexes **6** and **7(a)-(d)** are reported in Table 3.1. The $^1$H NMR signals indicated differences in shifts of the cymene aromatic protons as the carbon chain length of the diphosphine was increased. The cymene protons $H_b$ and $H_c$ of **7(a)** appear to be deshielded than that of the four complexes (*see figure 3.2*). The downfield shift of the protons $H_b$ and $H_c$ were observed because of the *trans* influence exerted by the phosphorus atoms. Less electron density on the carbons results in deshielding the nuclei of the protons $H_b$ and $H_c$, consequently increasing the acidity of these protons. Complex **7(b)** showed $H_b$ and $H_c$ signals that are deshielded relative to the $H_b$ and $H_c$ signals of complexes **6** and **7(d)** (*see figure 3.2*) which suggested strong interaction between the osmium centre and the phosphorus atoms of complex **7(b)**. The coupling constants for $H_b$ and $H_c$ protons are dependent on the dihedral angle between these protons. Different coupling constants are obtained because of the non-planarity of the cymene-ring protons as determined by crystallography measurements.

Complex **7(c)** showed $H_b$ and $H_c$ signals that are slightly deshielded relative to complexes **6** and **7(d)**. The cymene aromatic protons of **6** and **7(d)** were observed to be shielded (*see figure 3.2*). The shift may be due to the *trans* influence of the phosphorus atoms. The $^1$H NMR data for complexes **6** and **7(d)** suggest that the Os−P bonds are slightly longer than those of complexes **7(a)-(c)**, which results in carbons *trans* to the phosphorus atoms competing for electrons during back-bonding and thus shielding the nucleus of the $H_b$ and $H_c$ protons. Hence, deshielded cymene aromatic protons $H_b$ and $H_c$ suggested that the

phosphorus *trans* to carbons on the cymene has a stronger interaction with the osmium centre, and as a result may lead to shortened Os−P bond lengths.

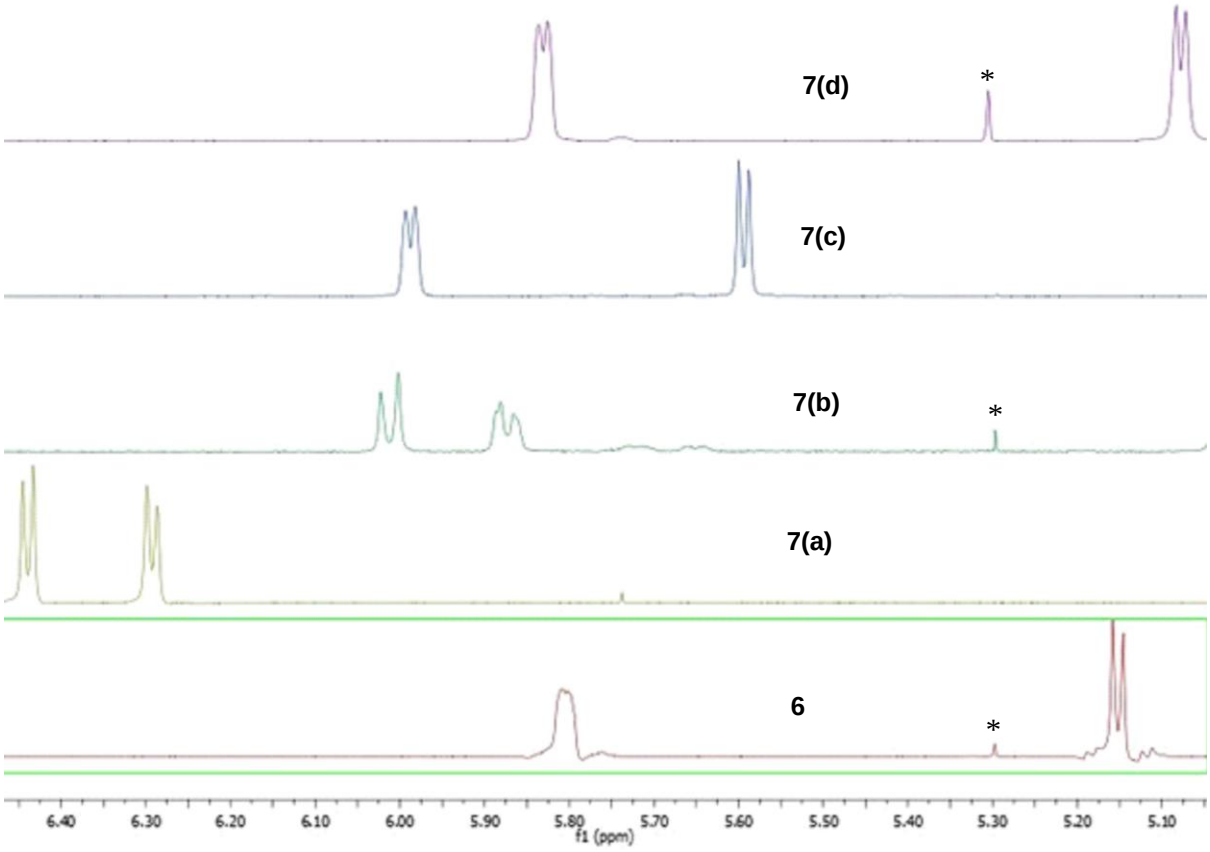


*Figure 3.2: The cymene protons $H_b$ and $H_c$ of **6** and **7(a)-(d)** with traces of $CH_2Cl_2$ (*).*

The proton $H_d$ also exhibits differences in signal shifts which were the opposite to that observed for protons $H_b$ and $H_c$ (*see table 3.1*). The signal due to $H_d$ for complex **6** was observed to be deshielded relative to complexes **7(a)-(d)**. Complex **7(d)** also shows a deshielded septet signal due to $H_d$ relative to complexes **7(a)-(c)**. Complex **7(c)** was deshielded compared to **7(b)** and **7(a)**. Complex **7(b)** was deshielded compared to **7(a)**. These results suggest that as the carbon chain length of the diphosphine ligand increases more electron density is shifted away from the cymene carbon bonded to the proton $H_d$.

*Table 3.1: $^{1}H$ NMR data of **6** and **7(a)-(b).***

| Assignment | **6** | | **7(a)*** | | **7(b)** | | **7(c)** | | **7(d)** | |
|---|---|---|---|---|---|---|---|---|---|---|
| | δ(ppm) | *J*(Hz) | δ(ppm) | *J*(Hz) | δ(ppm) | *J*(Hz) | δ(ppm) | *J*(Hz) | δ(ppm) | *J*(Hz) |
| $H_e$ (d) | 1.20 | 6.9 | 0.91 | 6.9 | 0.89 | 7.0 | 0.75 | 6.8 | 0.97 | 6.9 |
| $H_a$ (s) | 2.15 | - | 1.45 | - | 1.26 | - | 1.37 | - | 1.17 | - |
| 4H,$PCH_2C\underline{H}_2C\underline{H}_2CH_2$ (br) | - | - | - | - | - | - | - | - | 1.58-2.27 | - |
| 2H, $PCH_2C\underline{H}_2CH_2P$ (m) | - | - | - | - | - | - | 1.77-2.54 | - | - | - |
| $H_d$ (sept) | 2.75 | 7.0 | 2.20 | 6.8 | 2.38 | 6.7 | 2.46 | 6.8 | 2.65 | 7.1 |
| 2H,$PCH_2$- (m) | - | - | - | - | 2.65, 2.99 | - | 3.21 | - | 3.90 | - |
| 2H, P-$CH_2$-P (dd) | - | - | 4.73 | 5.4 | - | - | - | - | - | - |
| $H_b$ (d) | 5.23 | 5.9 | 6.31 | 5.9 | 5.87 | 4.1 | 5.58 | 5.9 | 5.05 | 5.9 |
| $H_c$ (d) | 5.80 | # | 6.45 | 5.9 | 6.01 | 6.4 | 5.97 | 5.4 | 5.80 | 5.4 |
| 20H, Ph (m) | - | - | 7.26-7.67 | - | 7.21-7.70 | - | 7.25-7.55 | - | 7.31-7.58 | - |
| 30H, Ph (m) | 7.23-7.37 | - | - | - | - | - | - | - | - | - |

*Spectra were recorded in $CDCl_3$ except for **7(a)** which was recorded in DMSO-$d_6$; # Poorly resolved doublet.

The $^{1}$H NMR data for **8(a)-(d)** are found in Table 3.2. A virtual triplet was observed for the bridging-methylene in **8(a)** at 4.88 ppm because the phosphorus-phosphorus coupling becomes larger resulting in the $^{1}$H NMR of the $-CH_2-$ being affected. In addition, complex **8(a)** is less sterically hindered (anti conformer), which has no mirror plane consequently the $-CH_2-$ protons are not equivalent, hence, a distorted triplet was observed rather than a doublet. Also, the aromatic protons $H_c$ for **8(a)** were displayed upfield relative to $H_c$ for **8(b)-(d)** (*see figure 3.3*). The $^{1}$H NMR signals of **8(b)** and **8(c)** were similar despite the additional $-CH_2-$ in **8(c)**. However, the aromatic protons $H_c$ of **8(c)** appeared downfield relative to $H_c$ of **8(b)**. Complex **8(d)** displayed $H_b$ and $H_c$ downfield relative to **8(a)-(c)**. The observation may be attributed to the competition of π-back bonding electrons between the P atoms and the aromatic cymene carbons.

*Table 3.2: $^{1}$H NMR data of **8(a)-(d).***

| Assignments | **8(a)** | | **8(b)** | | **8(c)** | | **8(d)** | |
|---|---|---|---|---|---|---|---|---|
| | δ(ppm) | *J*(Hz) | δ(ppm) | *J*(Hz) | δ(ppm) | *J*(Hz) | δ(ppm) | *J*(Hz) |
| $H_e$ (d) | 0.94 | 6.4 | 0.79 | 6.9 | 0.82 | 7.0 | 0.75 | 7.0 |
| 4H, $PCH_2CH_2$ (br) | – | – | 0.95 | − | 0.99 | – | 0.91 | – |
| 2H,$PCH_2$ (br) | 1.90 | – | – | – | – | – | – | – |
| $H_a$ (s) | 2.09 | – | 1.95 | – | 1.97 | – | 1.98 | – |
| $H_d$ (sept) | 2.52 | 6.9 | 2.48 | 6.9 | 2.51 | 6.9 | 2.49 | 7.0 |
| 4H,$PCH_2$- (br) | – | – | 2.64 | – | 2.66 | – | 2.51 | – |
| 2H, $PCH_2$ (m) | 3.49-3.71 | – | – | – | – | – | – | – |
| Virtual triplet, 1H,$CH_2$ | 4.88 | 7.3 | - | – | – | – | – | – |
| $H_b$ (d) | 5.07 | 4.7 | 5.15 | 5.9 | 5.17 | 5.9 | 5.20 | 5.9 |
| $H_c$ (d) | 5.31 | 5.9 | 5.29 | 5.9 | 5.31 | 5.3 | 5.36 | 5.3 |
| 20H, Ph (m) | 7.04-7.59 | – | 7.24-7.52 | – | 7.24 – 7.56 | – | 7.27-7.68 | – |

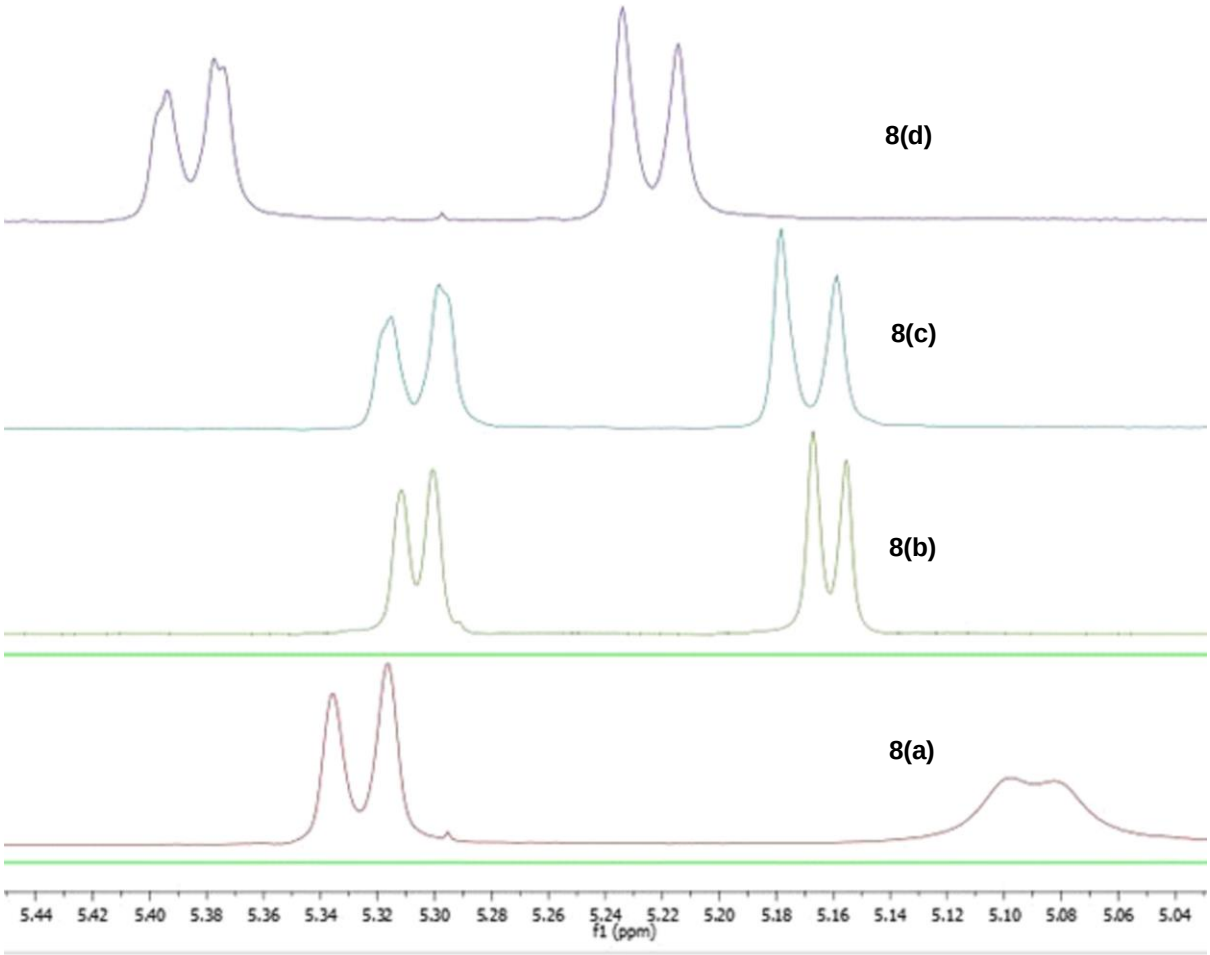


*Figure 3.3: $^{1}H$ NMR spectra of **8(a)-8(d)** showing the $H_b$ and $H_c$ protons.*

3.3.1.2 $^{13}C$ NMR data

The $^{13}C$ NMR data supports the $^{1}H$ NMR data and Table 3.3 contains the $^{13}C$ data for **6** and **7(a)-(d)**. Complex **6** shows shielded aromatic cymene carbons relative to **7(a)**, **7(b)** and **7(d)**. Complex **7(a)** showed a deshielded $^{13}C$ signal due to the dppm methylene carbon relative to the free ligand (28.07 ppm). This is because of the two phosphorus atoms withdrawing electrons from the carbon atom during σ-bonding to the metal. The two complexes **7(b)** and **7(c)** exhibit virtual triplets at 27.80 ppm with $J$ = 24 Hz and 23.79 ppm with $J$ = 20 Hz respectfully which are due to P−C coupling (*see table 3.3*).[6] This was observed because the *ortho* carbons on the phenyl group coupled to the P atom appear as virtual triplet and the *ipso* carbons as a second order multiplet under the influence of strong coupling of the two phosphorus atoms.[13]

Complex **7(d)** shows the cymene aromatic carbons downfield relative to **6** and **7(a)-(c)**. These observations indicate that the cymene ligand in **7(d)** is a stronger σ-donor relative to **6** and **7(a)-(c)**.

*Table 3.3: $^{13}C$ NMR data of **6** and **7(a)-(d)**.*

| Assignment | **6** δ(ppm) | **7(a)** δ(ppm) | **7(b)** δ(ppm) | **7(c)** δ(ppm) | **7(d)** δ(ppm) |
|---|---|---|---|---|---|
| $\underline{C}H_3C_6H_4$ | 15.30 | 16.37 | 15.52 | 15.60 | 14.99 |
| $CH(\underline{C}H_3)_2$ | 21.79 | 21.64 | 21.44 | 21.12 | 21.57 |
| $PCH_2\underline{C}H_2$ | - | - | 29.72 | 21.47 | 22.66 |
| $PCH_2$ | - | - | 27.80 ($J_{(P-C)}$ = 24Hz), | 23.79 ($J_{(P-C)}$ = 20Hz) | 28.83 |
| $\underline{C}H(CH_3)_2$ | 31.63 | 29.86 | 30.50 | 30.54 | 30.70 |
| $PCH_2$ | - | 43.69 | - | - | - |
| $\eta^6$-$C_6H_4$ | 96.42, 89.37, 81.30, 73.13 | 112.98, 95.79, 84.37, 81.07 | 117.56, 95.40, 85.96 ($J$ = 3Hz), 83.41($J$ = 8 Hz) | 94.00, 86.32, 85.15, 70.60 | 126.25, 92.45, 87.53, 83.32 |
| $C_{Aromatic}$ | 128.31-134.71 | 128.44-131.70 | 128.49-135.03 | 128.73-136.02 | 128.88-133.35 |

The $^{13}C$ NMR data of complexes **8(a)-(d)** are reported in Table 3.4. The $^{13}C$ data also supported the $^{1}H$ NMR data. The $^{13}C$ signal due to $P\underline{C}H_2P$ for **8(a)** appeared at $\delta$ = 53.65 ppm. This was attributed to the withdrawing of electron density by the two electronegative P atoms from $-CH_2-$ resulting in the carbon becoming electron deficient, thus exposing the nucleus of that carbon. Complex **8(b)** showed a virtual triplet for the $PCH_2$ at $\delta$ = 26.72 ppm with $J(^{31}P-^{13}C)$ = 23 Hz. This was observed because of the strong phosphorus–phosphorus coupling which result in each phosphorus atom coupling both two carbons on the dppe chain length. The triplet arises when both doublets are very close to one another because of the phosphorus-phosphorus coupling, which result in combination of the similar inner signals. Hence, a triplet was observed which is caused by a second order effects.

Complex **8(c)** showed a doublet of doublets at $\delta$ = 26.52 ppm with $J(^{31}P-^{13}C)$ = 15 Hz. This observation was attributed to the strong phosphorus-phosphorus coupling which results in each phosphorus atom coupling with both the two carbon atoms in an alkyl chain length $P\underline{C}H_2\underline{C}H_2CH_2P$. Complex **8(d)** showed only two signals due to the bridged-dppb at $\delta$ = 22.65 and 29.69 ppm because of the symmetry of the binuclear complex.

The signals due to aromatic cymene carbons appear similar for the four diphosphine-bridged complexes (*see table 3.4*). This observation may be due to similar interactions of the diphosphine ligands to the osmium centre.

*Table 3.4: $^{13}C$ NMR data of **8(a)-(d).***

| Assignment | **8(a)** δ (ppm) | **8(b)** δ (ppm) | **8(c)** δ (ppm) | **8(d)** δ (ppm) |
|---|---|---|---|---|
| $\underline{C}H_3C_6H_4$ | 18.71 | 17.80 | 17.61 | 17.49 |
| $P\underline{C}H_2\underline{C}H_2$ | – | 19.30 | 19.14 | 22.65 |
| $CH(\underline{C}H_3)_2$ | 22.49 | 21.87 | 21.69 | 21.48 |
| $PCH_2$ | – | 26.72(*J*=23Hz) | 26.52(*J*=15Hz) | 29.69 |
| $\underline{C}H(CH_3)_2$ | 30.45 | 30.22 | 30.04 | 30.03 |
| $PCH_2P$ | 53.65 | – | – | – |
| $\eta^6$-$C_6H_4$ | 101.66, 87.52, 82.95, 78.28 | 100.59, 86.19, 82.72(*J*=3Hz), 78.09(*J*=6Hz) | 100.43, 85.98, 82.50, 77.90(*J*=6Hz) | 99.86, 85.45, 82.81, 77.92 |
| $C_{Aromatic}$ | 127.04-134.54 | 128.05-133.48 | 127.85-133.33 | 128.11-133.39 |

### 3.3.1.3 $^{19}F$ NMR data of **6** and **7(a)-(d)**

The $^{19}F$ NMR confirmed the presence of the $BF_4$ counter ion in complexes **6** and **7(a)-(d)**. Two $^{19}F$ signals were observed; the low intensity signal was attributed to $^{10}B$-F coupling because of 19.58% of $^{10}BF_4$ ($^{10}B$, $I$ = 3) (*see figure 3.4*). The high intensity signal was attributed to $^{11}B$-F coupling because of the 80.42% of $^{11}BF_4$ ($^{11}B$, $I$ = 3/2).[14,15] The two signals appear separated due to the isotope shift since the two boron isotopes exhibit different electronic properties in bonding.

The $^{19}F$ NMR signals for $[Os(\eta^6\text{-}p\text{-cymene})(NCCH_3)_2Br]BF_4$ was observed as two singlets at −151.84 and −151.89 ppm. Complex **6** shows the fluorine chemical shifts at −157.67 and −157.72 ppm. Complex **7(a)** shows two singlet fluorine peaks at −143.46 and −143.52 ppm, complex **7(b)** at −152.86 and −152.92 ppm, complex **7(c)** at −152.51 and −152.56 ppm, complex **7(d)** at −152.85 and −152.91 ppm (*see figure 3.4*).

Complex **6** displayed $^{19}F$ signals upfield relative to the signals for $[Os(\eta^6\text{-}p\text{-cymene})(NCCH_3)_2Br]BF_4$. This observation may be attributed to weaker interaction between the complex ion and the $BF_4$ ion caused by the bulkiness on the cation complex. Complex **7(a)** shows deshielded fluorine peaks due to the solvent effect. This observation may be due to interaction between the S atom of the DMSO solvent and the F atom of $BF_4$ counter ion.

Hence, electron density on the fluorine atoms would be reduced consequently deshielding the fluorine nucleus. Complex **7(b)** and **7(d)** displayed similar $^{19}F$ signals; this may be attributed to similar electrostatic interactions of the complex ions with the counter ion. Complex **7(c)** showed $^{19}F$ signals slightly downfield relative to **7(b)** and **7(d)** because of the difference in electrostatic interactions.

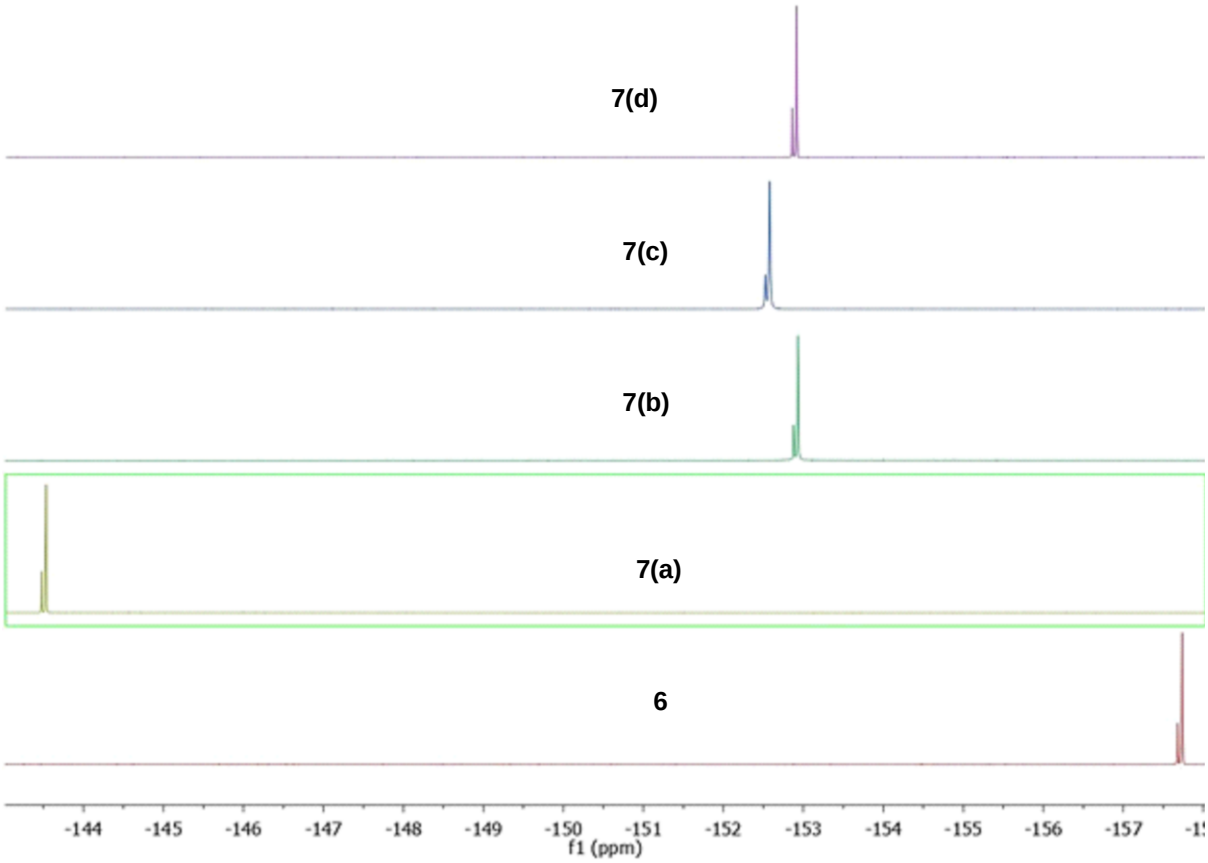


*Figure 3.4: $^{19}F$ NMR spectra of **6** and **7(a)-(d)** showing fluorine peaks.*

3.3.1.4 $^{31}$P NMR data

The $^{31}$P NMR data for complexes **6** and **7(a)-(d)** are discussed below. Complex **6** showed a single $^{31}$P peak at −28.94 ppm with two sets of satellite peaks. The first set of satellite peaks at −28.85 and −29.03 ppm with $J(^{187}\text{Os}–^{31}\text{P})$ = 271 Hz. The second set of satellite peaks was observed at −28.27 and −29.61 ppm attributed to the spinning side bands with $^{1}J$ = 36 Hz (*see figure 3.5*). The presence of two sets of satellite peaks in complex **6** may be due to the NMR active isotope of osmium which is $^{187}$Os and the spinning side bands.[16] In literature, $^{31}$P NMR studies in solution reported satellites peaks due to the less abundant $^{187}$Os isotope.[17] The satellites peaks due to $^{189}$Os isotope are reported to be observed only in solid-state $^{31}$P NMR studies because of the extremely efficient quadrupolar relaxation in solution.[18] As explained in Chapter 2, the two sets of satellite peaks were assigned to spinning side bands (high intensity peaks with $J$ = 36 Hz) and $^{187}$Os (low intensity peaks with $J$ = 271 Hz).

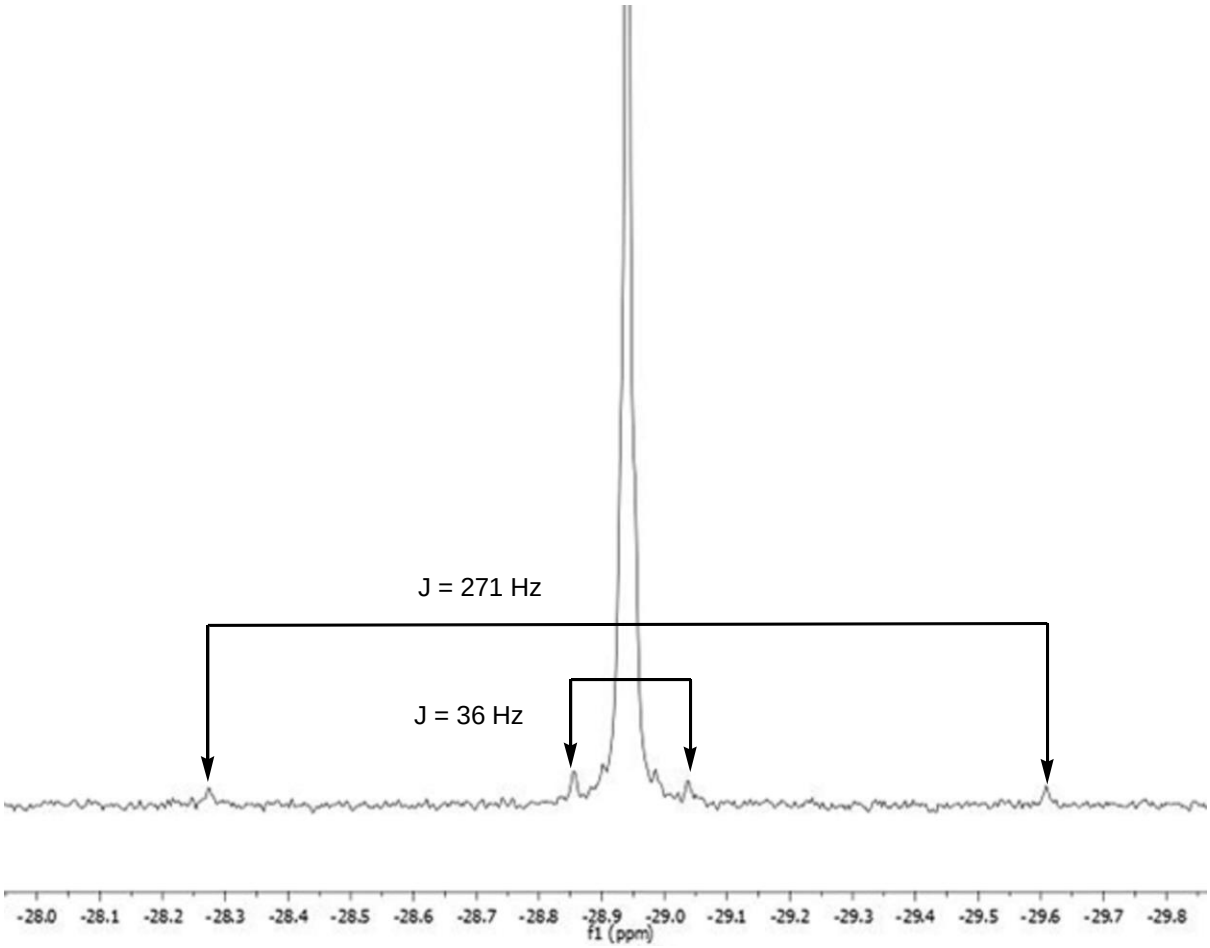


*Figure 3.5: $^{31}$P NMR spectrum of **6** with two sets of satellite peaks.*

A single $^{31}$P peak for complex **7(a)** appeared at −43.52 ppm, more shielded than the free dppm ligand (−22.51ppm). The satellite peaks appeared at −42.98 and −44.06 ppm with $J(^{187}\text{Os}–^{31}\text{P})$ = 218 Hz (*see figure 3.6*). Complex **7(b)** showed a single phosphorus peak at 30.33 ppm, more deshielded than the free dppe ligand (−12.64 ppm). The two satellite peaks appear at 29.88 and 32.01 ppm with $J(^{187}\text{Os}–^{31}\text{P})$ = 259 Hz. Complex **7(c)** showed a phosphorus peak at −25.00 ppm, which is more deshielded than the free ligand (−17.52ppm). The satellite peaks appeared at −24.39 and −25.62 ppm with $J(^{187}\text{Os}–^{31}\text{P})$ = 249 Hz (*see figure 3.6*). Complex **7(d)** showed the P peak at −17.10 ppm, which was slightly shielded than the free dppb ligand (−16.19 ppm). The two satellite peaks appeared with $J$ = 260 Hz due to $^{187}$Os –$^{31}$P coupling. The $J_{(\text{Os-P})}$ values of the chelated diphosphine complexes were found to follow the decreasing trend: **7(d)** > **7(b)** > **7(c)** > **7(a)**.

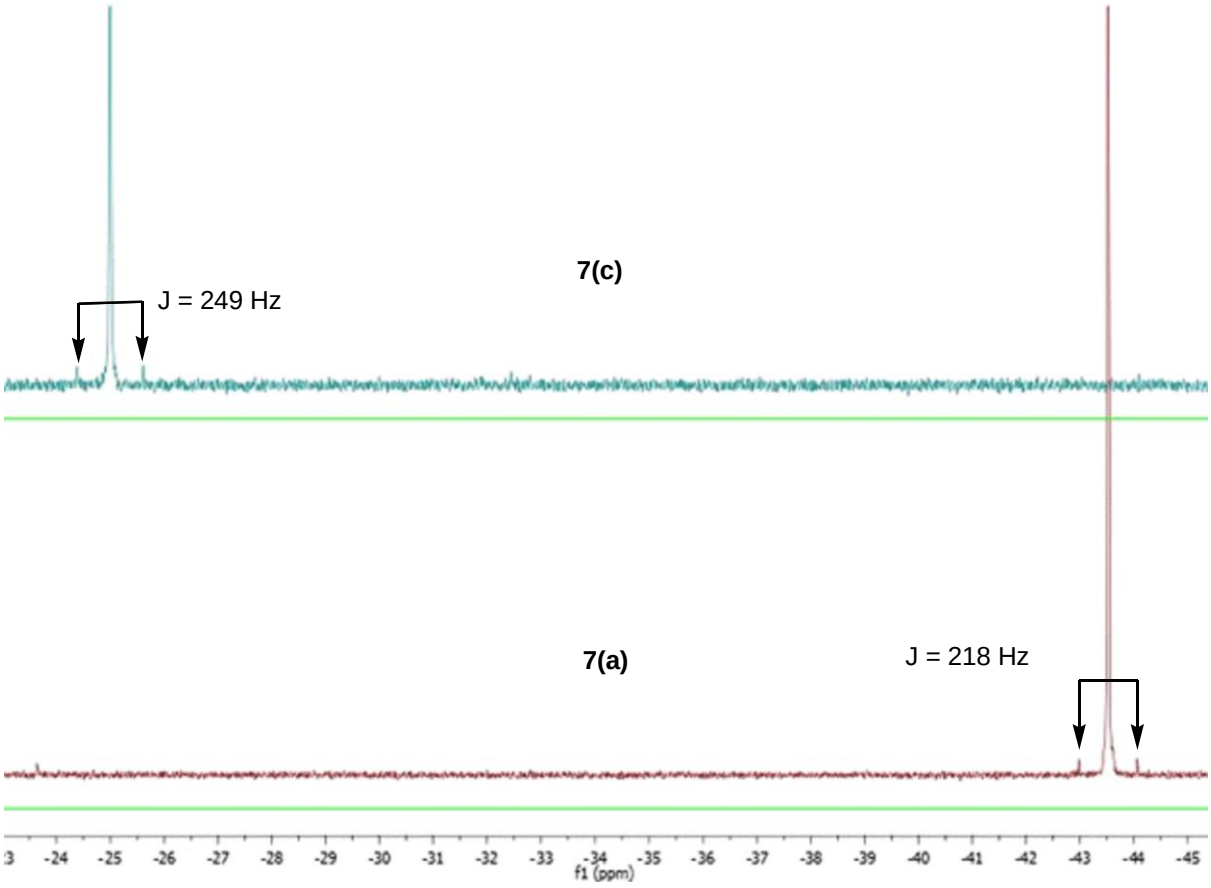


*Figure 3.6: $^{31}$P NMR spectra of **7(a)** and **7(c)** showing satellite peaks.*

The $^{31}P$ NMR chemical shifts are dependent of the electronic environment on the phosphorus atom, the bond angle as well as the shielding cones of unsaturated systems.[16] The alkyl groups bonded to phosphorus atoms are electron donating groups hence more electron density will be observed on the phosphorus atom as well as π-back bonding with the central metal. The P donor atoms in **7(a)** were more shielded and that suggests that the dppm is a good π-acceptor ligand and the C−P−C bond angles may have deviated towards tetrahedral geometry (109.5º). This would result in increased C−P−C bond angles consequently shifting the $^{31}P$ chemical shift upfield relative to the free dppm ligand. Complex **7(b)** showed a P signal, which was the most deshielded, compared to **7(a)**, **7(c)** and **7(c)**. This may be attributed to the change in geometry of the dppe in the chelated metal complex.

The P signal of **7(c)** appeared upfield relative to the free ligand, which suggests a change in the dppp ligand geometry upon coordination and π-back bonding. Complex **7(d)** appeared more deshielded compared to **7(a)-(c)**; which suggests that the dppb ligand is a less effective π-acceptor compared to the dppm, dppe and dppp ligands. Furthermore, the increased ring size is expected to have a negligible effect on the C−P−C bond angle upon coordination to osmium; hence, only a slight shift in signal was observed relative to the free dppb ligand. The above observations suggest that the ability of the diphosphine ligand to chelate decreases as the carbon chain length increases.

The ring contribution ($\Delta_r$) to $^{31}P$ NMR for the chelating diphosphine osmium complexes was calculated with respect to the monodentate bis(phosphine) osmium complex **6**. Table 3.5 contains the ring contribution factors for complexes **7(a)-(d)**.

The four membered ring complex **7(a)** was found to be the most shielded with a ring contribution of 2.40 ppm while **7(b)** showed the most downfield ring contribution (*see table 3.5).*[6,19] Complexes **7(c)** and **7(d)** also showed some downfield ring contribution compared to **7(a)**. The ring contribution of the chelate moiety increases with an increase in ring size with respect to monodentate bis($PPh_3$) complex. The four membered chelate ring complex **7(a)** and the six membered chelate ring complex **7(c)** gave a ring contribution which appears upfield whereas the five membered chelate ring complex **7(b)** and the seven membered chelate ring complex **7(d)** gave a ring contribution which appeared downfield. The chelating osmium complexes showed similar pattern to that reported by Garrou[19] for platinum complexes and also reported later by Jensen and co-workers[6] with ruthenium complexes. The

observation may have an implication with respect to the Os–P bond lengths and the Os–P bond stability which will be discussed later in the thermal studies and crystallography.

*Table 3.5: Ring contribution to $^{31}P$ NMR coordination shifts of [Os($\eta^6$-p-cymene)($L_2$)Br]$^+$ complexes relative to the monodentate $PPh_3$.*

| $L_2$ | δ ($^{31}$P) Complex | δ ($^{31}$P) Free ligand | Coordination shift (Δ δ)* | Ring contribution ($\Delta_r$)$^{\#}$ | Ring size |
|---|---|---|---|---|---|
| $2PPh_3$ | −28.94 | −5.53 | −23.41 | − | − |
| dppm | −43.52 | −22.51 | −21.01 | 2.40 | 4 |
| dppe | 30.13 | −12.64 | 42.77 | 66.18 | 5 |
| dppp | −25.00 | −17.52 | −7.48 | 15.93 | 6 |
| dppb | −17.10 | −16.19 | −0.91 | 22.50 | 7 |

Δδ* = δ ($^{31}$P) complex – δ ($^{31}$P) free ligand

$\Delta_r^{\#}$ = Δδ (chelate) – Δδ (monodentate)

The $^{31}$P NMR data for the bridging-diphosphine osmium complexes **8(a)-(d)** are discussed below. Complex **8(a)** exhibited a single $^{31}$P peak at −28.73 ppm with two satellite peaks giving $^1J(^{187}Os–^{31}P)$ = 274 Hz. Complex **8(b)** showed a single $^{31}$P peak at −25.22 with two satellite peaks attributed to $^{187}$Os with coupling constant as $^1J(^{187}Os–^{31}P)$ = 273 Hz. The $^{31}$P signal of **8(c)** appeared as a single peak at −25.44 ppm with satellite peaks giving coupling constants $^1J(^{187}Os–^{31}P)$ = 274 Hz. Complex **8(d)** showed a single peak due to P at −23.77 ppm. The non-chelate ring complexes also exhibited negative phosphorus chemical shifts. The environments of phosphorus atoms for the bridging compounds are expected to be less sterically crowded. The bond angles on the phosphorus atoms are expected to be less strained and consequently show downfield chemical shifts.

### 3.3.2 Infra-Red (IR) Spectroscopy

The stretching frequency of the B−F bonds was also observed in the infra-red spectra supporting the $^{19}$F NMR data for complexes **6** and **7(a)-(d)**. The stretching frequency due to $\nu_{(B\text{-}F)}$ was observed as a single peak for complex **6** at 1052 cm$^{-1}$ and 1046 cm$^{-1}$ for **7(a).** The three complexes **7(b)**, **7(c)** and **7(d)** show the presence of a B−F band at 1061 cm$^{-1}$. The observed difference in the B−F stretching frequency may be attributed to the stronger electrostatic interaction between the $BF_4$ and the complex cation of **7(a)**. The cation complex

comes closer to the counter ion resulting in possible hydrogen bonding between the fluorine atoms and the hydrogens on the arenes.

### 3.3.3 Raman Spectroscopy

The presence of the metal-halide bonds was confirmed by Raman spectroscopy for all nine complexes in this chapter. Complexes **6** and **7(a)-(d)** showed a single medium intensity vibrational peak due to the presence of a single Os−Br bond. Complex **6** displayed the Os−Br medium peak at 201 $cm^{-1}$ and a weak peak at 1056 $cm^{-1}$ attributed to $\nu_{(B\text{-}F)}$. Complex **7(a)** displayed the Os−Br medium peak at 205 $cm^{-1}$ and a weak peak due to at 1059 $cm^{-1}$. Complex **7(b)** displayed the Os−Br peak at 202 $cm^{-1}$ and a weak peak at 1056 $cm^{-1}$ due to $\nu_{(B\text{-}F)}$. Complex **7(c)** displayed a medium peak due to $\nu_{(Os\text{-}Br)}$ at 205 $cm^{-1}$ and a weak peak due to $\nu_{(B\text{-}F)}$ at 1060 $cm^{-1}$. Complex **7(d)** displayed a medium peak due to $\nu_{(Os\text{-}Br)}$ at 199 $cm^{-1}$ and a weak peak due to $\nu_{(B\text{-}F)}$ at 1057 $cm^{-1}$.

The four-bridged complexes **8(a)-(d)** displayed two peaks due to the two pairs of bromido ligands on each osmium centre. The two vibrational peaks were observed as an indication that the bromido ligands are bonded in a *cis* mode hence two bromide atoms exhibit symmetrical (intense peak) and anti-symmetrical (low intense peak) stretching vibrations. Complex **8(a)** exhibits two vibrational medium peaks at 208 and 183 $cm^{-1}$ (*see figure 3.7*), **8(b)** at 203 and 182 $cm^{-1}$, **8(c)** at 203 and 182 $cm^{-1}$, **8(d)** at 205 and 186 $cm^{-1}$. The Os–Br bands were assigned according to the literature data.[20]

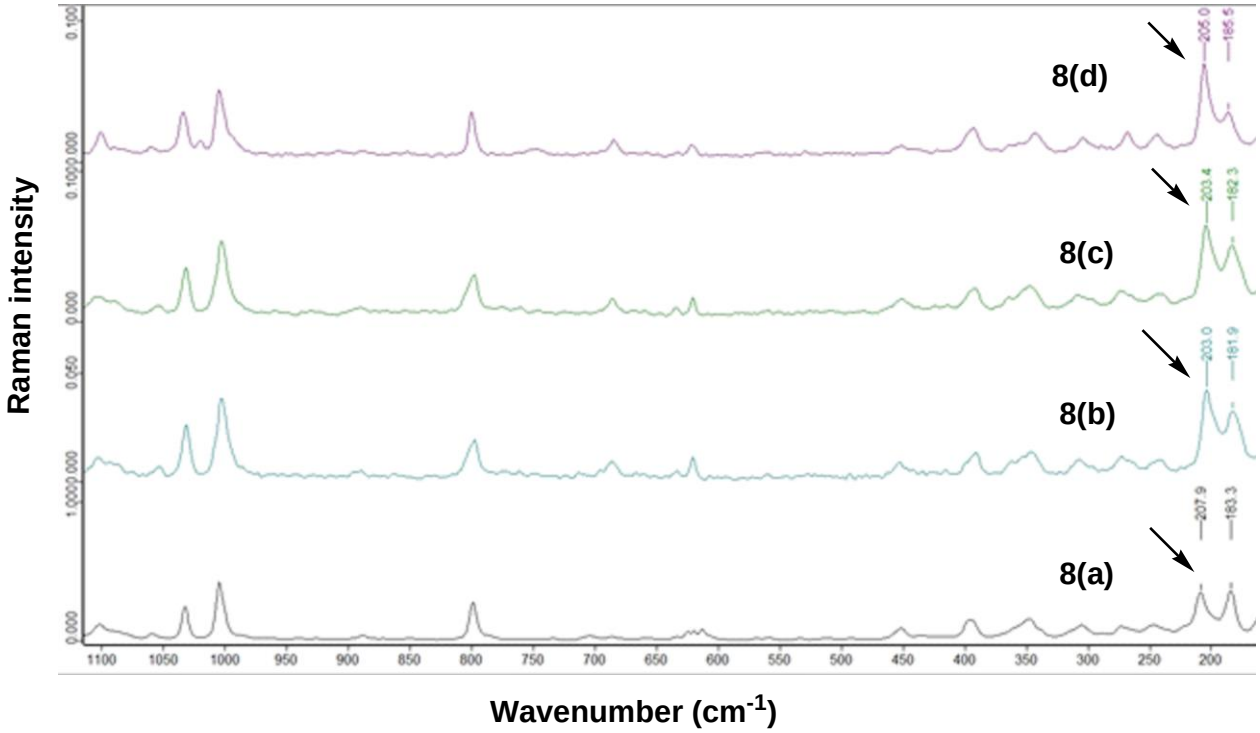


*Figure 3.7: Raman spectra of **8(a)-(d)** showing two Os−Br signals.*

3.3.4 Thermogravimetric analysis (TGA)

The thermal stability of the complexes was studied and the results show some similarity in degradation for complexes **6** and **7(a)-(d)**. Complex **6** shows four separate degradation steps (*see figure 3.8*). The first step corresponds to the loss of cymene at 227.6 to 267.9 ºC accounting for 12.5% mass loss. The second degradation step of 17.5% at 267.9 to 333.3 ºC was attributed to $BF_4$ counter ion and Ph fragment. The third degradation at 333.3 to 607.3 ºC accounting for 19.1% was attributed to the loss of $PPh_2$ fragment. The fourth degradation step at 607.3 to 774.8 ºC accounting for 7.9% was attributed to the loss of the Br ligand. The remaining 43% was attributed to [$Os(PPh_3)$] fragment.

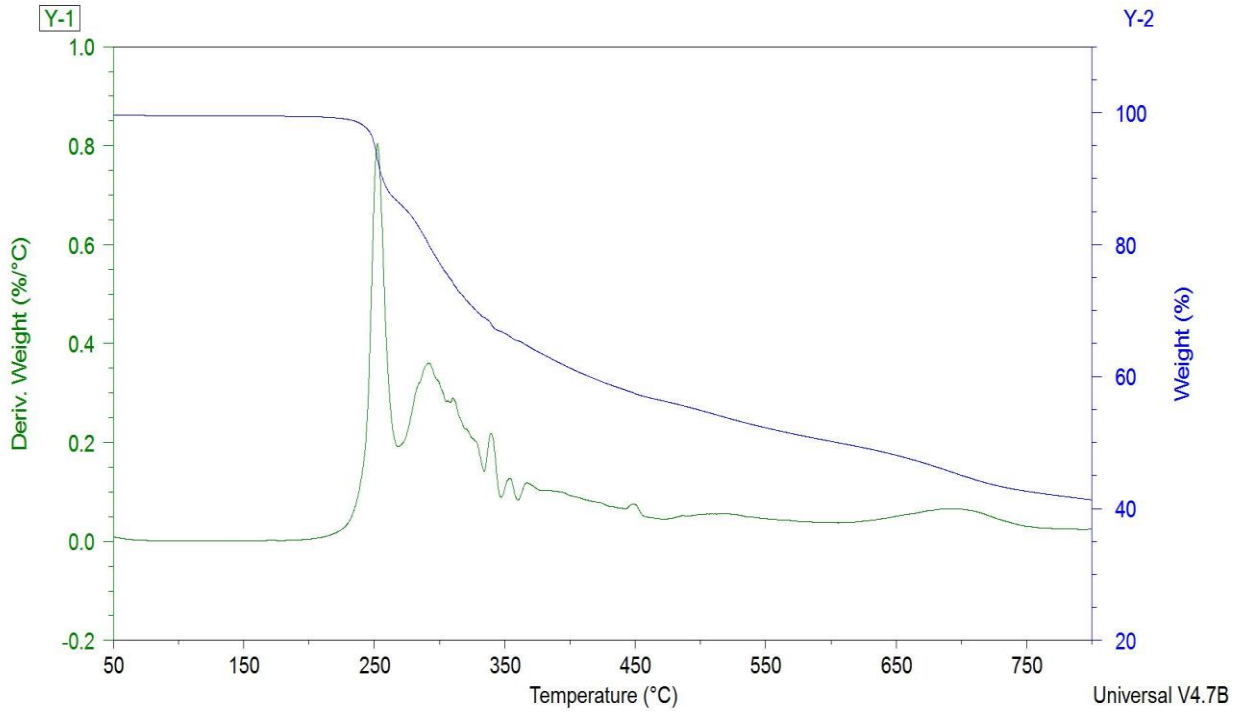


*Figure 3.8: TGA thermogram of **6** with DTG curve.*

In contrast, the chelated complexes **7(a)-(d)** degrade differently compared to the monodentate complex **6**. Complex **7(a)** shows 5.2% mass loss at 110.6 ºC attributed to the $CH_2Cl_2$ solvent. The onset decomposition of **7(a)** was observed at 287.1 to 380.9 ºC accounting for 30.5% mass loss attributed to cymene, Br and $BF_4$ counter ion. The second degradation was observed at 585.6 to 794.6 ºC accounting for 8.4% mass loss attributed to one phenyl group. The remaining 43% was attributed to the [$Os\{Ph_2P(CH_2)PPh\}$] fragment. Complex **7(b)** shows the mass loss at 108.1 ºC attributed to the $CH_2Cl_2$ solvent as observed in $^1H$ NMR data

accounting for 1.3%. The onset decomposition of **7(b)** was observed at 279.0 to 371.29 ºC accounting for 31.4% attributed to cymene, $BF_4$ and Br (*see figure 3.9*). The second degradation step at 476.7 to 586.9 ºC accounting for 8.9% mass loss was attributed to the loss of one phenyl group. The third degradation step was observed at 631.0 to 798.9 ºC accounting for 8.9% mass loss attributed to the second phenyl group. The remaining 38% of the mass was attributed to the [Os{PhP$(CH_2)_2$PPh}] fragment.

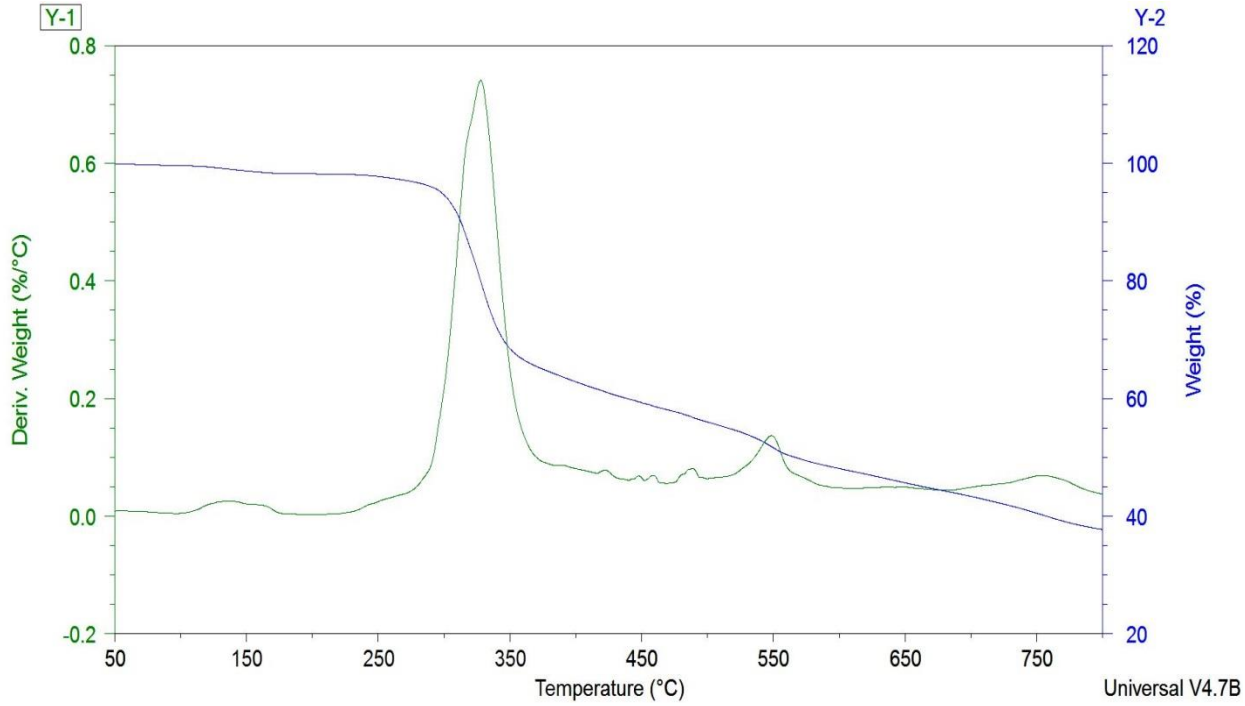


*Figure 3.9: TGA thermogram of **7(b)** with DTG curve.*

Complex **7(c)** shows the onset decomposition at 240.2 to 365.2 ºC accounting for 32.0% mass loss due to the cymene, $BF_4$ and Br. The second degradation was observed at 365.2 to 466.1 ºC accounting for 9.6% mass loss attributed to one phenyl group. The third degradation was observed at 537.6 to 722.5 ºC accounting for 8.9% attributed to the loss of the second phenyl group. The remaining 44% was attributed to [Os{PhP$(CH_2)_2$PPh}] fragment. Complex **7(d)** shows the onset decomposition at 217.99 to 353.6 ºC accounting for 32.1% mass loss attributed to cymene, $BF_4$ and Br. The second degradation step was observed at 355.0 to 516.0 ºC accounting for 14.4% mass loss attributed to the loss of one phenyl group and –$CH_2CH_2CH_2CH_2$– group. The remaining 53% fragment was attributed to [Os($PPh_2$)(PPh)] fragment (*see figure 3.10*). The chelated-diphosphine complexes shows a decrease in thermal stability as the alkyl chain length of the diphosphine ligand is increased to be: **7(a)** >**7(b)** > **7(c)** > **7(d)**.

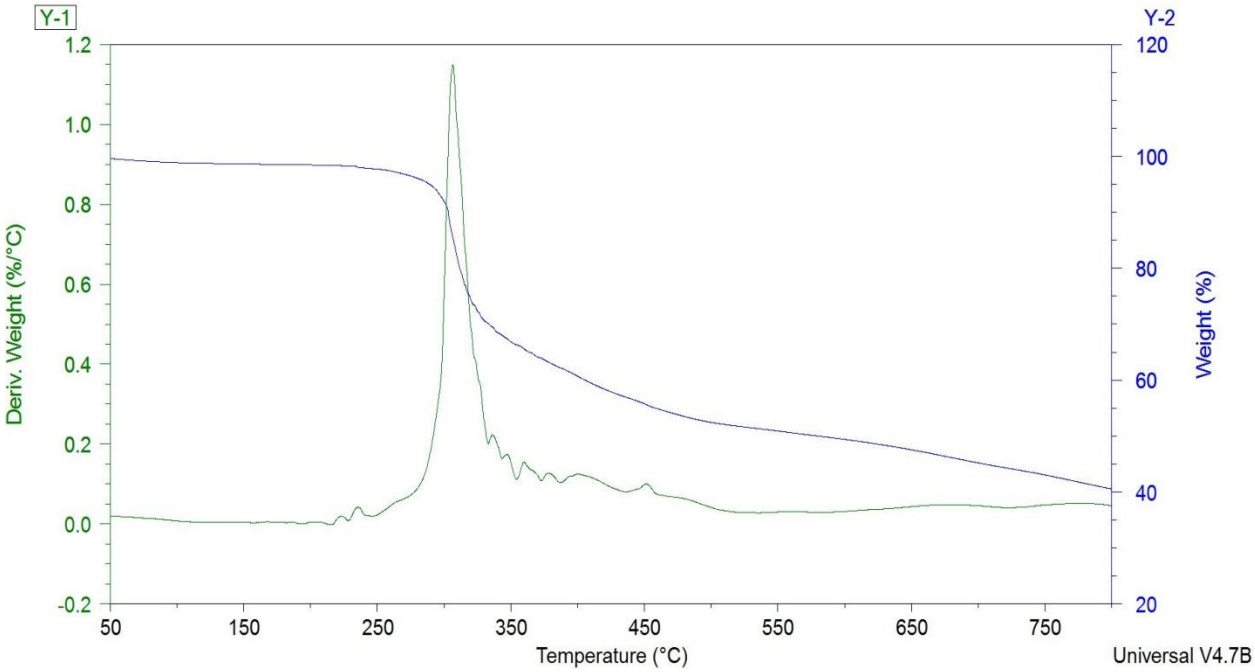


*Figure 3.10: TGA thermogram of **7(d)** with DTG curve.*

The bridging diphosphine osmium complexes **8(a)-(d)** were also tested for thermal stability. A two-step decomposition process followed by continuous degradation was observed for all four complexes. Complex **8(a)** degrades in several steps. The first step at 113.6 to 154.4 ºC was attributed to the loss of $CH_2Cl_2$ solvent. The onset decomposition was observed at 223.3 to 253.4 ºC accounting for 8.7% mass loss attributed to one cymene group. At 253.4 to 265.8

ºC the mass loss attributed to $CH_3CHCH_3$ group accounting for 2.9%. The next degradation was observed at 265.8 to 328.2 ºC accounting for 12.6% mass loss which was attributed to toluene and a phenyl group. At 328.2 to 385.2 ºC a mass loss of 7.3% was attributed to the phenyl group and the $-CH_2-$ fragments. At 385.2 to 554.1 ºC a mass loss of 28.4% was attributed to the loss of two bromide ligands and $P_2Ph_2$ fragment. At 662.8 to 799.9 ºC a mass loss of 19% was attributed to the loss of two bromide ligands and the reduction of the oxidised osmium compounds ($OsO_2/OsO_4$) to the Os metal which account for 12% residue.[21] Complex **8(b)** shows three degradation steps. The onset decomposition of **8(b)** was observed at 240.2 to 340.9 ºC accounting for 31.4% mass loss attributed to two cymene ligands and two bromide ligands (*see figure 3.11*). The second degradation was observed at 340.9 to 532.0 ºC accounting for 17.9% mass loss attributed to three phenyl groups. The third degradation was observed at 532.0 to 570.6 ºC accounting for 4.1% mass loss attributed to $PCH_2CH_2-$ fragment. The remaining [Br−Os−(PhP)−Os−Br] fragment account for 48% residue.

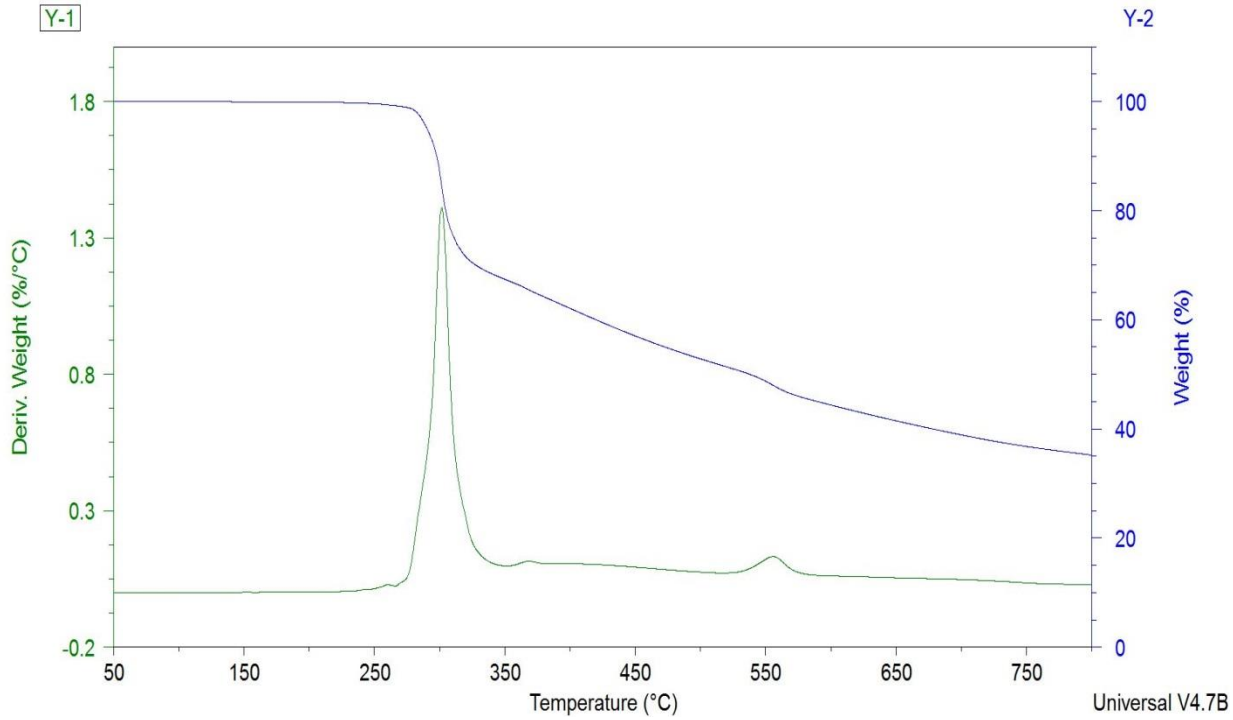


*Figure 3.11: TGA thermogram of **8(b)** with DTG curve.*

Complex **8(c)** shows the first degradation step at 235.4 to 355.9 ºC accounting for 31.2% mass loss, which was attributed to two cymene ligands and two Br ligands. The second step of degradation was observed at 355.9 to 509.4 ºC accounting for 13.2% mass loss attributed to two phenyl groups and $-CH_2CH_2CH_2-$ fragment. At 509.4 to 591.3 ºC, there was a mass loss of 6.1% attributed to one phenyl group. The last degradation step of 9.3% was observed at 591.3 to 770.1 ºC attributed to the loss of P–Ph fragment. The remaining 38.4% was attributed to [Br–Os(P)–Os–Br] fragment. Surprisingly, complex **8(d)** degrade in a similar manner as **8(c)**. The onset decomposition of **8(d)** was observed at 270.4 to 347.1 ºC accounting for 31.9% mass loss attributed to two cymene ligands and two Br ligands. The second degradation step was observed at 353.1 to 520.7 ºC accounting for 14.5% mass loss attributed to two phenyl groups and $-CH_2CH_2CH_2CH_2-$ fragment. The third degradation step was observed at 534.8 to 783.3 ºC accounting for 13.4% mass loss attributed to $P-Ph_2$ fragment. The remaining 38.4% residue was attributed to [Br–Os(P)–Os–Br] fragment. The three complexes **8(b)-(d)** shows similar pattern of fragment loss with **8(d)** being the most thermally stable followed by **8(b)** whereas **8(c)** was the least thermally stable complex. In general, the thermal stability trend of the bridged-diphosphine complexes was found to be: **8(d)** > **8(b)** > **8(c)** > **8(a)**.

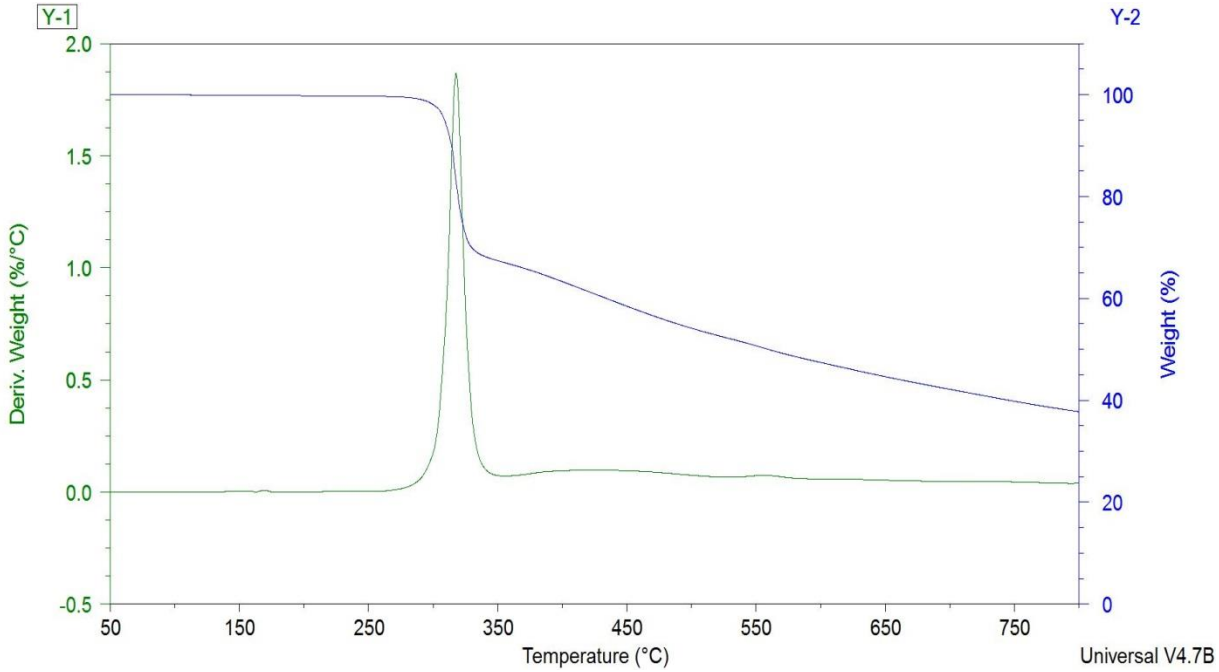


*Figure 3.12: TGA thermogram of **8(d)** with DTG curve.*

### 3.3.5 Conductivity studies

The five complexes **6** and **7(a)-(d)** were tested for conductivity because of their salt-like structures. Table 3.6 contains the molar conductivity data of complexes **6** and **7(a)-(d)**. The literature values for molar conductivities of 1:1 electrolytes in nitrobenzene at $10^{-3}$ M are found within the given range 20 − 30 S $cm^2$/mol.[22] Complex **6** recorded a value within the expected range (*see table 3.6*). These results may be attributed to the high mobility of the involved ions. Complexes **7(b)** and **7(d)** gave the molar conductivity values, which are within the expected range for complexes in nitrobenzene (*see table 3.6*). However, complexes **7(a)** and **7(c)** gave values that are lower than the expected range. The reason for these lower molar conductivities for complexes **7(a)** and **7(c)** may be attributed to their chemical structures, which contribute to their poor mobility in nitrobenzene.

*Table 3.6: The molar conductivity values of **6** and **7(a)-(d)** in nitrobenzene solvent.*

| Complex | $c \times 10^{-3}$M | Conductance ($c \times \mu$S)* | $\Lambda_M$ (S cm$^2$/mol) |
|---|---|---|---|
| **6** | 1.4 | 41.55 | 22.56 |
| **7(a)** | 1.1 | 27.45 | 18.97 |
| **7(b)** | 1.0 | 30.25 | 22.99 |
| **7(c)** | 1.2 | 25.45 | 16.12 |
| **7(d)** | 1.1 | 31.55 | 21.80 |

* The conductance of the samples were obtained after subtracting the value of the blank; Nitrobenzene = 3.45 μS from the measured values.

The molar conductivities of the complexes were obtained by the following calculations.

For complex **6**

$$\kappa = G \times K \quad \ldots\ldots [1]$$

Where $\kappa$ = conductivity (S/cm), G = conductance (S), K = cell constant (cm$^{-1}$)

Converting the conductivity to the molar conductivity the following equation was used:

$$\Lambda_M = \kappa / C_M \quad \ldots\ldots [2]$$

Where $\Lambda_M$ is the molar conductivity and $C_M$ is the molar concentration of **6** = $1.4 \times 10^{-3}$ M

Then substituting the values into equation [2] we obtain

$$\Lambda_M = 22.56 \text{ S cm}^2\text{/mol}$$

3.3.6 Crystallography

The molecular structures of complexes **6** and **7(a)-(d)** were confirmed by the single crystal X-ray diffraction. Table 3.7 contains the crystal data and structure refinements of complexes **6** and **7(a)-(d)**. Table 3.8 contains selected bond, interatomic and Os–centroid distances while Table 3.9 contains bond and torsion angles of complexes **6** and **7(a)-(d)**.

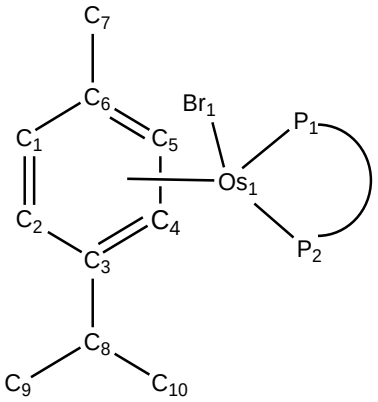


*Figure 3.13: The assignment pattern of molecular structures of complexes* ***6*** *and* ***7(a)-(d)*** *in this chapter.*

3.3.6.1 Molecular structure of **6**.

Crystals of **6** suitable for X-ray diffraction were obtained by slow diffusion of diethyl ether into dichloromethane solution at room temperature. Complex **6** was found to crystallise in a monoclinic crystal system with space group $P2_1/n$. Figure 3.11 shows the molecular structure of **6** with the fluorine atoms ellipsoids bigger than expected. Vibrations of the fluorine atoms within the crystal pockets may cause this ellipsoids to be bigger. The results of **6** showed alternating short and long C−C bonds around the cymene ligand which indicated loss of aromaticity. The sets of carbons, C(1)−C(2), C(3)−C(4) and C(5)−C(6) were observed to be longer than C(2)−C(3), C(4)−C(5) and C(6)−C(1). The torsion angle C(3)−C(2)−C(1)−C(6) supports the loss of aromaticity of the cymene ligand.

The cymene aromatic carbons bonded directly to the osmium centre display different bond distances. Carbon atoms C(2), C(3), C(4) and C(6) have longer bond distances to the osmium centre than C(1) and C(5). This was an indication of the *trans* influence of the strong π-acceptor phosphorus atoms. The distance from the osmium centre to the centroid of the cymene was found to be 1.784 Å. In contrast, the ruthenium analogue (ESOLUT[†7]) measured 1.793 Å which was slightly longer than the osmium analogue.[3] The observation was attributed to stronger interaction of the osmium and the cymene ligand. The loss of planarity was measured along the mean plane of C(1), C(2) and C(4), C(5). The C(3) showed some deviation by 0.067 Å above the mean plane and C(6) was 0.037 Å below the mean plane,

[†7] The CIF file used for comparison was obtained from the CCDC database.

which result in the cymene ligand adopting a chair conformation. The deviation from the mean plane was attributed to the presence of strong π-acceptor ability of the $PPh_3$ group.

The bond distances of the two phosphorus atoms bonded to the osmium centre were slightly different to each other. The Os(1)−P(1) bond distance was found to be longer relative to Os(1)−P(2) which indicated less interaction. In contrast, the Os(1)−P(2) bond distance was found to be shorter with the difference of 0.0339 Å compared to Os(1)−P(1). The interatomic distance of the two phosphorus atoms was measured as 3.600 Å at 98.00º influenced by steric crowding at the metal centre due to the bulky phenyl groups. This was supported by the chelate bite angle P(1)−Os(1)−P(2) which was above 90º an indication of distortion from the known octahedral geometry. The difference in M−P bond lengths, P(1)···P(2) interatomic distance and the P(1)−M−P(2) bite angles between the osmium and ruthenium analogues is negligible. In complex **6**, the longest bond was found to be the Os(1)−Br(1) which indicated weak interaction between the Os−Br bond.

Complex **6** shows four intramolecular and two intermolecular hydrogen bonding. The four intramolecular hydrogen bonding were all due to C−H···Br interaction. The intramolecular hydrogen bond C−H···Br due to hydrogen on C(10) measured 3.051 Å at 128.04º which indicated a weaker interaction. The other two intramolecular hydrogen bonds C−H···Br due to hydrogens on two phenyl groups on the same $PPh_3$ measures 3.017 Å at 146.91º and 2.782 Å at 128.43º (*see figure 3.14*). The last intramolecular hydrogen bond C–H···Br due to the hydrogen on the phenyl of the other $PPh_3$ measures 2.937 at 125.13º. The two intermolecular hydrogen bonds were on one fluorine atom bonding to two hydrogens of neighbouring carbons on the phenyl ring of one $PPh_3$ ligand (*see figure 3.14*). The two C−H···F hydrogen bonds measures 2.899 Å at 127.63º and 2.937 Å at 126.24º which was a weak interaction.[23]

The effect of coordination of two $PPh_3$ ligands at one metal centre is discussed here relative to the free $PPh_3$ ligand. The molecular structure of the free $PPh_3$ ligand (PTRPHE03[†8]) reported the C−P−C bond angles at 103.08º, 103.44º and 101.66º.[24] The coordinated $PPh_3$ in this study has C−P(1)−C bond angles measured at 97.12º, 100.23º and 106.88º. The second $PPh_3$ shows C−P(2)−C bond angles that were at 97.02º, 102.58º and 105.51º. The reduced C−P−C bond angle of the coordinated ligand indicates steric effects on the coordinated $PPh_3$ whereas the increased C−P−C bond angles may result from π-π repulsion between the phenyl groups. Therefore, the deviation of the C−P−C bond angles from the free ligand geometry

[†8] The CIF file used for comparison was obtained from the CCDC database.

towards the tetrahedral geometry (109.5º) may also have an impact on the upfield shift of $^{31}P$ NMR in solution. In addition, the free $PPh_3$ ligand has C−P bond lengths of 1.827 Å, 1.831 Å and 1.832 Å. However, in this study the C−P bond lengths were measured as 1.829 Å, 1.842 Å and 1.845 Å on P(1) atom while 1.836 Å, 1.837 Å and 1.842 Å were measured on P(2) atom.

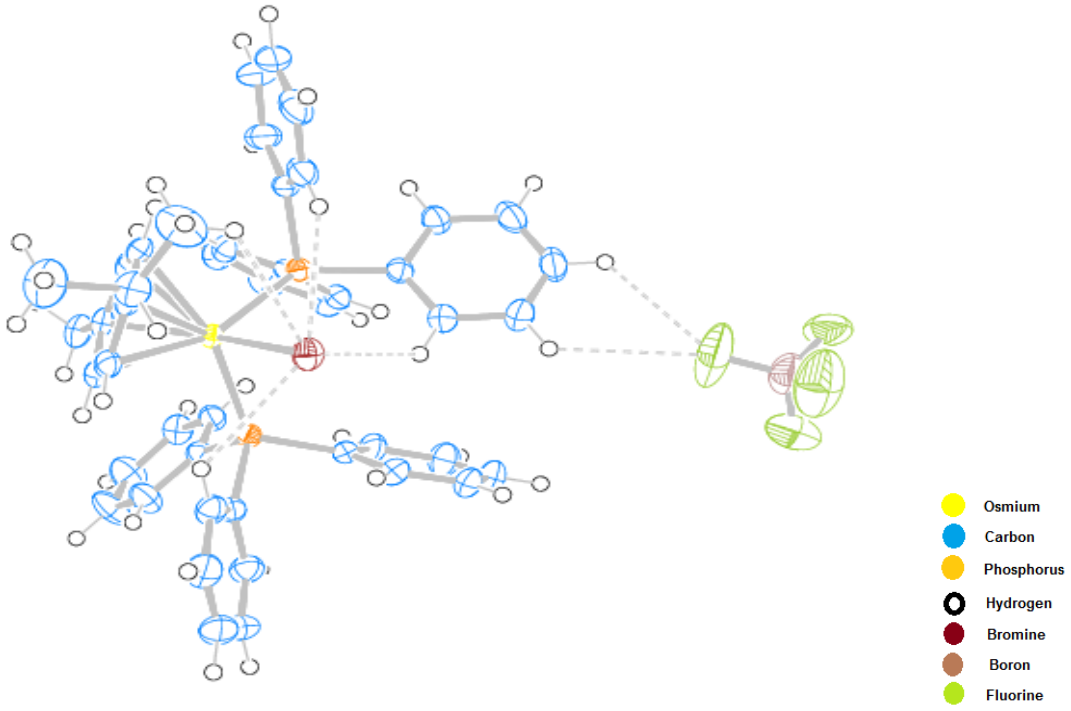


*Figure 3.14: Molecular structure of **6** at 50% probability thermal ellipsoids.*

3.3.6.2 The molecular structure of **7(a)**.

Crystals of **7(a)** suitable for single crystal X-ray diffraction were obtained by slow diffusion of diethyl ether into a dichloromethane solution. Complex **7(a)** was found to crystallise an orthorhombic system with space group $P2_12_12_1$. Figure 3.12 shows complex **7(a)** as a four membered chelate ring with one phenyl ring disordered at the P(2) atom. The carbon atoms on the phenyl groups show some disorientation resulting in larger ellipsoids than observed for aromatic carbons around the cymene. Loss of aromaticity was observed on the cymene ligand because of alternating long and short C−C bonds. C(2)−C(3), C(4)−C(5) and C(5)−C(6) were longer than C(1)−C(2), C(3)−C(4) and C(6)−C(1). In addition, the different Os−C bonds lengths were observed because of the *trans* influence of the P-donor ligands. In this case the both C atoms of the cymene and P atoms *trans* to each other share the *s* and *d*-orbitals, hence,

additional participation of *s* and *d* orbitals in the Os−P bond because of π-bonding capacity of P-donor ligands will result in a weaker Os−C bond. The ligands or C atoms *cis* to the P-donor ligand uses an independent *s* and *d* orbitals, therefore, would be less affected. The three carbon atoms on the cymene; C(3), C(4) and C(6) bonded to Os(1) atom exhibited longer bond lengths because of the phosphorus atoms *trans* to this three carbons. The distance from the osmium centre to the cymene centroid was observed to be 1.756 Å. In comparison, the ruthenium analogue (RAZLES[†9]) measured the Ru−centroid distance as 1.760 Å which is slightly longer than the Os−centroid distance in this study.[25]

Complex **7(a)** displayed steric strain with one phenyl group on P(2) showing some disorder. The disorder may be due to the steric effect caused by shorter chain length on the diphosphine. In addition, the steric effect hypothesis was also supported by the shortness of the Os−P bonds. The shorter carbon chain length of the diphosphine ligand also affects the bond angle which was observed to be smaller than in the free dppm ligand (73º).[26] Consequently, these factors bring more steric influence on the central metal and change the geometry at the metal centre. The two P-donor atoms exhibited a difference in M−P bond lengths of 0.0137 Å. Taking into account the two phenyl groups on each P atoms, limited space is available to accommodate the four phenyl groups on the four-membered chelate ring. This resulted in one phenyl group being forced to deviate from the natural dppm structure. The *π*-*π* stacking caused by the attractions or repulsions of π-systems may also be the reason one phenyl group on P(2) was disordered. The Os(1)−Br(1) bond was the longest bond which indicated weaker interaction of bromide ligand and the osmium centre.

Intermolecular hydrogen bonding between one fluorine atom and the H atoms on C(1), C(2) and one phenyl group were observed. The C−H···F hydrogen bond with the shortest distance was found on C(1) measuring 2.263 Å at 141.31º which indicated strong hydrogen bonding.[23] The fluorine involved in hydrogen bonding was found to have a shorter B−F bond (1.317 Å) than the other three B−F bonds. The hydrogen on C(2) showed two possible C−H···F hydrogen bonds with different fluorine atoms. The C−H···F hydrogen bonds on C(2) measures 2.782 Å at 144.05º and 2.660 Å at 130.01º (*see figure 3.15*). A further C−H···F hydrogen bond with an H atom on the phenyl group measures 2.666 Å at 128.02º. The loss of planarity on the cymene ligand was measured along the mean plane defined by C(1), C(2), C(4) and C(5). The deviation from planarity of C(3) was measured as 0.038 Å above the

[†9] The CIF file used for comparison was obtained from the CCDC database.

mean plane and for C(6) was measured as 0.071 Å above the mean plane. In this case, the cymene ligand adopts the boat conformation.

Coordination of the dppm ligand results in significant changes in bond lengths and angles, which are discussed below. The molecular structure of the free dppm ligand (GEHGAB02[†10]) measured the bond angle due to P−C−P at 107.63º and the coordinated dppm in this study measured at 93.50º.[27] This was attributed to the steric effects of the phenyl rings and the cymene ligand. The bond angles for the free dppm ligand due to C−P−C are reported at 103.12º and 101.53º for C($sp^3$)−P−($sp^2$) as well as 101.98º for C($sp^2$)−P−C($sp^2$). The second P atom of the free dppm ligand measured C($sp^3$)–P–C($sp^2$) at 99.94º and 103.17º while the C($sp^2$)−P−C($sp^2$) was measured at 101.22º.[27] In this study the C−P−C bond angles were measured at 106.58º for C($sp^3$)−P(1)−C($sp^2$), 110.20º for C($sp^3$)−P(1)−C($sp^2$) and 100.00º for C($sp^2$)–P(1)–C($sp^2$). The two C($sp^3$)–P(1)–C($sp^2$) bond angles at P(1) approach the tetrahedral value (109.5º) while the C($sp^2$)–P(1)–C($sp^2$) value remains similar to the values of the free dppm ligand.

On the P(2) atom with disorder the C–P–C bond angles were measured at 107.00º for C($sp^3$)–P(2)–C($sp^2$), 108.60º for C($sp^2$)–P(2)–C($sp^2$) and 102.50º for another C($sp^3$)–P(2)–C($sp^2$). The other set of bond angles are 92.50º for C($sp^2$)–P(2)–C($sp^2$), 114.60º for C($sp^3$)–P(2)–C($sp^2$) and 17.40º for another C($sp^2$)–P(2)–C($sp^2$). The C($sp^3$)–P(2)–C($sp^2$) and the C($sp^2$)–P(2)–C($sp^2$) values approaches that of the tetrahedral value while the other C($sp^3$)–P(2)–C($sp^2$) value remains within the values of the free dppm ligand. The dppm ligand has been strongly affected by electronic and steric effects upon coordination to the metal centre. The significant changes of the C–P–C bond angles towards tetrahedral geometry (109.5º) may also be an additional reason **7(a)** gave the most upfield shift in $^{31}$P NMR solution.

The C($sp^3$)−P bond lengths of the coordinated dppm ligand measured 1.846 Å for P(1) and 1.841 Å for P(2) while the free dppm measured C($sp^3$)−P as 1.847 Å and 1.855 Å. However, C($sp^2$)−P bond lengths of the free dppm ligands were measured as 1.827 Å and 1.837 Å on one P atom and the second P atom measured 1.830 Å and 1.841 Å. The coordinated dppm measured 1.803 Å and 1.821 Å on P(1) and 1.801 Å and 1.895 Å (disordered) on P(2) atom.

†[10] The CIF file used for comparison was obtained from the CCDC database.

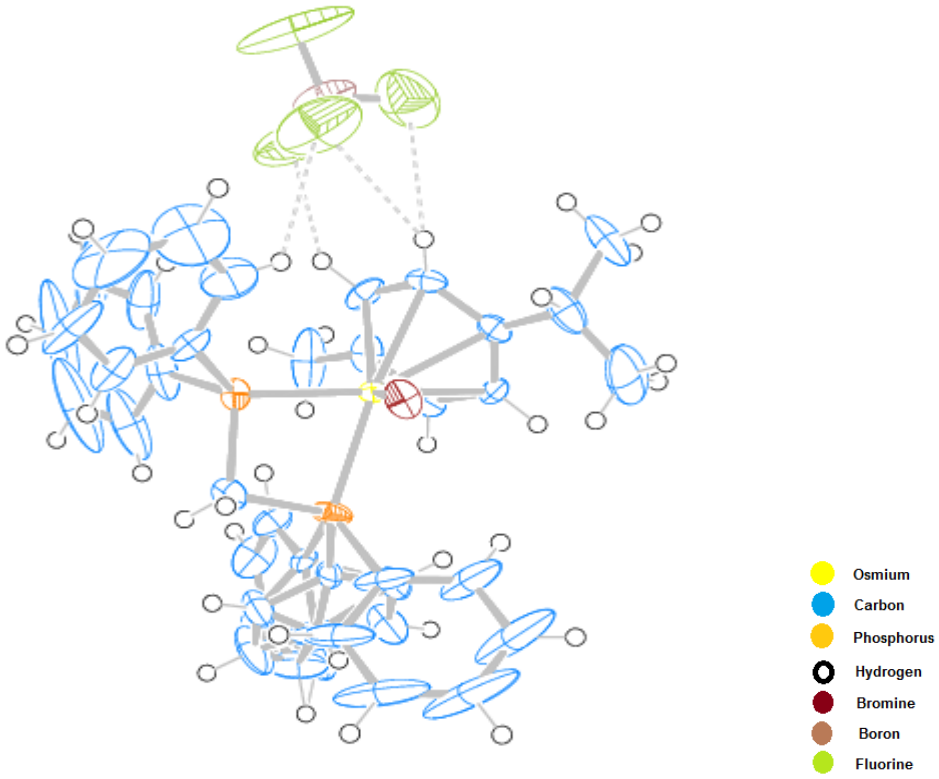


*Figure 3.15: Molecular structure of **7(a)** at 50% probability thermal ellipsoids.*

3.3.6.3 Molecular structure of **7(b)**.

Crystals of **7(b)** suitable for X-ray diffraction were obtained by slow diffusion of diethyl ether into a dichloromethane solution at room temperature. Complex **7(b)** crystallises in the orthorhombic system with a space group $P2_12_12_1$. Figure 3.16 shows the molecular structure of **7(b)** with short contacts due to hydrogen bonding. Loss of aromaticity in the cymene ligand was observed with alternating short and long C–C bonds. The sets of carbons with longer C–C bonds were C(2)–C(3) and C(4)–C(5), the shorter sets of carbons were C(1)–C(2) and C(3)–C(4) whereas C(5)–C(6) and C(6)–C(1) measured bond lengths which are intermediate. Complex **7(b)** measured different bond lengths from the Os centre to the carbons of the cymene. The Os(1)–C(3) and Os(1)–C(4) were found to measure longer bond lengths, whereas Os(1)–C(1), Os(1)–C(2) and Os(1)–C(5) were found to measure shorter bond lengths. The longer Os–C bonds indicated the effect of back bonding by the π-acceptor P atoms. The distance from the centroid to the metal centre was measured as 1.771 Å. In

contrast, the ruthenium analogue (RAHLIW[†11]) measured 1.786 Å for Ru−centroid$_{cymene}$ which is slightly longer than that of Os−centroid$_{cymene}$ distance.[25] This is an indication of stronger Os−cymene interaction compared to the Ru−cymene interaction.

The loss of planarity of the cymene ligand also supported the differences in Os−C bond lengths. The mean plane was defined by C(1), C(2), C(4) and C(5). C(3) measured 0.043 Å above the mean plane and C(6) measured 0.078 Å also above the mean plane. The steric effect and π-back bonding may be responsible for the deviation of C(3) and C(4) from the mean plane. The two carbon atoms, C(1) and C(4) measures 0.032 Å above the mean plane whereas C(2) and C(5) measures 0.033 Å and 0.032 Å below the mean plane respectively.

The bite angle P(1)–Os(1)–P(2) of **7(b)** measures 82.85º which is more acute than the ideal 90º expected in an octahedral arrangement. This observation may be attributed to the shorter carbon chain length of the dppe ligand. The interatomic distance of the two P atoms measured 3.087 Å at 180º. Two intermolecular hydrogen bonding were observed in the molecular structure of **7(b)**. The first C–H···F intermolecular hydrogen bond due to an H atom on one of the phenyl groups of P(2) measures 2.503 Å at 145.35º. The second C–H···F intermolecular hydrogen bond due to an H of the carbon on the alkyl backbone of the dppe measured 2.657 Å at 125.62º.

Similarly, the bond lengths and angles of the coordinated dppe and the free ddpe ligands were compared. The molecular structure of the free dppe ligand (DPPETH02[†12]) reported the following C–P–C bond angles. The bond angles were measured at 101.05º for C($sp^2$)–P–C($sp^2$), 100.22º and 102.37º for C($sp^2$)–P–C($sp^3$).[28] The C–P–C bond angles of **7(b)** were measured at 104.53º for C($sp^2$)–P(1)–C($sp^2$) and 98.66º for C($sp^2$)–P(2)–C($sp^2$). The other bond angles were measured at 103.58º and 104.34º for C($sp^2$)–P(1)–C($sp^3$) while bond angles on P(2) atom were measured at 104.52º and 105.33º. The small C($sp^2$)–P(2)–C($sp^2$) bond angle was caused by steric hindrance. The coordinated dppe measured the C($sp^3$)−P bond lengths as 1.831 Å in both P(1) and P(2) atoms but the uncoordinated dppe ligand measured C($sp^3$)−P bond length as 1.844 Å. The short C($sp^3$)−P bonds were caused by Os−P−C back-bonding.

†11 The CIF file used for comparison was obtained from the CCDC database.
†12 The CIF file used for comparison was obtained from the CCDC database.

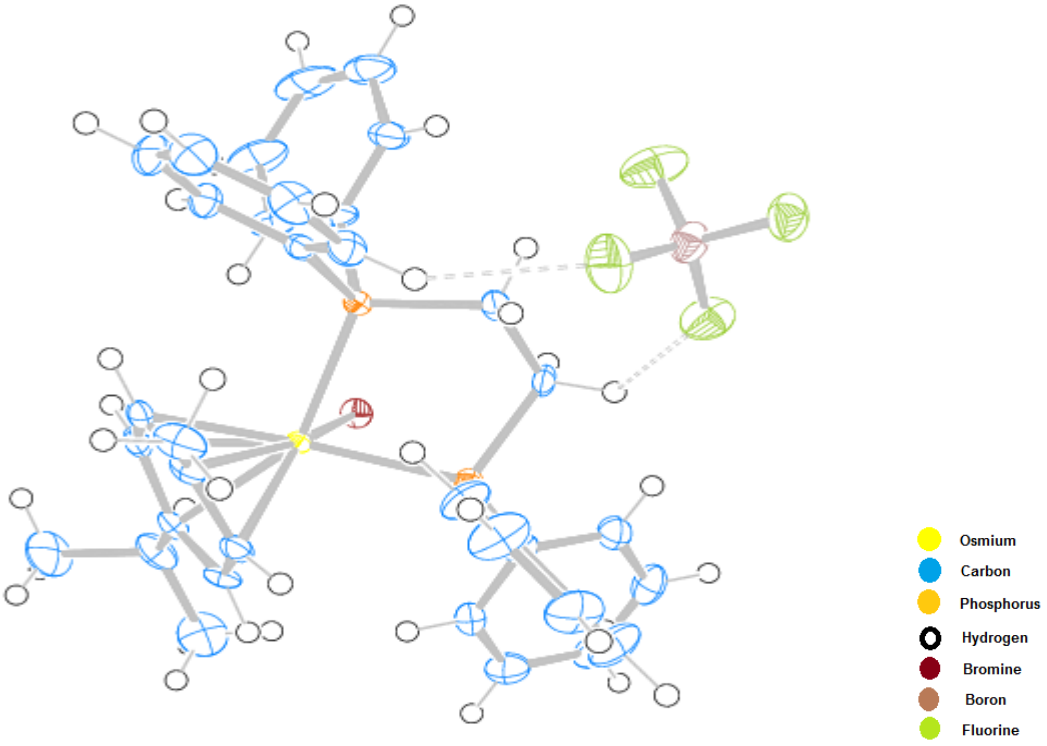


*Figure 3.16: Molecular structure of **7(b)** at 50% probability thermal ellipsoid.*

3.3.6.4 Molecular structure of **7(c)**.

Crystals of **7(c)** suitable for single crystal X-ray diffraction were obtained by slow diffusion of diethyl ether into dichloromethane solution at room temperature. The complex crystallises in a monoclinic crystal system with a space group $P2_1/n$. Figure 3.14 shows the molecular structure of **7(c)** as a six-membered chelate ring with short hydrogen contacts. The observed alternating short and long C–C bonds indicated loss of aromaticity of the cymene ligand. The three sets of carbons, C(2)–C(3), C(4)–C(5) and C(6)–C(1) measured longer bonds than C(1)–C(2), C(3)–C(4) and C(5)–C(6). The distance from the osmium to the centroid of the cymene was found to be 1.762 Å. The three carbon atoms C(3), C(4) and C(6) are observed to have longer bond distances to the osmium centre than three carbon atoms C(1), C(2) and C(5) on the cymene. An indication of how the π-back bonding affect the carbons on the cymene *trans* to the phosphorus atoms. The Os–P bond distances showed to be similar indicating a slight difference of 0.0025 Å.

The P(1)–Os(1)–P(2) bite angle measured greater than 90° to accommodate the long carbon chain length and four phenyl groups. The Os(1)–Br(1) bond was found to be longer than all bonds in the complex with 2.5545 Å because of weaker interaction due to the poor π-acceptor ability of the bromido ligand. One intramolecular and three intermolecular hydrogen bonds were observed. The weaker intramolecular hydrogen bond was due to C–H···Br, which measured 3.233 Å at 121.27º (*see figure 3.17*). The three intermolecular hydrogen bonds due to C–H···F measured 2.694 Å at 160.79º and 2.596 Å at 140.26º with the same F atom while the weak C–H···F hydrogen bond measured 2.993 Å at 128.56º with the second F atom (*see figure 3.17*). Loss of planarity of the cymene ligand as measured along the C(1), C(2), C(4) and C(5) mean plane was observed. The deviation of C(3) was measured as 0.006 Å above the mean plane and for C(6) was 0.035 Å above the mean plane. The cymene ligand adopted a boat conformation. The molecular structure of the free dppp ligand was reported with disorder; hence, the chelated-dppp in this study was not compared to the free dppp ligand.

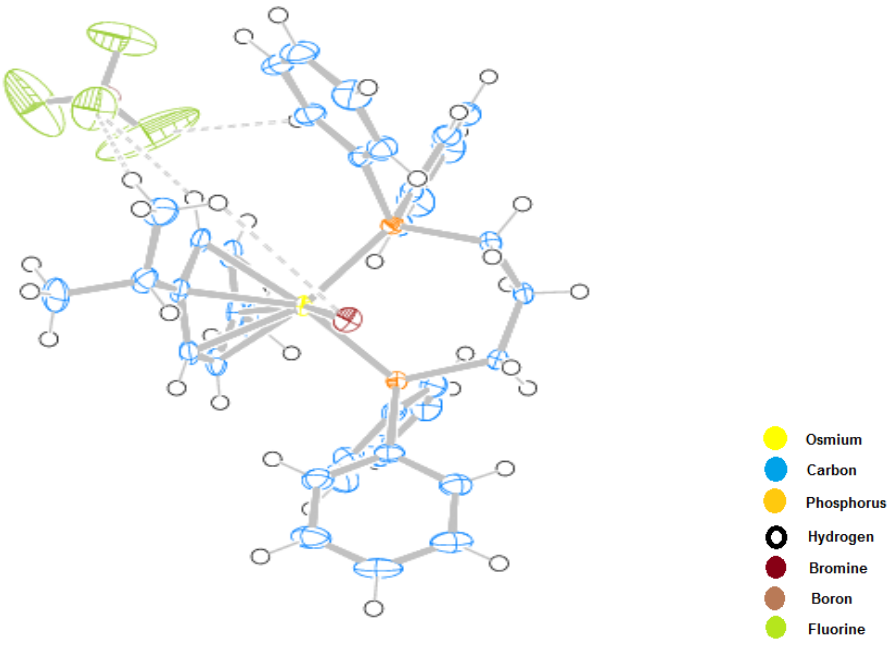


*Figure 3.17: Molecular structure of **7(c)** at 50% probability thermal ellipsoids.*

3.3.6.5 Molecular structure of **7(d)**.

Crystals of **7(d)** suitable for X-ray diffraction were obtained by slow diffusion of diethyl ether into a dichloromethane solution at room temperature. Complex **7(d)** crystallises in a monoclinic crystal system with $P2_1/n$ space group. Figure 3.15 shows the molecular structure of **7(d)**, which has a seven-membered chelate ring. The fluorine atoms of the $BF_4$ counter ion show disorder with large ellipsoids. This may result from vibrations or electronic effects during interactions with the complex ion. The loss of aromaticity was observed in the cymene ligand with alternating short and long C–C bond lengths. The three sets of carbons which measured shorter bond lengths were C(1)–C(2), C(3)–C(4) and C(5)–C(6) compared to C(2)–C(3), C(4)–C5) and C(6)–C(1) which measured longer C–C distances. The Os−C bond lengths showed evidence of the *trans* influence of the P atoms because of different Os−C bond lengths. The four carbons C(1), C(2), C(5) and C(6) have shorter distances to the Os centre compared to C(3) and C(4).

The distance from the Os centre to the centroid of the cymene was measured at 1.770 Å. The bite angle P(1)–Os(1)–P(2) was measured at 94.45º. The P–Os–P bite angle increases with an increase in carbon chain length. Hence, the coordinated dppb exhibits slight differences in $^{31}P$ NMR data compared to the free ligand. The Os(1)–Br(1) bond distance was observed to be the longest bond length compared to all bonds in the complex because electronegative atoms keeps their electrons towards themselves resulting in weaker interactions.

There were two intramolecular and two intermolecular hydrogen bonding interactions observed. The weak intramolecular interaction of C–H···Br measured 2.899 Å at 123.81º due to an H atom of the alkyl carbon on the dppb (*see figure 3.18*). A weak intramolecular bond C–H···Br measured 3.107 Å at 126.45º due to interaction of an H atom on C(10) (*see figure 3.18*). The two intermolecular hydrogen bonds were due to two hydrogens of neighbouring carbon atoms on the phenyl ring and the two fluorine atoms of $BF_4$ anion (*see figure 3.18*). The intermolecular C–H···F hydrogen bond measured 2.676 Å at 145.69º. The second intermolecular C–H···F hydrogen bond measured 2.649 Å at 129.95º (*see figure 3.18*).The loss of planarity was measured along the mean plane defined by C(1), C(2), C(4) and C(5). The deviation of C(3) from the mean plane was found to be 0.025 Å above the mean plane and C(6) deviated by 0.037 Å above the mean plane, which suggest that the cymene ligand adopted a boat conformation. The torsion angle of C(3) to C(6) along C(1) and C(2) was measured at 3.90º also supports the claim of loss of planarity. This may be attributed to the

steric crowding around the osmium centre by the phenyl rings resulting in the bending of the methyl and propyl substituents of the cymene above the mean plane. The *trans* influence of the P-donor atoms also contributed to the loss of planarity of the cymene ligand.

The effects of coordination of the dppb ligand relative to the free dppb ligand were compared. The molecular structure of the free dppb ligand (GASVUR01[†13]) measured the bond angles due to C($sp^2$)–P–C($sp^2$) at 100.63º, C($sp^2$)–P–C($sp^3$) at 100.83º and 102.24º.[29] In this study, the C–P–C angles were measured at 101.52º for C($sp^2$)–P(1)–C($sp^2$), 99.82º and 103.52º for C($sp^2$)–P(1)–C($sp^3$). On the second P atom, the bond angles were measured at 103.78º for C($sp^2$)–P(2)–C($sp^2$), 101.85º for C($sp^2$)–P(2)–C($sp^3$) and another C($sp^2$)–P(1)–C($sp^3$) at 98.96º. There was a slight difference between the C($sp^3$)−P(1) (1.828 Å) and C($sp^3$)−P(2) (1.838 Å) bond lengths of the coordinated dppb, which are slightly shorter than the C($sp^3$)−P (1.847 Å) of the free dppb ligand. The differences were attributed to the Os−P−C back bonding. There was a negligible effect on the bond angles of the coordinated dppb relative to the free dppb ligand.

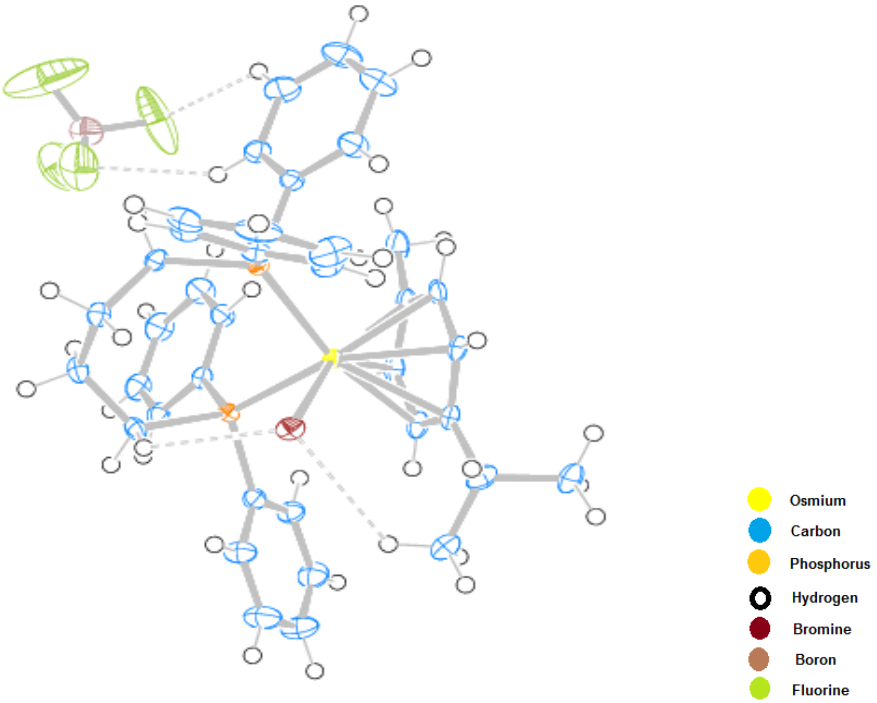


*Figure 3.18: Molecular structure of **7(d)** at 50% probability thermal ellipsoids.*

†[13] The CIF file used for comparison was obtained from the CCDC database.

*Table 3.7: Crystal data and structure refinement of **6** and **7(a)-(d)**.*

| | **6** | **7(a)** | **7(b)** | **7(c)** | **7(d)** |
|---|---|---|---|---|---|
| Chemical formula | $C_{46}H_{44}BBrF_4OsP_2$ | $C_{35}H_{36}BBrF_4OsP_2$ | $C_{36}H_{38}BBrF_4OsP_2$ | $C_{37}H_{40}BBrF_4OsP_2$ | $C_{38}H_{42}BBrF_4OsP_2$ |
| Chemical formula weighed | 1015.67 | 874.99 | 889.52 | 903.55 | 917.58 |
| Crystal system | Monoclinic | Orthorhombic | Orthorhombic | Monoclinic | Monoclinic |
| Space group | $P2_1/n$ | $P2_12_12_1$ | $P2_12_12_1$ | $P2_1/n$ | $P2_1/n$ |
| Crystal colour and shape | Reddish cubes | Yellow cubes | Yellow cubes | Yellow cubes | Yellow rectangles |
| a(Å) | 11.0792(7) | 11.7760(5) | 12.4702(13) | 11.1986(5) | 11.2054(9) |
| b(Å) | 30.180(2) | 15.3492(6) | 15.2982(15) | 24.2160(12) | 24.899(2) |
| c(Å) | 12.4379(9) | 18.4176(6) | 17.2694(17) | 12.7674(6) | 12.6930(9) |
| α(º) | 90.00 | 90.00 | 90.00 | 90.00 | 90.00 |
| β(º) | 103.606(3) | 90.00 | 90.00 | 98.859(2) | 97.223(2) |
| γ(º) | 90.00 | 90.00 | 90.00 | 90.00 | 90.00 |
| V(Å$^3$) | 4042.2(5) | 3329.0(2) | 3294.5(6) | 3421.0(3) | 3513.3(5) |
| Z | 4 | 4 | 4 | 4 | 4 |
| T(K) | 243(2) | 173(2) | 173(2) | 173(2) | 173(2) |
| $D_{calc}$ (mg/m$^3$) | 1.669 | 1.746 | 1.793 | 1.754 | 1.735 |
| Reflections collected | 49781 | 124299 | 71858 | 105074 | 100808 |
| Independent reflections | 9770 [R(int) = 0.0667] | 8049 [R(int) = 0.0583] | 7950 [R(int) = 0.0815] | 8249 [R(int) = 0.0594] | 8458 [R(int) = 0.1271] |
| F(000) | 2008 | 1710 | 1744 | 1776 | 1808 |
| Final R indices [I>2σ(I)] | R1 = 0.0241, wR2 = 0.0484 | R1 = 0.0249, wR2 = 0.0527 | R1 = 0.0238 wR2 = 0.0530 | R1 = 0.0258, wR2 = 0.0536 | R1 = 0.0323, wR2 = 0.0756 |
| R indices (all data) | R1 = 0.0351, wR2 = 0.0503 | R1 = 0.0256, wR2 = 0.0531 | R1 = 0.0258 wR2 = 0.0544 | R1 = 0.0326, wR2 = 0.0566 | R1 = 0.0403, wR2 = 0.0802 |
| Goodness-of-fit on $F^2$ | 0.965 | 1.114 | 1.077 | 0.884 | 1.111 |
| Largest diff. peak and hole | 0.814 and −1.144 e.Å$^{-3}$ | 0.709 and −0.760 e.Å$^{-3}$ | 0.625 and −1.107 e.Å$^{-3}$ | 1.341 and −0.938 e.Å$^{-3}$ | 1.423 and −1.501 e.Å$^{-3}$ |

*Table 3.8: Selected bond lengths (Å), Os–centroid$_{cymene}$ distance (Å) and interatomic distances (Å) of **6** and **7(a)-(d)**.*

| **Atom type label** | **6** | **7(a)** | **7(b)** | **7(c)** | **7(d)** |
|---|---|---|---|---|---|
| Os(1)–C(1) | 2.217(2) | 2.220(4) | 2.243(4) | 2.242(3) | 2.249(3) |
| Os(1)–C(2) | 2.286(2) | 2.243(4) | 2.243(4) | 2.244(3) | 2.252(3) |
| Os(1)–C(3) | 2.346(2) | 2.323(4) | 2.347(4) | 2.307(3) | 2.327(3) |
| Os(1)–C(4) | 2.260(2) | 2.283(4) | 2.288(4) | 2.283(3) | 2.291(4) |
| Os(1)–C(5) | 2.233(3) | 2.192(4) | 2.189(3) | 2.211(3) | 2.201(4) |
| Os(1)–C(6) | 2.291(2) | 2.269(4) | 2.278(4) | 2.266(3) | 2.258(4) |
| C(1)–C(2) | 1.416(3) | 1.402(7) | 1.397(6) | 1.404(5) | 1.396(5) |
| C(2)–C(3) | 1.402(3) | 1.427(7) | 1.436(6) | 1.426(5) | 1.427(5) |
| C(3)–C(4) | 1.411(3) | 1.104(6) | 1.388(6) | 1.400(5) | 1.402(6) |
| C(4)–C(5) | 1.402(3) | 1.432(6) | 1.427(6) | 1.428(5) | 1.418(6) |
| C(5)–C(6) | 1.418(3) | 1.420(6) | 1.415(6) | 1.403(5) | 1.409(6) |
| C(6)–C(1) | 1.404(4) | 1.411(7) | 1.417(6) | 1.420(5) | 1.411(6) |
| Os(1)–P(1) | 2.4019(6) | 2.3138(11) | 2.3386(10) | 2.3379(8) | 2.3507(9) |
| Os(1)–P(2) | 2.3680(7) | 2.3275(11) | 2.3265(10) | 2.3354(8) | 2.3605(9) |
| P(1)···P(2) | 3.600 | 2.6862(18) | 3.087 | 3.368 | 3.458 |
| Os(1)–Br(1) | 2.5345(3) | 2.5302(4) | 2.5401(4) | 2.5545(3) | 2.5483(4) |
| Os(1)–centroid$_{cymene}$ | 1.784 | 1.756 | 1.771 | 1.762 | 1.770 |

*Table 3.9: Selected bond and torsion angles (°) of **6** and **7(a)-(d)**.*

| **Bond angles** | **6** | **7(a)** | **7(b)** | **7(c)** | **7(d)** |
|---|---|---|---|---|---|
| P(1)–Os(1)–P(2) | 98.00(2) | 70.73(5) | 82.85(3) | 92.23(3) | 94.45(3) |
| P(1)–Os(1)–Br(1) | 90.200(17) | 85.28(3) | 81.41(3) | 81.99(2) | 87.96(2) |
| P(2)–Os(1)–Br(1) | 88.266(17) | 84.04(3) | 89.71(3) | 84.84(2) | 84.75(2) |
| **Torsion angles** | | | | | |
| C(3)–C(2)–C(1)–C(6) | 3.0(4) | 1.2(7) | 4.6(6) | 1.9(5) | 3.9(5) |
| C(3)–C(4)–C(5)–C(6) | 0.2(4) | 4.2(6) | 7.7(5) | 4.7(5) | 5.0(5) |

## 3.4 Conclusions

In this chapter, nine novel osmium cymene complexes with phosphine ligands are reported. The spectroscopic techniques (NMR, IR and Raman) played an important role in characterisation of the nine osmium cymene complexes in this chapter. The cationic complexes have shown interesting electrostatic interaction with $BF_4$ anion in $^{19}F$ NMR studies. The $^{31}P$ NMR studies revealed additional osmium satellite peaks with small coupling constant, which were postulated to be caused by the most abundant $^{189}Os$ isotope.

Single crystal X-ray diffraction confirmed the molecular structures of **6** and **7(a)-(d)**. The ability of the diphosphine ligands to form strong chelates increase with a decrease in carbon chain length on the diphosphine backbone, observed from their M–P bond lengths. The bite angles of the complexes **7(a)-(d)** increases with an increase in carbon chain length. Complex **6** and **7(d)** shows longer Os–P bond lengths than the complexes **7(a)-(c)** which supports the $^1H$ NMR data. Hence, the downfield shift of the aromatic cymene protons $H_b$ and $H_c$ suggest shorter Os–P bond lengths and upfield aromatic cymene $H_b$ and $H_c$ suggest longer Os–P bond lengths. The *trans* influence of the P-donor atoms has affected the same aromatic carbons of the cymene ligand, which indicated that the chelating diphosphines are coordinated in a similar manner. Also the electronic effects of the diphosphine ligands with regards to the deviation from the mean plane seem to decreases with an increase in carbon chain length.

The Os-centroid$_{cymene}$ distance was observed to be larger for **7(b)** and **7(d)**, however, **7(a)** and **7(c)** have shorter Os-centroid$_{cymene}$ distances. The B–F bonds for all the complexes in this study were found to fall within the range 1.317 – 1.395 Å which were comparable to the values in literature.[30] Complexes **6**, **7(c)** and **7(d)** have at least one intramolecular hydrogen bonding interaction with the bromine ligand. All the cation complexes have at least one intermolecular hydrogen bonding interaction with the $BF_4$ counter ion. The *in vitro* anticancer activity results of the nine complexes reported here will be discussed in Chapter 5.

## 3.5 References


(1) Barthel-Rosa, L. P.; Maitra, K.; Nelson, J. H. *Inorg. Chem.* **1998**, *37*, 633.

(2) Polam, J. R.; Porter, L. C. *Inorg. Chim. Acta* **1993**, *205*, 119.

(3) Lalrempuia, R.; Carroll, P. J.; Kollipara, M. R. *J. Coord. Chem.* **2003**, *56*, 1499.

(4) Berners-Price, S. J.; Johnson, R. K.; Giovenella, A. J.; Faucettem, L. F.; Mirabelli, C. K.; Sadler, P. J. *J. Inorg. Biochem.* **1988**, *33*, 285.

(5) Deeming, A. J.; Donovan-Mtunzi, S.; Kabir, S. E. *J. Organomet. Chem.* **1984**, *276*, 65.

(6) Jensen, S. B.; Rodger, S. J.; Spicer, M. D. *J. Organomet. Chem.* **1998**, *556*, 151.

(7) Chaplin, A. B.; Fellay, C.; Laurenczy, G.; Dyson, P. J. *Organomet.* **2007**, *26*, 586.

(8) Karami, K.; Hosseini-Kharat, M.; Sadeghi-Aliabadi, H.; Lipkowski, J.; Mirian, M. *Eur. J. Med. Chem.* **2014**, *73*, 8.

(9) Ozer, Z.; Ozkar, S. *Turk. J. Chem.* **1999**, *23*, 9.

(10) Casey, C. P.; Petrovich, L. M. *J. Am. Chem. Soc.* **1995**, *117*, 6007.

(11) Tang, J.-H.; Shao, J.-Y.; He, Y.-Q.; Wu, S.-H.; Yao, J.; Zhong, Y.-W. *Chem. Eur. J.* **2016**, *10*, 1002.

(12) Bennett, M. A.; Byrnes, M. J.; Willis, A. C. *Dalton Trans.* **2007**, 1677.

(13) Fiedler, T.; Bhuvanesh, N.; Hampel, F.; Reibenspiesa, J. H.; Gladysz, J. A. *Dalton Trans.* **2016**, *45*, 7131.

(14) Akitt, J. W. *J. Chem. Soc., Faraday Trans. 1* **1975**, *71*, 1557.

(15) Gillespiej, R. J.; Hartmanan, S.; Parekh, D. M. *Can. J. Chem.* **1968**, *46*, 1601.

(16) Kühl, O. *Phosphorus-31 NMR Spectroscopy A Concise Introduction for the Synthetic Organic and Organometallic Chemist*; Springer-Verlag: Berlin Heidelberg, 2008.

(17) Clayton, H. S.; Makhubela, B. C. E.; Su, H.; Smith, G. S.; Moss, J. R. *Polyhedron* **2009**, *28*, 1511.

(18) Eichele, K.; Wasylishen, R. E.; Corrigan, J. F.; Taylor, N. J.; Carty, A. J.; Feindel, K. W.; Bernard, G. M. *J. Am. Chem. Soc.* **2002**, *124*, 1541.

(19) Garrou, P. E. *Chem. Rev.* **1981**, *81*, 229.

(20) Bottger, G. L.; Damsgard, C. V. *Spectrochim. Acta* **1972**, *28A*, 1631.

(21) Brown, M. E. *Introduction to thermal analysis: techniques and applications*; Chapman and Hall Ltd: London and New York 1988.

(22) Geary, W. J. *Coord. Chem. Rev.* **1971**, *7*, 81.

(23) Desiraju, G. R. *Acc. Chem. Res.* **1991**, *24*, 290.

(24) Bruckmann, J.; Kruger, C.; Lutz, F. *Z. Naturforsch.* **1995**, *50*, 351.

(25) Daguenet, C.; Scopelliti, R.; Dyson, P. J. *Organomet.* **2004**, *23*, 4849.

(26) Birkholz, M.-N.; Freixa, Z.; van Leeuwen, P. W. N. M. *Chem. Soc. Rev.* **2009**, *38*, 1099.

(27) Burrow, R. A.; Wouters, F. C.; Borges de Castro, L.; Peppe, C. *Acta Cryst.* **2007**, *63*, 9.

(28) Tiekink, E. R. T. *Z. Kristallogr. NCS* **2001**, *216*, 69.

(29) Bruckmann, J.; Kruger, C. *J. Organomet. Chem.* **1997**, *536*, 465.

(30) Kuratieva, N. V.; Tkach, V. S.; Suslov, D. S.; Bykov, M. V.; Gromilov, S. A. *J. Struct. Chem.* **2011**, *52*, 813.

# CHAPTER 4

## SYNTHESIS OF OSMIUM CYMENE COMPLEXES WITH N- AND/OR P-DONOR LIGANDS

### 4.1 Background

The chemistry of monodentate N-donor ligands has been studied extensively.[1,2] The widely used polar aprotic solvent acetonitrile ($CH_3CN$) is commonly incorporated as a labile ligand in transition metal complexes. The preparation method of ruthenium arene complex $[Ru(\eta^5\text{-}C_5H_5)(CH_3CN)_3]^+$ with acetonitrile ligands were reported by Moriaty and co-workers.[3] The ruthenium complex with two different arene ligands $[Ru(\eta^5\text{-}C_5H_5)(\eta^6\text{-}C_6H_6)]PF_6$ irradiated in $CH_3CN$ solution yielded the trisacetonitrile cyclopentadienyl ruthenium species $[Ru(\eta^5\text{-}C_5H_5)(CH_3CN)_3]PF_6$ which can be used as a starting material for the synthesis of a variety of ruthenium arene complexes. Thorburn and co-workers[4] reported the synthesis of ruthenium complexes $[\{Ru(dppb)(CH_3CN)\}_2\mu\text{-}Cl_3]PF_6$ and *fac*-$[RuCl(dppb)(CH_3CN)_3]PF_6$ from $Ru_2Cl_5(dppb)_2$. The *fac*-tris(acetonitrile) ruthenium complex has shown some catalytic properties for homogenous hydrogenation of terminal olefins and imines.

Complexes with $PPh_3$ and $CH_3CN$ ligands on the same metal centres are also known. Copper complexes with $PPh_3$ and $CH_3CN$ with distorted tetrahedral geometry have been reported.[5] The ruthenium complex $[Ru(\eta^6\text{-}p\text{-cymene})Cl(CH_3CN)(PPh_3)]^+$ with both N-donor and P-donor ligands was reported by Chaplin and co-workers.[6] Transition metal complexes with ligands that contain borderline donor N- and hard donor O-ligating sites have been reported.[7] These types of complexes exhibit various electronic and steric properties as well as various coordination modes. The 2-aminobenzamide ligand has been coordinated to 3d transition metals such as Cu(II), Ni(II) and Zn(II) which chelates through the N-amino and O-amido functional groups to form stable six-membered chelate ring complexes.[7]

In medicine, ruthenium arene complexes with labile ligands such as $CH_3CN$ were found to be inactive against ovarian because of the poor stability of the complex.[8] Ruthenium arene complexes with a $PPh_3$ ligand however, were found to exhibit enhanced anticancer activities attributed to the presence of the $PPh_3$ ligand.[9] The organic benzamide derivatives are known

to exhibit biological activities such as anticancer, antimicrobial, antimalarial, analgesic and anti-inflammatory properties.[10] Hence, when coordinated to transition metals such as Co(II), Cu(II) and Ni(II), these benzamide derivatives exhibit antimicrobial and anticancer activities.[10] In this chapter, osmium cymene complexes with monodentate N- and P-donor ligands are reported.

### 4.2 Preparation of monodentate N- and P-donor osmium cymene complexes

The use of metal arene dimers bridged with halides presented an opportunity to synthesise bisacetonitrile complexes at room temperature.[11] The halides bridge the two metal centres by forming a dative bond and a coordinate bond to the metal centres. This results in the halide having reduced electron density; hence, an electron pair donor solvent easily cleaves the metal-halide dative bond resulting in a vacant coordinate site. This allows a σ-donor ligand such as $CH_3CN$ to coordinate to the metal centre. The preparation of **9** was adopted with modifications from the method reported by Jensen and co-workers.[11] The bromide bridged osmium dimer was stirred at room temperature in excess acetonitrile in the presence of $NH_4BF_4$ salt. Complex **10** was prepared with the method adopted from Chaplin and co-workers[6] with some modifications. Complex **9** was then further reacted with $PPh_3$ (*see scheme 4.1*).

Complex **11** was prepared from the osmium dimer $[Os(\eta^6\text{-}p\text{-cymene})Br_2]_2$ and 2-aminobenzamide in the presence of $NH_4BF_4$ in $CH_2Cl_2$ at room temperature. The expected $[Os(\eta^6\text{-}p\text{-cymene})(\kappa^2\text{-}N,N'\text{-}C_7H_8N_2O)Br]BF_4$ product was not obtained instead **11** was isolated where the 2-aminobenzamide coordinates as a monodentate ligand. Complex **11** was isolated because the N atom of the amine group offers more electrons towards σ-bonding than the N atom of the amido group. On the amido group, electrons are being pulled towards the electronegative O atom, consequently reducing the electron density on the N atom.

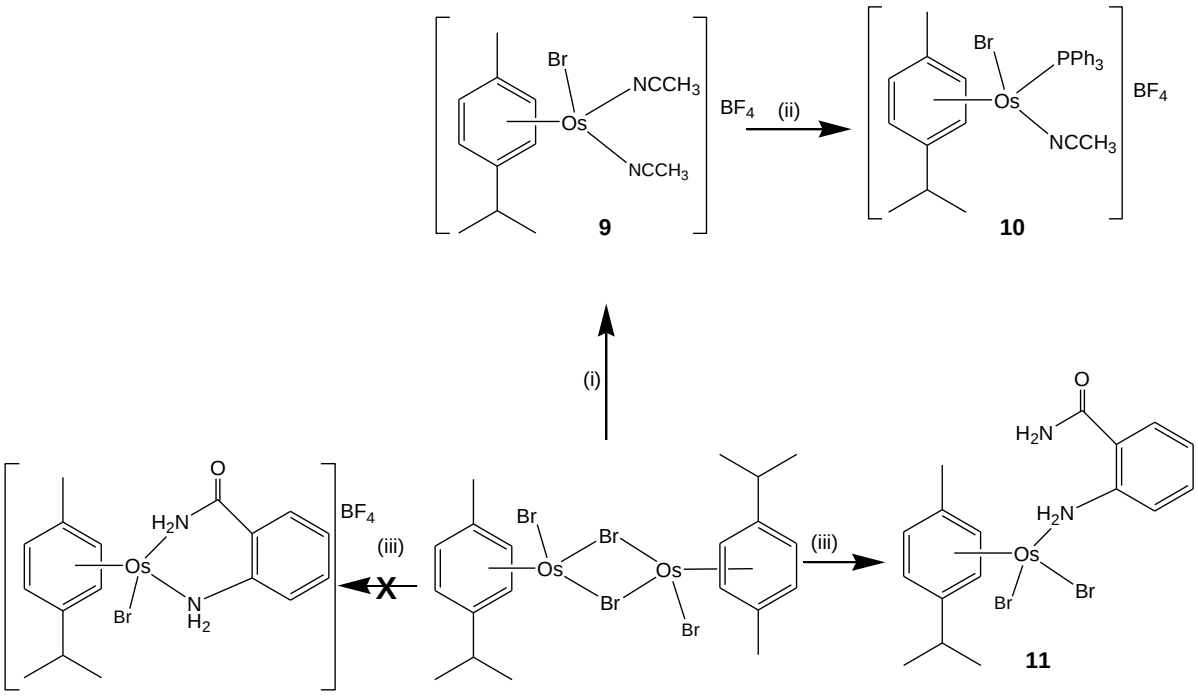


Reaction conditions : (i) $NCCH_3$, $NH_4BF_4$, R.T., 16 h.
(ii) $PPh_3$, $CH_2Cl_2$, R.T., 16 h.
(iii) $C_7H_8N_2O$, $NH_4BF_4$, $CH_2Cl_2$, R.T., 16 h.

**Scheme 4.1**

## 4.3 Results and Discussion

### 4.3.1 Nuclear Magnetic Resonance (NMR) Spectroscopy

#### 4.3.1.1 $^{1}$H NMR data

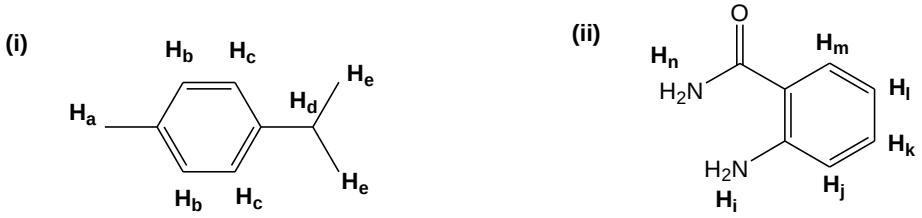


*Figure 4.1: $^{1}$H NMR for the (i) cymene and (ii) 2-aminobenzamide will be discussed according to this assignment and standard IUPAC naming for carbons will be used for 2-aminobenzamide.*

The $^{1}$H NMR data were collected for complexes **9**, **10** and **11**. Complexes **9** and **10** are similar in structure except for replacement of one of the $CH_3CN$ ligands in **9** by the $PPh_3$ ligand in **10**, hence, different electronic properties were observed. A singlet due to six protons of the two $CH_3CN$ ligands on **9** was observed at 2.74 ppm downfield relative to the free $CH_3CN$ ligand (2.10 ppm). A singlet due to three protons of the $CH_3CN$ in **10** was observed at 2.18 ppm slightly downfield relative to the free $CH_3CN$ ligand. The observation may be attributed to the σ-donor ability of the $CH_3CN$ ligand. Upon coordination, the N atom of the $CH_3CN$ ligand becomes electron deficient, resulting in electrons being pulled from the $CH_3$– by inductive effect deshielding the $CH_3$– protons. Complex **11** displayed a minor downfield shift on protons $H_i$, $H_j$, $H_k$, $H_l$ and $H_m$ relative to the free 2-aminobenzamide ligand (*see figure 4.1(ii)*).

The $H_b$ and $H_c$ protons of **9** appeared upfield at 5.86 and 6.05 ppm respectively, relative to the $H_b$ (6.02 ppm) and $H_c$ (6.15 ppm)[12] protons of the starting material. This observation may be attributed to the $CH_3CN$ ligand as a good σ-donor but a poor π-acceptor, consequently back bonding electrons are donated to the carbons of the cymene ligand. Complex **10** displayed four sets of $H_b$ and $H_c$ protons because of the *R* and *S* isomers that co-exist in $CDCl_3$ solution. Complex **11** displayed two sets of doublets due to $H_b$ (6.03 ppm) and $H_c$ (6.09 ppm). The protons $H_c$ were slightly upfield relative to the $H_c$ protons of the starting material $[Os(\eta^6\text{-}p\text{-cymene})Br_2]_2$. This observation was attributed to the competition of back-

bonding electrons by aromatic cymene carbons and the N atom coordinated to the osmium centre.

#### 4.3.1.2 $^{13}$C NMR data

The $^{13}$C NMR data for complexes **9**, **10**, **11** support the $^{1}$H NMR data. A peak for the $CH_3$– group of $CH_3CN$ ligand for complexes **10** was observed upfield relative **9** (*see table 4.1*). The upfield shift of this signal in **10** was attributed to the presence of the $PPh_3$. The C≡N carbon of $CH_3CN$ in **9** appears upfield while for **10** this signal appears downfield (*see table 4.1*). The observation may be attributed to the effect of $PPh_3$ by participating in competing for back-bonding electrons as compared to **9** where the cymene, Br and $CH_3CN$ ligands were present. The aromatic carbons of the cymene appeared downfield for **10** relative to the upfield shift of the aromatic carbons of the cymene in **9**. This observation may be attributed to the poor π-acceptor $CH_3CN$ ligands in **9**. However, the strong π-acceptor $PPh_3$ ligand in **10** offers competition of back-bonding electrons deshielding the aromatic carbons. Complex **11** displayed carbon signals similar to the free 2-aminobenzamide ligand.

*Table 4.1: $^{13}$C NMR data of **9** and **10**.*

| Assignments | **9** δ(ppm) | **10** δ(ppm) |
|---|---|---|
| $\underline{C}H_3CN$ | 4.19 | 3.32 |
| $\underline{C}H_3C_6H_4$ | 18.97 | 18.36 |
| $CH(\underline{C}H_3)_2$ | 22.63 | 20.92 |
| $\underline{C}H(CH_3)_2$ | 31.40 | 31.06 |
| $\eta^6$-$C_6H_4$ | 97.67, 94.41, 78.69, 75.74 | 121.92, 109.88 (*J*=7 Hz), 96.99, 89.14 (*J*=6 Hz), 83.43, 80.61 |
| $\underline{C}$≡N | 122.09 | 130.05 |
| $C_{Aromatic}$ | - | 128.72-135.07 |

4.3.1.3 Heteronuclear Single Quantum Correlation (HSQC) NMR

Complex **11** was characterised by a 2D HSQC NMR experiment to confirm the assignments. The $H_a$ protons (2.22 ppm) appear as a singlet peak correlating to the carbon signal at 18.45 ppm (*see figure 4.2*). The $H_e$ protons (1.20 ppm) appear as a doublet correlating to a carbon signal at 21.74 ppm. The $H_d$ proton (2.83 ppm) appears as a septet correlating to a carbon signal at 30.16 ppm. The $H_b$ (6.03 ppm) and $H_c$ (6.09 ppm) protons appear as two pairs of doublets correlating to carbon signals at 78.21 and 78.75 ppm respectively (*see figure 4.2*). The 2-aminobenzamide ligand protons were assigned below. The triplet of doublets due to proton $H_l$ (6.48 ppm) correlates to the carbon signal (C5) at 114.83 ppm. This triplet of doublets is observed because of $H_l$ coupling with $H_m$ and $H_k$ to give two signals of doublets; in addition, the third doublet occurs because of a long-range $^4$J-coupling of $H_l$ with $H_j$. The doublet of doublets due to proton $H_j$ (6.69 ppm) correlate to the carbon signal (C3) at 116.84 ppm. The set of triplet of doublets due to proton $H_k$ (7.12 ppm) correlate to the carbon signal (C4) at 132.31 ppm. The doublet of doublets due to proton $H_m$ (7.52 ppm) correlates to the carbon signal (C6) at 129.17 ppm.

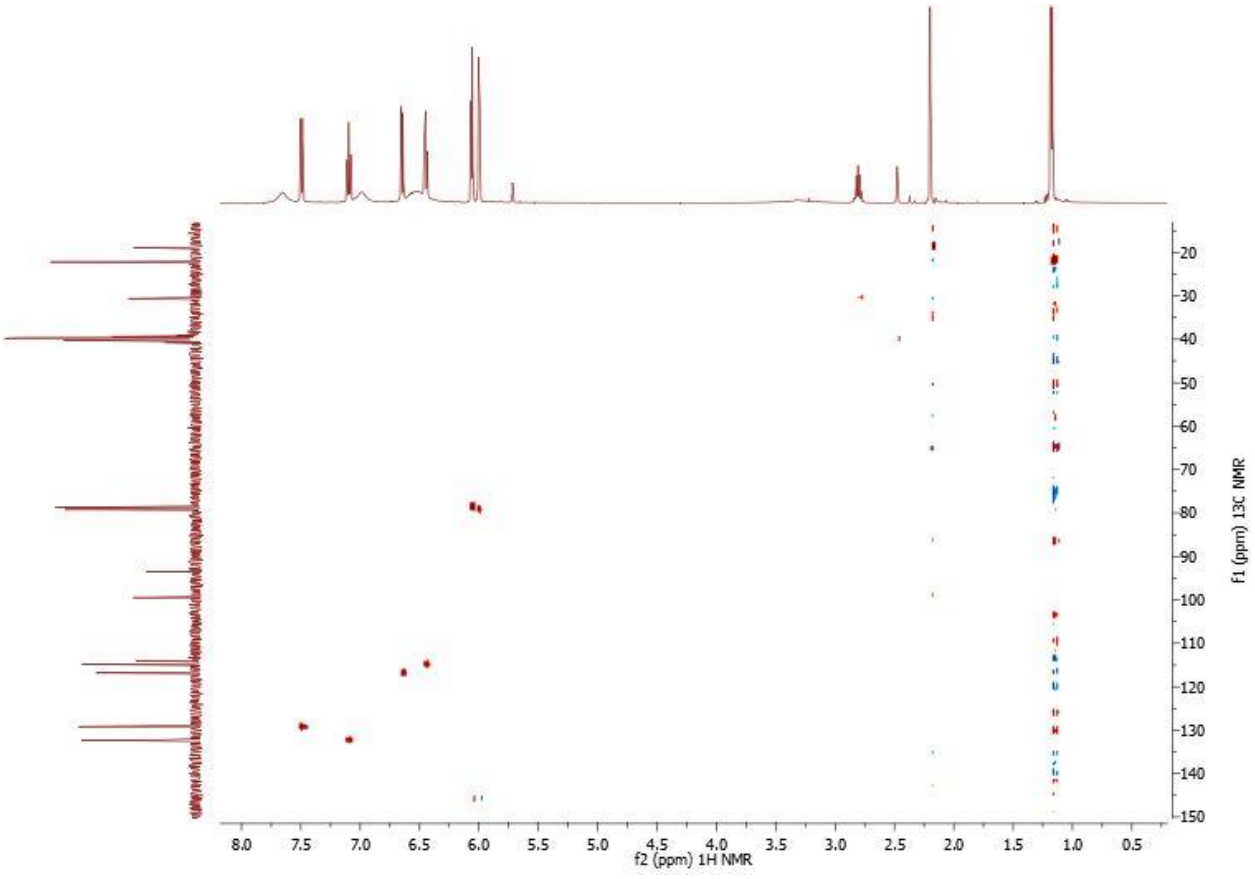


*Figure 4.2: The 2D HSQC NMR spectrum of **11** showing C−H correlations.*

4.3.1.4 $^{19}F$ NMR data of **9** and **10**

A $^{19}F$ NMR study was carried out to confirm the presence of the $BF_4$ counter ion in **9** and **10**. Complex **9** shows two F signals at −151.84 and −151.89 ppm found to be upfield relative to $NH_4BF_4$ (−148.88 and −148.94 ppm) which was used as a reagent (*see figure 4.3*). Complex **10** displayed two F signals at −152.31 and −152.37 ppm slightly upfield relative to **9** which was used as a starting material for the synthesis of **10**. The $^{19}F$ signals also appear shifted from $NH_4BF_4$ to **9** then to **10** because of the significant changes in cationic complex structures. In addition, two $^{19}F$ signal were observed due to the co-existence of the two boron isotopes ($^{10}B$ and $^{11}B$) in solution.[13,14]

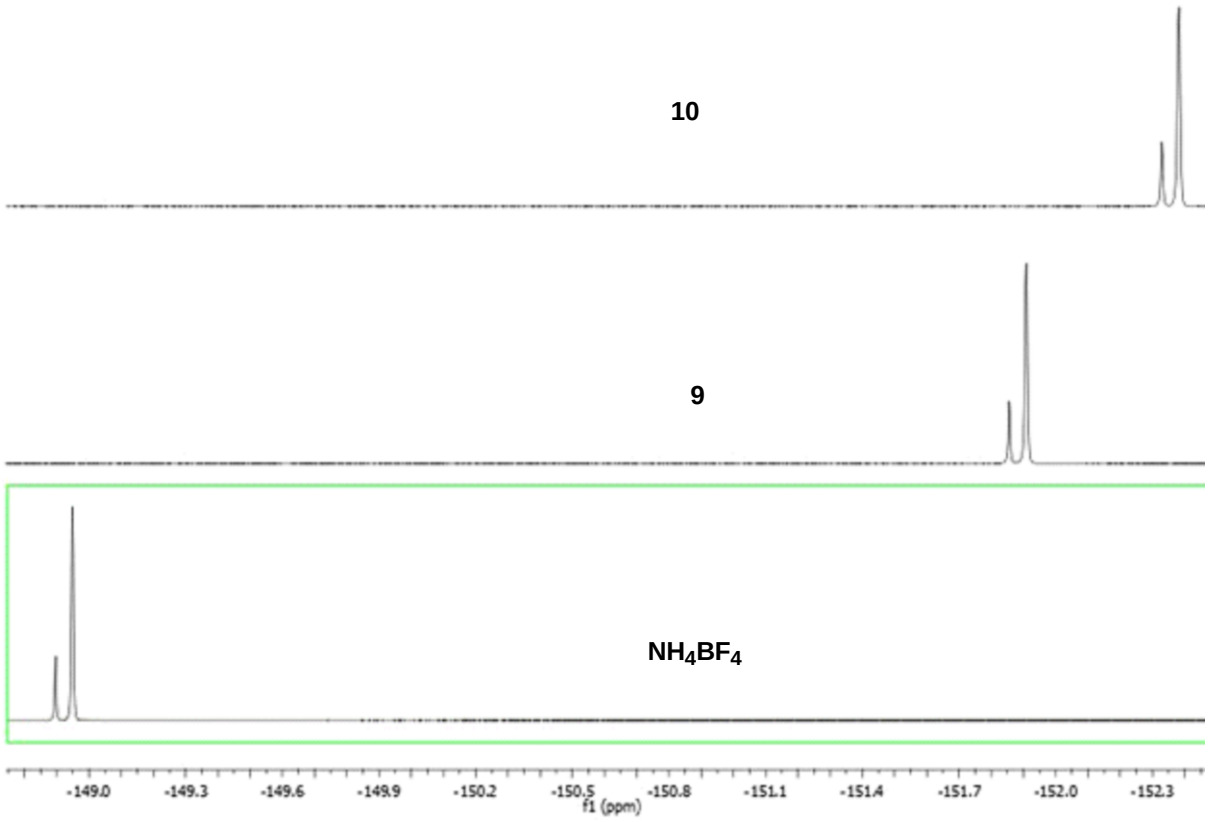


*Figure 4.3: $^{19}F$ NMR spectra for **9** and **10** showing the shift in fluorine signals.*

4.3.1.5 $^{31}$P NMR data of **10**

Complex **10** displayed a P signal at –2.69 ppm with two sets of satellites peaks at –2.56 and –2.84 ppm with $^{1}J$ = 56 Hz attributed to the spinning side bands.[15] Another pair of satellite peaks was observed at –2.02 and –3.36 ppm with $^{1}J(^{187}Os–^{31}P)$ = 271 Hz due to the NMR active isotope of osmium (*see figure 4.4*). [15,16] In Chapter 2, the assignment of the two sets of satellite peaks was explained; hence, a similar assignment was used in this chapter. The P signal appeared to be deshielded relative to the free $PPh_3$ ligand at –5.53 ppm. This deshielding may be attributed to the competition for the back-donated electrons influenced by other ligands around the osmium centre. In addition, the bond angle (C–P–C) on the coordinated ligand may be less strained with phenyl groups far away from each other because of the absence of the lone pair lobe.

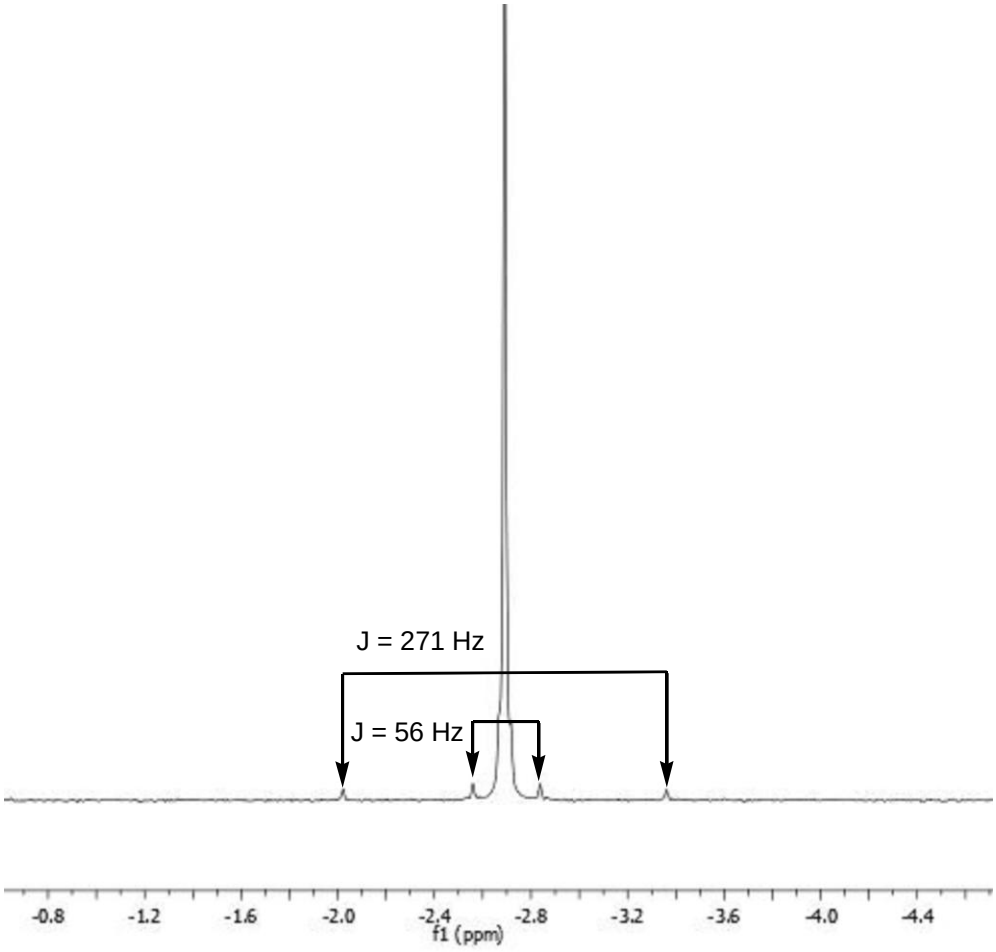


*Figure 4.4: $^{31}$P NMR spectrum of **10** showing two sets of satellite peaks.*

### 4.3.2 Infra-Red (IR) Spectroscopy

The IR data shows that **9** exhibits two weak peaks at 2331 and 2303 $cm^{-1}$ due to the reduced C≡N triple bond in the two acetonitrile groups in different environments. A strong peak assigned to the B−F bond was observed at 1052 $cm^{-1}$. However, as expected **10** exhibits a single medium peak due to C≡N triple bond of the acetonitrile at 2322 $cm^{-1}$ and the B−F bond as a strong peak at 1054 $cm^{-1}$. Complex **11** shows a stretching frequency due to $\nu_{(C=O)}$ at 1660 $cm^{-1}$, as well as N−H peaks at 3332, 3263, 3177 and 3112 $cm^{-1}$.

### 4.3.3 Raman Spectroscopy

The IR results were supported by Raman spectroscopy data where additional evidence of the Os-Br bonds were obtained. Complex **9** exhibited a vibrational peak of medium intensity due to Os−Br at 203 $cm^{-1}$ which agrees with the Raman data by Bottger and co-workers.[17] The two vibrational strong peaks due to $\nu_{(C\equiv N)}$ at 2331 and 2303 $cm^{-1}$ which support the IR data (*see figure 4.6*). Complex **10** shows a Os−Br stretch at 202 $cm^{-1}$, a weak peak due to $\nu_{(B-F)}$ at 1061 $cm^{-1}$ and a medium peak at 2327 $cm^{-1}$ attributed to $\nu_{(C\equiv N)}$. Complex **11** shows two vibrational peaks due to Os−Br in different environments at 178 and 200 $cm^{-1}$ as well as peak at 1669 $cm^{-1}$ due to $\nu_{(C=O)}$.

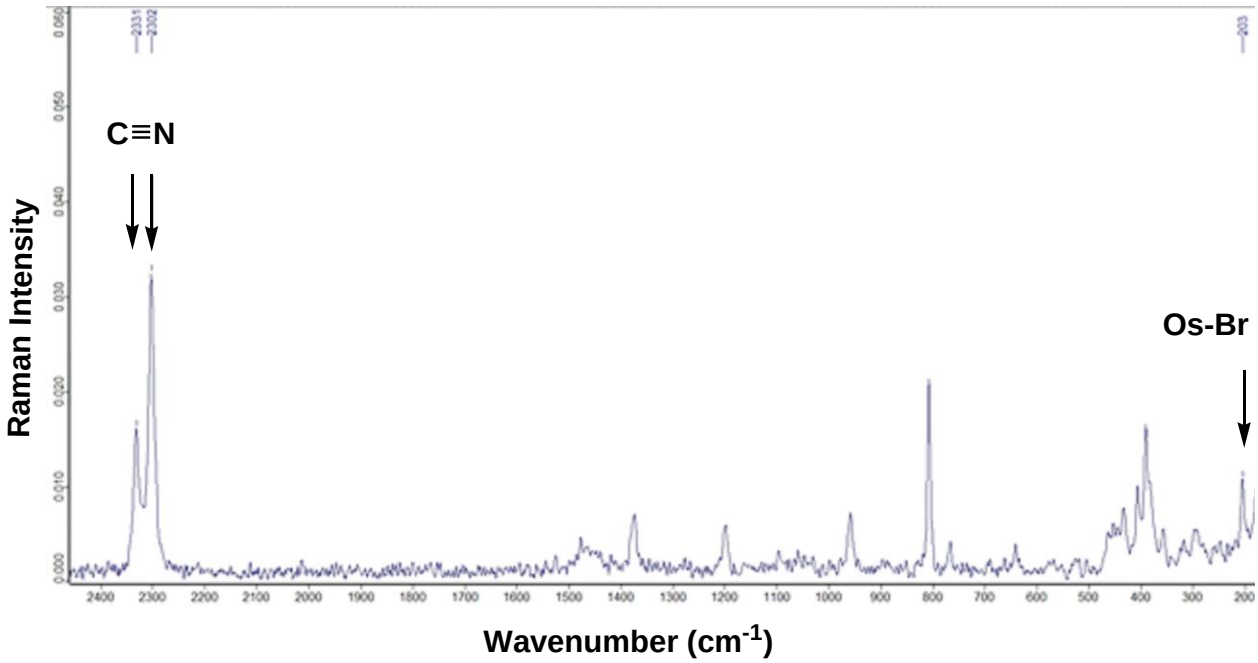


*Figure 4.5: Raman spectrum of **9** showing Os−Br and two C≡N stretching bands.*

4.3.4 Thermogravimetric analysis (TGA)

The thermal decomposition of the three complexes showed some similarity. Complex **9** shows 2.1% mass loss between 80.8 to 135.3 ºC attributed to the acetonitrile solvent. The onset decomposition of **9** was observed at 163.9 to 287.3 ºC with 30.4% mass loss attributed to $BF_4$ counter ion and two $NCCH_3$ ligands. At 287.3 to 337.4 ºC a mass loss of 19.7% was attributed to the loss of the cymene. two $CH_3CN$ ligands and the $BF_4$ counter ion. The loss of 13.7% mass at 394.0 to 684.3 ºC was attributed to the Br ligand (*see figure 4.6*). At 684.3 ºC oxidation of Os metal to $OsO_2$ and/or $OsO_4$ takes place resulting in a residue of about 26% at 800 ºC attributed to Os metal. [18]

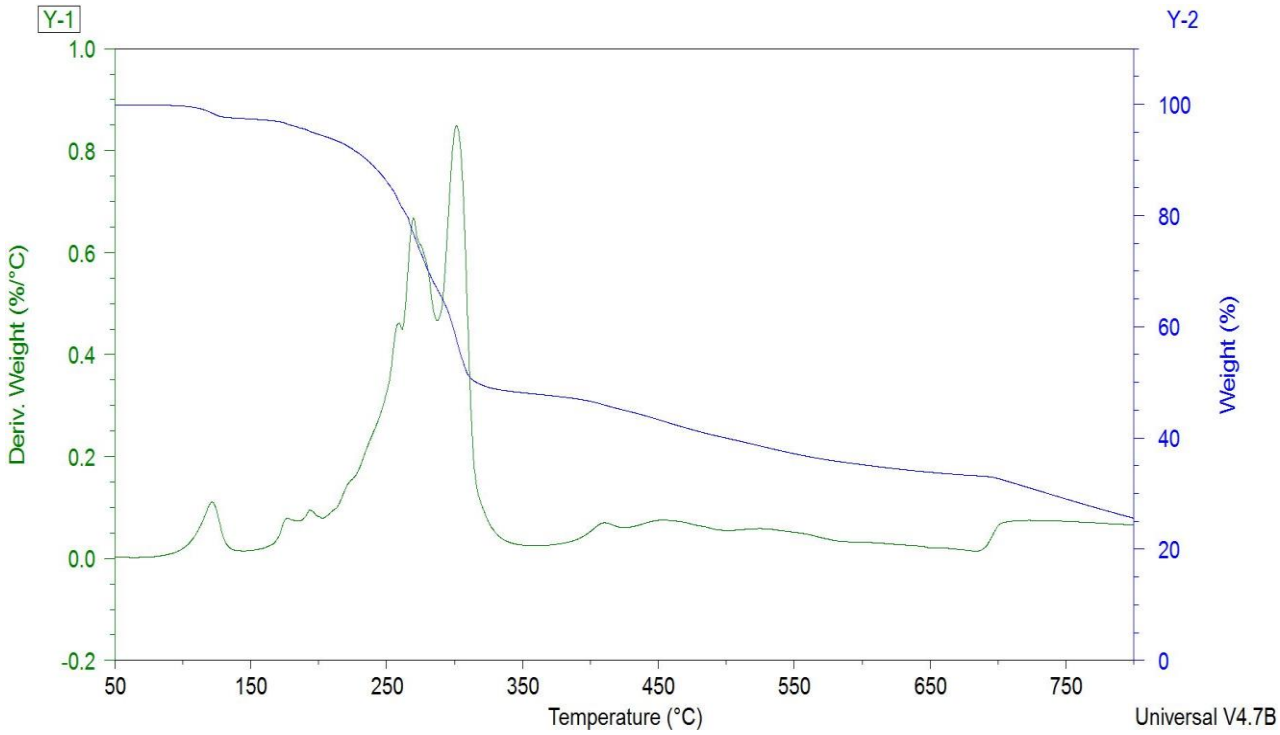


*Figure 4.6:TGA thermogram of **9** with DTG curve.*

Complex **10** shows an initial 2.6% loss in mass at 80.1 to 174.3 ºC attributed to the loss of the acetonitrile solvent. The onset decomposition of **10** was observed at 176.1 to 327.9 ºC with 34.5% mass loss attributed to the loss of the $CH_3CN$ and cymene ligands as well as the $BF_4$ counter ion. At 426.5 to 764.5 ºC a mass loss of 16.5% was observed, attributed to the loss of Br and one phenyl. The remaining 39% mass was attributed to Os–$PPh_2$ fragment. Complex **11** shows mass loss of 32.2% at 140.8 to 303.7 ºC attributed to the loss of the cymene and one Br ligands. The second degradation of 12.6% was attributed to the loss of the second Br ligand at temperatures from 267.9 to 347.1 ºC (*see figure 4.7*). The third degradation of 50.2% fragment was attributed to the loss of 2-aminobenzamide group and the Os metal undergoing oxidation to $OsO_2$/$OsO_4$ followed by reduction to Os metal at temperatures between 416.2 ºC to 539.7 ºC.[18] The presence of the $PPh_3$ ligand has a significant impact on the thermal stability of **10** relative to **9**. The thermal studies of **9** and **10** have shown that the $CH_3CN$ and cymene ligand decomposes first at temperatures around 170 ºC. The Os–N bonds of the $CH_3CN$ ligand in **9** and **10** are thermally less stable relative to the Os–N bond of the 2-aminobenzamide in **11**.

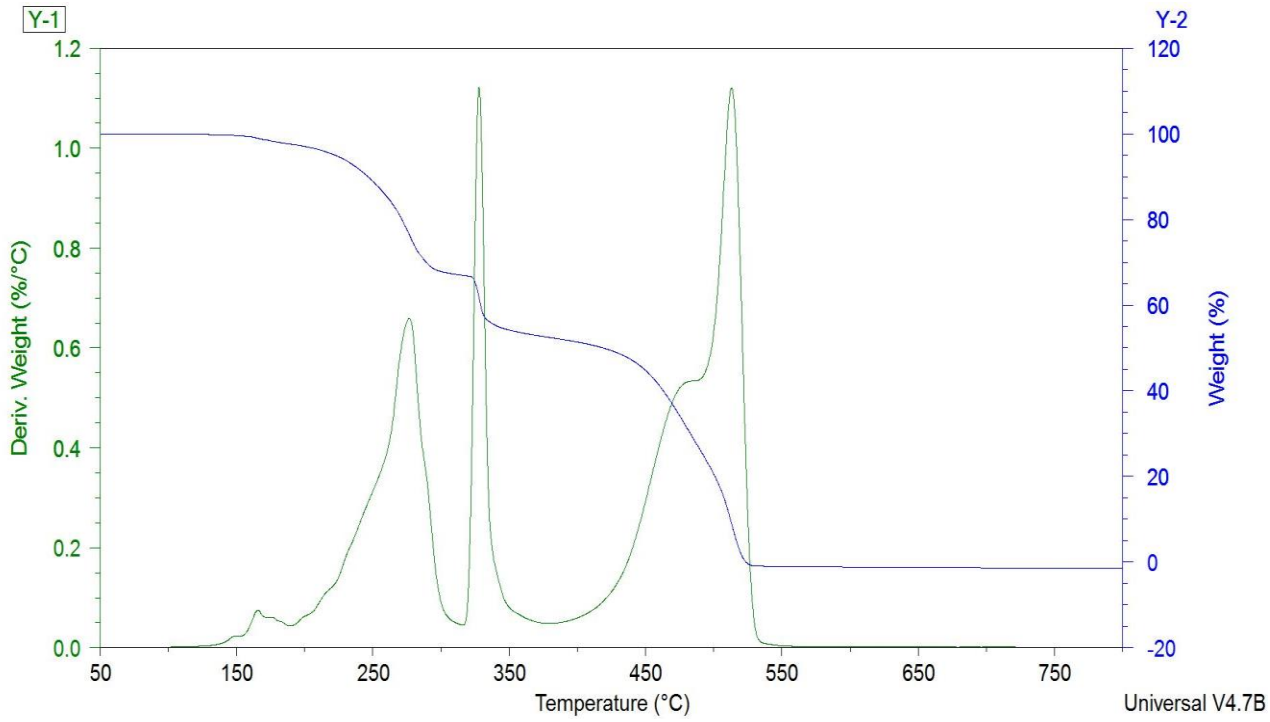


*Figure 4.7: TGA thermogram of **11** with DTG curve.*

## 4.3.5 Conductivity studies

Conductivity studies were also carried out on complexes **9** and **10**. For 1:1 complexes at *ca.*$10^{-3}$ M in nitrobenzene solvent it is expected that the molar conductivity ($\Lambda_M$) measurement be within the range 20–30 $Scm^2mol^{-1}$.[19] Complex **9** gave a molar conductivity value found to be below the expected range (*see table 4.2*). This may be attributed to lability of the $CH_3CN$ ligand, which destabilizes the complex. Complex **10** gave a value that is within the range (*see table 4.2*). This may be attributed to the inertness of the complex after the coordination of the $PPh_3$ ligand. This result supports the theory of lower molar conductivity than the expected range due to the lability of the $CH_3CN$ ligand.

*Table 4.2: The concentrations, conductance and molar conductivity values of **9** and **10**.*

| Complex | c × $10^{-3}$ M | Conductance (c × μS)* | $\Lambda_M$ (S $cm^2$ $mol^{-1}$) |
|---|---|---|---|
| **9** | 1.1 | 20.55 | 14.20 |
| **10** | 1.1 | 29.35 | 20.28 |

*The conductance of the samples were obtained after subtracting the value of the blank; Nitrobenzene = 3.45 μS from the measured values.

The molar conductivities were calculated using the following equations:

For complex **9**.

$\kappa = G \times K$ . . . . . [1]

Where $\kappa$ = conductivity (S/cm), G = conductance (S), K = cell constant ($cm^{-1}$)

Taking that G = 20.55 μS and K = 0.76 $cm^{-1}$, then substituting the values in equation [1],

Converting the conductivity to the molar conductivity the following equation was used:

$\Lambda_M = \kappa / C_M$ . . . . . [2]

= 14.20 S $cm^2$/mol

4.3.6 Crystallography

Complex **11** co-crystallized with a disordered 2-aminobenzamide molecule. Table 4.3 contains the crystal data and structure refinement and Table 4.4 contains selected bond lengths and bond angles of **11**.

Crystals of **11** suitable for X-ray diffraction was obtained by slow diffusion of the diethyl ether into a dichloromethane solution at room temperature. Figure 4.7 shows the molecular structure of **11**, which crystallised in a triclinic crystal system with *P-1* space group. The C–C bond lengths measured different distances around the aromatic cymene, an indication of loss of aromaticity. The set of C–C bonds which measured longer bond lengths are; C(2)–C(3), C(3)–C(4) and C(4)–C(5). The C−C set which measured shorter bond lengths are; C(1)−C(2), C(5)−C(6), and C(6)−C(1). The Os–C bond lengths also measured different distances, attributed to the loss of planarity. The Os(1)–C(1) and Os(1)–(6) measured shortest bond lengths compared to other carbons around the aromatic cymene, which indicated stronger interactions. The Os(1)–C(3) and Os(1)–C(4) measured the longest bond lengths, influenced by back-bonding from the N(2) atom on *trans* position, which is in agreement with $^1$H NMR data. The Os–centroid$_{cymene}$ distance was measured as 1.653 Å. In addition, the loss of planarity was measured along the mean plane defined by C(2), C(3), C(5) and C(6). C(1)

measured 0.029 Å below the mean plane and C(3) measured 0.006 Å also below the mean plane. The coordinated 2-aminobenzamide ligand was observed to be out of plane with a torsion angle [centroid$_{cymene}$–Os(1)–N(2)–C(12)] measured at 26.09º.

Complex **11** co-crystallised with a molecule of 2-aminobenzamide. Complex **11** and co-crystallised 2-aminobenzamide were found to be held together by C−H···N intermolecular hydrogen bonding (*see figure 4.8*). The short contact was measured as 2.602 Å at 148.91º due to one hydrogen of C(10) of the cymene with N(3) of the co-crystallised 2-aminobenzamide, which is classified as a strong hydrogen bond.[20] The two intramolecular hydrogen bonds were observed as results of N−H···O and C−H···Br interactions (*see figure 4.8*). The N−H···O interaction was due to the hydrogen of N(2) with O(1) on the coordinated 2-aminobenzamide. This N−H···O intramolecular interaction was measured as 1.951 Å at 143.85º, which is classified as a strong hydrogen bonding.[20] The C−H···Br intramolecular interaction was measured as 3.358 Å at 127.65º, which was due to the hydrogen on C(13) of the 2-aminobenzamide and Br(1). The C−H···Br intramolecular hydrogen bond was observed to have an influence on the Os(1)–Br(1) bond length. The two Br atoms measured different Os–Br bond lengths, with Br(1) longer than Br(2).

The Br(1)···Br(2) measured an interatomic distance of 3.469 Å at an angle subtended at the Os centre of 85.87º. The bond angles Br(1)−Os(1)−Br(2) were measured at 85.87º, Br(1)−Os(1)−N(2) measured at 81.87º and Br(2)−Os(1)−N(2) measured at 80.50º. The torsion angle C(1)–C(6)–C(5)–C(4) was measured at 3.45º which support the loss of planarity of the cymene ligand.

The effect of coordination of 2-aminobenzamide was observed relative to the co-crystallized 2-aminobenzamide and the free 2-aminobenzamide ligand (JIXCIC[†14]). The crystal structure of the free 2-aminobanzamide was reported by Kashino and co-workers.[21] The free 2-aminobenzamide measured C(2)–N(2) as 1.391 Å and the co-crystallized 2-aminobenzamide in this study measured C(24)–N(3) as 1.377 Å whereas the coordinated ligand measured C(12)–N(2) as 1.439 Å. This observation in coordinated 2-aminobenzamide was attributed to the strong σ-donor ability of N(2). Furthermore, in JIXCIC the C(7)–N(1) measured 1.327 Å and the co-crystallised 2-aminobenzamide measured C(24)–N(3) as 1.398 Å whereas the coordinated 2-aminobenzamide ligand measured C(17)–N(1) as 1.332 Å. The C−H···N

[†14] The CIF file used for comparison was obtained from the CCDC database.

hydrogen bonding have an effect on the C–N bond of the co-crystallized 2-aminobenzamide ligand. The N−H···O hydrogen bonding has a significant effect on the C–O bond of the coordinated 2-aminobenzamide.

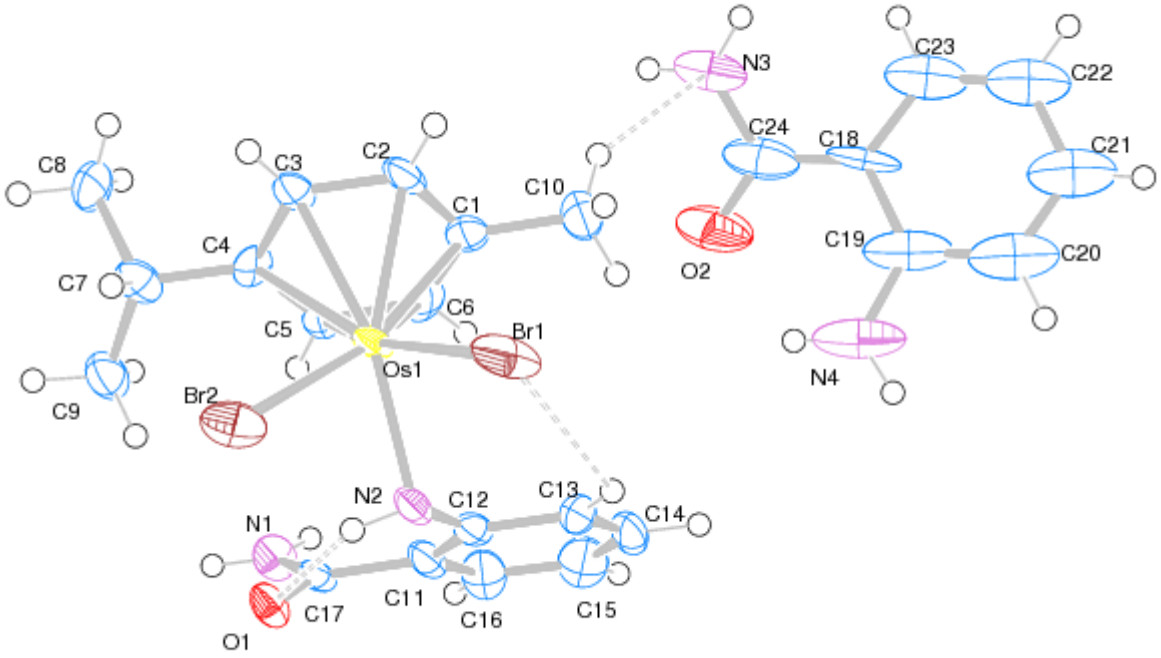


*Figure 4.8: Molecular structure of **11** at 50% probability thermal ellipsoids.*

*Table 4.3: Crystal data and structure refinement of **11**·2-aminobenzamide.*

| | |
|---|---|
| Chemical formula | $C_{24}\ H_{25}\ Br_2\ N_4\ O_2Os$ |
| Molecular mass | 687.45 |
| Crystal system | Triclinic |
| Space group | P-1 |
| Crystal colour and shape | Yellow-brownish cubes |
| a(Å) | 8.483(2) |
| b(Å) | 9.938(3 |
| c(Å) | 14.914(4) |
| α(°) | 87.285(11) |
| β(°) | 74.264(11) |
| γ(°) | 67.131(11) |
| V(Å$^3$) | 1112.7(5) |
| Z | 2 |
| T(K) | 173(2) |
| $D_{calc}$ (mg/m$^3$) | 2.052 |
| Absorption coefficient | 9.339 mm$^{-1}$ |
| Reflections collected | 56810 |
| Independent reflections | 5361 [R(int) = 0.4236] |
| Data / restraints / parameters | 5361 / 54 / 280 |
| F(000) | 654 |
| Final R indices [I>2σ(I)] | R1 = 0.0895, wR2 = 0.2259 |
| R indices (all data) | R1 = 0.0972, wR2 = 0.2400 |
| Goodness-of-fit on F$^2$ | 1.034 |
| Largest diff. peak and hole | 7.043 and −8.175 e.Å$^{-3}$ |

*Table 4.4: Selected bond lengths (Å), bond angles (º) and torsion angles (º) of **11**.*

| **Atom type label** | **11** |
|---|---|
| Os(1)–C(1) | 2.158(15) |
| Os(1)–C(2) | 2.178(12) |
| Os(1)–C(3) | 2.189(11) |
| Os(1)–C(4) | 2.196(10) |
| Os(1)–C(5) | 2.175(13) |
| Os(1)–C(6) | 2.162(15) |
| C(1)–C(2) | 1.400(2) |
| C(2)–C(3) | 1.432(17) |
| C(3)–C(4) | 1.440(17) |
| C(4)–C(5) | 1.441(16) |
| C(5)–C(6) | 1.399(18) |
| C(6)–C(1) | 1.380(2) |
| Os(1)–N(2) | 2.180(10) |
| Os(1)–Br(1) | 2.5634(15) |
| Os(1)–Br(2) | 2.5292(16) |
| Br(1)···Br(2) | 3.469 |
| Os(1)–centroid$_{cymene}$ | 1.653 |
| **Bond angles** | |
| Br(1)–Os(1)–Br(2) | 85.87(7) |
| Br(1)–Os(1)–N(2) | 81.87(3) |
| Br(2)–Os(1)–N(2) | 80.50(3) |
| **Torsion angles** | |
| C(1)–C(6)–C(5)–C(4) | 3.45 |
| C(1)–C(2)–C(3)–C(4) | −0.03 |

## 4.4 Conclusions

The novel osmium cymene complexes with monodentate N- and P-donor ligands were synthesised and fully characterised. The presence of a $PPh_3$ ligand was found to play a significant role on the electronic and electrolytic properties of **10**. Complex **10** was found to be thermally stable relative to **9** because of the substitution of the labile $CH_3CN$ ligand by the non-labile $PPh_3$ ligand. In addition, the electrolytic properties of **10** were found to be good, with **10** exhibiting higher molar conductivity than the substrate complex **9** attributed to the $PPh_3$ ligand. The 2-aminobenzamide in **11** coordinates to the osmium centre with the most

electron rich amino group. Steric hindrance has an influence on the choice of coordination of 2-aminobenzamide with only monodentate N atom as opposed to chelation with N,O or N,N′ atoms.

The effects of coordination of 2-aminobenzamide with N atom of the amino group has significant effects on the cymene ligand according to NMR and crystallography data. Hydrogen bonding plays an important role in co-crystallization of **11** with 2-aminobenzamide ligand. The *in vitro* anticancer activity results of complexes **9** and **10** will be discussed in Chapter 5.

## 4.5 References


(1) Liang, H.-C.; Kim, E.; Incarvito, C. D.; Rheingold, A. L.; Karlin, K. D. *Inorg. Chem.* **2002**, *41*, 2209.

(2) Nagao, H.; Hirano, T.; Tsuboya, N.; Shiota, S.; Mukaida, M.; Oi, T.; Yamasaki, M. *Inorg. Chem.* **2002**, *41*, 6267.

(3) Moriarty, R. M.; Gill, U. S.; Ku, Y. Y. *J. Organomet. Chem.* **1988**, *350*, 157.

(4) Thorburn, I. S.; Rettig, S. J.; James, B. R. *J. Organomet. Chem.* **1985**, *296*, 103.

(5) Yang, L.; Powell, D. R.; Houser, R. P. *Dalton Trans.* **2007**, 955.

(6) Chaplin, A. B.; Fellay, C.; Laurenczy, G.; Dyson, P. J. *Organomet.* **2007**, *26*, 586.

(7) Dharmaraja, J.; Subbaraj, P.; Esakkidurai, T.; Shobana, S. *J. Coord. Chem.* **2015**, *68* 4314.

(8) Aird, R. E.; Cummings, J.; Ritchie, A. A.; Muir, M.; Morries, R. E.; Chen, H.; Salder, P. J.; Jodrell, D. I. *Br. J. Cancer* **2002**, *86*, 1652.

(9) Scolaro, C.; Chaplin, A. B.; Hartinger, C. G.; Bergamo, A.; Cocchietto, M.; Keppler, B. K.; Sava, G.; Dyson, P. J. *Dalton Trans.* **2007**, 5065.

(10) Tyagi, P.; Chandra, S.; Saraswat, B. S.; Sharma, D. *Spectrochim. Acta* **2015**, *143*, 1.

(11) Jensen, S. B.; Rodger, S. J.; Spicer, M. D. *J. Organomet. Chem.* **1998**, *556*, 151.

(12) Clayton, H. S.; Makhubela, B. C. E.; Su, H.; Smith, G. S.; Moss, J. R. *Polyhedron* **2009**, *28*, 1511.

(13) Akitt, J. W. *J. Chem. Soc., Faraday Trans. 1* **1975**, *71*, 1557.

(14) Gillespiej, R. J.; Hartmanan, S.; Parekh, D. M. *Can. J. Chem.* **1968**, *46*, 1601.

(15) Eichele, K.; Wasylishen, R. E.; Corrigan, J. F.; Taylor, N. J.; Carty, A. J.; Feindel, K. W.; G.M., B. *J. Am. Chem. Soc.* **2002**, *124*, 1541.

(16) Bell, A. G.; Kozminski, W.; Linden, A.; von Philipsborn, W. *Organomet.* **1996**, *15*, 3124.

(17) Bottger, G. L.; Damsgard, C. V. *Spectrochim. Acta* **1972**, *28A*, 1631.

(18) Brown, M. E. *Introduction to thermal analysis: techniques and applications*; Chapman and Hall Ltd: London and New York 1988.

(19) Geary, W. J. *Coord. Chem. Rev.* **1971**, *7*, 81.

(20) Steiner, T.; Desiraju, G. R. *Chem. Commun.* **1998**, 891.

(21) Kashino, S.; Tateno, S.; Tanabe, H.; Haisa, M.; Katsube, Y. *Acta Cryst.* **1991**, *47*, 2236.

# CHAPTER 5

## ANTICANCER STUDIES OF OSMIUM CYMENE COMPLEXES WITH CHELATED O,O′ AND P,P′ AS WELL AS MONODENTATE N- AND P-DONOR LIGANDS

### 5.1 Background

#### 5.1.1 Platinum complexes as chemotherapeutic agents

Platinum complexes have been found to be cytotoxic against a variety of cancer cell lines. Cisplatin has been used since 1978 for treatment of a number of tumours such as ovarian, non-small cell, small cell lung, neck, head, and testicular cancers.[1] It is understood that Cisplatin is activated by hydrolysis of one or both chloride ligands. The resulting platinum aqua adduct then coordinates covalently with the DNA bases and subsequently induces programmed cell death, apoptosis (*see scheme 5.1*).[2] The second generation of platinum complexes such as Carboplatin and Oxaliplatin were approved world-wide for treatment of Cisplatin resistant tumours in 1993 and 2003 respectively (*see chart 5.1*).[3,4] The presence of O,O′- and N,N′-chelate rings on Carboplatin and the O,O′-chelate ring on Oxaliplatin brings inertness towards hydrolysis. These complexes exhibit a different mode of anticancer activity against Cisplatin resistant tumours such as colon carcinoma.[5]

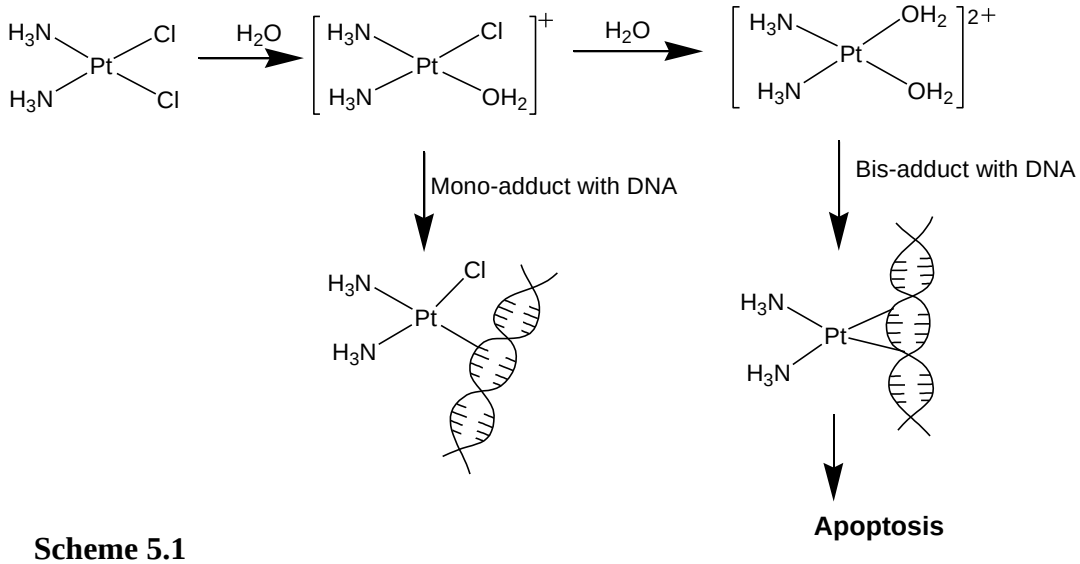


**Scheme 5.1**

Nedaplatin has been approved for clinical use in Japan against ovarian carcinomas, head and neck tumours as well as oesophageal and bladder cancer (*See chart 5.1*).[6] Lobaplatin is a platinum complex with both O,O′- and N,N′-chelate rings which is approved in China for treatment of non-small-cell-lung cancer, breast tumours and certain forms of leukaemia.[7] Heptaplatin is a platinum complex with six-membered and seven-membered O,O′-chelate rings on the platinum centre. This platinum based complex is currently in clinical use for gastric cancer, head and neck squamous cancers in South Korea.[6] Satraplatin, Picoplatin and BBR3464 are currently in clinical trials in the United States for treatment of various tumours such as malignancies, lymphomas, colorectal, prostate, melanoma, pancreatic and lung cancers (*see chart 5.1*).[8] However, platinum complexes as anticancer agents are still limited by challenges such as drug resistance[9] and side effects.[10] As a result, many platinum complexes have been abandoned in early phases of clinical trials.[8] Hence, there is a need for non-platinum complexes to overcome the challenges observed with platinum complexes.

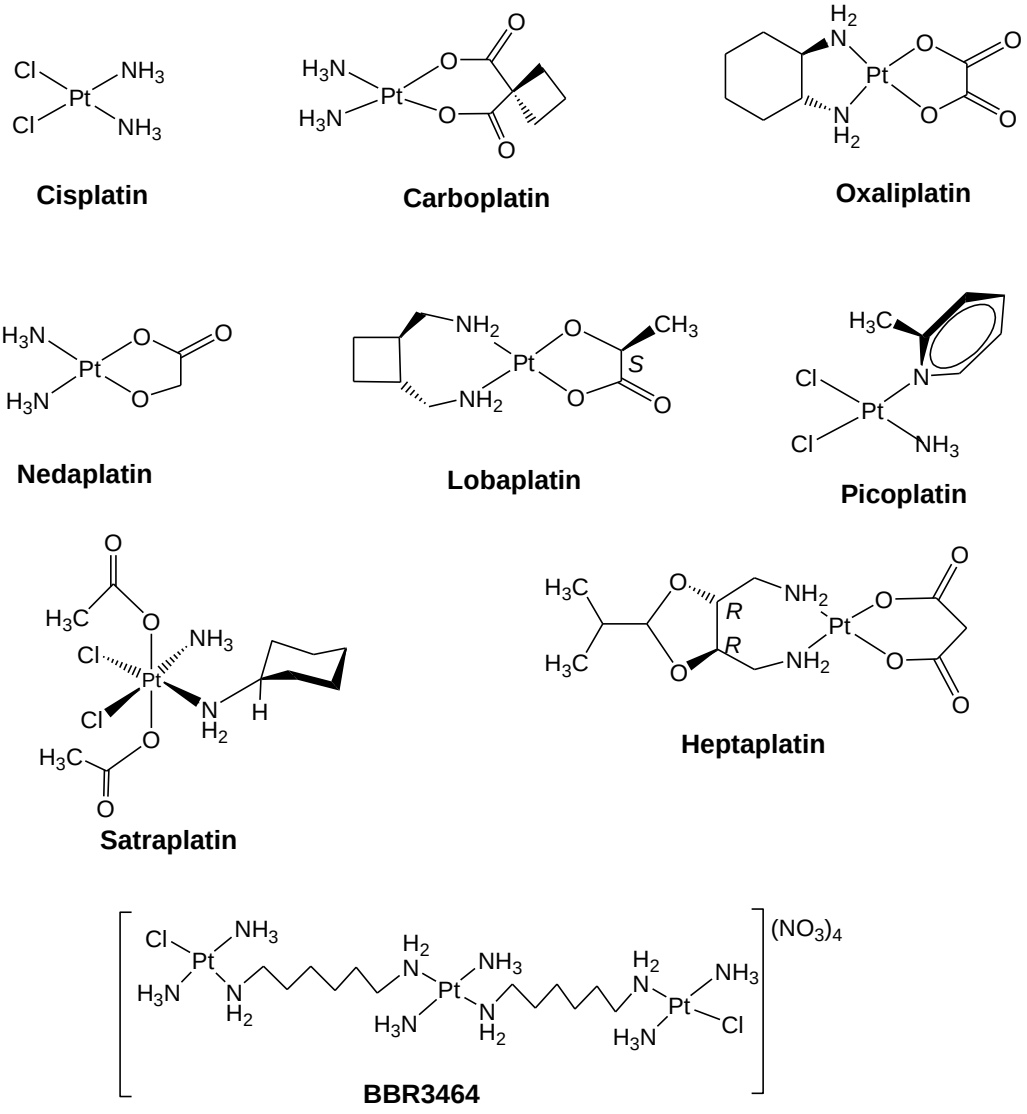


*Chart 5.1: Platinum complexes with anticancer activity.*

5.1.2 Ruthenium complexes as promising cancer chemotherapy agents

After the discovery of the limitations of the platinum complexes, ruthenium chemistry was developed rapidly to tackle challenges faced by platinum complexes in treatment of cancer. Ruthenium complexes have been found to have interesting properties in biological systems. Ruthenium complexes can undergo oxidation/reduction, exhibit lower toxicity relative to other platinum group metals, have lower rate of ligand exchange and can mimic the binding of iron to certain biological molecules.[11] Ruthenium complexes have been found to exhibit anticancer, antimalarial and antibiotic activities.[11] The two classical ruthenium coordination complexes NAMI-A[12] and KP1019[13] have been undergoing clinical trials since 1999 and

2003 respectively for their potency against colorectal cancer. These complexes have been found to be soluble and selectively potent against solid tumours.[1,13] The ruthenium complex NAMI-A is currently undergoing phase II clinical trials.[14]

The development of ruthenium arene complexes for anticancer screening contributed to the fast developing field of bio-organometallic chemistry. These half-sandwich ruthenium complexes with "piano-stool" geometry have been coordinated with a number of N,N′-, O,O′-, N,O-[15] and P,P′-[16,17] chelating ligands as well as N-, P- and O- monodentate ligands. In 2001, Morris and co-workers[18] reported ruthenium arene complexes bonded to ethylenediamine. These complexes were found to be potent against human ovarian (A2780) cancer cells. The synthesis of ruthenium arene PTA (PTA = 1,3,5-triaza-7-phosphatricyclo[3.3.1.1]decane) complexes was first reported in 2005.[19] The RAPTA complexes were found to be selective towards the TS/A mouse adenocarcinoma cancer cell line but non-active against the HBL-100 human mammary (non-tumour) cell line.[19] Introduction of the $PPh_3$ ligand to the RAPTA complex to form [Ru($\eta^6$-*p*-cymene)Cl(PTA)($PPh_3$)]$BF_4$ was found to increase the cytotoxicity towards the TS/A adenocarcinoma and the non-tumourigenic HBL-100 cancer cells.[20] The ruthenium arene moiety has been coordinated to biologically active molecules and the effect of ruthenium metal on biological activities of the molecule/adduct was investigated.[11]

### 5.1.3 Osmium complexes as emerging cancer chemotherapy agents

Osmium complexes have been recently studied as potential metallopharmaceuticals against cancerous cells. Osmium complexes were synthesised based on ruthenium analogues and the biological activities were investigated.[21] The complexes of osmium were found to prefer higher oxidation states, exhibit stronger π-back donation at lower oxidation states and hydrolyse slower depending on the ligand system compared to the ruthenium analogues.[22,23] Kostrhunova and co-workers[24] investigated the ability of osmium arene complexes to bind to DNA. Their results showed binding of osmium biphenyl complexes to the DNA guanine nucleotide. The contact was found to be a noncovalent interaction of the guanine and the arene ligands. Filak and co-workers[25] in 2010 reported the synthesis of ruthenium cymene and osmium cymene complexes with indolo[3,2-*c*]quinolones and indolo[3,2-*d*]benzazepines. The complexes were tested for cytotoxicity against ovarian carcinoma (CH1), colon

adenocarcinoma (SW480) and non-small-cell lung carcinoma (A549) and were found to be potent against all the three cell lines.

Fu and co-workers[26] in 2011 reported the osmium cymene phenylazopyridine complex with a higher cytotoxicity than the isostructural ruthenium analogue. More recently, van Rijt and co-workers[27] in 2014 investigated the mechanism of action of the compound first reported by Fu and co-workers in 2011. The group found that [Os($\eta^6$-*p*-cymene)($NMe_2$-phenylazopyridine)I]$PF_6$ induces apoptosis which is linked to the involvement of mitochondrial pathways. Again in 2013 Fu and co-workers[28] reported the anticancer activity of osmium cymene complexes with chiral centres which were found to have different selectivity patterns. The development of osmium complexes for medicinal application was further advanced by the work of Filak and co-workers[29] when they reported chelated osmium cymene indolo[3,2,-*c*]-quinoline complexes which exhibited higher potency than the ruthenium analogues.

These results suggest that osmium complexes exhibit different mechanisms of actions. In addition, osmium complexes can exhibit more potency towards cancer cells relative to their ruthenium analogues depending on the ligand system. Hence in this study, the osmium cymene complexes with various ligand systems were investigated against a range of cancer cell lines.

### 5.1.4 The role of the arene ligands in anticancer complexes

Arenes play an important role in the field of bioinorganic chemistry. The arene ligand which donates π-electrons to the oxidized metal ion brings stability to the whole metal complex. The arene ligands also increase the hydrophobicity of the complex, which increases the cellular uptake of the complexes. As a result, there is increased cytotoxicity of complexes towards cancer cells. The size of the arene ligand also plays a role because larger size arenes are more hydrophobic and are taken up by the cells to a greater degree than complexes with small size arene ligands.[15] There are reports of some metal coordinated arene ligands having non-covalent interactions with the DNA.[24]

### 5.1.5 The role of labile ligands in anticancer complexes

The labile ligands play an important role in biological studies of metal complexes where interaction of complexes studied is covalent with the specific biomolecule. These labile groups are weak bases with high electronegativity. These species are known to hold onto their electrons as a result forming weaker bonds with metal ions. They also play a role in the rate of ligand substitution. Larger labile groups have a steric effect on the central metal hence leave easily resulting in $S_N1$ process being faster for the entering group. Likewise, a smaller leaving group will favour an $S_N2$ process depending on the nature of the entering group. The bonds between the labile group and the metal can easily be cleaved with the introduction of a stronger binding ligand. The labile group is influenced by the ancillary ligands as well as the metal ion charge. The M-X bond (where X is a labile group) can break easily influenced by the trans effect, back bonding as well as the bulkiness of the ancillary ligands.[30]

In the fields of catalysis and bioinorganic chemistry, halides are preferred as labile groups because of their high electronegativity and readiness to depart. Romero-Canelon and co-workers[31] discovered that different halides bring different properties to the metal complex such as the chlorido complexes activating twice faster than the iodido complexes. In their study of ruthenium and osmium arene azo- and imido-pyridine complexes, they discovered that the iodido complex increases polarization of the positive charge on the chelated face of the pseudo-octahedral complexes than the chlorido complexes. These iodido complexes were found to be more potent and selective towards cancer cells than the analogous chlorido complexes.[31]

van Rijt and co-workers[27] reported osmium biphenyl complexes with iodido and chlorido ligands. The iodido complex was found to be more potent than the chlorido complex. Karami and co-workers[32] compared the influence of the bromide and chloride ligands on the palladium(II) binuclear complexes with a bridging diphosphine ligand. They discovered that the bromido complex exhibits higher cytotoxicity against the HeLa, HT-29 and K562 cell lines than the chlorido complex. The property of the iodide ligand to undergo slower hydrolyses than the chloride ligand offers a more suitable leaving group for metallopharmaceuticals. Dougan and co-workers[33] observed that the iodide ligand can act as a two electron donor ligand forming stronger bonds with metal centres than the more electronegative chloride ligand. Furthermore, the iodide ligand hydrolyse slower than the

chloride ligand; however the iodide ligand is being considered a stronger ligand than the chloride ligand.[33]

### 5.2 SRB vs. MTT assays

There are various methods of anticancer assays which are known to be effective. However, these methods are not without drawbacks. The two most widely used assay methods will be discussed below namely: the 3-(4,5-dimethylthiazol-2-yl)-2,5-diphenyltetrazolium bromide (MTT) and sulforhodamine B (SRB) assay methods. The MTT assay determines the cell viability by measuring the reduced activity of enzymes inside the cell. These enzymes convert colourless tetrazolium compound into the water insoluble purple formazan crystals by dehydrogenase.[34,35] In contrast, the SRB assay method determine the cell viability by measuring cellular protein content. The sulforhodamine B dye interacts electrostatically with the basic amino acids of cellular proteins depending on the pH of the environment (*see figure 5.1*).[36]

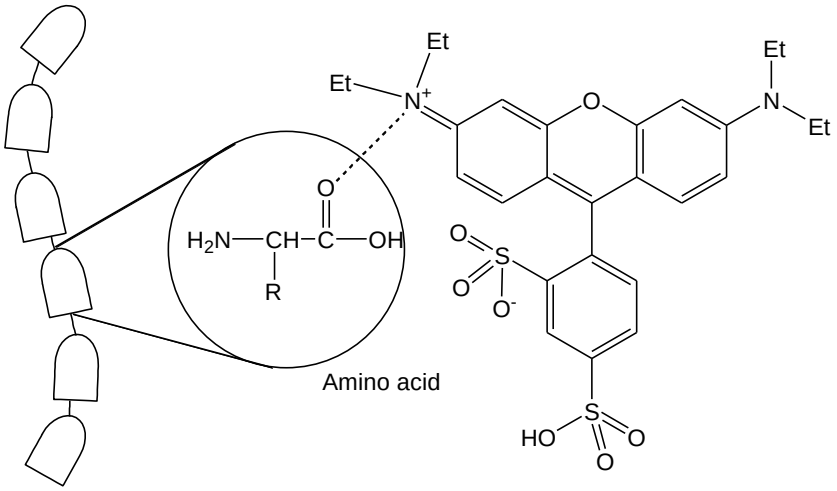


*Figure 5.1: Illustration of electrostatic interaction between sulforhodamine B and the amino acids from the primary protein structure.*

The MTT assay method suffers drawbacks because several enzymatic activities are involved within the cells. The MTT assay method entirely depends on the mitochondrial succinic

dehydrogenases to convert tetrazolium dye to formazan.[34] Also the MTT assay method was found to suffer from sensitivity and interferences because few cells are used to minimize the non-linearity of the assay method.[34,37] The SRB assay methods was found to have higher sensitivity and better linearity with the cell number and free of cell metabolic activity.[34,38,39] In addition, the staining of plates for SRB assays were found to be stable for use in several weeks to months as compared to the less stable stained plates for MTT assay.

Therefore, in this study the SRB assay method was used to determine the cytotoxicity of the fourteen osmium cymene complexes against four cancer cell lines.

### 5.3 Results and Discussion

Osmium cymene complexes chelated with α-diketones, diphosphines and monodentate N- and P-donor ligands exhibit interesting potency against renal (TK-10), melanoma (UACC-62), breast (MCF-7) and HeLa cancer cells. The complexes reported here have some similarity in structure however show some differences in anticancer activities. Table 5.1 contains the $IC_{50}$ values of the fourteen complexes against the TK-10, UACC-62, MCF-7 and HeLa cancer cell lines.

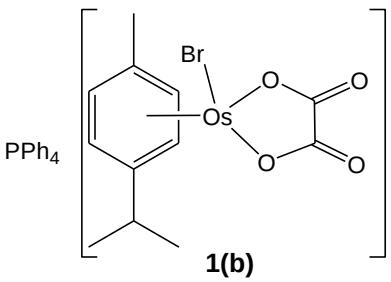


**1(b)**

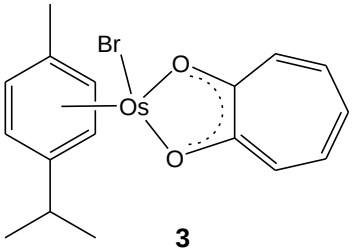


**3**

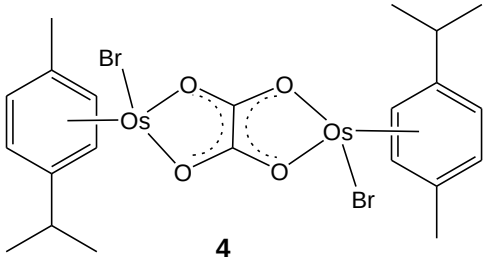


**4**

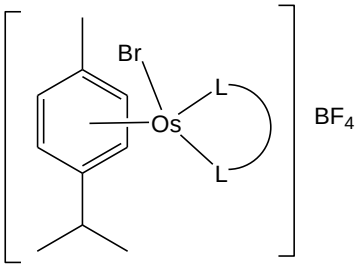


**7(a)** $L_2$ = dppm
**7(b)** $L_2$ = dppe
**7(c)** $L_2$ = dppp
**7(d)** $L_2$ = dppb

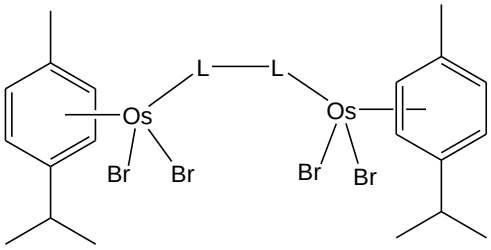


**8(a)** $L_2$ = dppm
**8(b)** $L_2$ = dppe
**8(c)** $L_2$ = dppp
**8(d)** $L_2$ = dppb

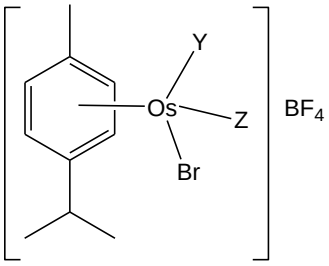


**6** : (YZ) = $(PPh_3)_2$
**9** : (YZ) = $(NCCH_3)_2$
**10** : (YZ) = $(NCCH_3)(PPh_3)$

*Chart 5.2: Complexes screened against TK-10, UACC-62, MCF-7 and HeLa cancer cells.*

5.3.1 Renal (TK-10) cell line

Complexes **1(b)**, **3** and **4** were evaluated against the TK-10 cancer cells. The chelated-O,O′ osmium complexes **1(b)**, **3** and **4** exhibited a wide range of activities. Complex **1(b)** was found to exhibit moderate activity against the renal cell line. Complex **3** also showed moderate activity against the renal cancer cells with $IC_{50}$ value of 33.46 μM. Complex **4** was found to exhibit low activity against the renal cancer cell line (*see chart 5.3*). The low activity of **4** may be attributed to the bulkiness of the binuclear complex, which limits the cellular uptake.

The P,P′-chelated complexes **7(a)-(d)** and the monodentate bis(phosphine) osmium complex **6** were screened against the TK-10 cancer cells. Complex **6** was found to exhibit an $IC_{50}$ value of 1.53 μM (*see table 5.1* p130). Complex **7(a)** was found to be slightly more potent than **6** against the renal cancer cells. The slight potency may be due to chelate effect of the dppm ligand, which contributes to the stability of **7(a)** relative to **6**. Structure modification of **7(a)** with addition of a methylene (−$CH_2$–) group to afford **7(b)** slightly increased the potency (*see chart 5.4*).

The addition of a second −$CH_2$– group which afforded **7(c)** increased the potency by 2-fold relative to **7(a)** and **7(b)**. The increase in potency may be attributed to the positioning of phenyl groups in suitable angles that allows increased exposure of interaction with the DNA bases as the alkyl chain was increased. In addition, the spreading of the phenyl rings may also contribute to exposure of the phenyl protons resulting hydrogen bonding.[40] Complex **7(d)** showed activity 3-times less than that of **7(c)** (*see chart 5.4*). This observation can be attributed to longer alkyl chain length which brings more flexibility at the phenyl groups resulting in floating of the phenyl groups in solution and hence deviation from the special angles required for intercalation. The spacers created by **7(b)** and **7(c)** upon coordination to the osmium centre may also be attributed to the high activity against the renal cancer cell line. The order of potency of the chelated-diphosphine complexes against the renal cell line was found to be: **7(d)** < **7(a)** < **7(b)** < **7(c)**.

The bridging diphosphine osmium cymene complexes were also screened against the TK-10 cancer cells. Complex **8(a)** was found to exhibit similar potency compared to **8(b)** and was 3 times more potent than **8(c)**. The activity was assumed to be because of the dppm ligand locks the two osmium centres closely together, reducing the movement of atoms and the size of the complex, which can easily get between DNA strands to allow intercalation or hydrogen bonding. The results showed that **8(b)** was potent but slightly less than **8(a)**. Complex **8(d)** was found to be inactive against the renal cancer cell line. This observation was attributed to the larger size of the **8(d)** hence less space to be accommodated on the DNA strand. The order of potency of bridged-diphosphine complexes against the renal cancer cell line was found to be: **8(d)** < **8(c)** < **8(b)** < **8(a)**.

The anticancer activities of N- and P-donor ligands in complexes **6**, **9** and **10** are discussed below. Complex **9** was found to exhibit low activity against the renal cancer cell line. This may be due to the lability of $CH_3CN$ ligands which result in the formation of non-active

adducts in the aqueous environment. Similar observations were reported by Aird and co-workers for the isostructural ruthenium complex against the human ovarian (A2780) cancer cells.[41] Structural modification of **9** by replacing one labile $CH_3CN$ ligand with one $PPh_3$ ligand to afford **10**, consequently, increases the potency by 2-3 fold (*see figure 5.4*). The increase in potency may be attributed to the presence of $PPh_3$ ligand, which brought stability to complex **10**. Addition of the second $PPh_3$ ligand to afford **6** further increased the potency by 33-fold. The increased potency was due to the increased stability of the complex combined with increased hydrophobicity.

### 5.3.2 Melanoma (UACC-62) cell line

For complexes with O,O′-chelating ligands **1(b)**, **3** and **4** were screened against the UACC-62 cancer cells. Complex **1(b)** was found to be 11-fold active than **3** while the binuclear complex **4** was less active against the melanoma cancer cells (*see chart 5.3*). Complex **1(b)** consists of two oppositely charged ions, which may be held strongly by electrostatic interactions. Hence, hydrogen bonding between the protons on the phenyl rings with the nitrogen of the adenine and oxygen of the thymine is possible.[40] Also, electrostatic charges may have played a role in the activity of **1(b)** through interaction of the positively charged complex with the negatively charged phosphate backbone of DNA. Complex **3** exhibited moderate activity against the melanoma cancer cell line. The inactivity of the binuclear complex **4** may be attributed to the size of the complex as well as the lability of the ligands.

The chelated-diphosphine osmium complexes and the monodentate bis(phosphine) complex **6** were found to exhibit diverse anticancer activities. Complex **6** exhibited high activity against the melanoma cells, which may be attributed to the stability and large surface area (*see chart 5.6*). Large surface area offers possible interactions, hence six phenyl rings of the two $PPh_3$ ligands offers large spectrum of reactivity with DNA nucleotides. Furthermore, the phenyl rings and the cymene ligand increase the hydrophobicity of the complex ion. There is also an increased probability of intercalation and hydrogen bonding of the phenyl and cymene protons to the nitrogen (adenine) and oxygen (thymine) atoms of the DNA bases.[40] Complexes **7(b)** and **7(d)** exhibited similar activities against the melanoma cancer cells (*see chart 5.4*). On the other hand, **7(a)** and **7(c)** exhibited lower activities against the melanoma cell line relative to **7(b)** and **7(d)**. The high potency of **7(b)** and **7(d)** may be attributed to the delocalization of the charge on the dppe and dppb ligands upon coordination. From the

molecular structures of **7(b)** and **7(d)**, the two complexes shows similar Os–centroid$_{cymene}$ distances. Also, the $BF_4$ anion is located alongside the dppe and dppb ligands whereas in **7(a)** and **7(c)** the $BF_4$ anion is located alongside the cymene ligand. This indicated that the formal charge in **7(b)** and **7(d)** may be delocalised on the dppe and dppb ligands. Hence, the two complexes exhibited similar reactivity against the melanoma cell line. Complex **7(a)** and **7(c)** may have the positive charge delocalised on the cymene ligand. Hence, low activity was observed because of small surface area for reactivity compared to two phenyl rings on each P atom. The increase in potency of the chelated diphosphine complexes against the melanoma cell was found to be: **7(a)** < **7(c)** < **7(b)** ≈ **7(d)**.

For the complexes with bridging-diphosphine ligands **8(a)-(d)**, a wide range of anticancer activities with melanoma cells was observed. Complex **8(a)** showed higher potency against the melanoma cell line compared to **8(b)**, **8(c)** and **8(d)** (*see chart 5.5*). The addition of methylene group (–$CH_2$–) on the diphosphine backbone **8(b)** was found to decrease the activity by 3-fold relative to **8(a)**. The high activity of **8(a)** may be attributed to the shorter carbon chain length of the dppm hence possible intercalation of the DNA strand. Complex **8(c)** shows a slight decrease in activity when compared to **8(b)**, and both complexes were found to be potent against the melanoma cell line. Complex **8(d)** was found to be inactive against the melanoma cell line. The inactivity of **8(d)** may be due to the increased stability, flexibility and bulkiness, which may cause difficulty in penetrating the cell membranes. The trend of increased potency against the melanoma cell line was found to be: **8(d)** < **8(c)** < **8(b)** < **8(a)**.

For complexes **6**, **9** and **10** with monodentate N- and P-donor ligands, various activities were observed. Complex **9** was found to be inactive against the melanoma while complex **10** was found to exhibit moderate activity against the melanoma cell line. The non-labile $PPh_3$ may be responsible for the moderate activity of **10**, because of increased stability and hydrophobicity as well as increased surface reactivity with DNA's helical structure. Addition of the second non-labile ligand $PPh_3$ to afford **6** was found to increase potency by 27-fold relative to **10** (*see chart 5.6*). The high activity may be attributed to enhanced stability and increased surface area for reactivity.

5.3.3 Breast (MCF-7) cell line

Complexes with O,O′-chelating ligands **1(b)**, **2** and **4** were screened against the breast cancer cell line. Complex **1(b)** was found to exhibit high potency against the breast cancer cell line. This activity may be due to electrostatic interaction of **1(b)** and the DNA nucleotides. Complex **3** exhibited moderate activity against the breast cancer cell line (*see chart 5.3*). Complex **4** also showed some weak activity against the breast cancer cell line, which may be due to the lability of the ligands around the central metal.

The chelating diphosphine osmium complexes **7(a)-(d)** and the bis(phosphine) osmium complex **6** exhibited a wide range of activities against breast cancer cell line. Complex **6** exhibited high activity with $IC_{50}$ value below 1μM against the breast cancer cell line. The activity of **7(a)** was found to be below 0.5 μM, which is twice as active as **6** but a similar activity to **7(d)**. Complex **7(b)** was found to be twice active than **7(a)** and **7(d)** as well as 4-fold active relative to **6**. The activity of **7(b)** may be due to the special bite angle of coordinated dppe which increases the exposure of the four phenyl rings towards the DNA nucleotides for interaction. Complex **7(c)** exhibited high activity, which is slightly more than that of 7(a), and **7(d)** (*see chart 5.4*). The free dppm and dppb ligands are found to be only moderately active against the breast (MCF7) cancer cell line with $IC_{50}$ values of $0.7 \pm 0.1$ μM and $0.8 \pm 0.5$ μM respectfully.[42] Therefore **7(a)** and **7(d)** has been found to exhibit increased anticancer activity relative to their respective free ligands. The increased activity may be attributed to the bite angles as well as the length of spacer upon coordination of the free ligands. The electronic properties of this coordinated dppe and dppp ligands may allow locking of P atoms by limiting movement of phenyl groups, hence increasing reactivity surface exposure. The trend of increased potency of the chelated complexes against the breast cancer cell line was found to be: **7(d)** ≈ **7(a)** < **7(c)** < **7(b)**.

The bridging-diphosphine osmium complexes **8(a)-(d)** exhibited a wide range of activities against the breast cancer cells. Complex **8(a)** showed an activity below 2 μM which was found to be 4-fold higher than that of **8(b)** and 5-fold higher than that of **8(c)** (*see chart 5.5*). Complex **8(b)** was found to be slightly higher in activity against breast cancer cell line compared to **8(c)**. Surprisingly **8(d)** was found to be inactive against the breast cancer cell line. The diphosphine-bridged binuclear complexes **8(a)** and **8(d)** were also found to exhibit

reduced activity against the breast cancer cell line relative to the respective free ligands. The reduced activity of **8(a)** may be due to the size of the complex whereas the inactive character of **8(d)** may be attributed to the larger size of the binuclear complex. The increased potency of the complexes with bridging-diphosphine ligands against the breast cancer cell line was found to be: **8(d)** < **8(c)** < **8(b)** < **8(a)**.

Complexes with monodentate N- and P-donor ligands **6**, **9** and **10** were also screened against the breast cancer cell line. Complex **9** was found to be inactive against the breast cancer cell lines. On replacement of one of the labile ligands with $PPh_3$, **10** were found to increase activity against the breast cancer cell line. The introduction of a non-labile ligand was found to increase the cytotoxicity towards cancer cells. This may be due to increased stability and cell uptake of **10** because of the hydrophobicity of the phenyl groups.[20] Replacement of the second labile ligand by another $PPh_3$ ligand to afford complex **6** increased the activity by 29-fold (*see chart 5.6*). The two $PPh_3$ ligands in **6** offer an increased surface reactivity and increased stability as well as increased cellular uptake.

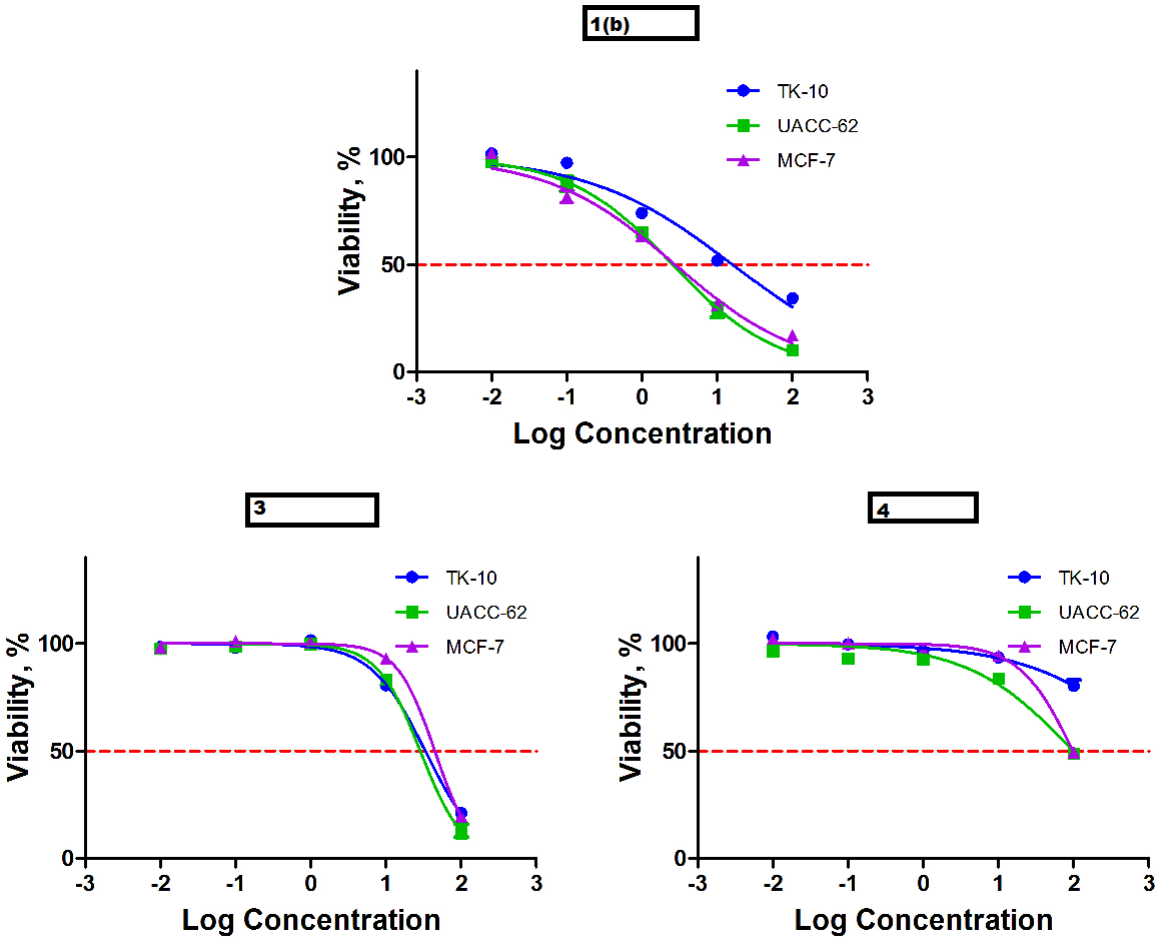


*Chart 5.3: The plot of log concentration versus percentage cell viability of* ***1(b)****,* ***3*** *and* ***4*** *against TK-10, UACC-62 and MCF-7.*

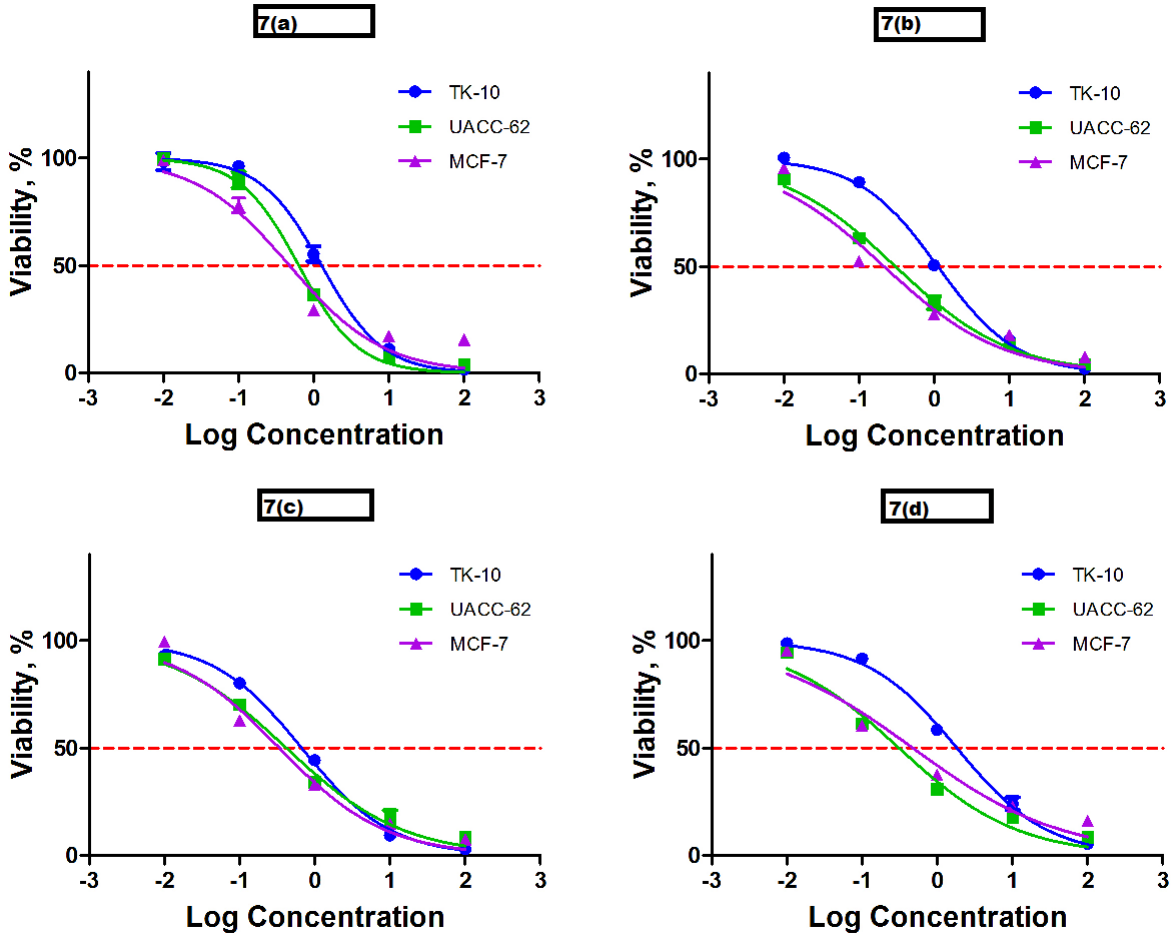


*Chart 5.4: The plot of log concentration versus percentage cell viability of complexes* ***7(a)-(d)*** *against TK-10, UACC-62 and MCF-7.*

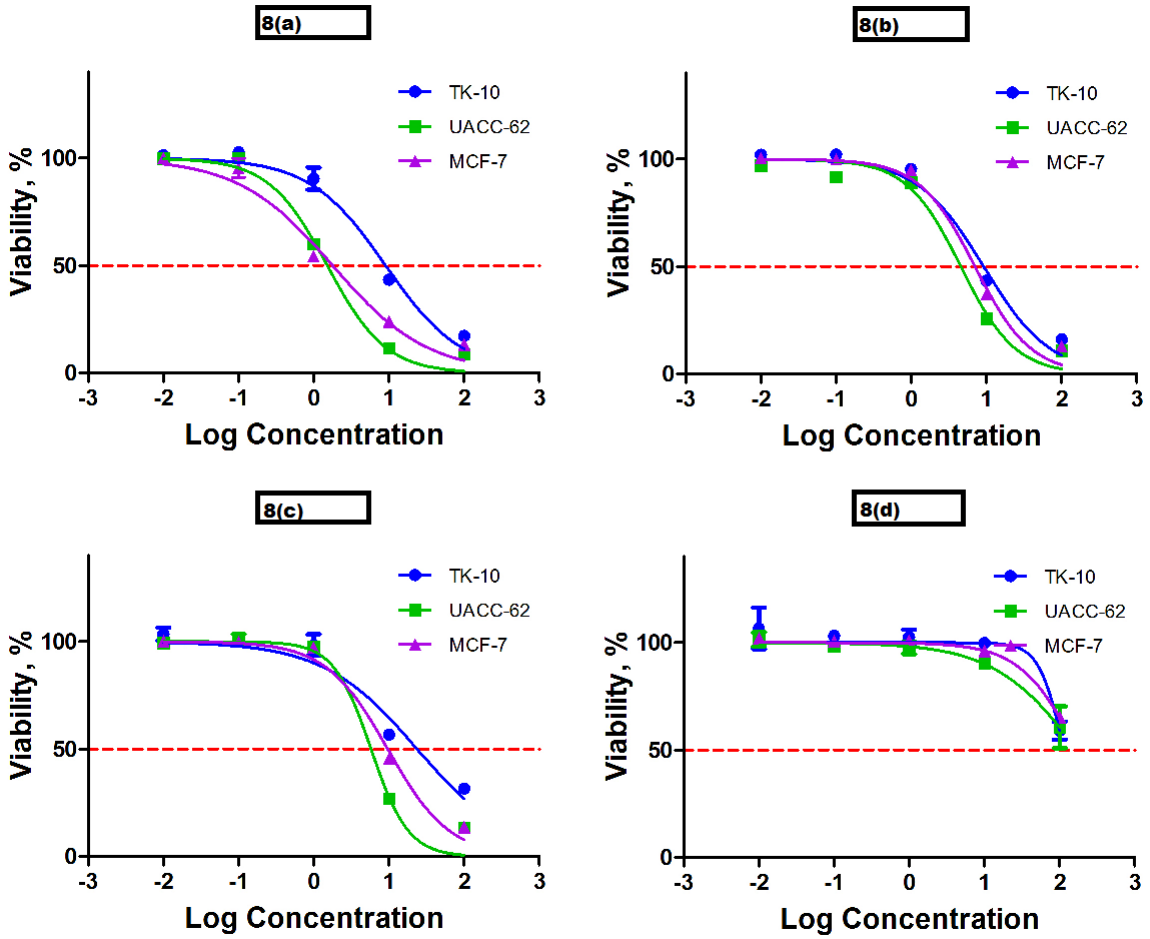


*Chart 5.5: The plot of log concentration versus percentage cell viability of complexes* ***8(a)-(d)*** *against TK-10, UACC-62 and MCF-7.*

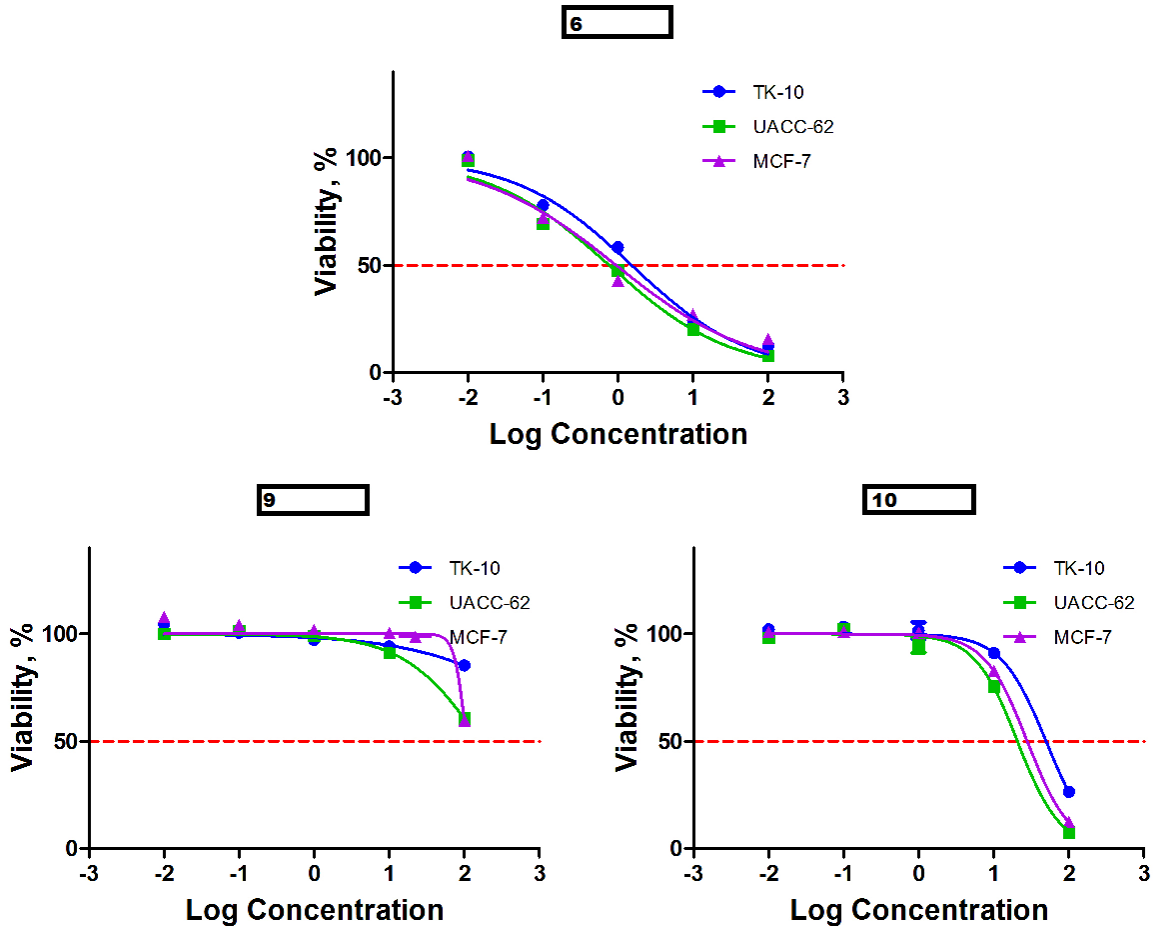


*Chart 5.6: The plot of log concentration versus percentage cell viability of **6**, **9** and **10** against TK-10, UACC-62 and MCF-7.*

5.3.4 HeLa cell line

The HeLa cell line was used to determine the general cytotoxicity of the fourteen complexes (*see chart 5.2*). The general cytotoxicity has been classified according to CSIR criteria as follows: low hazard ($IC_{50}$ value > 100 μM), weak hazard (100 μM > $IC_{50}$ value > 50 μM), moderate hazard (50 μM > $IC_{50}$ value > 10 μM) and high hazard ($IC_{50}$ value < 10 μM).[43]

Complexes with O,O′-chelating ligands **1(b)**, **3** and **4** showed a wide range of cytotoxicity against the HeLa cell line. Complex **1(b)** exhibited a moderate activity and **3** showed low activities which were considered a weak hazard against the HeLa cell. Complex **4** was inactive against the HeLa cell line, which was considered a low hazard complex.

For chelated-P,P′ osmium complexes and the monodentate bis(phosphine) osmium complex **6** a wide range of anticancer activities against the HeLa cancer cells was observed. Complex **6**

was found to exhibit potency below 1 μM against the HeLa cell line. This may be due to the stability of the complex combined with the hydrophobicity provided by six phenyl groups of the two $PPh_3$ ligands, which in turn increases cellular uptake of the complex. The may be possible intercalation as well as hydrogen bonding between the nucleotides with the phenyl protons. Also the cationic character of the osmium cymene complex may contribute to the potency of the complex because of electrostatic interactions with the electronegative sugar phosphate ions of the DNA.[40] Therefore, complex **6** was considered a high hazard according to the CSIR criteria.

The chelated-diphosphine mononuclear complexes **7(a)-(d)** were found to be potent against the HeLa cell lines. The potency of **7(a)** was found to be below 4 μM against the HeLa cell line. This may be due to the decreased spacer of **7(a)** relative to **7(b)-(d)**. Complex **7(b)** was found to be more active against the HeLa cell line relative to **7(a)**. Complex **7(c)** shows slightly higher potency against **7(a)** but slightly lower than **7(b)**. Complex **7(d)** shows activity slightly lower than that of **7(b)** and **7(c)** but slightly higher than that of **7(a)**. Since all the $IC_{50}$ values of the complexes **7(a)-(d)** series were all below 10 μM. All the chelated-diphosphine complexes were considered hazardous towards the HeLa cell line (*see table 5.1*).

The bridged-diphosphine binuclear complexes **8(a)-(d)** exhibited different anticancer activities against the HeLa cells. Complex **8(a)** showed high potency against the HeLa cancer cell line whereas structural modification of **8(a)** by addition of $-CH_2-$ group to afford complex **8(b)** reduces the potency. The reduction in activity may be due to the larger size of **8(b)** as the carbon chain length was increased. The higher the carbon chain length of the diphosphine the more flexible the whole binuclear complex becomes, therefore the loss of fixed positions of the atoms. Complex **8(c)** exhibited weak activity against the HeLa cell line. The loss of activity may be due to the increased carbon chain length, which increases the flexibility of the whole complex. Complex **8(d)** was also found to be inactive against the HeLa cell line.

The bridged-diphosphine binuclear complexes exhibited interesting behaviour against the HeLa cell line. The trend of increased potency against the HeLa cell line was found to be: **8(d)** < **8(c)** < **8(b)** < **8(a)**. The trend of increased hazardousness against the HeLa cell line was found to be: **8(d)** < **8(c)** < **8(b)** < **8(a)**. Therefore, **8(c)** and **8(d)** exhibited weak hazard relative **8(b)** and **8(a)** against the HeLa cell line.

For complexes with monodentate N- and P-donor ligands, screening against the HeLa cell line exhibited a wide range of activities. Complex **9** exhibited low potency against the HeLa cell line while **10** exhibit a moderate potency against the HeLa cell line. The labile $CH_3CN$ ligands of **9** may be the reason lower potency was observed against the HeLa cell line. The introduction of $PPh_3$ in **10** enhances stability, hence an increased potency was observed. Complex **6** exhibited higher potency relative to **9** and **10** because of increased stability, increased hydrophobicity and increased surface reactivity. Therefore **9** were found to exhibit lower hazard and **10** exhibit moderate hazards and **6** exhibit high hazards.

*Table 5.1: The $IC_{50}$ (μM) results against TK-10, UACC-62, MCF-7 and HeLa cell lines.*

| Complexes | TK-10 (renal) | UACC-62 (melanoma) | MCF-7 (breast) | HeLa |
|---|---|---|---|---|
| **1(b)** | 16.02 | 2.56 | 2.76 | 21.3 |
| **3** | 33.46 | 28.71 | 44.76 | 96.1 |
| **4** | >100 | 99.07 | 98.56 | >100 |
| **6** | 1.53 | 0.77 | 0.95 | 0.78 |
| **7(a)** | 1.28 | 0.64 | 0.48 | 3.66 |
| **7(b)** | 1.12 | 0.31 | 0.22 | 1.93 |
| **7(c)** | 0.67 | 0.42 | 0.34 | 2.36 |
| **7(d)** | 1.83 | 0.31 | 0.48 | 3.02 |
| **8(a)** | 9.07 | 1.52 | 1.79 | 7.71 |
| **8(b)** | 9.22 | 4.58 | 7.07 | 29.5 |
| **8(c)** | 23.75 | 5.8 | 9.67 | 66 |
| **8(d)** | >100 | >100 | >100 | >100 |
| **9** | >100 | >100 | >100 | >100 |
| **10** | 49.77 | 20.7 | 27.98 | 45.9 |

## 5.4 Conclusions

Osmium cymene complexes have demonstrated a range of anticancer activity against three cancer cell lines (TK-10, UACC-62 and MCF-7) depending on the ligand system and the general cytotoxicity against the HeLa cells. However, a challenge remains the poor selectivity of these osmium cymene complexes between the three cancer cell lines and the HeLa cell line.

The phosphine containing complexes **6**, **7(a)-(d)**, **8(a)** and **8(b)** were found to be very active against the renal cancer cell line whereas **1(b)**, **3**, **4**, **8(c)**, **8(d)**, **9** and **10** were found to be less active. The melanoma cancer cell line showed some susceptibility against **1(b)**, **6**, **7(a)-(d)** and **8(a)-(c)** in this study; however, some resistance was observed against **3**, **4**, **8(d)**, **9** and **10**. The breast cancer cell line also showed similar susceptibility to the same complexes and similar resistance to the same complexes as the melanoma cell line with more or less $IC_{50}$ values. Complexes **6**, **7(a)-(d)** and **8(a)** showed to be the only active complexes against the HeLa cancer cells while **1(b)**, **3**, **4**, **8(b)-(d)**, **9** and **10** were found to be less active. The renal and HeLa cancer cell lines were observed to be resistance to all the O,O′ chelated complexes suggesting a similar mode of action of these O,O′ complexes.

It has been found that the most potent complexes **6** and **7(a)-(d)** have strongly bound phosphine ligands. Hence, the metal centre was assumed not to have covalent interaction with the DNA bases as Cisplatin does. The high potency of **6** and **7(a)-(d)** may be attributed to the intercalation of phenyl groups on the diphosphine backbone, electrostatic interaction of the cationic osmium complex and/or the hydrogen bonding of phenyl protons to the thymine and adenine DNA bases. The presence of the phenyl groups had a positive influence on the anticancer activity of these complexes, in a sense that, they enhance the hydrophobicity on the metal complex moiety. Also the chelated-diphosphine complexes **7(a)-(d)** have shown high anticancer activity against the four cancer cells relative to the monodentate bis(phosphine) complex **6**.

The carbon chain length on the diphosphine complexes plays a key role in the activity of the bridged-diphosphine osmium complexes. The shorter chain length of the bridged-diphosphine binuclear complexes exhibit enhanced anticancer activity against cancer cell lines compared to the longer carbon chain length of the bridged-diphosphine binuclear complexes.

## 5.5 Future work

The mechanisms of action of the most potent complexes need further investigation. Complexes with activity lower than 1μM may be subjected to DNA binding studies in order to understand the selectivity of the complexes.

## 5.6 References


(1) Dabrowiak, J. C. *Metals in Medicine*; John Wiley & Sons, Ltd. : United Kingdom, 2009.

(2) Johnstone, T. C.; Suntharalingam, K.; Lippard, S. J. *Chem. Rev.* **2016**, *116*, 3436.

(3) Page, S. *Education in Chemistry* **2012**, 26.

(4) Gore, M. E.; Fryatt, I.; Wiltshaw, E.; Dawson, T.; Robinson, B. A.; Calvert, A. H. *Br. J. Cancer* **1989**, *60*, 767.

(5) Stordal, B.; Pavlakis, N.; Davey, R. *Cancer Treat. Rev.* **2007**, *33*, 347.

(6) Boulikas, T.; Pantos, A.; Bellis, E.; Christofis, P. *Cancer Therapy* **2007**, *5*, 537.

(7) Wu, Q.; Qin, S.-K.; Teng, F.-M.; Chen, C.-J.; Wang, R. *J. Hematol. Oncol.* **2010**, *3*, 1.

(8) Pasetto, L. M.; D'Andrea, M. R.; Brandes, A. A.; Rossi, E.; Monfardini, S. *Crit. Rev. Oncol. Hematol.* **2006**, *60*, 59.

(9) Eckstein, N. *J. Exp. Clin. Canc. Res* **2011**, *30*, 6.

(10) Florea, A.-M.; Busselberg, D. *Cancers* **2011**, *3*, 1351.

(11) Allardyce, C. S.; Dyson, P. J. *Platin. Met. Rev.* **2001**, *45*, 62.

(12) Rademaker-Lakhai, J. M.; van den Bongard, D.; Pluim, D.; Beijnen, J. H.; Schellens, J. H. M. *Clin. Cancer Res.* **2004**, *10*, 3717.

(13) Jakupec, M. A.; Arion, V. B.; Kapitza, S.; Reisner, E.; Eichinger, A.; Pongratz, M.; Marian, B.; Graf van Keyserlingk, N.; Keppler, B. K. *Int. J. Clin. Pharm. Th.* **2005**, *43*, 595.

(14) Leijen, S.; Burgers, S. A.; Baas, P.; Pluim, D.; Tibben, M.; van Werkhoven, E.; Alessio, E.; Sava, G.; Beijnen, J. H.; Schellens, J. H. M. *Invest New Drugs* **2015**, *33*, 201.

(15) Habtemariam, A.; Melchart, M.; Fernandez, R.; Parsons, S.; Oswald, I. D. H.; Parkin, A.; Fabbiani, F. P. A.; Davidson, J. E.; Dawson, A.; Aird, R. E.; Jodrell, D. I.; Sadler, P. J. *J. Med. Chem.* **2006**, *49*, 6858.

(16) Daguenet, C.; Scopelliti, R.; Dyson, P. J. *Organomet.* **2004**, *23*, 4849.

(17) Jensen, S. B.; Rodger, S. J.; Spicer, M. D. *J. Organomet. Chem.* **1998**, *556*, 151.

(18) Morris, R. E.; Aird, R. E.; Murdoch, P. d. S.; Chen, H.; Cummings, J.; Hughes, N. D.; Parsons, S.; Parkin, A.; Boyd, G.; Jodrell, D. I.; Sadler, P. J. *J. Med. Chem.* **2001**, *44*, 3616.

(19) Scolaro, C.; Bergamo, A.; Brescacin, L.; Delfino, R.; Cocchietto, M.; Laurenczy, G.; Geldbach, T. J.; Sava, G.; Dyson, P. J. *J. Med. Chem.* **2005**, *48*, 4161.

(20) Scolaro, C.; Chaplin, A. B.; Hartinger, C. G.; Bergamo, A.; Cocchietto, M.; Keppler, B. K.; Sava, G.; Dyson, P. J. *Dalton Trans.* **2007**, 5065.

(21) Maksimoska, J.; Williams, D. S.; Atilla-Gokcumen, G. E.; Smalley, K. S. M.; Carroll, P. J.; Webster, R. D.; Filippakopoulos, P.; Knapp, S.; Herlyn, M.; Meggers, E. *Chem.* **2008**, *14*, 4816.

(22) Peacock, A. F. A.; Habtemariam, A.; Moggach, S. A.; Prescimone, A.; Parsons, S.; Sadler, P. J. *Inorg. Chem.* **2007**, *46*, 4049.

(23) Hanif, M.; Babak, M. V.; Hartinger, C. G. *Drug Discovery Today* **2014**, *00*, 1.

(24) Kostrhunova, H.; Florian, J.; Novakova, O.; Peacock, A. F. A.; Sadler, P. J.; Brabec, V. *J. Med. Chem.* **2008**, *51*, 3635.

(25) Filak, L. K.; Muhlgassner, G.; Jakupec, M. A.; Heffeter, P.; Berger, W.; Arion, V. B.; Keppler, B. K. *J. Biol. Inorg. Chem.* **2010**, *15*, 903.

(26) Fu, Y.; Habtemariam, A.; Basri, A. M. B. H.; Braddick, D.; Clarkson, G. J.; Sadler, P. J. *Dalton Trans.* **2011**, *40*, 10553.

(27) van Rijt, S. H.; Romero-Canelon, I.; Fu, Y.; Shnyder, S. D.; Sadler, P. J. *Metallomics* **2014**, *6*, 1014.

(28) Fu, Y.; Soni, R.; Romero, M. J.; Pizarro, A. M.; Salassa, L.; Clarkson, G. J.; Hearn, J. M.; Habtemariam, A.; Wills, M.; Sadler, P. J. *Chem. Eur. J.* **2013**, *19*, 15199.

(29) Filak, L. K.; Göschl, S.; Heffeter, P.; Samper, K. G.; Egger, A. E.; Jakupec, M. A.; Keppler, B. K.; Berger, W.; Arion, V. B. *Organomet.* **2013**, *32*, 903.

(30) Huang, J.; Serron, S.; Nolan, S. P. *Organomet.* **1998**, *17*, 4004.

(31) Romero-Canelon, I.; Salassa, L.; Sadler, P. J. *J. Med. Chem.* **2013**, *56*, 1291.

(32) Karami, K.; Hosseini-Kharat, M.; Sadeghi-Aliabadi, H.; Lipkowski, J.; Mirian, M. *Eur. J. Med. Chem.* **2014**, *73*, 8.

(33) Dougan, S. J.; Habtemariam, A.; McHale, S. E.; Parsons, S.; Sadler, P. J. *Proc. Natl. Acad. Sci.* **2008**, *105*, 11628.

(34) van Tonder, A.; Joubert, A. M.; Cromarty, A. D. *BMC Res. Notes* **2015**, *8*, 1.

(35) Denizot, F.; Lang, R. *J. lmmunol. Methods* **1986**, *89*, 271.

(36) Skehan, P.; Storeng, R.; Scudiero, D.; Monks, A.; McMahon, J.; Vistica, D.; Warren, J. T.; Bokesch, H.; Kenney, S.; Boyd, M. R. *J. Natl. Cancer Inst.* **1990**, *82*, 1107.

(37) Banasiak, D.; Barnetson, A. R.; Odell, R. A.; Mameghan, H.; Russell, P. J. *Radiat. Oncol. Invest.* **1999**, *7*, 77.

(38) Keepers, Y. P.; Pizao, P. E.; Peters, G. J.; van Ark-Otte, J.; Winograd, B.; Pinedo, H. M. *Eur. J. Cancer* **1991**, *27*, 897.

(39) Vichai, V.; Kirtikara, K. *Nat. Protoc.* **2006**, *1*, 1111.

(40) Sirajuddin, M.; Ali, S.; Badshah, A. *J. Photochem. Photobiol.* **2013**, *124*, 1.

(41) Aird, R. E.; Cummings, J.; Ritchie, A. A.; Muir, M.; Morries, R. E.; Chen, H.; Salder, P. J.; Jodrell, D. I. *Br. J. Cancer* **2002**, *86*, 1652.

(42) Meyer, A.; Gutiérrez, A.; Ott, I.; Rodríguez, L. *Inorg. Chim. Acta* **2013**, *398*, 72.

(43) Fouche, G.; Cragg, G. M.; Pillay, P.; Kolesnikova, N.; Maharaj, V. J.; Senabe, J. *Journal of Ethnopharmacology* **2008**, *119*, 455.

# CHAPTER 6

## EXPERIMENTAL

### 6.1 Standard procedures and materials

All synthetic procedures were carried under an argon atmosphere using standard Schlenk techniques unless otherwise stated in the relevant synthetic method. All solvents, phosphine (ddpm, dppe, dppp, dppb and $PPh_3$) and tropolone ligands used were obtained from Sigma-Aldrich. Potassium osmate salt was kindly donated by Anglo-Platinum research laboratory. Phellandrene was purchased from Fluka and used as received. The $(NH_4)_2C_2O_4{\cdot}H_2O$ used was purchased from Kanto Chemical Co. Inc. and used as received. The $Ag_2C_2O_4$ used was prepared in our laboratory from $AgNO_3$ and $(NH_4)_2C_2O_4{\cdot}H_2O$ according to literature methods.[1] Solvents were dried and purified by standard methods. Methanol was dried by distilling over $Mg/I_2$, acetonitrile ($CH_3CN$) over calcium hydride ($CaH_2$), dichloromethane ($CH_2Cl_2$) stored over calcium chloride ($CaCl_2$) for 24 hours followed by distillation over calcium hydride and nitrobenzene ($C_6H_5NO_2$) was dried over phosphorus pentaoxide ($P_2O_5$) followed by distillation prior to use.

### 6.2 Instrumentation

Agilent technologies 500 MHz premium Compact NMR was used to collect data $^{1}H$ (500 MHz), $^{13}C$ (125 MHz), $^{19}F$ (470 MHz) and $^{31}P$ (202 MHz). IR data was collected from Bruker vertex 70 FTIR instrument employing ATR with diamond crystal. The data was collected within the spectral range of 400 - 4000 $cm^{-1}$, resolution of 4 and 32 numbers of scans. Raman data was also collected from the Bruker Raman II instrument within the spectral range 0 – 5000 $cm^{-1}$, resolution 4 and 128 numbers of scans employing laser with pellets.

Elemental Analysis data were obtained from Carlo Erba NA 1500 Nitrogen Carbon Sulphur Analyser. The instrument uses Gas Chromatography (GC) to separate the gases, i.e. N (in the form of $N_2$), C (in the form of $CO_2$) and S (in the form of $SO_2$), using a He carrier gas and a thermal conductivity detector. The instrument is from Agricultural Research Council-Institute for Soil, Climate and Water analysed by Mr. M. Philport. Thermogravimetric Analysis of the

all complexes in this study was carried out with Thermogravimetric analyser (TGA/DSC) SQ600 between 50 and 800 ºC at a heating rate 20 ºC/min and gas flow rate of 10 mL/min under nitrogen atmosphere in our laboratories. Conductance data was collected from the Metrohm 644 conductometer in our laboratory.

Single crystal XRD data were obtained from the diffractometer Bruker Venture D8 Photon CMOS with graphite-monochromated MoK$\alpha_1$ ($\lambda$ = 0.71073 Å) radiation at 173 K using an Oxford Cryostream 600 cooler at Wits University collected by Professor A. Lemmerer.

Ms. N. Kolesnikova at the CSIR Boiscience laboratories carried out anticancer testing.

### 6.3 Methods for cancer testing against four cancerous cell lines

The human cell lines TK10, UACC62 and MCF7 and were obtained from the National Cancer Institute (NCI) in the framework of collaborative research program between CSIR and NCI. The TK10, UACC62 and MCF-7 cell lines were routinely maintained as monolayer cell culture at 37 ºC, 5% $CO_2$, 95% air and 100% relative humidity in RPMI containing 5% fetal bovine serum, 2 mM L-glutamine and 50 µg/ml gentamicin.

For screening experiment of TK10, UACC62 and MCF-7, the cells (3-19 passages) were inoculated in a 96-well microtiter plates at plating densities of 7-10 000 cells/well and were incubated for 24 h. After 24 h the cells were treated with the experimental osmium complexes which were previously dissolved in DMSO and diluted in medium to produce 5 concentrations. Cells without osmium complex addition served as control. The blank contains complete medium without cells. Parthenolide was used as a standard.

The HeLa cell line (Human Negroid cervix epitheloid adenocarcinoma, ECACC) was routinely maintained as a monolayer cell culture at 37 ºC, 5% $CO_2$, 95% air and 100% relative humidity in EMEM containing 5% fetal bovine serum, 2 mM L-glutamine and 50 µg/ml gentamicin.

For screening experiment of HeLa, the cells (3-16 passages) were inoculated in a 96-well microtiter plates at plating densities of 7 000 cells/well and were incubated for 24 h. After 24 h the cells were treated with the experimental osmium complexes which were previously dissolved in DMSO and diluted in medium to produce 5 concentrations. Cells without the

osmium complex addition served as control. The blank contains complete medium without cells. Emetine was used as a standard.

All the plates were incubated for 48 h after addition of osmium complexes. Viable cells were fixed to the bottom of each well with cold 50% trichloroacetic acid, washed, dried and dyed by Sulforhodamine B (SRB). Unbound dye was removed and protein-bound dye was extracted with 10mM Tris base for optical density determination at the wavelength 540 nm using a multiwell spectrophotometer.

Data analysis was performed using GraphPad Prism software. The 50% of cell growth inhibition ($IC_{50}$) was determined by non-linear regression.

6.3.1 Assay conditions

The samples (14) were screened with the following assay conditions: samples were tested at concentrations of 100 – 0.01 μM (5 × 10-fold serial dilutions), reference standards of Parthenolide (100 – 0.01 μM) and Emetine (100 – 0.01 μM, 5 × 10-fold serial dilutions), the absorbance reading was recorded at 540 nm and the assay prerequisites of *Z' factor > 0.5.

## 6.4 Preparation of complexes

6.4.1 Synthesis of starting material $[Os(\eta^6\text{-}p\text{-cymene})Br_2]_2$

The osmium dimer $[Os(\eta^6\text{-}p\text{-cymene})Br_2]_2$ was used as starting material for the synthesis of the osmium cymene complexes studied in this work. The preparation of the starting material was followed as reported in the literature.[2]

6.4.2 Preparation of **1(a)** $Ag[Os(\eta^6\text{-}p\text{-cymene})Br(\kappa^2\text{-}O,O'\text{-}C_2O_4)]$

The starting material $[Os(\eta^6\text{-}p\text{-cymene})Br_2]_2$ (2.130 g, 2.20 mmol) and excess $Ag_2C_2O_4$ (2.757 g, 9.08 mmol) were stirred in $CH_2Cl_2/CH_3OH$ solution (100 mL 1:1 v/v) at room temperature overnight. The Schlenk tube was covered with aluminium foil to prevent decomposition of silver oxalate to AgO by UV radiation. The milky yellow solution was filtered to remove AgBr formed and unreacted $Ag_2C_2O_4$ salt. The yellow filtrate developed yellow and grey suspensions on standing. The solvent was removed *in vacuo* and the yellow precipitate was dissolved in $CH_2Cl_2$ (10 mL) and the grey precipitate was filtered off. The

solvent was removed again *in vacuo* under reduced pressure resulting in a yellow product. The product was dried *in vacuo*. Yield 55% (1.437 g, 2.40 mmol). $^{1}$H NMR (500 MHz, dmso-$d_6$) δ: 1.24 (d, 6H, CH(C$\underline{H}_3$)$_2$, $J_{(HH)}$ = 6.9 Hz); 2.17 (s, 3H, C$\underline{H}_3$C$_6$H$_4$); 2.67 (sept, 1H, C$\underline{H}$(CH$_3$)$_2$, $J_{(HH)}$ = 6.8 Hz); 6.09 (d, 2H, η$^6$-C$_6$H$_4$, $J_{(HH)}$ = 6.4 Hz); 6.22 (d, 2H, η$^6$-C$_6$H$_4$, $J_{(HH)}$ = 5.9 Hz). $^{13}$C{$^{1}$H} NMR δ: 17.25 $\underline{C}$H$_3$C$_6$H$_4$; 22.34 CH($\underline{C}$H$_3$)$_2$; 30.65 $\underline{C}$H(CH$_3$)$_2$; {95.41, 90.77, 78.80, 77.46} η$^6$-C$_6$H$_4$; 163.78 ($\underline{C}$O). IR (cm$^{-1}$): $\nu_{asym(OCO)}$ 1688vs/1671sh/1640sh, 1595vs/1574sh; $\nu_{sym(OCO)}$ + $\nu_{(CC)}$ 1457vw/1422m; $\nu_{sym(OCO)}$ 1265m; $\nu_{(CC)}$ 911vw/876w; $\nu_{(CC)}$ + $\delta_{(OCO)}$ 794s.

6.4.3 Preparation of **1(b)** PPh$_4$[Os(η$^6$-*p*-cymene)Br(κ$^2$-O,O′-C$_2$O$_4$)]

Complex **1(a)** (0.507 g, 0.84 mmol) was dissolved in $CH_2Cl_2$ (50 mL). To this was added a solution of tetraphenylphosphonium bromide (PPh$_4$Br) (0.426 g, 1.02 mmol) in $CH_2Cl_2$ (20 mL) mixed dropwise with stirring for 30 minutes at room temperature. The yellow solution was reduced to *ca.* 20mL. Hexane (40mL) was added dropwise, the solution shaken to give bright yellow suspension, which was washed with hexane for 2 h. The bright yellow product was isolated by filtration and dried *in vacuo*. Yield 74% (0.522 g, 0.63 mmol). $^{1}$H NMR (500 MHz, $CDCl_3$): 1.27 (d, 6H, CH(C$\underline{H}_3$)$_2$, $J_{(HH)}$ = 6.8 Hz); 2.23 (s, 3H, C$\underline{H}_3$C$_6$H$_4$); 2.80 (sept, 1H, C$\underline{H}$(CH$_3$)$_2$, $J_{(HH)}$ = 6.9 Hz); 5.64 (d, 2H, η$^6$-C$_6$H$_4$, $J_{(HH)}$ = 5.9); 5.91 (d, 2H, η$^6$-C$_6$H$_4$, $J_{(HH)}$ = 5.4 Hz); 7.57 - 7.91 (m, 20H, PPh$_4$). $^{13}$C{$^{1}$H} NMR δ: 18.91 $\underline{C}$H$_3$C$_6$H$_4$; 23.01 CH($\underline{C}$H$_3$)$_2$; 31.66 $\underline{C}$H(CH$_3$)$_2$; {117.82, 117.15, 71.76, 68.86} η$^6$-C$_6$H$_4$; 130.79 – 135.75 C$_{Aromatic}$; 166.90 ($\underline{C}$O). $^{31}$P{$^{1}$H}: 24.06 (s, PPh$_4$). IR (cm$^{-1}$): $\nu_{asym(OCO)}$ 1695s/1674s/1653s; $\nu_{sym(OCO)}$ + $\nu_{(CC)}$ 1483w/1436m; $\nu_{sym(OCO)}$ 1378s/1317w; $\nu_{(CC)}$ 910vw/886vw; $\nu_{(CC)}$ + $\delta_{(OCO)}$ 787s. Elemental analysis (%) for C$_{36}$H$_{34}$BrO$_4$OsP · 0.1 mol CH$_3$(CH$_2$)$_4$CH$_3$: Calculated – C 51.98, H 4.12; found – C 52.26, H 4.46.

6.4.4 Preparation of **2** [Os(η$^6$-*p*-cymene)Br(κ$^2$-O,O′-C$_2$O$_4$)PPh$_3$]

The method for preparation of complexes **2** was adopted from Yan and co-workers with some modifications.[3] Complex **1(a)** (0.354 g, 0.59 mmol) and an excess PPh$_3$ (0.570 g, 2.17 mmol) were placed into the Schlenk tube. The solids were dissolved in $CH_2Cl_2$/$CH_3OH$ (1:1 20 mL) solution. The orange yellow solution was stirred with reflux at 44 ºC overnight. The yellow solution was cooled to room temperature and filtered. The solvent was removed *in vacuo* to yield yellow oil. The yellow oil was washed in hexane over 24 h. The yellow precipitate was

obtained by filtration and dried *in vacuo*. Yield 79% (0.316 g, 0.47 mmol) $^{1}$H NMR (500 MHz, $CDCl_3$) δ: 1.16 (d, 6H, CH(C<u>H</u>$_3$)$_2$, $J_{(HH)}$ = 6.9 Hz); 2.01 (s, 3H, C<u>H</u>$_3$C$_6$H$_4$); 2.47 (sept, 1H, C<u>H</u>(CH$_3$)$_2$, $J_{(HH)}$ = 6.8 Hz); 5.29 (d, 2H, η$^6$-C$_6$H$_4$, $J_{(HH)}$ = 5.4 Hz); 5.51 (d, 2H, η$^6$-C$_6$H$_4$, $J_{(HH)}$ = 5.9 Hz); 7.41 - 7.50 (m, 15H, Ph). $^{13}$C{$^{1}$H} NMR δ: 18.04 <u>C</u>H$_3$C$_6$H$_4$; 22.70 CH(<u>C</u>H$_3$)$_2$; 31.00 <u>C</u>H(CH$_3$)$_2$; {98.82 ($J$ = 3 Hz), 88.39, 79.35 ($J$ = 5 Hz), 79.10 ($J$ = 4 Hz)} η$^6$-C$_6$H$_4$; 128.91 - 134.40 $C_{Aromatic}$; 164.22 CO. $^{31}$P{$^{1}$H}: 1.78 (s, $PPh_3$). IR (cm$^{-1}$): $\nu_{asym(OCO)}$ 1706sh/1693s/1669s; $\nu_{sym(OCO)}$ + $\nu_{(CC)}$ 1482vw/1433w; $\nu_{sym(OCO)}$ 1371sh/1363sh/1356s; $\nu_{(CC)}$ 904vw/875w; $\nu_{(CC)}$ + $\delta_{(OCO)}$ 786s. Elemental analysis (%) for $C_{30}H_{29}O_4OsP$: Calculated – C 53.40, H 4.33; found – C 53.40, H 4.24.

6.4.5 Preparation of **3** [Os(η$^6$-*p*-cymene)Br(κ$^2$-O,O′-$C_7H_5O_2$)]

The procedure for preparation of complex **3** was adopted from Melchart and co-workers.[4] The starting material [Os(η$^6$-*p*-cymene)Br$_2$]$_2$ (1.037 g, 1.07 mmol) and sodium tropolonate (0.448 g, 3.11 mmol) were weighed into a Schlenk tube. Methanol (100 mL) was added to the Schlenk tube and the reddish-orange solution was stirred overnight at room temperature. A dark brown solution was obtained. The solution was filtered and the solvent was removed *in vacuo*. The product was extracted with $CH_2Cl_2$ (80 mL). The resulting solution was reduced to *ca.* 20mL and hexane (40 mL) was added into the brown solution and shaken to give an opaque solution. Then the solution was filtered again to give a reddish solution. The solvent was removed to give a dark brown precipitate and dried *in vacuo*. Yield 72% (0.807 g, 1.54 mmol). $^{1}$H NMR (500 MHz, $CDCl_3$) δ: 1.29 (d, 6H, CH(C<u>H</u>$_3$)$_2$, $J_{(HH)}$ = 6.9 Hz); 2.38 (s, 3H, C<u>H</u>$_3$C$_6$H$_4$); 2.76 (sept, 1H, C<u>H</u>(CH$_3$)$_2$, $J_{(HH)}$ = 6.9 Hz); 5.78 (d, 2H, η$^6$-C$_6$H$_4$, $J_{(HH)}$ = 5.5 Hz); 6.00 (d, 2H, η$^6$-C$_6$H$_4$, $J_{(HH)}$ = 5.8 Hz); 6.80 – 6.87 (tt, 1H, trop-O,O′, $J_{(HH)}$ = 8.8 Hz); 7.20 – 7.31 (m, 4H, trop-O,O′). $^{13}$C{$^{1}$H} NMR δ: 19.56 <u>C</u>H$_3$C$_6$H$_4$; 23.00 CH(<u>C</u>H$_3$)$_2$; 32.02 <u>C</u>H(CH$_3$)$_2$; {91.00, 87.26, 71.76, 69.63} η$^6$-C$_6$H$_4$; 185.85 (<u>C</u>O); 127.42 – 138.07 (trop-C). IR (cm$^{-1}$): $\nu_{(CC)}$ 1588s; $\nu_{(CO)}$ + $\nu_{(CC)}$ 1512s; $\nu_{(CC)}$ 1424vs; $\delta_{(CH)}$ 1407vs; $\nu_{(CO)}$ 1353/1341. Elemental analysis (%) for $C_{17}H_{19}BrO_2Os$: Calculated – C 38.86, H 3.64; found – C 38.73, H 3.72.

6.4.6 Preparation of **4** [{Os(η$^6$-*p*-cymene)Br}$_2$ (μ-$C_2O_4$)]

The method for the preparation of **4** was adopted from Yan and co-workers with some modifications.[3] The starting material [Os(η$^6$-*p*-cymene)Br$_2$]$_2$ (2.348 g, 2.43 mmol) and excess $(NH_4)_2C_2O_4{\cdot}H_2O$ (4.180 g, 29.53 mmol) were stirred in $CH_2Cl_2$/$CH_3OH$ solution (40 mL 1:1 v/v) at room temperature overnight. The $NH_4Br$ salt formed was filtered off. The yellow

filtrate was concentrated to *ca.* 5 mL under reduced pressure to produce yellow oil. The oil was redissolved in $CH_2Cl_2$ (10 mL) and diethyl ether (20 mL) was added dropwise. The yellow product was obtained by filtration then washed with ethanol (30 mL) and diethyl ether (20 mL). The precipitate was dried *in vacuo*. Yield 82% (1.785 g, 1.99 mmol).$^1$H NMR (500 MHz, $CDCl_3$) δ: 1.32 (d, 6H, $CH(C\underline{H}_3)_2$, $J_{(HH)}$ = 6.8 Hz); 2.28 (s, 3H, $C\underline{H}_3C_6H_4$); 2.77 (sept, 1H, $C\underline{H}(CH_3)_2$, $J_{(HH)}$ = 6.8 Hz); 5.97 (d, 2H, $\eta^6$-$C_6H_4$, $J_{(HH)}$ = 5.9 Hz); 6.21 (d, 2H, $\eta^6$-$C_6H_4$, $J_{(HH)}$ = 5.9 Hz). $^{13}C\{^1H\}$ NMR δ: 19.51 $\underline{C}H_3C_6H_4$; 22.94 $CH(\underline{C}H_3)_2$; 32.07 $\underline{C}H(CH_3)_2$; {90.68, 86.64, 71.97, 69.75} $\eta^6$-$C_6H_4$; 175.39 ($\underline{C}O$). IR ($cm^{-1}$): $\nu_{asym(C\text{-}O)}$ 1611vs; $\nu_{sym(OCO)}$ 1387/1341vs; $\nu_{sym(OCO)}$ + $\nu_{(CC)}$ 1468w; $\nu_{(CC)}$ 891sh/881w; $\nu_{(CC)}$ + $\delta_{(OCO)}$ 803sh/796w. Elemental analysis (%) for $C_{22}H_{28}Br_2Os_2$: Anal. Found – C 29.44, H 3.19. $C_{22}H_{28}Br_2Os_2$ Calculated – C 29.47, H 3.15.

6.4.7 Preparation of **5** [Os($\eta^6$-*p*-cymene)$Br_2$($PPh_3$)]

The method for the preparation of 5 was adopted with modifications from Clayton and co-workers.[2] The starting material $[Os(\eta^6\text{-}p\text{-cymene})Br_2]_2$ (0.202 g, 0.21 mmol) and $PPh_3$ (0.130 g, 0.50 mmol) were dissolved in dichloromethane (20 mL). The reddish-orange solution was stirred overnight at room temperature. A reddish-orange solution was obtained and the solvent was removed *in vacuo*. The orange precipitate obtained was washed with hexane (30 mL) overnight. The orange precipitates were obtained by filtration then dried *in vacuo*. Yield 70% (0.218 g, 0.29 mmol) $^1$H NMR (300 MHz, $CDCl_3$) δ: 1.17 (d, 6H, $CH(C\underline{H}_3)_2$, $J_{(HH)}$ = 7.0 Hz); 1.96 (s, 3H, $C\underline{H}_3C_6H_4$); 2.98 (sept, 1H, $C\underline{H}(CH_3)_2$, $J_{(HH)}$ = 7.0 Hz); 5.11 (d, 2H, $\eta^6$-$C_6H_4$, $J_{(HH)}$ = 5.3 Hz); 5.46 (d, 2H, $\eta^6$-$C_6H_4$, $J_{(HH)}$ = 5.9 Hz); 7.31 - 7.75 (m, 15H, Ph). $^{13}C\{^1H\}$ NMR δ: 18.38 $\underline{C}H_3C_6H_4$; 22.54 $CH(\underline{C}H_3)_2$; 30.72 $\underline{C}H(CH_3)_2$; {104.70, 89.40, 81.21 ($J$ = 5 Hz), 80.13 ($J$ = 2 Hz)} $\eta^6$-$C_6H_4$; 128.91 - 134.40 $C_{Aromatic}$; 164.22 CO. $^{31}P\{^1H\}$: –17.55 (s, $PPh_3$).

6.4.8 Attempted preparation of $[\{Os(\eta^6\text{-}p\text{-cymene})(PPh_3)\}_2\ \mu\text{-}C_2O_4](BF_4)_2$

The procedure for the attempted preparation of $[\{Os(\eta^6\text{-}p\text{-cymene})(PPh_3)\}_2\ \mu\text{-}C_2O_4](BF_4)_2$ was adopted from Yan and co-workers.[3] Complex **4** (0.516 g, 0.58 mmol) and excess $PPh_3$ (1.500 g, 5.72 mmol) were placed in a Schlenk tube. To this was added $NH_4BF_4$ (0.157 g, 1.50 mmol) and dissolved in $CH_2Cl_2$ (20 mL). A yellow solution was stirred at room temperature overnight. The reddish-orange solution was filtered and the solvent was removed *in vacuo* to give reddish-orange oil. The oil was washed with (60 mL) hexane for 72 h with

decanting the hexane solution. The orange product was obtained by filtration and dried *in vacuo*. Yield 76% (0.625 g, 0.44 mmol). $^{1}$H NMR (500 MHz, $CDCl_3$) δ: 1.17 (d, 6H, $CH(C\underline{H}_3)_2$, $J_{(HH)}$ = 6.9 Hz); 1.18 (d, 6H, $CH(C\underline{H}_3)_2$, $J_{(HH)}$ = 6.9 Hz); 1.94 (s, 3H, $C\underline{H}_3C_6H_4$); 2.01 (s, 3H, $C\underline{H}_3C_6H_4$); 2.47 (sept, 1H, $C\underline{H}(CH_3)_2$, $J_{(HH)}$ = 6.8 Hz); 2.96 (sept, 1H, $C\underline{H}(CH_3)_2$, $J_{(HH)}$ = 7.0 Hz); 5.10 (d, 2H, $\eta^6$-$C_6H_4$, $J_{(HH)}$ = 5.4 Hz); 5.30 (d, 2H, $\eta^6$-$C_6H_4$, $J_{(HH)}$ = 5.9 Hz); 4.45 (d, 2H, $\eta^6$-$C_6H_4$, $J_{(HH)}$ = 5.9 Hz); 5.52 (d, 2H, $\eta^6$-$C_6H_4$, $J_{(HH)}$ = 5.9 Hz); 7.31 - 7.73 (m, 30H, Ph). $^{13}$C{$^{1}$H} NMR δ: 18.02, 18.33 $\underline{C}H_3C_6H_4$; 22.49, 22.71 $CH(\underline{C}H_3)_2$; 30.65, 30.98 $\underline{C}H(CH_3)_2$; {104.61 ($J$ = 6 Hz), 98.75 ($J$ = 3 Hz), 89.37, 88.41, 81.15 ($J$ = 5 Hz), 80.10 ($J$ = 2 Hz), 79.36 ($J$ = 5 Hz), 79.10 ($J$ = 4 Hz)} $\eta^6$-$C_6H_4$; 127.82-134.97 $C_{Aromatic}$; 164.23 CO. $^{31}$P{$^{1}$H}: 1.77, –17.54 (s, $2PPh_3$). IR ($cm^{-1}$): $\nu_{asym(OCO)}$ 1705s, 1694s; $\nu_{(OCO)}$ 1670s. Elemental analysis (%) for $C_{58}H_{58}Br_2O_4Os_2P_2$: Calculated – C 48.54, H 4.07; found – C 46.96, H 3.95.

6.4.9 Preparation of **6** $[Os(\eta^6\text{-}p\text{-cymene})Br(PPh_3)_2]BF_4$

The complex $[Os(\eta^6\text{-}p\text{-cymene})Br(NCCH_3)_2]BF_4$ (2.068 g, 3.61 mmol) was reacted with excess $PPh_3$ (3.632 g, 13.85 mmol) in $CH_2Cl_2$ (50 mL). The orange solution was stirred at room temperature overnight. The reddish-orange solution was filtered and the solvent was removed *in vacuo*. Reddish-orange oil was obtained and washed with hexane (80 mL) over 48 hours. The reddish-orange precipitate was obtained by filtration and dried *in vacuo*. Yield 77% (2.803 g, 2.76 mmol). $^{1}$H NMR (500 MHz, $CDCl_3$) δ: 1.20 (d, 6H, $CH(C\underline{H}_3)_2$, $J_{(HH)}$ = 6.9 Hz); 2.15 (s, 3H, $C\underline{H}_3C_6H_4$); 2.75 (sept, 1H, $C\underline{H}(CH_3)_2$, $J_{(HH)}$ = 7.0 Hz); 5.23 (d, 2H, $\eta^6$-$C_6H_4$, $J_{(HH)}$ = 5.9 Hz); 5.80 (d, 2H, $\eta^6$-$C_6H_4$, $J_{(HH)}$ = 2.9 Hz); 7.23 - 7.37 (m, 30H, Ph). $^{13}$C{$^{1}$H} NMR δ: 15.30 $\underline{C}H_3C_6H_4$; 21.79 $CH(\underline{C}H_3)_2$; 31.63 $\underline{C}H(CH_3)_2$; {96.42, 89.37, 81.30, 73.13} $\eta^6$-$C_6H_4$; 128.31 - 134.71 $C_{Aromatic}$. $^{19}$F{$^{1}$H} NMR δ: –157.67, –157.72. $^{31}$P{$^{1}$H}: –28.94 (s, $2PPh_3$). IR ($cm^{-1}$): $\nu_{(B\text{-}F)}$ 1052s.

6.4.10 Preparation of **7(a)-(d)** $[Os(\eta^6\text{-}p\text{-cymene})(\kappa^2\text{-}PPh_2(CH_2)_nPPh_2)Br]BF_4$ (n = 1 - 4)

Complexes **7(a)-(d)** were synthesized by the general method below adopted from literature by Jensen et al. with modifications.[5]

The complex $[Os(\eta^6\text{-}p\text{-cymene})(NCCH_3)_2Br]BF_4$ was weighed into the Schlenk tube. To this was added $PPh_2(CH_2)_nPPh_2$ (where n = 1 – 4). Dichloromethane (50 mL) was then added and the resulting solution was stirred at room temperature overnight. A yellow-brown solution

was filtered and the solvent was reduced to *ca.* 10 mL *in vacuo*. Diethyl ether (20mL) was added and solution cooled to −15 ºC for 24 h. The yellow product was washed with hexane for 72 h. The yellow product was obtained by filtration and dried *in vacuo*. The quantities of starting materials used for the four complexes are given below.

For preparation of complex **7(a)**: $[Os(\eta^6\text{-}p\text{-cymene})(NCCH_3)_2Br]BF_4$ (1.202 g, 2.10 mmol) and dppm (1.105 g, 2.87 mmol). The product was obtained as a bright yellow solid. Yield 91% (1.673 g, 1.91 mmol). $^1$H NMR (500 MHz, dmso-$d_6$) δ: 0.91 (d, 6H, $CH(C\underline{H}_3)_2$, $J_{(HH)}$ = 6.9 Hz); 1.45 (s, 3H, $C\underline{H}_3C_6H_4$); 2.20 (sept, 1H, $C\underline{H}(CH_3)_2$, $J_{(HH)}$ = 6.8 Hz); 4.77, 4.68 (dd, 2H, $PCH_2P$); 6.31 (d, 2H, $\eta^6$-$C_6H_4$, $J_{(HH)}$ = 5.9 Hz); 6.45 (d, 2H, $\eta^6$-$C_6H_4$, $J_{(HH)}$ = 5.9 Hz); 7.26 - 7.67 (m, 20H, Ph). $^{13}C\{^1H\}$ NMR δ: 16.37 $\underline{C}H_3C_6H_4$; 21.64 $CH(\underline{C}H_3)_2$; 29.86 $\underline{C}H(CH_3)_2$; 43.69 $P\underline{C}H_2P$; {112.98, 95.79, 84.37, 81.07} $\eta^6$-$C_6H_4$; 128.44 - 131.70 $C_{Aromatic}$. $^{19}F\{^1H\}$ NMR δ: −143.46, −143.52. $^{31}P\{^1H\}$ NMR δ: −43.52 (s, dppm). IR ($cm^{-1}$): $\nu_{(B\text{-}F)}$ 1046s.

For preparation of complex **7(b)**: $[Os(\eta^6\text{-}p\text{-cymene})(NCCH_3)_2Br]BF_4$ (1.203 g, 2.10 mmol) and dppe (0.879 g, 2.21 mmol). The product was obtained as a yellow solid. Yield 70% (1.308 g, 1.47 mmol). $^1$H NMR (500 MHz, $CDCl_3$) δ: 0.89 (d, 6H, $CH(C\underline{H}_3)_2$, $J_{(HH)}$ = 7.0 Hz); 1.26 (s, 3H, $C\underline{H}_3C_6H_4$); 2.38 (sept, 1H, $C\underline{H}(CH_3)_2$, $J_{(HH)}$ = 6.7 Hz); 2.65, 2.99 (m, 2H, $PCH_2$); 5.87 (d, 2H, $\eta^6$-$C_6H_4$, $J_{(HH)}$ = 4.1 Hz); 6.01 (d, 2H, $\eta^6$-$C_6H_4$, $J_{(HH)}$ = 6.4 Hz); 7.21-7.77 (m, 20H, Ph). $^{13}C\{^1H\}$ NMR δ:1 5.52 $\underline{C}H_3C_6H_4$; 21.44 $CH(\underline{C}H_3)_2$; 30.50 $\underline{C}H(CH_3)_2$; 27.80, $J_{(P\text{-}C)}$ = 24 Hz, $PCH_2$; 29.72 $PCH_2CH_2$; {117.56, 95.40, 85.96 ($J$ = 3 Hz), 83.41 ($J$ = 8 Hz)} $\eta^6$-$C_6H_4$; 128.70 – 135.97 $C_{Aromatic}$. $^{19}F\{^1H\}$ NMR δ: −152.86, −152.92. $^{31}P\{^1H\}$ NMR δ: 30.92 (s, dppe). IR ($cm^{-1}$): $\nu_{(B\text{-}F)}$ 1061s. Elemental analysis (%) for $C_{36}H_{38}BBrF_4OsP_2$: Calculated – C 48.61, H 4.31; found – C 48.37, H 4.51.

For preparation of complex **7(c)**: $[Os(\eta^6\text{-}p\text{-cymene})(NCCH_3)_2Br]BF_4$ (2.053 g, 3.58 mmol) and dppp (1.513 g, 3.67 mmol). The product was obtained as a yellow solid. Yield 73% (2.374 g, 2.63 mmol). $^1$H NMR (500 MHz, $CDCl_3$) δ: 0.75 (d, 6H, $CH(C\underline{H}_3)_2$, $J_{(HH)}$ = 6.8 Hz); 1.37 (s, 3H, $C\underline{H}_3C_6H_4$); 1.77 - 2.54 (m, 2H, $PCH_2C\underline{H}_2CH_2P$); 2.46 (sept, 1H, $C\underline{H}(CH_3)_2$, $J_{(HH)}$ = 6.8 Hz); 3.21 (m, 2H,$PCH_2$); 5.58 (d, 2H, $\eta^6$-$C_6H_4$, $J_{(HH)}$ = 5.9 Hz); 5.97 (d, 2H, $\eta^6$-$C_6H_4$, $J_{(HH)}$ = 5.4 Hz); 7.25 - 7.55 (m, 20H, Ph). $^{13}C\{^1H\}$ NMR δ: 15.60 $\underline{C}H_3C_6H_4$; 21.12 $CH(\underline{C}H_3)_2$; 21.47 $PCH_2CH_2$; 23.79, $J$ = 20 Hz, $PCH_2$; 30.54 $\underline{C}H(CH_3)_2$; {94.00, 86.32, 85.15, 70.60} $\eta^6$-$C_6H_4$; 128.73 - 136.02 $C_{Aromatic}$. $^{19}F\{^1H\}$ NMR δ: −152.51, −152.56. $^{31}P\{^1H\}$ NMR δ: −25.00 (s, dppp). IR ($cm^{-1}$): $\nu_{(B\text{-}F)}$ 1061s.

For preparation of complex **7(d)**: $[Os(\eta^6\text{-}p\text{-cymene})(NCCH_3)_2Br]BF_4$ (2.032 g, 3.55 mmol) and dppb (1.593 g, 3.74 mmol). The product was obtained as a yellow solid. Yield 72% (2.339 g, 2.55 mmol). $^1$H NMR (500 MHz, $CDCl_3$) δ: 0.97 (d, 6H, $CH(C\underline{H}_3)_2$, $J_{(HH)}$ = 6.9 Hz); 1.17 (s, 3H, $C\underline{H}_3C_6H_4$); 1.58 - 2.27 (m, 4H, $PCH_2C\underline{H}_2C\underline{H}_2CH_2P$); 2.65 (sept, 1H, $C\underline{H}(CH_3)_2$, $J_{(HH)}$ = 7.1 Hz); 3.90 (m, 2H,$PCH_2$); 5.05 (d, 2H, $\eta^6$-$C_6H_4$, $J_{(HH)}$ = 5.9 Hz); 5.80 (d, 2H, $\eta^6$-$C_6H_4$, $J_{(HH)}$ = 5.4 Hz); 7.31 - 7.58 (m, 20H, Ph). $^{13}C\{^1H\}$ NMR δ: 14.99 $\underline{C}H_3C_6H_4$; 21.57 $CH(\underline{C}H_3)_2$; 22.66 $PCH_2CH_2$; 28.83 $PCH_2$; 30.70 $\underline{C}H(CH_3)_2$; {126.25, 92.45, 87.53, 83.32} $\eta^6$-$C_6H_4$; 128.88 - 133.35 $C_{Aromatic}$. $^{19}F\{^1H\}$ NMR δ: –152.85, –152.91. $^{31}P\{^1H\}$ NMR δ: –17.10 (s, dppb). IR ($cm^{-1}$): $\nu_{(B\text{-}F)}$ 1061s. Elemental analysis (%) for $C_{38}H_{42}BBrF_4OsP_2 \cdot 0.3(CH_2Cl_2)$: Calculated – C 49.74, H 4.61; found – C 48.85, H 4.64.

6.4.11 Preparation of 8(a)-(d) $[\{Os(\eta^6\text{-}p\text{-cymene})Br_2\}_2\ \mu\text{-}PPh_2(CH_2)_nPPh_2]$ (n = 1 - 4)

Complexes **8(a)-(d)** were prepared by the general method below.

The starting material $[Os(\eta^6\text{-}p\text{-cymene})Br_2]_2$ was weighed in a Schlenk tube and dissolved in $CH_2Cl_2$ (20 mL). To this was added a solution of $PPh_2(CH_2)_nPPh_2$ (where n = 1 − 4) in $CH_2Cl_2$ (20 mL) dropwise over 4 h. The resulting reddish-orange solution was stirred at room temperature overnight. The reddish-orange solution was filtered and then the filtrate was reduced to *ca.* 10 mL *in vacuo*. Diethyl ether (20 mL) was added to give an orange precipitate. The orange precipitate was washed with hexane (40 mL) over 72 h to remove excess diphosphine. The product was obtained by filtration and dried *in vacuo*. The quantities of starting materials used for preparation of the four complexes are found below.

For preparation of **8(a)**: $[Os(\eta^6\text{-}p\text{-cymene})Br_2]_2$ (1.194 g, 1.23 mmol) and dppm (0.509g, 1.32mmol). Yield 82% (1.374 g, 1.02 mmol). $^1$H NMR (500 MHz, $CDCl_3$) δ: 0.94 (d, 6H, $CH(C\underline{H}_3)_2$, $J_{(HH)}$ = 6.4 Hz); 1.90 (b, 2H,$PCH_2$); 2.09 (s, 3H, $C\underline{H}_3C_6H_4$); 2.52 (sept, 1H, $C\underline{H}(CH_3)_2$, $J_{(HH)}$ = 6.9 Hz); 4.88 (virtual triplet, 1H,$CH_2$, $J_{(HH)}$ = 7.3 Hz); 5.07 (d, 2H, $\eta^6$-$C_6H_4$, $J_{(HH)}$ = 4.7 Hz); 5.31 (d, 2H, $\eta^6$-$C_6H_4$, $J_{(HH)}$ = 5.9 Hz); 7.04 - 7.59 (m, 20H, Ph). $^{13}C\{^1H\}$ NMR δ: 18.71 $\underline{C}H_3C_6H_4$; 22.49 $CH(\underline{C}H_3)_2$; 30.45 $\underline{C}H(CH_3)_2$; 53.65 $PCH_2P$; {101.66, 87.52, 82.95, 78.28} $\eta^6$-$C_6H_4$; 127.04-134.54 $C_{Aromatic}$. $^{31}P\{^1H\}$ δ: –28.73 (s, dppm). Elemental analysis (%) for $C_{45}H_{50}Br_4Os_2P_2$: Calculated – C 39.95, H 3.73; found – C 39.94, H 3.72.

For preparation of **8(b)**: $[Os(\eta^6\text{-}p\text{-cymene})Br_2]_2$ (2.093 g, 2.16 mmol) and dppe (0.862 g, 2.16 mmol). Yield 84% (2.471 g, 1.81 mmol). $^1$H NMR (500 MHz, $CDCl_3$) δ: 0.79 (d, 6H, $CH(C\underline{H}_3)_2$, $J_{(HH)}$ = 6.9 Hz); 0.95 (b, 4H,$PCH_2\underline{CH}_2$); 1.95 (s, 3H, $C\underline{H}_3C_6H_4$); 2.48 (sept, 1H, $C\underline{H}(CH_3)_2$, $J_{(HH)}$ = 6.9 Hz); 2.64 (b, 4H,$PCH_2$); 5.15 (d, 2H, $\eta^6$-$C_6H_4$, $J_{(HH)}$ = 5.9 Hz); 5.29 (d, 2H, $\eta^6$-$C_6H_4$, $J_{(HH)}$ = 5.9 Hz); 7.24 - 7.52 (m, 20H, Ph). $^{13}C\{^1H\}$ NMR δ: 17.80 $\underline{C}H_3C_6H_4$; 19.30 $PCH_2\underline{CH}_2$; 21.87 $CH(\underline{C}H_3)_2$; 26.72 ($J$ = 23 Hz) $PCH_2$; 30.22 $\underline{C}H(CH_3)_2$; {100.59, 86.19, 82.72 ($J$ = 3 Hz), 78.09 ($J$ = 6 Hz)} $\eta^6$-$C_6H_4$; 128.05 – 133.48 $C_{Aromatic}$. $^{31}P\{^1H\}$ δ: –25.22 (s, dppe). Elemental analysis (%) for $C_{46}H_{52}Br_4Os_2P_2$: Calculated – C 40.42, H 3.83; found – C 40.47, H 3.92.

For preparation of **8(c)**: $[Os(\eta^6\text{-}p\text{-cymene})Br_2]_2$ (0.502 g, 0.52 mmol) and dppp (0.300 g, 0.73 mmol). Yield 84% (0.597 g, 0.43 mmol). $^1$H NMR (500 MHz, $CDCl_3$) δ: 0.82 (d, 6H, $CH(C\underline{H}_3)_2$, $J_{(HH)}$ = 7.0 Hz); 0.99 (b, 4H,$PCH_2\underline{CH}_2$); 1.97 (s, 3H, $C\underline{H}_3C_6H_4$); 2.51 (sept, 1H, $C\underline{H}(CH_3)_2$, $J_{(HH)}$ = 6.9 Hz); 2.66 (b, 4H,$PCH_2$); 5.17 (d, 2H, $\eta^6$-$C_6H_4$, $J_{(HH)}$ = 5.9 Hz); 5.31 (d, 2H, $\eta^6$-$C_6H_4$, $J_{(HH)}$ = 5.3 Hz); 7.24 - 7.56 (m, 20H, Ph). $^{13}C\{^1H\}$ NMR δ: 17.61 $\underline{C}H_3C_6H_4$; 19.14 $PCH_2\underline{CH}_2$; 21.91 $CH(\underline{C}H_3)_2$; 26.52 ($J$ = 15 Hz) $PCH_2$; 30.04 $\underline{C}H(CH_3)_2$; {100.43, 85.98, 82.50, 77.90 ($J$ = 6 Hz)} $\eta^6$-$C_6H_4$; 127.85-133.33 $C_{Aromatic}$. $^{31}P\{^1H\}$ δ: –25.35 (s, dppp). Elemental analysis (%) for $C_{47}H_{54}Br_4Os_2P_2$: Calculated – C 40.88, H 3.94; found – C 39.55, H 3.94.

For preparation of **8(d)**: $[Os(\eta^6\text{-}p\text{-cymene})Br_2]_2$ (0.514 g, 0.53 mmol) and dppb (0.295 g, 0.69 mmol). Yield 82% (0.606 g, 0.43 mmol). $^1$H NMR (500 MHz, $CDCl_3$) δ: 0.75 (d, 6H, $CH(C\underline{H}_3)_2$, $J_{(HH)}$ = 7.0 Hz); 0.91 (b, 4H, $PCH_2\underline{CH}_2$); 1.98 (s, 3H, $C\underline{H}_3C_6H_4$); 2.49 (sept, 1H, $C\underline{H}(CH_3)_2$, $J_{(HH)}$ = 7.0 Hz); 2.51 (b, 4H,$PCH_2$); 5.20 (d, 2H, $\eta^6$-$C_6H_4$, $J_{(HH)}$ = 5.9); 5.36 (d, 2H, $\eta^6$-$C_6H_4$, $J_{(HH)}$ = 5.3); 7.27 - 7.68 (m, 20H, Ph). $^{13}C\{^1H\}$ NMR δ: 17.49 $\underline{C}H_3C_6H_4$; 21.48 $CH(\underline{C}H_3)_2$; 22.65 $PCH_2\underline{CH}_2$; 29.69 $PCH_2$; 30.03 $\underline{C}H(CH_3)_2$; {99.86, 85.45, 82.81, 77.92} $\eta^6$-$C_6H_4$; 128.11-133.39 $C_{Aromatic}$. $^{31}P\{^1H\}$: –23.77 (s, dppb). Elemental analysis (%) for $C_{48}H_{56}Br_4Os_2P_2 \cdot 0.5(CH_2Cl_2)$: Calculated – C 41.33, H 4.05; found – C 40.41, H 4.17.

6.4.12 Preparation of **9** [Os($\eta^6$-*p*-cymene)($NCCH_3$)$_2$Br]$BF_4$

The starting material [Os($\eta^6$-*p*-cymene)$Br_2$]$_2$ (5.226 g, 5.39 mmol) was weighed into the Schlenk tube. To this was added a solution of $NH_4BF_4$ (1.14 g, 10.89 mmol) in $CH_3CN$ (100 mL) to give an orange solution which was stirred at room temperature overnight. The yellow-orange solution was filtered to remove $NH_4Br$. The solvent was reduced *in vacuo* to give an orange oil. Dichloromethane (30 mL) was added to redissolve the oily product and diethyl ether (50 mL) was also added to make a two layer solution which was left to precipitate over 24 h at room temperature. A yellow precipitate was obtained by filtration then dried *in vacuo*. Yield 75% (4.629 g, 8.08 mmol). $^1$H NMR (500 MHz, $CDCl_3$) δ: 1.26 (d, 6H, CH(C<u>H</u>$_3$)$_2$ $J_{(HH)}$ = 6.8 Hz); 2.34 (s, 3H, C<u>H</u>$_3$C$_6$H$_4$); 2.74 (s, 6H, $NCCH_3$); 2.80 (sept, 1H, C<u>H</u>(CH$_3$)$_2$ $J_{(HH)}$ = 6.8 Hz); 5.86 (d, 2H, $\eta^6$-C$_6$H$_4$ $J_{(HH)}$ = 5.9 Hz); 6.05 (d, 2H, $\eta^6$-C$_6$H$_4$ $J_{(HH)}$ = 5.9 Hz). $^{13}$C{$^1$H} NMR δ: 4.19 NC<u>C</u>H$_3$; 18.97 <u>C</u>H$_3$C$_6$H$_4$; 22.63 CH(<u>C</u>H$_3$)$_2$; 31.40 <u>C</u>H(CH$_3$)$_2$; {97.67, 94.41, 78.69, 75.74} $\eta^6$-C$_6$H$_4$; 122.09 N≡C. $^{19}$F{$^1$H} NMR δ: −151.84, −151.89. IR (cm$^{-1}$): $\nu_{(N\equiv C)}$ 2331w, 2303w; $\nu_{(B\text{-}F)}$ 1052s.

6.4.13 Preparation of **10** [Os($\eta^6$-*p*-cymene)($NCCH_3$)Br($PPh_3$)]$BF_4$

Complex **9** (2.073 g, 3.62 mmol) and one mole equivalent of $PPh_3$ (0.961 g, 3.66 mmol) were placed in a Schlenk tube. Dichloromethane (30mL) was added to give a brownish solution which was stirred at room temperature overnight. The brownish-orange solution was filtered and the solvent was removed *in vacuo* to give yellow oil. The yellow oil was washed in hexane for 24 h to remove unreacted $PPh_3$. The yellow precipitate was obtained by filtration and dried *in vacuo*. Yield 86% (2.413g, 3.10mmol). $^1$H NMR (500 MHz, $CDCl_3$) δ: 1.24 (d, 6H, CH(C<u>H</u>$_3$)$_2$, $J_{(HH)}$ = 6.9 Hz), 1.32 (d, 6H, CH(C<u>H</u>$_3$)$_2$, $J_{(HH)}$ = 6.8 Hz); 1.88 (s, 6H, C<u>H</u>$_3$C$_6$H$_4$); 2.18 (s, 3H, $NCCH_3$); 3.00 (sept, 1H, C<u>H</u>(CH$_3$)$_2$, $J_{(HH)}$ = 6.8 Hz); 4.75 (d, 2H, $\eta^6$-C$_6$H$_4$, $J_{(HH)}$ = 5.9); 5.66 (d, 2H, $\eta^6$-C$_6$H$_4$, $J_{(HH)}$ = 5.9 Hz); 5.89 (d, 2H, $\eta^6$-C$_6$H$_4$, $J_{(HH)}$ = 5.9 Hz); 6.46 (d, 2H, $\eta^6$-C$_6$H$_4$, $J_{(HH)}$ = 5.4 Hz); 7.23 – 7.57 (m, 15H, Ph). $^{13}$C{$^1$H} NMR δ: 3.32 (NC<u>C</u>H$_3$); 18.36 <u>C</u>H$_3$C$_6$H$_4$; 20.92 CH(<u>C</u>H$_3$)$_2$; 31.06 <u>C</u>H(CH$_3$)$_2$; {121.92, 109.88 (J=7 Hz), 96.99, 89.14 ($J$ = 6 Hz), 83.43, 80.61} $\eta^6$-C$_6$H$_4$; 130.05 (N≡C); 128.72 – 135.07 C$_{Aromatic}$. $^{19}$F{$^1$H} NMR δ: −152.31, −152.37. $^{31}$P{$^1$H} δ: −24.06 (s, $PPh_3$). IR (cm$^{-1}$): $\nu_{(N\equiv C)}$ 2322w; $\nu_{(B\text{-}F)}$ 1054s.

6.4.14 Preparation of **11** [Os($\eta^6$-*p*-cymene)($C_7H_8N_2O$)$Br_2$]

The starting material [Os($\eta^6$-*p*-cymene)$Br_2$]$_2$ (1.118 g, 1.15 mmol) and an excess of 2-aminobenzamide ($C_7H_8N_2O$) (0.698 g, 5.13 mmol) were placed in a Schlenk tube. To this was added $NH_4BF_4$ (0.328 g, 3.13 mmol) and $CH_2Cl_2$ (40 mL). The reddish-orange solution was stirred at room temperature overnight. The reaction mixture was filtered to remove a white suspension of unreacted $NH_4BF_4$. The solvent was then removed under reduced pressure to give a yellow-brownish solid. The yellow-brownish solid was washed with $CH_2Cl_2$ (30 mL) to remove impurities. The yellow solid was isolated by filtration and dried *in vacuo*. Yield 81% (1.172 g, 1.87 mmol). $^1$H NMR (500 MHz, $CDCl_3$) δ: 1.20 (d, 6H, CH(C$\underline{H}_3$)$_2$, $J_{(HH)}$ = 7.0 Hz); 2.22 (s, 3H, C$\underline{H}_3$C$_6$H$_4$); 2.83 (sept, 1H, C$\underline{H}$(CH$_3$)$_2$, $J_{(HH)}$ = 7.0 Hz); 3.34 (b, 2H, $NH_2$); 6.03 (d, 2H, $\eta^6$-C$_6$H$_4$, $J_{(HH)}$ = 5.9 Hz); 6.09 (d, 2H, $\eta^6$-C$_6$H$_4$, $J_{(HH)}$ = 5.9 Hz); 6.42 – 7.51 (m, 4H, Ph); 7.70 (b, 2H, $NH_2$C(=O)). $^{13}$C{$^1$H} NMR δ: 18.45 C$\underline{H}_3$C$_6$H$_4$; 21.74 CH(C$\underline{H}_3$)$_2$; 30.16 C$\underline{H}$(CH$_3$)$_2$; {116.38, 114.37, 78.75, 78.21} $\eta^6$-C$_6$H$_4$; 93.16 - 131.85 $C_{Aromatic}$; 150.13 N-(C)Ph; 171.26 N$\underline{C}$(=O). $^{19}$F{$^1$H} NMR δ: –148.19, –148.24. IR (cm$^{-1}$): $\nu_{(C=O)}$ 1660s; $\nu_{(N-H)}$ 3332m, 3263m, 3177m, 3112m.

## 6.5 References


(1) Pourmortazavi, S. M.; Hajimirsadeghi, S. S.; Kohsari, I.; Alamdari, R. F.; Rahimi-Nasrabadi, M. *Chem. Eng. Technol.* **2008**, *31*, 1532.

(2) Clayton, H. S.; Makhubela, B. C. E.; Su, H.; Smith, G. S.; Moss, J. R. *Polyhedron* **2009**, *28*, 1511.

(3) Yan, H.; Suss-Fink, G.; Neels, A.; Stoeckli-Evans, H. *J. Chem. Soc., Dalton Trans.* **1997**, 4345.

(4) Melchart, M.; Habtemariam, A.; Parsons, S.; Moggach, S. A.; Sadler, P. J. *Inorg. Chim. Acta* **2006**, *359*, 3020.

(5) Jensen, S. B.; Rodger, S. J.; Spicer, M. D. *J. Organomet. Chem.* **1998**, *556*, 151.

# APPENDICES

## APPENDIX A: ADDITIONAL IR AND RAMAN SPECTRA OF COMPLEXES IN CHAPTER 2

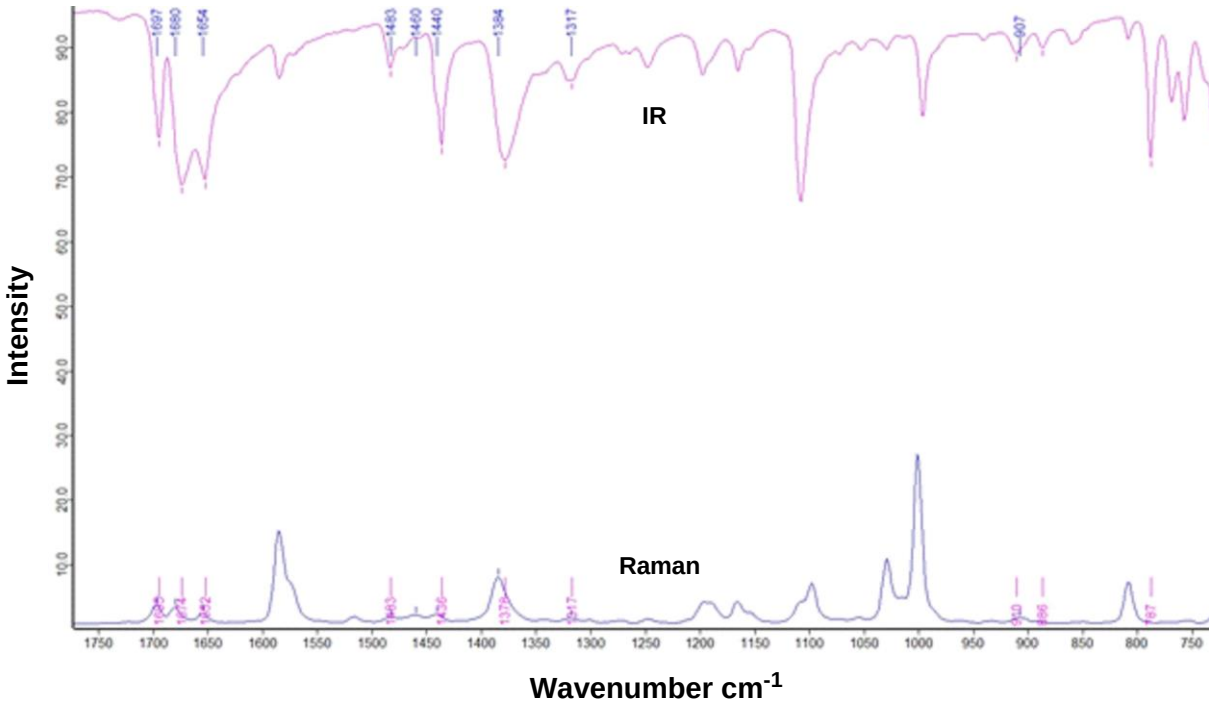


*Figure A-1: The combined infra-red and raman spectra of* ***1(b)***.

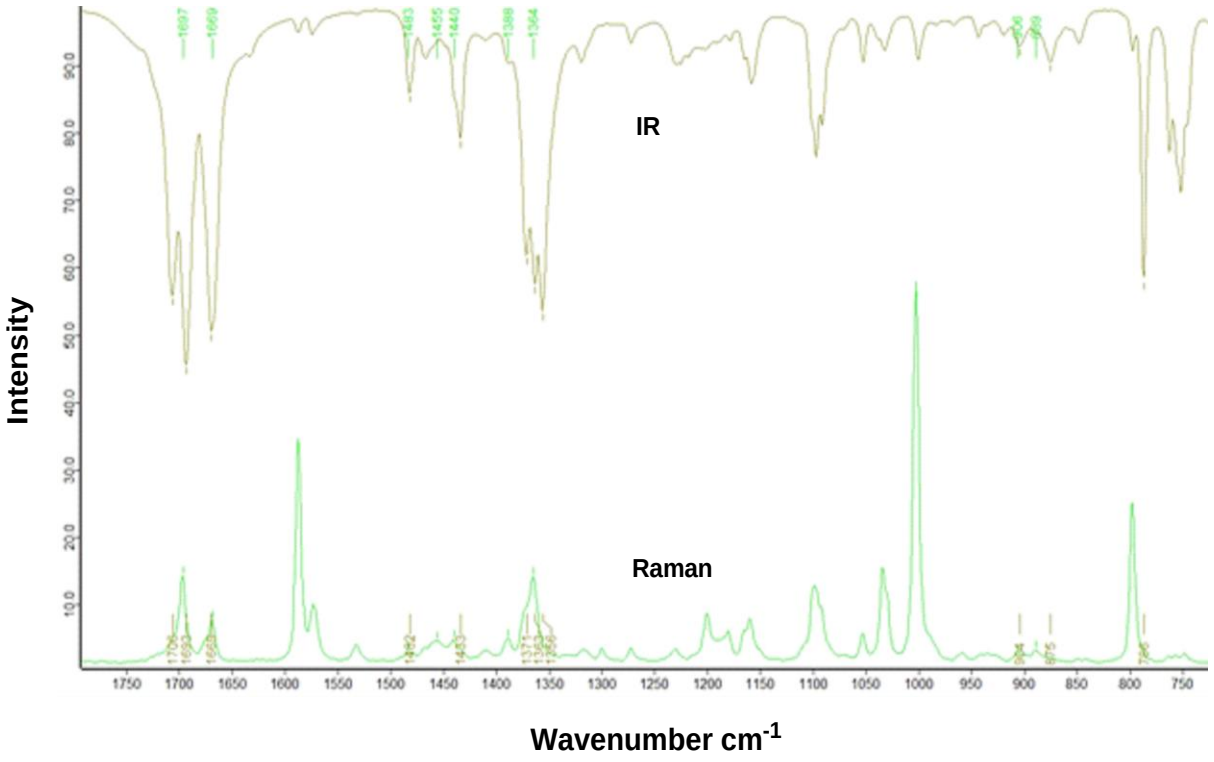


*Figure A-2: The combined infra-red and raman spectra of **2**.*

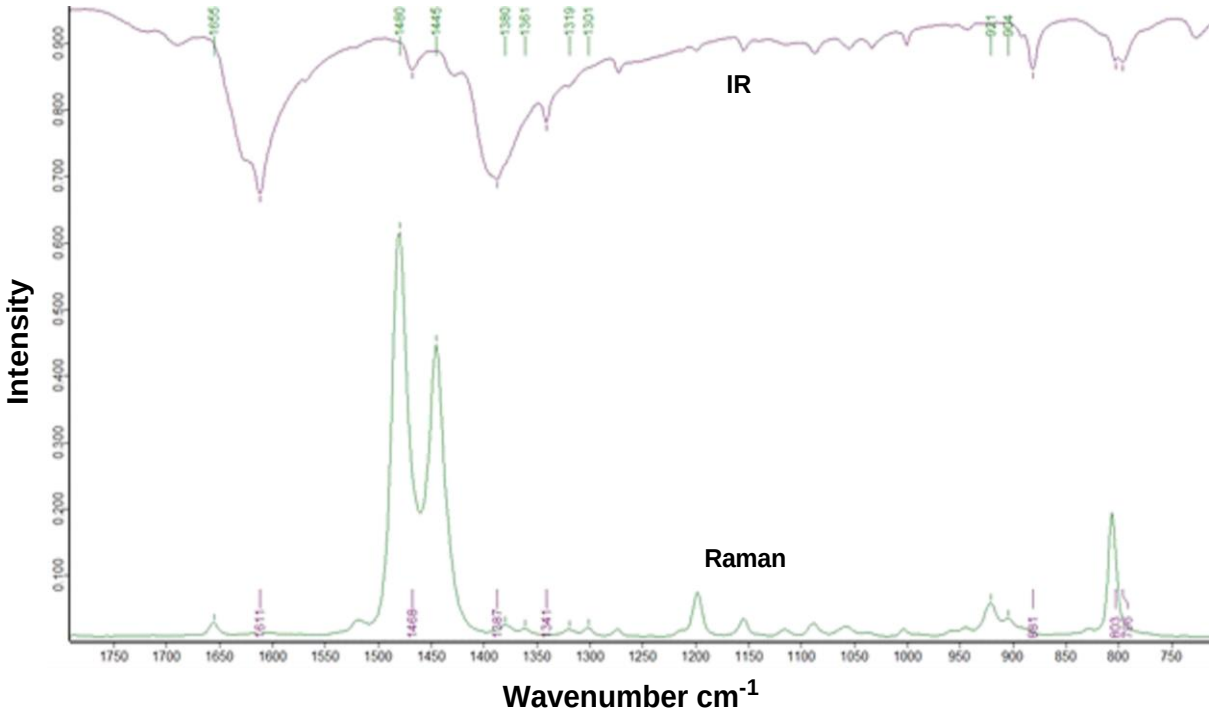


*Figure A-3: The combined infra-red and raman spectra of **4**.*

## APPENDIX B: TGA THERMOGRAMS WITH DTG CURVES

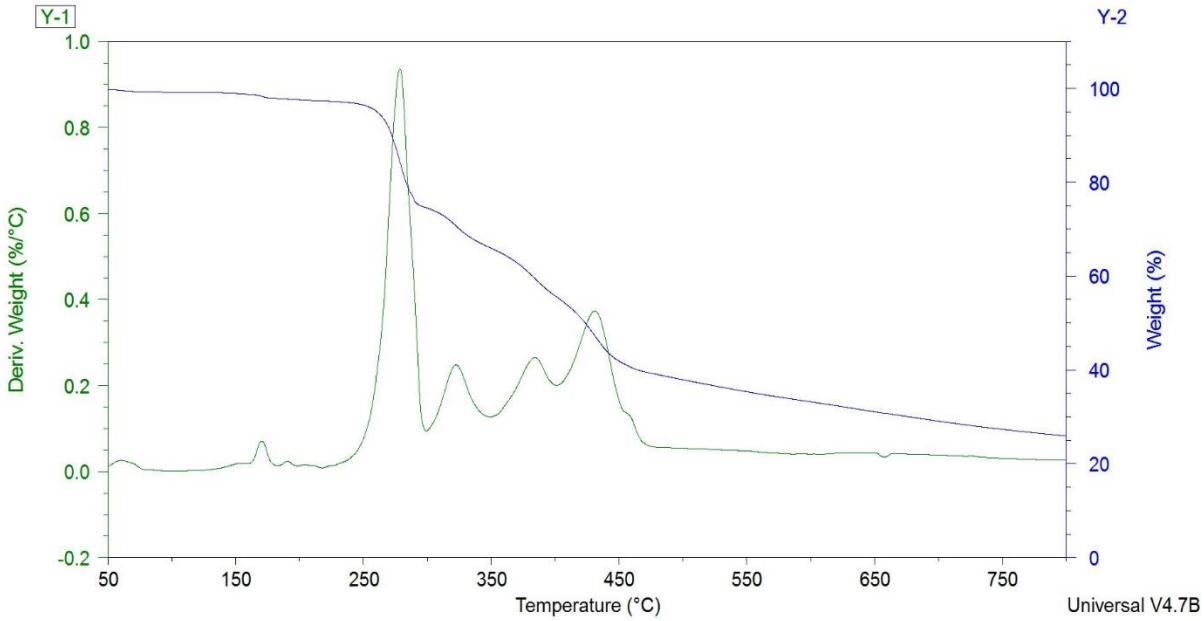


*Figure B-1: TGA thermogram of **1(b)** with DTG curve.*

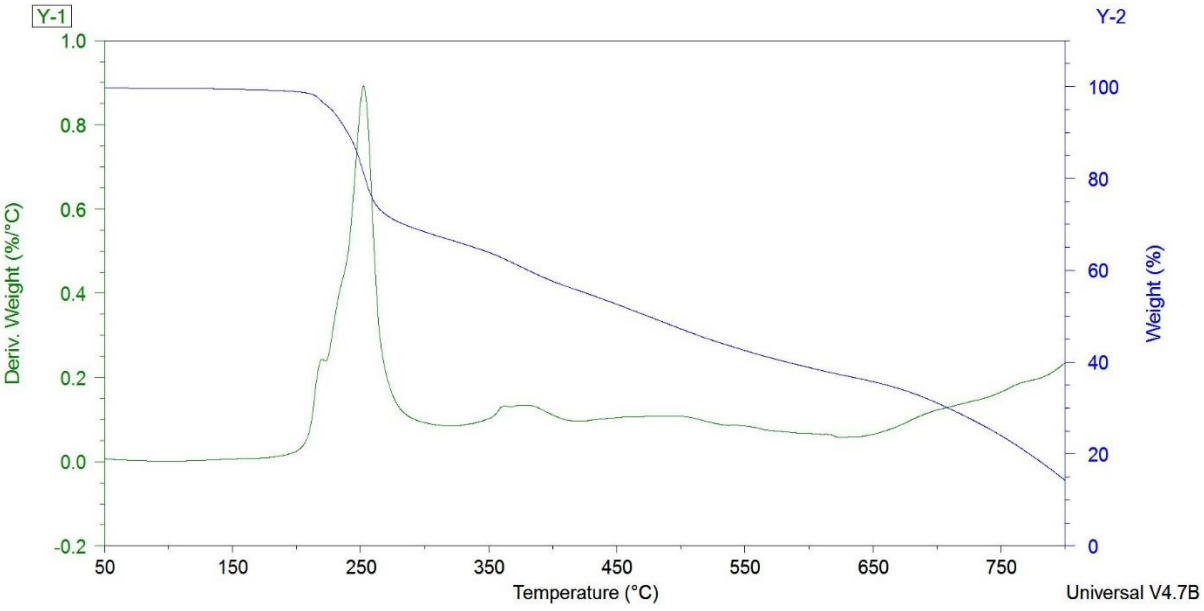


*Figure B-2: TGA thermogram of **2** with DTG curve.*

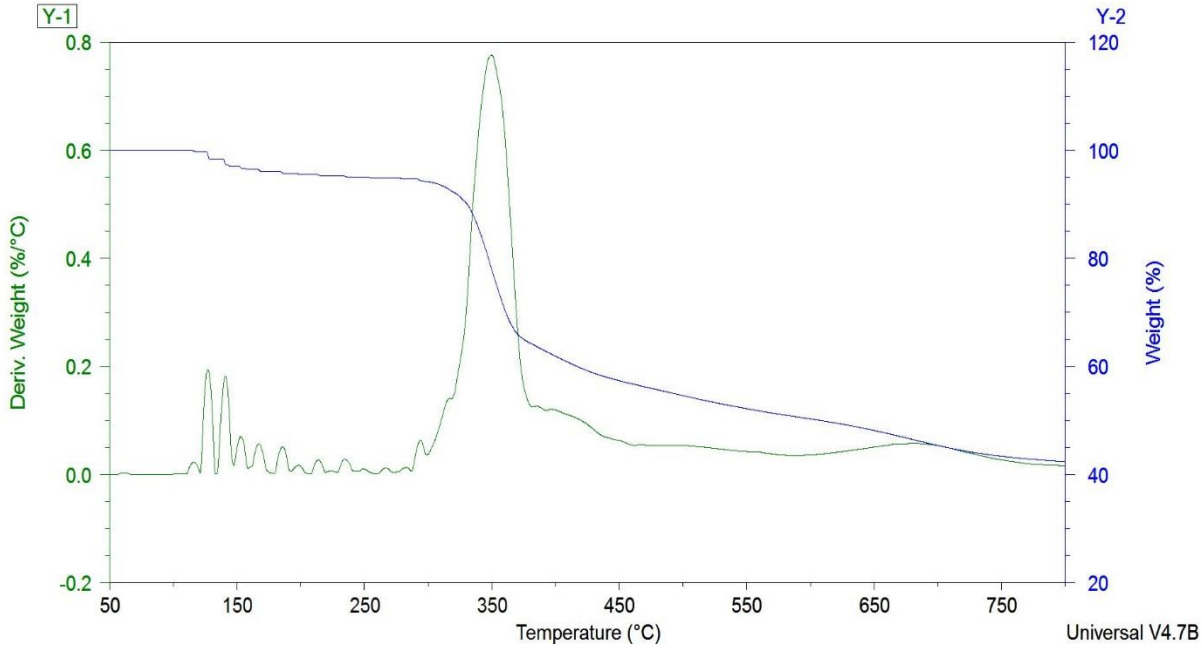


*Figure B-3: TGA thermogram of **7(a)** with DTG curve.*

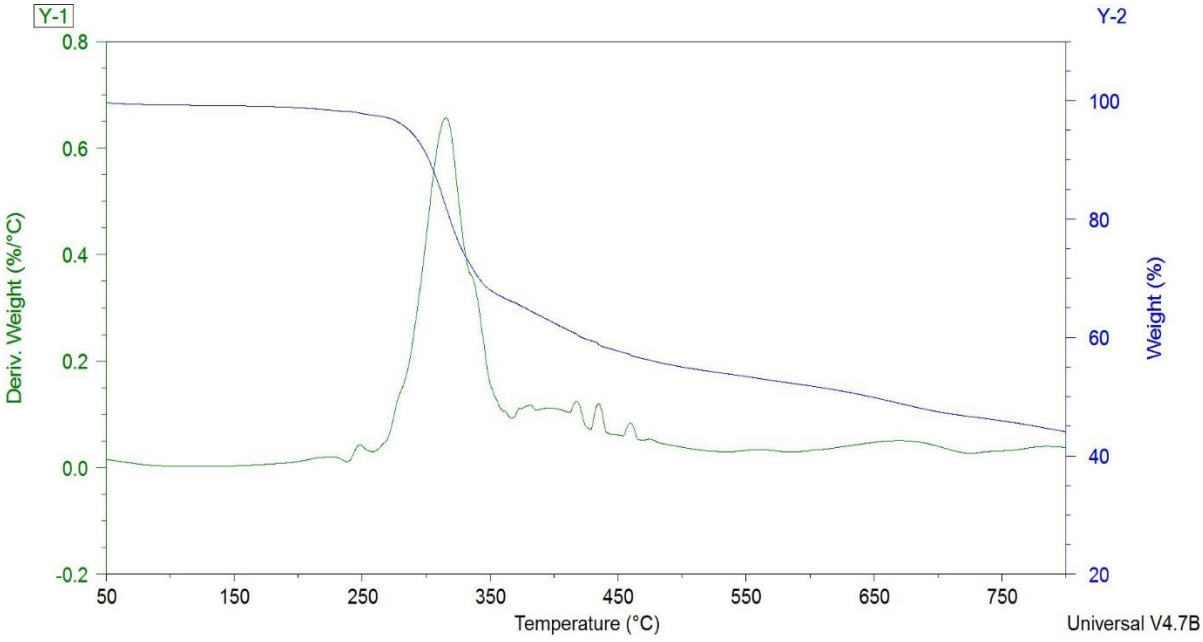


*Figure B-4: TGA thermogram of **7(c)** with DTG curve.*

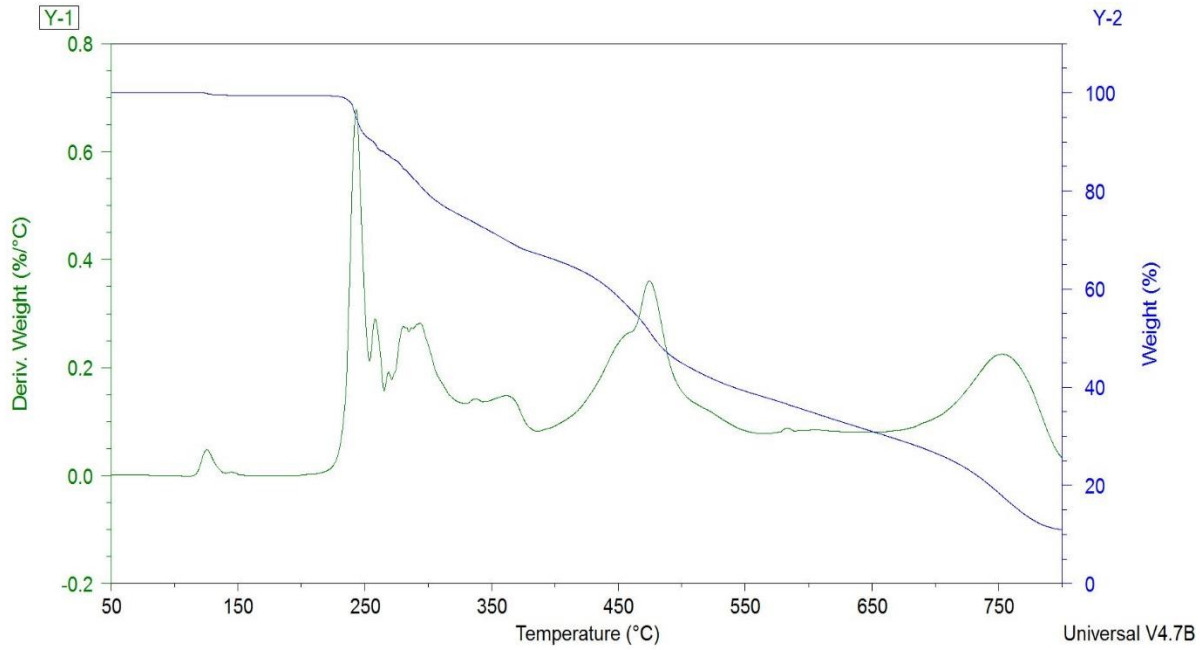


*Figure B-5: TGA thermogram of **8(a)** with DTG curve.*

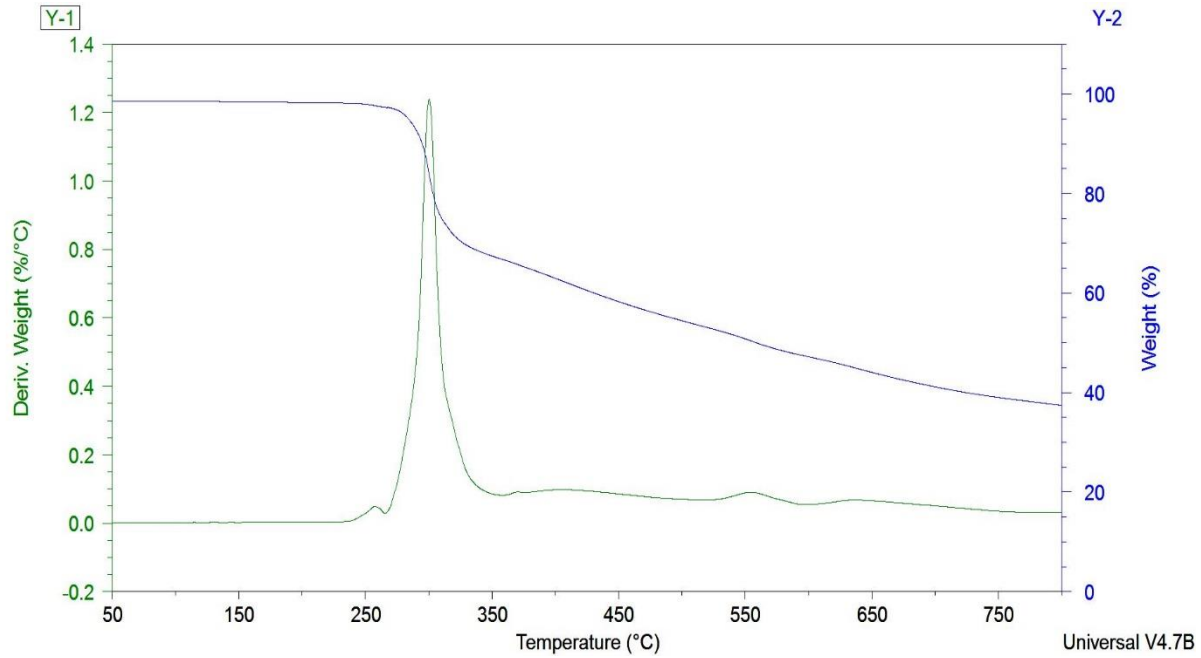


*Figure B-6: TGA thermogram of **8(c)** with DTG curve.*

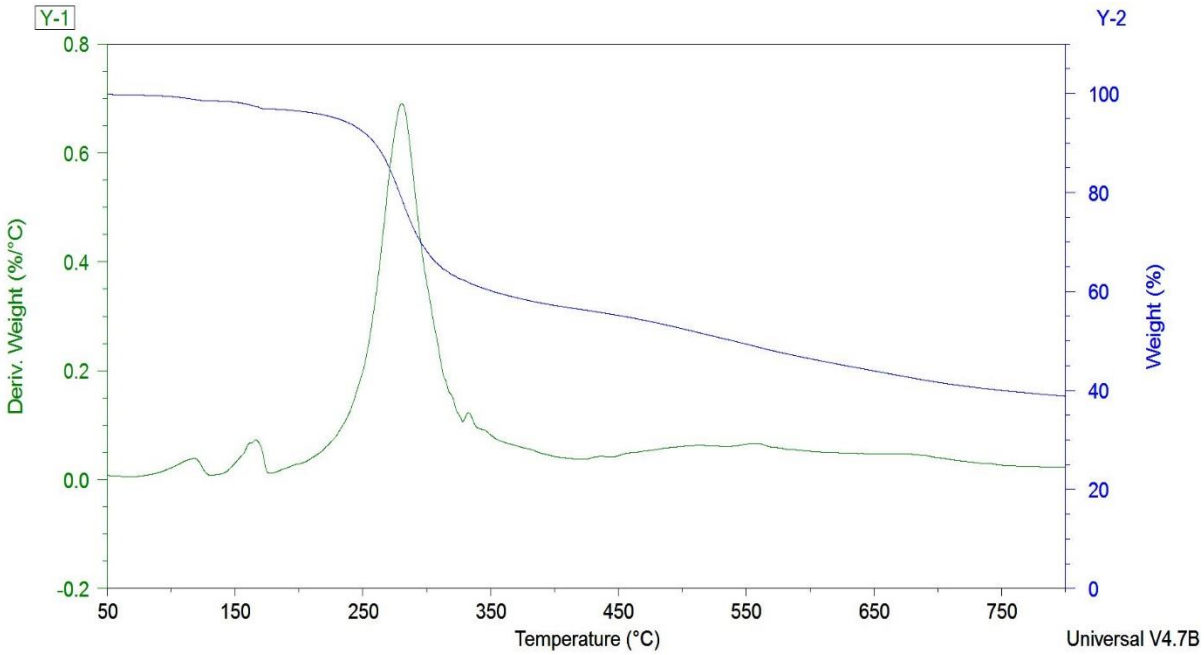


*Figure B-7: TGA thermogram of **10** with DTG curve.*